

# Flood Risk Prediction under Global Vegetated Hydrody- namics

A Bayesian Network

Muhammad Hassan Khan NIAZI

Technische Universiteit Delft





# FLOOD RISK PREDICTION UNDER GLOBAL VEGETATED HYDRODYNAMICS

## A BAYESIAN NETWORK

by

**Muhammad Hassan Khan NIAZI**

Correspondence: [hassaniazi@gmail.com](mailto:hassaniazi@gmail.com)

in partial fulfillment of the requirements for the degree of

**Master of Science** in Civil Engineering  
and M.Sc. in Coastal and Marine Engineering and Management

at the Delft University of Technology,  
to be defended publicly on Thursday July 18, 2019 at 10:00 AM.

Thesis Committee:

Dr. Morales Nápoles O. (Oswaldo)	TU Delft
Dr. van Wesenbeeck, B.K. (Bregje)	TU Delft & Deltares
ir. Smith, G.M. (Gregory)	TU Delft & Van Oord
ir. Lashley, C.H. (Christopher)	TU Delft

## Thesis Support Institutions:



*Student No.:* 4767365  
*Duration:* February 7, 2019 – July 10, 2019

*Keywords:* Flood risk, Disaster risk reduction, Climate change, Nature-based solutions, Building with Nature, Vegetation, Hydrodynamics, Infragravity waves, XBeach Non-Hydrostatic, Probabilistic methods, Non-Parametric Bayesian network, UNINET, Decision support systems.

*Front & Back:* An artist's impression of what this thesis serves to avoid. *Back:* Intriguing cover art by Hania Nawaz Khan that captures the entire content of this thesis in a single illustration.

*This thesis is confidential and cannot be made public until August 14, 2019.*

An electronic version of this thesis is available at <http://repository.tudelft.nl/>.

محمد نیازی

Copyright © 2019 by Muhammad Hassan Khan NIAZI



The Erasmus+: Erasmus Mundus Master of Science in Coastal and Marine Engineering and Management (CoMEM) is an integrated programme including mobility organized by five European partner institutions, coordinated by Norwegian University of Science and Technology (NTNU).

The joint study programme of 120 ECTS credits (two years full-time) has been obtained at two or three of the five CoMEM partner institutions:

Technische Universiteit Delft (TU Delft)	Delft, The Netherlands
Norges Teknisk-Naturvitenskapelige Universitet (NTNU)	Trondheim, Norway
Universitat Politècnica de Catalunya (UPC BarcelonaTech)	Barcelona, Spain
University of Southampton (SOTON)	Southampton, UK
City University London (City)	London, UK

During the first three semesters of the programme, students study at two or three different universities depending on their track of study. In the fourth and final semester an MSc project and thesis has to be completed. The two-year CoMEM programme leads to a multiple set of officially recognized MSc diploma certificates. These will be issued by the universities that have been attended by the student. The transcripts issued with the MSc Diploma Certificate of each university include grades/marks and credits for each subject.

Information regarding the CoMEM programme can be obtained from the programme coordinator:

Øivind A. Arntsen, Dr.ing.

Associate Professor in Marine Civil Engineering

Department of Civil and Environmental Engineering, NTNU, Norway

Telephone: +4773594625 Cell: +4792650455 Fax: + 4773597021

Email: [ovind.arntsen@ntnu.no](mailto:ovind.arntsen@ntnu.no)

URL: <https://www.ntnu.edu/studies/mscomem>





*We make to ourselves pictures of facts.  
The picture presents the facts in logical space,  
the existence and non-existence of atomic facts.  
The picture is a model of reality.  
The picture is a fact.*

*That the elements of the picture are combined,  
with one another in a definite way,  
represents that the things are so combined with one another.  
Thus the picture is linked with reality; it reaches up to it.  
It is like a scale applied to reality.*

*The representing relation consists of the co-ordinations,  
of the elements of the picture and the things.  
These co-ordinations are as it were the feelers of its elements,  
with which the picture touches reality.  
The picture can represent every reality whose form it has.*

*The picture, however, cannot represent its form of representation; it shows it forth.  
But the picture cannot place itself outside of its form of representation.  
If the form of representation is the logical form,  
then the picture is called a logical picture.  
Every picture is also a logical picture.  
The logical picture can depict the world.*

*The picture depicts reality by representing a possibility,  
of the existence and non-existence of atomic facts.  
The picture represents a possible state of affairs in logical space.  
The picture contains the possibility of the state of affairs which it represents.*

*The picture represents what it represents,  
independently of its truth or falsehood,  
through the form of representation.  
What the picture represents is its sense.*

*In order to discover whether the picture is true or false,  
we must compare it with reality.  
There is no picture which is a priori true.*

*The logical picture of the facts is the thought.  
“An atomic fact is thinkable”—means: we can imagine it.  
What is thinkable is also possible.*

Ludwig Wittgenstein in Tractatus Logico-Philosophicus  
[Wittgenstein \(1922\)](#)



This thesis is dedicated to

*... my family*

*... all the underprivileged yet extremely talented  
struggling to make their mark*

*... all the unaided flood affected*



# CONTENTS

<b>List of Figures</b>	<b>ix</b>
<b>List of Tables</b>	<b>xi</b>
<b>Summary</b>	<b>xiii</b>
<b>Samenvatting</b>	<b>xv</b>
<b>Preface</b>	<b>xvii</b>
<b>I PART I: BACKGROUND</b>	<b>1</b>
<b>1 Introduction</b>	<b>3</b>
1.1 Motivation . . . . .	4
1.1.1 Problem . . . . .	4
1.1.2 Solution . . . . .	9
1.1.3 Thought Experiment . . . . .	11
1.2 Scoping & Significance . . . . .	12
1.2.1 Research Gaps & Value Addition . . . . .	12
1.2.2 Research Aims & Objectives . . . . .	13
1.2.3 Research Questions . . . . .	14
1.3 Methodology . . . . .	15
1.3.1 Limitations. . . . .	16
1.3.2 Thesis Structure . . . . .	18
<b>2 Literature Review</b>	<b>21</b>
2.1 Hybrid Flood Defence System . . . . .	22
2.1.1 Run-up & Overtopping. . . . .	23
2.1.2 Hydrodynamic Forcing. . . . .	23
2.2 Vegetation Hydrodynamics . . . . .	25
2.2.1 Flow Variation . . . . .	26
2.2.2 Wave Attenuation . . . . .	35
2.3 Extreme Behavior Modeling: XBeach . . . . .	39
2.3.1 XBeach Formulation . . . . .	40
2.3.2 Abstractions & Simplifications . . . . .	42
2.3.3 Wave Dissipation by Vegetation . . . . .	43
2.4 Bayesian Networks . . . . .	43
2.4.1 Building Blocks & Theoretical Framework . . . . .	44
2.4.2 Non-Parametric Bayesian Networks . . . . .	47
2.4.3 Dependence Modelling by UNINET . . . . .	49

<b>II</b>	<b>PART II: MODELING ACTION, REACTION &amp; PREDICTION</b>	<b>51</b>
<b>3</b>	<b>Action: Global Vegetated Hydrodynamic System</b>	<b>53</b>
3.1	System Idealization . . . . .	54
3.1.1	Schematization . . . . .	54
3.1.2	Input Parameters . . . . .	56
3.2	Stochastic Modeling . . . . .	62
3.2.1	Stochastic Model Setup . . . . .	62
3.2.2	Marginal Distributions . . . . .	63
3.2.3	Copulas & Correlations . . . . .	65
3.3	Results & Discussion: Global Vegetated Hydrodynamics . . . . .	73
3.3.1	Correlations Matrices . . . . .	75
3.3.2	Monte Carlo Sampling . . . . .	75
<b>4</b>	<b>Reaction: Numerical Model &amp; Vegetation Response</b>	<b>79</b>
4.1	Global Model Setup . . . . .	81
4.1.1	Model Settings . . . . .	81
4.1.2	Vegetation Implementation . . . . .	85
4.2	Analysis & Post-Processing . . . . .	85
4.2.1	Outputs . . . . .	86
4.2.2	Analysis Methods . . . . .	87
4.3	Results & Discussion: Vegetation Response . . . . .	89
4.3.1	Case Model Results . . . . .	89
4.3.2	Global Model Results . . . . .	92
<b>5</b>	<b>Prediction: Probabilistic Model and Bayesian Network</b>	<b>99</b>
5.1	Non-Parametric Bayesian Network . . . . .	100
5.1.1	Vegetated Systems . . . . .	100
5.1.2	Flood Risk . . . . .	102
5.2	Results & Discussion: Flood Risk Prediction . . . . .	103
5.2.1	Prediction Tool . . . . .	103
5.2.2	Dependence . . . . .	106
5.2.3	Empirical Parameterization . . . . .	107
5.3	Validation . . . . .	112
5.3.1	Does the model represent reality? . . . . .	112
5.3.2	Dependence Structure Validation . . . . .	113
5.3.3	Predictive Skill Validation . . . . .	114
<b>6</b>	<b>Conclusions &amp; Way Forward</b>	<b>119</b>
6.1	Novelty . . . . .	120
6.2	Conclusions . . . . .	120
6.3	Recommendations . . . . .	122
6.4	Way Forward . . . . .	123
	<b>Bibliography</b>	<b>125</b>

---

<b>III PART III: SUPPLEMENTARY</b>	<b>147</b>
<b>A Parameter Sampling</b>	<b>149</b>
A.1 Alternative System Idealizations . . . . .	150
A.2 Marginal Distributions . . . . .	151
A.3 Copulas & Correlations . . . . .	154
<b>B Model Setups &amp; Pre-Processing</b>	<b>159</b>
B.1 Pseudocodes . . . . .	160
B.2 XBeach Input Files . . . . .	161
B.3 XBeach Sensitivity Tests . . . . .	165
B.4 Stochastic Model . . . . .	166
<b>C Extended Results</b>	<b>169</b>
C.1 Spectral Evolution. . . . .	170
C.2 CoWebs of Bayesian Network . . . . .	171



# LIST OF FIGURES

1.1	Spatial mean annual wave power for the globe and the different ocean basins	5
1.2	Share of loss due to natural disasters.	6
1.3	Relative Interest in nature-based solutions, dike, saltmarsh, mangrove, and seawall	7
1.4	Relative Interest about nature-based solutions worldwide in last 5 years	7
1.5	Hybrid and nature-based flood defense solutions	9
1.6	Global distribution of Types of Vegetation	10
1.7	Thesis Outline and Process flow	11
1.8	Wave spectrum & classification. (Munk, 1950)	13
1.9	Research plan and Work flow	17
2.1	Risk reduction cascade	22
2.2	Interaction of seagrass-saltmarsh environment with hydrodynamics	25
2.3	Summary of general mechanics of wave height reduction through habitats	27
2.4	Flow variation in Emergent Vegetation	28
2.5	Regimes of flow variation in all types of vegetation	28
2.6	Drag Coefficients review (van Zelst, 2018).	30
2.7	Types of BN structures: undirected, directed, weighted, and bipartite graphs	48
2.8	Steps for Stochastic modeling in UNINET	50
3.1	Idealized profile used for XBeach modeling including six output points	55
3.2	Vegetated hydrodynamic system schematization	56
3.3	Saltmarsh parameter values	59
3.4	Vegetation parameters values for Mangroves	60
3.5	Bivariate matrix of hydraulic parameters	65
3.6	Gaussian copula and correlations from global wave climate data for $H_{m0}$ and $(S_T)$	66
3.7	Copula and correlations from field data	68
3.8	Copula and correlations from global wave climate data for $H_{m0}$ and $T_p$	69
3.9	Structured expert judgment-ANDURIL	70
3.10	Bayesian network for stochastic modeling of saltmarsh input parameters	73
3.11	Bayesian network for stochastic modeling of mangroves input parameters	74
3.12	Correlations in global vegetated hydrodynamic conditions in saltmarshes and mangroves	76
3.13	Profile samples from 10 random models.	78
4.1	Scripts overview for vegetation modeling in XBeach using MATLAB	81
4.2	Numerical model setup based on system idealization	82
4.3	Pseudocode setup.m for XBeach model setup.	83

4.4	Implementation of all three types of vegetation in XBeach . . . . .	85
4.5	Pseudocode process .m for post-processing the XBeach results . . . . .	88
4.6	Wave amplitude timeseries . . . . .	89
4.7	Comparison of spectral evolution of the case model with and without vegetation . . . . .	90
4.8	Case model results showing wave height evolution, water levels and wave setup along with bed levels. . . . .	91
4.9	Violin Plot combining box and whiskers plot and probability density plots. . . . .	93
4.10	Bulk model results of attenuated wave heights . . . . .	94
4.11	Bulk model results of mean water levels and set-up . . . . .	95
4.12	Bulk model results of run-up . . . . .	96
4.13	Bulk model results of attenuation and transmission coefficients . . . . .	97
5.1	Flood risk prediction tool (non-parametric Bayesian network) for seagrass-saltmarsh environments. . . . .	104
5.2	Flood risk prediction tool (non-parametric Bayesian network) for seagrass-mangroves environment. . . . .	105
5.3	Inter-parameter dependence in saltmarshes and mangroves . . . . .	106
5.4	Maximum dependence of Run-up ( $R_{H2\%}$ ) and Attenuation coefficient ( $K_{r,M}$ ) . . . . .	108
5.5	Empirical parameterization of Run-up and wave attenuation coefficient for Saltmarshes . . . . .	110
5.6	Empirical parameterization of Run-up and wave attenuation coefficient for Mangroves . . . . .	111
5.7	Statistical validation of developed non-parametric Bayesian networks . . . . .	113
5.8	Dependence structure validation of non-parametric Bayesian networks . . . . .	114
5.9	Predictive skill validation of seagrass-saltmarshes non-parametric Bayesian network . . . . .	117
A.1	Alternative System Idealizations based on vegetation forest platform . . . . .	150
A.2	Copula and correlations from field data . . . . .	154
A.3	Copula and correlations from field data . . . . .	154
A.4	Gaussian copula and correlations from global wave climate data for $H_{m0}$ and ( $S_r$ ) . . . . .	155
A.5	Gaussian copula and correlations from global wave climate data for $T_p$ and $S_r$ . . . . .	155
A.6	Gaussian copula and correlations from field data for $H_{m0}$ and $h$ . . . . .	156
B.1	Parent file calling all the functions to run the XBeach simulation . . . . .	160
B.2	The pseudocode run .m to run XBeach global model simulations . . . . .	161
B.3	Grid points sensitivity for running duration and spin up . . . . .	165
B.4	XBeach sensitivity test based on dxmax and ARC . . . . .	166
C.1	Spectral evolution of the case model with and without vegetation . . . . .	172
C.2	CoWebs and density plots of Saltmarsh and Mangroves non-parametric Bayesian Networks . . . . .	173

# LIST OF TABLES

2.1	Vegetation classifications . . . . .	26
2.2	Review of experimental work in vegetation hydrodynamics . . . . .	31
2.2	Review of experimental work in vegetation hydrodynamics . . . . .	32
2.2	Review of experimental work in vegetation hydrodynamics . . . . .	33
3.1	Sea-state classification based on peak wave period $T_p$ and peak frequency $f_p$ . . . . .	58
3.2	Input parameters for vegetated hydrodynamic system . . . . .	64
3.3	World wave climate . . . . .	69
3.4	Rank correlations between global saltmarsh system . . . . .	71
3.5	Conditional (partial) rank correlations between input parameters . . . . .	72
3.6	Correlation matrix of stochastic model for saltmarshes . . . . .	75
3.7	Monte Carlo samples from stochastic model to be used as input conditions for XBeach global model runs . . . . .	77
4.1	Input conditions for a sample XBeach case model run. All case model results are based on this simulation. . . . .	89
5.1	Validation of flood risk prediction tool: seagrass-saltmarshes and seagrass-mangroves non-parametric Bayesian network . . . . .	115
A.1	Random variables in stochastic modeling for parameter sampling . . . . .	153
A.2	Data Specifications for bivariate dependence matrix of hydraulic parameters . . . . .	157



# SUMMARY

Coasts are headsprings of opportunities with positive externalities but concurrently are vulnerable to hazards like floods. The increasing frequency and intensity of extreme events due to global warming and climate change is increasing flood risk. To act, rather than react, nature-based solutions (NBS) involving vegetation and wetlands are being explored on top of conventional solutions like dikes.

There was a dire need for global study quantifying the potential of vegetation in reducing flood risk and eventually make a decision support tool which enables quick assessments about flood risk reduction in a vegetated hydrodynamic system. The developed tool can predict flood risk anywhere in the world without rigorous modeling through user defined conditionalization of in-situ hydrodynamic or vegetation characteristics.

The effectiveness of seagrasses, salt marshes, and mangroves in reducing hydrodynamic loads globally have been investigated. A hybrid system of wetlands and dikes have been numerically modeled through a non-hydrostatic model resolving full spectrum of high and low frequency waves. A non-parametric Bayesian network-based flood risk prediction tool has been developed from the synthetic dataset developed from the simulations.

Multivariate dependence among parameters of schematized system can exhibit characteristics of vegetated hydrodynamics. To ensure global representation of vegetated hydrodynamics a copula-based multivariate stochastic model was developed which caters global ranges of each parameter, their probability distributions and the inter-parameter dependencies through ranked correlations.

Bulk results conclude that saltmarshes attenuate waves by 87% and mangroves by 94% as a mean value. That being the case, huge reduction in costs of conventional flood defenses could be enjoyed if hybrid flood defenses are adopted. Wave attenuation, flood risk reduction and wave run-up manifests maximum dependence on offshore wave height, water depth, drag coefficient, vegetation height, frontal width, and forest length.

To the author's knowledge no such study exists which captures natural variability of hydrodynamics and vegetation together in a probabilistic model over global scales. Additionally, no such study exist which applies non-parametric Bayesian networks to predict flood risk. The dependence modeling which skims out the most critical parameters is also unique.

This work advocates for using nature-based solutions like vegetation for combating detrimental effects of climate change like increasing flood risk along with value addition of enhanced ecosystem. The flood risk prediction tool would help decision makers in implementing NBS, in making better informed decisions about early warnings and policy making related to flood risk reduction and climate change adaptation by incorporating vegetation.



# SAMENVATTING

Kustgebieden zijn koplopers van kansen met positieve externe effecten, maar tegelijkertijd zijn ze kwetsbaar voor gevaren zoals overstromingen. Door de toenemende frequentie en intensiteit van extreme gebeurtenissen als gevolg van opwarming van de aarde en klimaatverandering neemt het overstromingsrisico toe. Om op te treden, in plaats van te reageren, worden natuurgerichte oplossingen (NBS) met betrekking tot vegetatie en kwelders actief onderzocht, naast conventionele oplossingen zoals dijken.

Er was een grote behoefte aan een wereldwijde studie die het potentieel van vegetatie kwantificeert in het verminderen van overstromingsrisico's en uiteindelijk een beslissingsondersteunende tool maakt die snelle beoordelingen mogelijk maakt van de vermindering van het risico op overstromingen in een begroeide hydrodynamische systeem. Het ontwikkelde hulpmiddel kan overstromingsrisico's overal ter wereld voorspellen zonder rigoureuze modellering door middel van de door de gebruiker gedefinieerde conditionalisatie van in-situ hydrodynamische of vegetatiekenmerken.

De effectiviteit van zeegrassen, kwelders en mangroven bij het wereldwijd verminderen van hydrodynamische belastingen is onderzocht. Een hybride systeem van wetlands en dijken is numeriek gemodelleerd door een niet-hydrostatisch model dat het volledige spectrum van hoog- en laagfrequente golven oplost. Een niet-parametrische Bayesiaanse netwerk-gebaseerde voorspellingstool voor overstromingsrisico's is ontwikkeld op basis van de synthetische dataset die is ontwikkeld op basis van de simulaties.

De multivariate afhankelijkheid tussen de parameters van het schematische systeem kan kenmerken van begroeide hydrodynamica vertonen. Om globale representatie van begroeide hydrodynamica te waarborgen, werd een op copula gebaseerd multivariabel stochastisch model ontwikkeld dat globale bereiken van elke parameter, hun waarschijnlijkheidsverdelingen en de inter-parameterafhankelijkheden op basis van gerangschikte correlaties verzorgt.

Bulkresultaten concluderen dat kwelders golven met 87% en mangroven met 94% als gemiddelde waarde verzwakken. Als dat het geval is, zou een enorme verlaging van de kosten van conventionele waterkeringen kunnen worden genoten als hybride waterkeringen worden toegepast. Golfverzwakking, overstromingsrisicovermindering en golfoploop manifesteren laten een maximale afhankelijkheid van offshore golfhoogte, waterdiepte, luchtweerstandscoefficiënt, vegetatiehoogte, frontale breedte en boslengte.

Voor zover de auteur weet, bestaat er geen dergelijke studie die de natuurlijke variabiliteit van hydrodynamica en vegetatie samenbrengt in een probabilistisch model over globale schalen. Bovendien bestaat er geen dergelijke studie die niet-parametrische Bayesiaanse netwerken toepast om overstromingsrisico's te voorspellen. De afhankelijkheidsmodellering die de meest kritische parameters wegschiet, is ook uniek.

Dit werk pleit voor het gebruik van op de natuur gebaseerde oplossingen zoals vegetatie voor het bestrijden van schadelijke effecten van klimaatverandering, zoals het verhogen van het overstromingsrisico en het toevoegen van toegevoegde waarde aan een verbeterd ecosysteem. Het voorspellingsinstrument voor overstromingsrisico's zou besluitvormers helpen bij de implementatie van NBS, bij het nemen van beter geïnformeerde beslissingen over vroege waarschuwingen en beleidsvorming met betrekking tot overstromingsrisicovermindering en aanpassing aan de klimaatverandering door de integratie van vegetatie.

# PREFACE

I come from highly vulnerable, low-income part of the world who is a first hand witness of adversity in the times of natural disasters. While I believe that water resources and the degree of control over it define nations; masters degree related to hydraulic engineering and interest in disaster risk reduction implored to do something about flood risk. The idea of this masters degree in general, and the thesis in particular, was to get to the core of fundamental engineering principles and use them for the society-oriented adaptive solutions in the systems set forth.

I believe that trickle down effect of economics holds true in societal dynamics as well which converged my motivation to develop an aid for the ones on top of the pyramid. I channeled my knowledge acquired over the past few years to bridge up science to policy with a flood risk prediction tool. The journey was not all alone but alot of individuals and institutions are to be commended for imprinting an impression on me and this thesis.

First of all, I value the love and appreciate the patience of my parents Ghazanfar and Nureed, brothers Hussain and Mohsin, and wife Hania for bearing with the distance, for understanding my 'mute-times' due to busy routine, and always believing in me. Secondly, I also acknowledge my mentors Dr. Shahid Ali and Dr. Mansoor A. Hashmi who were not directly involved in this MSc journey but thanks to them for their encouragement when it mattered the most.

I want to thank my thesis committee comprising of Dr. Oswaldo Morales Nápoles as the chairman and Dr. Bregje K. van Wesenbeeck, Greg M. Smith, and Chris H. Lashley as the supervisors. I am grateful for their time and effort with especially the contribution in identifying the blindspots which I might had missed.

If it wasn't Oswaldo I believe I would not have been able to satisfy my intellectual quench of looking into system-wide world of possibilities. I'd cherish him being an amicable chairman, be it by always answering to my walk-in questions or by dropping by my room to check how am I holding up. I thank Bregje whose biggest contribution was not only the supervision but the inspiration that I drew from the way she advocates for nature-based solutions as an expert world wide. Greg could not be thanked more for the most meaningful conversations and most encouraging comments, I wish he had joined the committee earlier. I thank Chris for meeting me every week, even sometimes when I had nothing to present. He indeed threw the sanity element into the mix whenever I got carried away with more and more ideas to implement.

I would like to acknowledge Dr. Bas Hofland for introducing me to the Dutch water-consulting hub and a place of great minds - Deltares, where I worked on WoodVer-susWaves project with Bregje and Bas. I also want to thank him for showing me how much energetic and exciting your life could be if you love what you do.

I also thank Professor Heidi Nepf and Dr. Chao Liu from Parsons Laboratory MIT and Dr. Khanh L. Phan from WaterLab TUDelft for agreeing to support and sharing their experimental datasets. Unfortunately, the datasets could not be used in the thesis but I am indebted to both the researchers for the kind gesture and practically believing in knowledge sharing.

I am highly obliged to Dr. Bas W. Borsje, Dr. Vincent Vuik, Dr. Siddharth Narayan, Alejandra G. Mancheño and Vincent van Zelst for the discussion meetings about global vegetation. I would like to appreciate Stuart G. Pearson for doing a similar work about coral reefs, such elaborated answers to my queries, and sharing the scripts which formed the basis of MATLAB scripting for this thesis. Also, Rabia Ilyas is to be thanked for giving insights on ecological and botanical aspects of coastal vegetation. I thank Mohsan for his invaluable logistical contribution and the free coffees ofcourse. I extremely admired the company of Joanneke, Bas, Jochum, Lluís, Akshay, Susana, and Camila while working, discussing and sharing with them.

I'd like to extend my gratitude to EU commission, NTNU administration and CoMEM consortium for accepting me as an Erasmus Mundus student and for the courteous human investment that EC has made. At NTNU, I thank Øivind A. Arntsen and Sonja M. Hammer for the waffle meetings and treating all of us as one of their own, Knut V. Høyland for being so courteous and considerate, and Micheal Muskulus for instilling in me the meaning of true understanding. At SOTON, I appreciate Professor Robert J. Nicholls for taking out the time and sitting with us for the commencement of this thesis. TUDelft as a front runner institution in water engineering and management has not only taught me alot but has also made me evolve as a person and so I express my gratitude to people and fellow students at TUDelft.

I am indebted to my entire CoMEM family for electing me as their Program Representative for two years. Furthermore, I truly enjoyed and learnt alot while living with my Holyrood clan Fred, Flo, Matteo, Ingrid, and Nikos which certainly means alot to me. I also want to thank Marlon, Ludovie, Ganga, Nauman, Fahad, Yasser, Khaled, Mazen, Sung, and Daniil for the time we've spent together. For the little things which helped throughout the courses and the thesis. For being my CoMEM fellows through the course of two years and the times to come.

*Muhammad Hassan Khan Niazi  
Delft, Netherlands  
July 2019*

# I

## PART I: BACKGROUND



# 1

## INTRODUCTION

*Whenever a man interferes with a system  
he becomes involved in its operation.  
To the degree that man upsets the natural balance of the system  
he end up his machines must do the work  
that nature did before.*

The Beach: A River of Sand

### Abstract

Flood risk is increasing due to climate change and increasing vulnerability. To counter that, nature-based solutions involving vegetation are being explored because they offer both engineering and ecosystem services. However, decision support tools which incorporates both detailed hydrodynamics and vegetation are scarce. Therefore, the global vegetated hydrodynamic system has been stochastically parameterized, numerically modeled and probabilistically expressed through a multivariate dependence model–Bayesian network. The resulting decision support tool will help decision makers to make quick assessments about flood risk and reduction potential of vegetation anywhere in the world. Motivation and scoping of the thesis in terms of aims, objectives, and research questions, followed by a brief methodology is presented in this chapter.

**C**OASTAL systems around the globe are headsprings of many opportunities with positive externalities like trade, tourism, transport, offshore energy, fisheries and more. On the flip side, while providing the positive services, these systems can be facing challenges like climate change, plastic pollution, flooding and erosion risks which affect people rather adversely. While we want to reap the benefits we need to limit the threats in order to maximize the utility.

This master thesis is a combination of numerical and probabilistic study aimed to deliver a flood risk prediction tool under global vegetated hydrodynamics and investigate the role of vegetation in reduction of coastal flooding. Probabilistic parameterization of global vegetated-hydrodynamic systems was extended towards numerically analyzing flood risk reduction by seagrasses, saltmarshes, and mangroves. The results were further extended to create the flood risk prediction tool under global vegetated hydrodynamics. Therefore, the thesis encompasses studying the effects generated by vegetated environments in varied hydrodynamic conditions, modeling the vegetated-hydrodynamic system and eventually developing a Bayesian network-based flood risk prediction tool.

The prediction tool would help decision makers in making quick assessments about flood risk mitigation and in optimal utilization of vegetation to deliver the function of flood risk reduction. The tool would eventually enable decision makers to make better informed nature-based flood risk mitigation plans.

## 1.1. MOTIVATION

The true motivation for this thesis lies in investigating environmental hydrodynamics in vegetated environments to aid disaster risk reduction through Nature-Based Solutions (NBS). At the core, this motivation is driven based on a problem-solution viewpoint which has been channeled through understanding hydrodynamics and the effects of vegetation in reducing the ferocity of the former when it touches its extremes.

The system of vegetated hydrodynamics involves various elements embracing a dependence structure in reality. Further to understanding the nature, an initiative for a robust tool catering detailed hydrodynamics and the dependence structure is imperative to be incorporated in decision making.

### 1.1.1. PROBLEM

Flood risk is a function of probability of flooding (hazard) and the magnitude of consequences (vulnerability) due to that flooding. The crux of the problem part of motivation has been synthesized in a problem statement presented hereunder.

#### **Problem Statement**

With climate change flood risk is increasing which is affecting most vulnerable parts of the world. To combat increasing flood risk, resource allocation has to be done by decision makers for whom improved tools should be available to make predictions about flood risk reduction potential of a possible nature-based solution – vegetation.

### HAZARD: INCREASING FLOOD RISK

Climate change is a challenge of global trends and scale. Flood risk, in low-lying areas with high vulnerability, is complementary to climate change (Kellens et al., 2013). Oceans form 75% of the earth's surface area and many studies including the very recent ones indicate increase in global wave power due to ocean warming (Reguero et al., 2019), see Figure 1.1. Regional and global analyses of sea-level rise scenarios indicate increasing flood risk (Nicholls et al., 1999). The foremost physical impact of sea-level rise is the increase in land submergence and flooding (IPCC et al., 2007; Nicholls & Cazenave, 2010) which has to be dealt with an emergency.

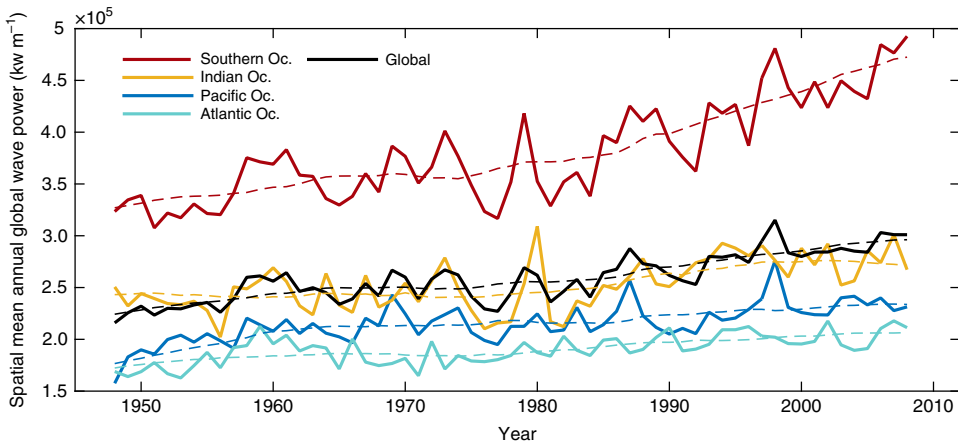


**Figure 1.1:** Spatial mean annual wave power for the globe and the different ocean basins. Wave power is a climate change indicator which represents cumulative transport of energy transmitted to wave motion by air-sea interactions (Donelan et al., 1997). A clear increasing trend is observed in the 10-year moving averages (dashed lines) of the wave power timeseries (solid lines). Figure is reproduced from Reguero et al. (2019).

The frequency and intensity of extreme events across the globe is increasing at an accelerating rate (Reguero et al., 2019). The frequency of coastal flooding would double in a 10-20cm sea-level rise scenario until 2050 (Vitousek et al., 2017). There has been an increase in the rate of global mean sea level rise since 2010 (Yi et al., 2015) which directly translates to increased flood risk through wave setup, swash, and runup (Stockdon et al., 2006).

The trends for increasing extreme values are more severe than the trends for increase in mean values (Young et al., 2011; Wang et al., 2009; Wang & Swail, 2001). The 95th percentile wave heights are increasing at a rate twice as much as 90th percentile wave heights (Young et al., 2011). ERA-40 re-analysis of meteorological observations concludes that even wave periods are increasing (Sterl & Caires, 2005; Uppala et al., 2005). More distant waves in future with higher extreme wave heights with longer periods means a significant increase in flood risk.

## VULNERABILITY: INCREASING EXPOSURE

Vulnerability and exposure for flood risk are accounted through the population prone to coastal flooding. About 40% of the world's population live within 100km of the coast and more than 10% live in low elevation coastal areas that are less than 10m above sea level (United Nations, 2017). The biggest hotspots of population are found in tropical and sub tropical areas. The population density in coastal areas have a three times higher average than the global average and is significantly higher than the non-coastal areas (Small & Nicholls, 2003). Most of the world's biggest metropolitan cities are situated on the coast (Brown et al., 2013) and many of these are located in large deltas (Neumann et al., 2015).

Not only does this showcases huge vulnerability already but the bigger pressing issue is that coastal areas tend to have higher rates of population growth and urbanization than inland areas (Neumann et al., 2015; Hugo, 2011). This increasing trend of coastal migration associated with global demographic changes scales up the current vulnerability (Hugo, 2011) and greatly contributes to flood losses and flood risk eventually.

The menace of flooding results in all sorts of individual, societal and economic losses. UNISDR (2018)<sup>1</sup> states that floods have the highest share of loss compared to other natural disaster, as observed in Figure 1.2. A global assessment of future flood losses in 136 largest coastal cities reveals a gigantic 10 times increase of flood losses per year in 2050 as compared to 2005 even if constant flood probability is maintained (Hallegatte et al., 2013). Therefore, to maintain current flood risk, flooding probabilities are to be reduced (Hallegatte et al., 2013) for which more robust solutions are required.

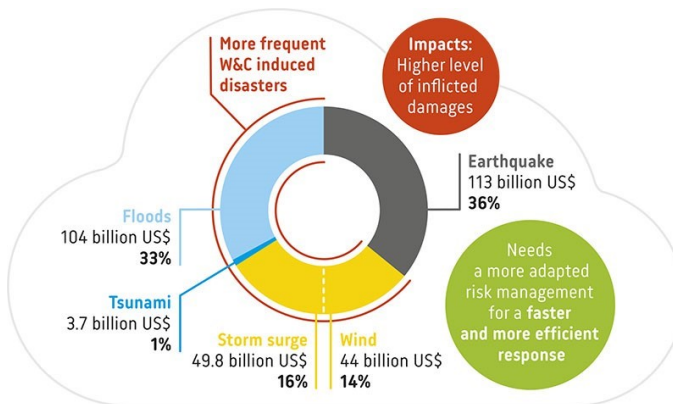


**Figure 1.2:** Share of loss due to natural disasters. Figure reproduced from (UNISDR, 2018) with data from Global Risk Assessment.

Increasing hazard and vulnerability uplifts flood risk which encourages to have greater interests in finding more adaptive solutions on top of conventional solutions. In order to quantify the utility of newer solutions better tools are necessary to be made available for decision makers.

<sup>1</sup>Currently known as UNDRR: United Nations Office for Disaster Risk Reduction formerly as UNISDR: United Nations International Strategy for Disaster Reduction.

RELATIVE INTEREST

A preliminary observation revealed that conventional solutions are more researched than nature-based solutions so there is a need for improving the understanding of NBS. A google trends comparison in Figure 1.3 shows that the relative interest<sup>2</sup> in dikes and seawalls is prominently more than nature-based solutions, saltmarshes, and mangroves. Also in the literature better principles, guidelines and standards have been developed for designing conventional solutions than NBS. Infact, only recently principles and guidance about successfully implementing and upscaling nature-based solutions (Cohen-Shacham et al., 2019; van Wesenbeeck et al., 2017) have started to appear in literature.

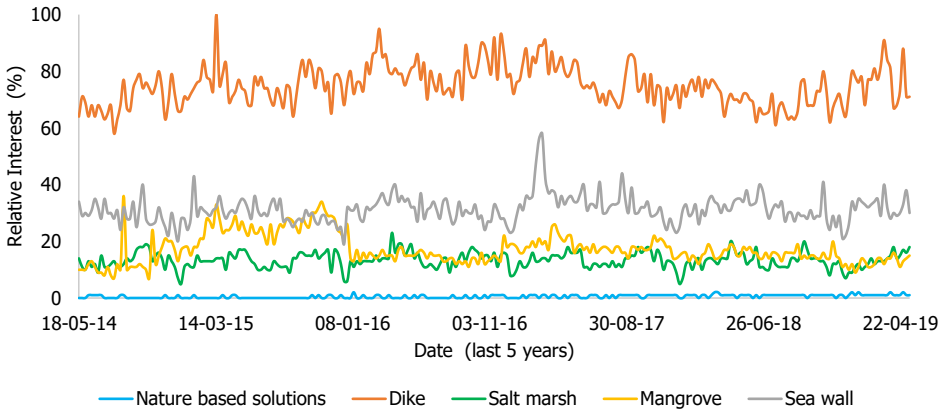


**Figure 1.3:** Relative Interest in nature-based solutions, dike, saltmarsh, mangrove, and seawall. Data taken from Google Trends.

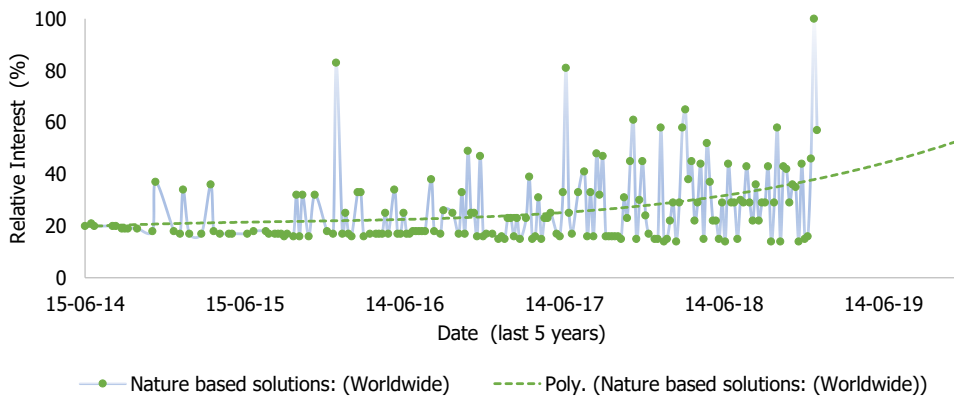


**Figure 1.4:** Relative Interest about nature-based solutions worldwide in last 5 years. The data has been taken from Google Trends.

<sup>2</sup>Relative interest is relative popularity which is calculated by dividing the term searches by the maximum searches of any term in a given period of time.

However, the realization that nature-based solutions add value to the overall flood defense system has led to its increased interest. The google trends analysis in Figure 1.4 depict increasing popularity and interest about nature-based solutions worldwide in last 5 years. Similar trends have been observed in number of scientific papers published related to nature-based solutions in Web of Science and Scopus portals ( $\approx 3$  times more in 2018 as compared to 2013).

### NEED FOR CUTTING EDGE PREDICTION TOOLS

Implementation of nature-based solutions for countering the complex and damaging effects of climate change necessitates highly informed decision makers. Better and effective decisions, especially about problems in future, depict better understanding (Kourgiyas et al., 2015; Sperotto et al., 2017) which directly correlates to the prediction tools available for the decision maker. The obligation of delivering state-of-the-art prediction tools to decision makers lies on the shoulders of scientific community.

Numerical model based predictions concerning nature-based solutions do exist for various system response elements. The models can predict results like drag forces in vegetated canopies (van Rooijen et al., 2018) or extreme run-up in coral reefs (Lashley et al., 2018) or swash dynamics and run-up (Roelvink et al., 2018). However, numerical model based predictions are greatly cumbersome and not everyone, especially the decision makers, can't use them. A simple user-friendly prediction model is needed which resolves most of the physical processes and uses the results to infer the dependence between various components of a vegetated-hydrodynamic system.

Plenty of tools exist for decision support related to ecosystem management. Tools like Ecosystem Management System Support (EMDS) can provide global ecological assessments, Ecosystem Assessment and Reporting Tool (EAR) can do spatial assessments for effective conservation, Drivers-Pressure-State-Impact-Response (DPSIR) can inform about inter-relations between ecological and economic dynamics of coastal zones, Dynamic and Interactive Vulnerability Assessment (DIVA) can assess coastal impact and so on. However, not many tools are able to incorporate both hydrodynamics and ecosystems to offer decision support for flood risk.

Closest attempt to the aim of this thesis was made in Foreshore Assessment using Space Technology (FAST) project which can predict wave attenuation on vegetated foreshores globally. However, it only takes into account the absence or non-absence of vegetation, except for 7 case study locations, while predicting wave attenuation potential. Single vegetation state per vegetation type, i.e. saltmarsh or mangroves, is taken and even for the 7 case study sites only vegetation density is varied. Furthermore, the underlying hydrodynamic model that FAST Project used to determine nearshore wave conditions doesn't resolve high frequency (wind waves). Therefore, there was a big void in decision support tools which couples detailed hydrodynamics and vegetation and, most importantly, takes into consideration the underlying dependence of such a dynamic system.

### 1.1.2. SOLUTION

In the realm of proposing solutions to mitigate the detrimental effects of climate change especially increasing flood risk, both hard and soft solutions are proposed (Carrick et al., 2018). Conventional or hard solutions involve building physical barriers like dikes, flood walls, revetments and breakwaters where as nature-based or soft solutions involve using natural features and processes to gain engineering as well as ecosystem services.

The solution for coastal systems facing hazardous prospects of climate change and increasing flood risk lies in designing flood defenses in an objective way where the primary objective should be flood risk reduction. In order to obtain the optimal solution for flood defense, both conventional and nature-based solutions could be coupled yielding hybrid solutions for problems as complex as increasing flood risk, refer to Figure 1.5 for the scope of nature-based solutions under the umbrella of hybrid solutions.

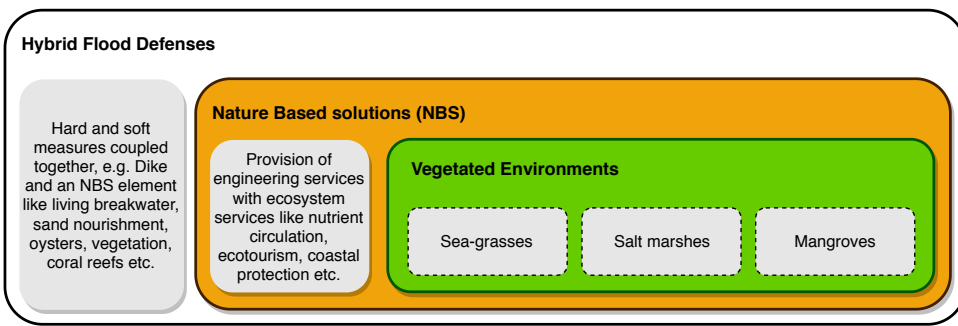


**Figure 1.5:** Hybrid and nature-based in hierarchy of flood defense solutions. Both could be used together to design flood defenses in an objective way.

### POTENTIAL OF NATURE-BASED SOLUTIONS

Provision of nature-based solutions (NBS) for climate change adaptation and flood risk mitigation could be conceived by using vegetation which could be seagrass, salt marshes, or mangroves. Vegetation in aquatic environments not only attenuates hydrodynamic forcing but also provides ecosystem services like seabed stabilization, fish sheltering, oxygen-carbon concentration regulation, coastal erosion reduction and water quality improvement (Green & Short, 2003; Nepf, 2012a). For water quality improvement alone global economic value was estimated to be \$3.8 trillion per year (Costanza et al., 1997). An estimate of the average economic value of entire biosphere is \$33 trillion per year ranging between \$16 to \$54 trillion per year (Costanza et al., 1997).

Nature-based solutions involving vegetation are becoming prominent because of their ability to enhance the engineering services with ecosystem services. Flood risk is a function of probability of flooding and the magnitude of consequences due to that flooding. If vegetation, as a nature-based solution, is employed it delivers a two fold advantage by reducing the hydraulic load as well as reducing the operational costs of conventional flood defenses. The same hydrodynamic forcing experienced by the conventional flood defenses could be reduced due to vegetation-induced wave attenuation and energy dis-

sipation. The decreased wave heights eventually reduces the flood risk by reducing probability of flooding.

Vegetation is a natural resource found across the global and its value, as a flood risk reduction measure, increases in coastal areas since biggest concentration of the population is found near coasts (Neumann et al., 2015; Brown et al., 2013). Figure 1.6, reproduced from Moffett et al. (2015), shows the existence of coastal vegetation in tropical and subtropical areas and it could be observed that vegetated foreshores exist alongside the biggest deltas (red triangles). Large population concentrations are alarming as vulnerability is large but at the same time the coexistence of coastal vegetation on foreshores of these deltas is relieving. The reason being that the utility of flood risk reduction obtained from vegetation would be maximized in such regions.

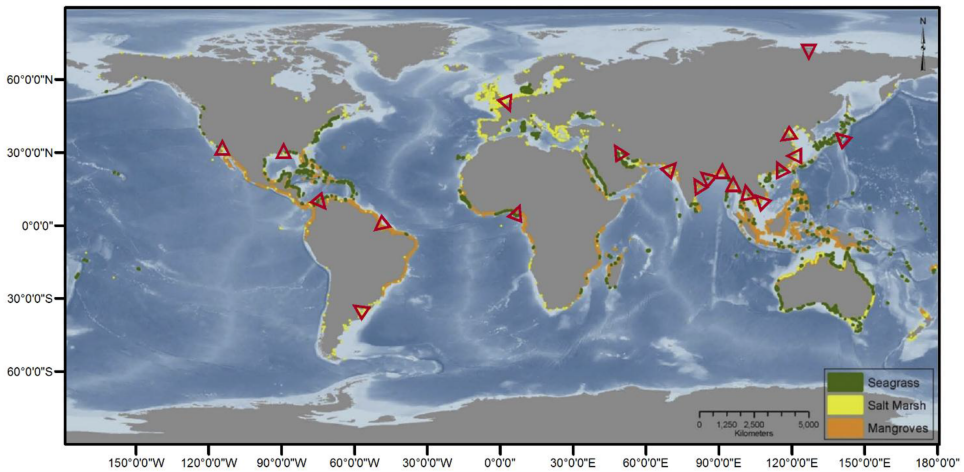


**Figure 1.6:** Global distribution of seagrass meadows, salt marshes, mangroves, and major deltas (red triangles) (Moffett et al., 2015)

While recently nature-based solutions are being explored (Vuik et al., 2015; Narayan et al., 2016; Saleh & Weinstein, 2016; Cohen-Shacham et al., 2019; Davies & Laforteza, 2019; Laforteza & Sanesi, 2019), wave attenuation due to vegetation is comprehensible and have been quantified through both modelling (Mattis et al., 2019; Phan et al., 2019; Wu et al., 2016; Karambas et al., 2016; Van Rooijen et al., 2015) and measurements (Reidenbach & Thomas, 2018; Maza et al., 2016; Möller et al., 2014; Horstman et al., 2014). However, as established earlier, the solutions are subject to uncertainty induced due to climate change, increasing hazard and increasing vulnerability. Vegetation has also been put under the same perspective and future response of global coastal wetlands to sea-level rise has been assessed through detailed geomorphological and anthropogenic system feedbacks (Schuerch et al., 2018). It has been suggested that coastal wetlands can certainly cope up with climate change if current accommodation space is available (Schuerch et al., 2018) and sufficient sediment supply is maintained (Nicholls & Cazenave, 2010).

## DECISION SUPPORT

Innovation and effectiveness of the solutions is a depiction of understanding of the system. The effectiveness of decision and policy making related to flood risk decreases due to increase in uncertainty because of lack of understanding (Carrick et al., 2018). Physical understanding of the system directly correlates with the value generated from probabilistic models (Jaeger, 2018).

This work resonates the same philosophy of trying to improve the understanding about effectiveness of vegetation in reducing flood risk. Improving understanding about global flood risk reduction potential of vegetation and better tools like Bayesian-based prediction models would help decision makes to make more informed decisions. Once the flood risk reduction potential of vegetation is established the whole system is extended to a flood risk prediction tool.

### 1.1.3. THOUGHT EXPERIMENT

The aftermath of the problem-solution driven motivation was the “thought experiment”, as described hereunder, which evolved as the thesis outline and process flow.

*“Seeing and feeling a physical situation almost tangibly, manipulating its elements, observing their changes – all of this imagined in the mind.”*

~ Robert Root-Bernstein in Sparks of Genius

The process flow is divided into four sequential yet intertwined phases which could be seen in Figure 1.7. These phases would be the part of an iterative process to reach to reliable results.

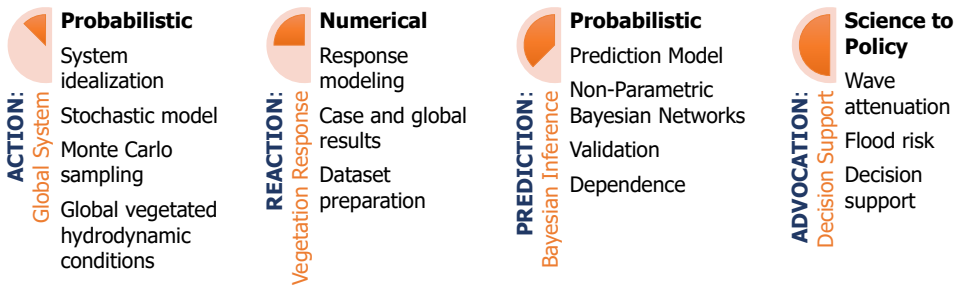


**Figure 1.7:** Thesis Outline and Process flow comprising of four phases of the thesis which are a combination of numerical and probabilistic methods.

### Action: Global Vegetated Hydrodynamic System

Various loading mechanisms contribute to challenge the resisting ability of flood defenses in case of extreme events. Hydrodynamics and vegetation form a vegetated hydrodynamic system in which both vary spatially and temporally. In reality, many components in this combined system exhibit dependence. The action phase would idealize this system, parameterize it, model through a stochastic model, and generate global conditions through Monte Carlo sampling from the copula-based multivariate stochastic model. Hydrodynamic, vegetation and hybrid parameters parameters can represent

the system in a model framework on global scale.

### **Reaction: Vegetation Response**

Seagrasses, salt marshes, and mangroves could be considered as nature-based solutions for flood defenses in coastal areas. This thesis would focus on vegetated foreshores in order to quantify wave attenuation effects of vegetation and resulting wave run-ups. In the reaction phase, the effects of vegetation would be modeled to generate a large synthetic dataset to be used as an input for Bayesian network.

### **Prediction: Non-Parametric Bayesian Network**

In order to derive flood risk predictions this thesis aims to develop a Non-Parametric Bayesian Network (NPBN) for all three types of vegetation under scope. The Bayesian network would be fed with the Monte Carlo samples global input conditions and the resulting dataset from numerical simulations. The Bayesian network would be used to unravel underlying dependence in hydrodynamic or vegetation parameters to run-up and flooding.

### **Advocacy: Flood Risk**

This phase would be a bridging phase to interpret scientific results in order to help in decision and policy making. When needed, the flood risk prediction tool shall be used for estimating wave attenuation potential of seagrass, saltmarshes, and mangroves. Predictions related to run-up and flooding could be also be made through the developed. What-if scenarios could be analyzed and decisions could be made accordingly. The tool will also show uncertainty associated with the prediction which is an essence of probabilistic tools only.

## **1.2. SCOPING & SIGNIFICANCE**

The scope related to hydrodynamics has been narrowed to model ordinary gravity waves, see Section 1.3.1 for limitations associated with this scoping. The plot in Figure 1.8 shows frequency of occurrence of the wave components. Only ordinary waves at the offshore boundary have been considered in the study which means free long waves are not modeled. However, based on harmonic modulations infragravity (bound long) waves are generated nearshore (Bertin et al., 2018). Therefore, separate effect of short wind (SW) waves, infragravity (IG) waves and very low frequency (VLF) waves on wave run-up and their interaction with vegetation would be studied.

### **1.2.1. RESEARCH GAPS & VALUE ADDITION**

This work builds on the work of (van Zelst, 2018; Songy, 2016; Janssen, 2016; S. G. Pearson et al., 2017) who have quantified global flood hazard reduction in saltmarshes, mangroves, and coral reefs. This study models full range of wave frequencies and uses continuous distributions of both hydrodynamic and vegetation parameters through a copula-based multivariate stochastic model. The value addition due to thesis would be:

- Resolving full spectrum of high and low frequency waves in a non-hydrostatic model instead of surfbeat model which was used by (van Zelst, 2018; Songy, 2016; Janssen, 2016).

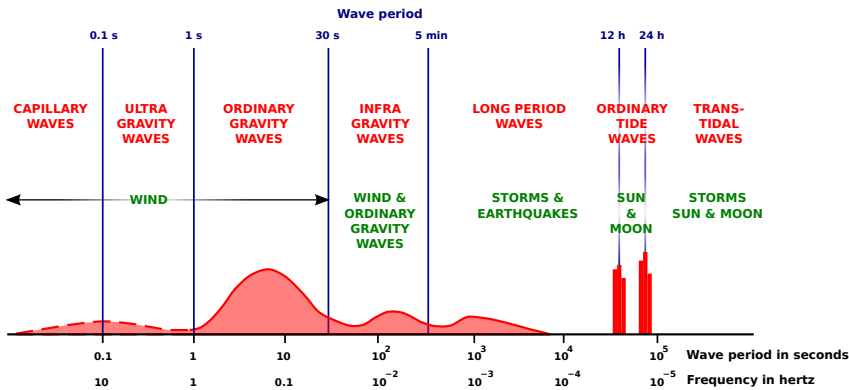


Figure 1.8: Wave spectrum & classification. (Munk, 1950)

- Full range of vegetation parameters found globally to be modeled which wasn't the case in (van Zelst, 2018).
- Continuous distributions of the parameters instead of discrete parameters.
- Non-parametric Bayesian networks instead of discrete Bayesian networks. van Zelst (2018) made a look-up table where as Songy (2016); S. Pearson (2016) used discrete Bayesian networks.
- Reduced number of simulations would be done but more information could be drawn due to use of non-parametric Bayesian networks.
- A robust global flood risk prediction tool in vegetated environments.

### 1.2.2. RESEARCH AIMS & OBJECTIVES

The research aim of this thesis is to improve the understanding of nature-based solutions involving vegetation in order to use them for climate change adaptation and flood risk mitigation. Specifically, it aims to quantify the potential of vegetation in countering the problem of coastal flooding and eventually making a flood risk prediction tool for decision support. To achieve the aims three major research objectives are enlisted hereunder:

1. Represent global vegetated hydrodynamic system as a multivariate stochastic model which captures underlying dependence and generates physical conditions globally.
2. Carry out numerical modeling for investigating and quantifying the role of vegetation in reducing flood risk during a range of conditions.
3. Develop a probabilistic model in the form of a Bayesian network to act as a flood risk prediction tool in vegetated environments for decision support.

### 1.2.3. RESEARCH QUESTIONS

To achieve research objectives certain research questions are defined in accordance with the objectives. Once these questions are answered according to methods proposed in Section 1.3 the aims and objectives are fulfilled.

#### Research Questions for Objective # 1

- How can the global vegetated hydrodynamic system be idealized and probabilistically parameterized for seagrasses, saltmarshes and mangroves?
- Does carrying out stochastic modeling add any value to the process of preparing synthetic dataset to feed the prediction tool?

Flow over vegetation would help to understand the important processes occurring on smaller scales for different types of vegetation. This would provide guidelines on how does different terms in conservation equations affect hydrodynamics and eventually wave attenuation in the presence of vegetation.

The primary element in changing the type of vegetation would be the height of vegetation resulting in a classification of *benthic*, *submerged* and *emergent* vegetation. For submerged vegetation, depth of flow experiencing the vegetation would determine its behaviour because of predominant vertical exchange of momentum (Nepf, 2012b). For emergent vegetation, the hydrodynamics is governed through longitudinal advection therefore, the spatial density would be varied from patches to canopy scale in order to change the stem morphology (Nepf & Vivoni, 2000; Nepf, 2012b). These variations in vertical and horizontal plane would enable to cover the range of vegetation like sea grasses as benthic vegetation, salt marshes as submerged vegetation, and mangroves as emergent vegetation.

#### Research Questions for Objective # 2

- What is the degree of effectiveness of vegetation in attenuating hydrodynamic forcing in a range of conditions?
- Is vegetation more effective in attenuating high frequency (sea-swell) waves or low frequency (infragravity) waves?
- Which vegetation type, saltmarshes or mangroves, is more effective in wave run-up reduction?

Vegetation-induced wave attenuation is well-established (Fonseca & Cahalan, 1992; Kobayashi et al., 1993; Paul & Amos, 2011; Sánchez-González et al., 2011; Pinsky et al., 2013; Horstman et al., 2014; Marsooli & Wu, 2014; Möller et al., 2014; Van Rooijen et al., 2015; Vuik et al., 2016; Reidenbach & Thomas, 2018; Mattis et al., 2019; Montgomery et al., 2019) however, the real question is how robust is the combination of hard and soft solutions? Utilizing the merits of numerical modeling can acknowledge the question. Furthermore, to assess the effectiveness of vegetation in wave damping, comparison through the model runs with bare and vegetated beds are needful. This concluded by detailed modeling of

range of global parameters would lead to emergence of critical parameters in the system which would be paid special attention while constructing a Bayesian network.

#### Research Questions for Objective # 3

- What are the critical parameters that govern the wave attenuation and wave run-up processes in a vegetated hydrodynamic system?
- How accurate is a non-parametric Bayesian network as a probabilistic model for predicting flood risk in a vegetated hydrodynamic system?
- How accurate is the developed flood risk prediction tool in predicting reality?
- How can the developed model help decision makers in implementing nature-based solutions involving vegetation for flood risk mitigation?

The limit state function would be analogous to the model function for the last child node in the Bayesian network. All the preceding network elements (nodes and arcs) would be hybrid in nature and dealt with Non-Parametric Bayesian Network (NPBN) methodology (A. Hanea et al., 2015).

The marginal distributions of the variables and the conditional rank correlations of the arcs would be derived from the synthetic dataset developed from the simulations done in XBeach global runs.

Once the Bayesian network is created, inference would be performed to make predictions for flooding for different limit state values. Morales Napoles et al. (2013) suggests that this could be done by computing rank correlation matrix and those different limit state values would represent real world scenarios and cases. The case specific predictions could be made by defining different combinations of resistance and solicitation (load) parameters.

### 1.3. METHODOLOGY

To create a flood risk prediction tool for vegetated environments under varied hydrodynamic conditions, the project would be carried out in four phases: Action, Reaction, Prediction, and Advocation phase (see Figure 1.7). Following methods have been utilized for carry out the aforementioned phases:

- Stochastic modeling explaining dependence among hydrodynamics-vegetation parameters globally.
- Numerical modeling using XBeach Non-Hydrostatic and MATLAB for vegetation response modeling.
- Probabilistic modeling for non-parametric Bayesian network-based flood risk prediction tool on UNINET.

In the action phase, global vegetated hydrodynamic system would be schematized and parameterized for seagrasses, saltmarshes and mangroves. The dependence modeling would be done and global vegetated hydrodynamic conditions would be sampled through

Monte Carlo simulation based on the dependence model.

In the reaction phase, the vegetated hydrodynamic systems would be modeled to generate a large synthetic dataset to be used as an input for creation of a Bayesian network. Precompiled version of the XBeach Non-Hydrostatic (XB-NH) model along with scripting in MATLAB would be used to carry out the numerical modeling. The effect of vegetation on hydrodynamics would be studied through set-up and wave attenuation.

Before stepping into probabilistic modeling the option of physical modeling was also considered to generate the dataset. Since the focus of the study revolves around extreme events and physical models are unfeasible to reproduce such conditions over globally varied environments therefore, the inexpensiveness and flexibility of numerical modeling over its counterpart led to its choice for generating a large dataset. However, they always go hand in hand for validation purposes of numerical models.

In the prediction phase, a Non-Parametric Bayesian Network (NPBN) is aimed to be developed yielding posterior flooding probabilities would result in a flood risk prediction tool. Flooding limit-state criteria would be defined by incorporating crest levels with wave run-up and overtopping. More outputs like wave attenuation coefficient and vegetation factor are also defined through functional relations among model parameters.

Finally, in the advocacy phase, the results would be interpreted to make a Decision Support System (DSS) helping decision makers in early warnings, rapid response and policy making related to flooding. Figure 1.9 accurately illustrates the work flow and broader methodology followed throughout the thesis.

### 1.3.1. LIMITATIONS

The limitations foreseen for this study are based on simplification choices and the restrictions of the tools used for the modeling. A process-based model XBeach Non-Hydrostatic is used for numerical modelling and UNINET is used for probabilistic modeling through Bayesian networks. Both models do come a long way in improving modeling aids available to users but they should only be trusted if the limitations doesn't compromise response of the system under study. The simplifications and the limitations are hereunder:

- Two dimensional depth-averaged (2DH) model  
XBeach Non-Hydrostatic was used which solves nonlinear shallow water equations (Van Rooijen et al., 2015) where as better formulations (Suzuki et al., 2019; Mattis et al., 2019; Losada et al., 2016; Maza et al., 2013) describing vegetated hydrodynamics exist. Depth averaging doesn't allow to study variation of hydrodynamic forcing and its interaction with vegetation in the vertical column.
- One dimensional (1D) cross-shore profile  
1D profile was chosen to be modelled keeping the aim, scope and time in mind. 1D profile would be able to explain the flow-vegetation interaction in crossshore direction which is critical for flooding. Also, computation expense would be greatly reduced which enables to model more cases eventually reducing the uncertainty in the predictions.
- Wave boundary conditions

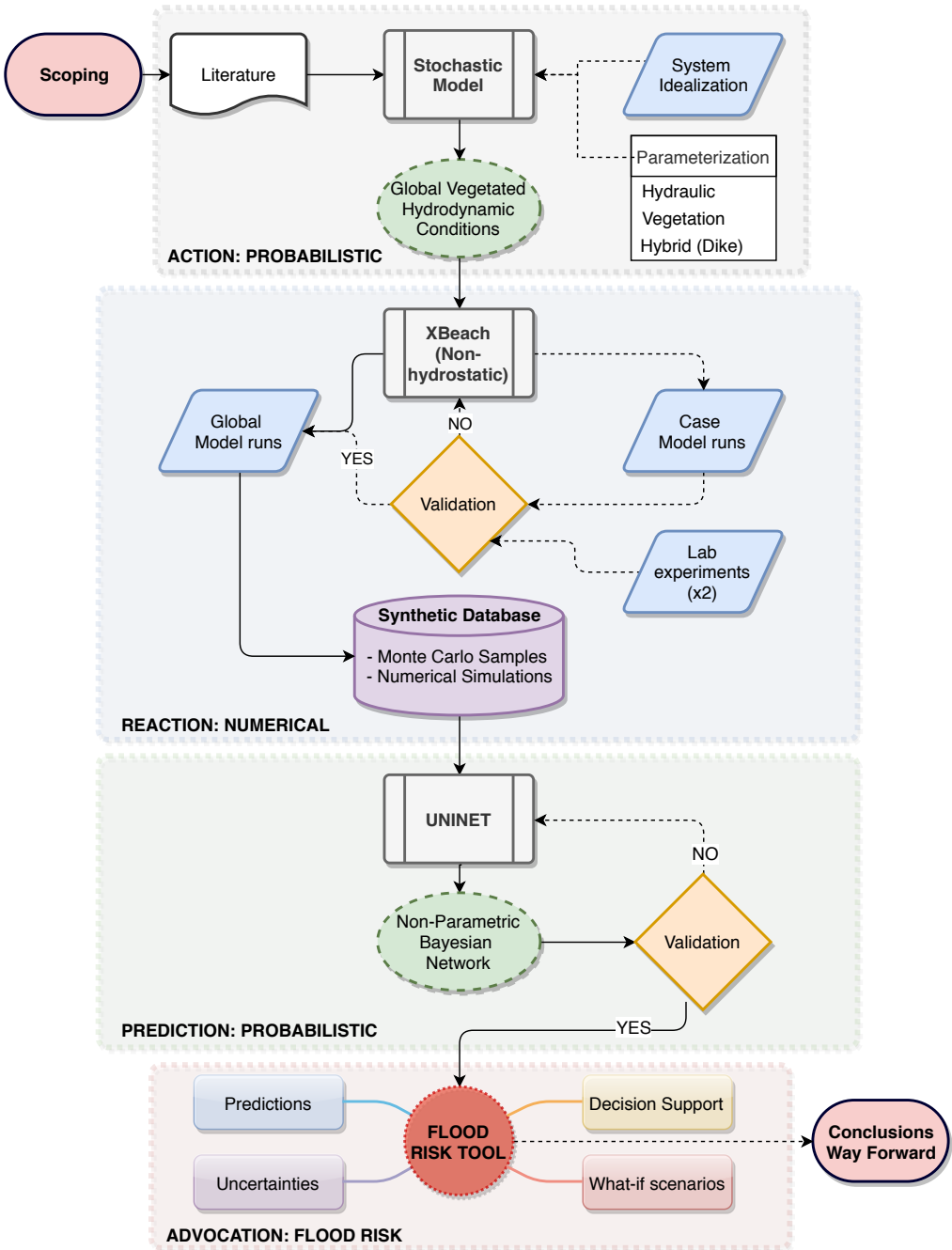


Figure 1.9: Research plan and Work flow

Waves are forced through unimodal JONSWAP spectrum therefore no low frequency forcing like incoming long waves, swell or tide is considered. XBeach for modelling vegetation-induced wave attenuation has been validated for short wave energy only (Van Rooijen et al., 2015). Also, due to single dimensionality of the model only long crested waves and JONSWAP spectra with no directional spreading are modelled. However, long crested waves should not be confused with regular waves as the modeled wave timeseries would be random.

- Rigid Cylindrical Vegetation

The vegetation is supposed to behave as rigid cylinders which do not undergo uprooting or breakage under storm conditions. The flexibility of vegetation changes the hydrodynamic response because the vegetation-induced drag forces change. In such conditions, drag forces become a function of effective vegetation height rather than full vegetation height and relative velocities between flow and vegetation rather than flow velocities. Rigidity is assumed because it has not been implemented in XBeach and only very recent studies (Lei & Nepf, 2019b,a; Mattis et al., 2019) have upscaled such fine process from blade scales to meadow scales.

- Data Availability

The input parameters in the schematized system are probabilistically specified through a range, distribution, and its correlations with other parameters. These parameters govern the global nature of the prediction model and ideally the statistical description should be derived from the data but limited data was available to perform stochastic modeling for input parameters.

- NPBN Graphs

Directed acyclic graphs were used for modelling NPBN where as more types of graphs exist which can cater the weightage of certain influences over others (Schmidt & Morup, 2013), see Figure 2.7.

- Gaussian Copula

Dependence structure throughout this study is assumed to be based on Gaussian copula for simplification. However, there is evidence of other dependence structures for the parameters under study.

In order to simulate numerous simulations and keep the modeling simple enough to avoid computation hitches while being able to capture significant processes the simplifications were necessary.

### 1.3.2. THESIS STRUCTURE

Chapter 1 finishes with mentioning research scope of the study and broader methodology. Chapter 2 builds the background knowledge to familiarize the reader with important concepts which are useful to have good reading experience of the thesis. It also presents state-of-the-art knowledge that has already been published related to the scope of the study. Chapter 3 presents the stochastic modeling to generate global vegetated hydrodynamic conditions for the action phase of the study. Chapter 4 presents the numerical modeling using XBeach. The chapter comprises of case models and global models used to generate the synthetic dataset. Chapter 5 shows the probabilistic model which is

referred to as flood risk prediction tool. The modeling chapters also interprets the results from their respective parts and eventually puts them into perspective through discussion. Chapter 6 concludes the study reiterating answers to research questions, novelty of the thesis, recommendations for improvement of current work and way forward for future extension of the work.



# 2

## LITERATURE REVIEW

*Literature Review is not about what to take;  
rather, about what to leave.*

Anwar Masood

### Abstract

A great deal of work has been done in proposing solutions for flood risk reduction including nature-based solutions involving vegetation. Flow-vegetation interaction and resulting wave attenuation has been well-established but gaps have been identified in putting knowledge to practice in terms of decision support tools. Concurrently, Bayesian networks have been applied for many systems and have shown great potential as prediction models. The chapter presents the background knowledge to build understanding about flood risk, decision support systems, vegetated hydrodynamics, numerical modeling using XBeach and the Bayesian networks.

THIS chapter elaborates the background knowledge on which this thesis builds on along with the current state-of-the-art knowledge published related to the field of vegetated hydrodynamics and Bayesian networks. Non-hydrostatic numerical model XBeach for extreme beach behaviour is being used to simulate vegetated environments. Seagrasses, saltmarshes and mangroves are being modeled to quantify wave reduction potential for the ranges of variables found over global scales. The resulting large synthetic dataset is being used to setup Bayesian network-based flood risk prediction model.

## 2.1. HYBRID FLOOD DEFENCE SYSTEM

Hybrid flood defenses are the flood defenses in which conventional and an element of nature-based flood defenses is combined (Carrick et al., 2018) to form a more robust defense (Niazi et al., 2018). These are proposed because in scenario of the sea level rise due to the climate change and increasing storm surges, vegetation can not efficiently reduce increase in water level as it can reduce waves.

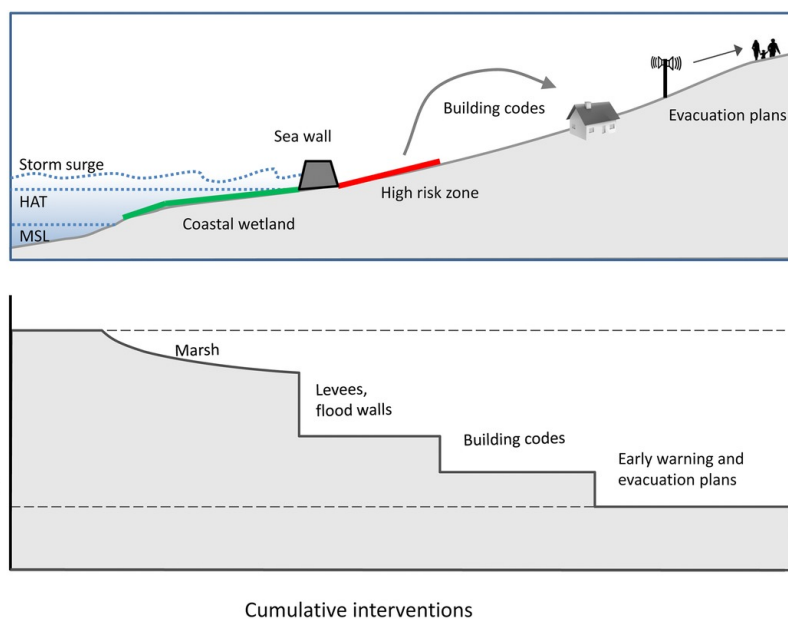


**Figure 2.1:** Cascade of protection measures forming hybrid defence for risk mitigation (Spalding et al., 2014)

Spalding et al. (2014) in Figure 2.1 presents the evolution of risk reduction through cascade of structural and non structural measures. Vegetation along with conventional solutions have the potential to reduce hazard levels to hit minimum risks. More non-structural measures would increase the resilience of the flood defenses eventually compensating lack of flexibility of conventional flood defenses and increasing the system robustness in an optimal way (Niazi et al., 2018).

### 2.1.1. RUN-UP & OVERTOPPING

Run up is the maximum traversing of water on a dike which is measured as a vertical distance. If the water level increases the height of the dike, the water starts transmitting on the crest which results in overtopping. [EurOtop \(2018\)](#) presents formulations to calculate run-up and overtopping.

$$\frac{R_{u2\%}}{H_{m0}} = 1.65 \cdot \gamma_b \cdot \gamma_f \cdot \gamma_\beta \cdot \xi_{m-1,0} \quad (2.1a)$$

with a maximum of:

$$\frac{R_{u2\%}}{H_{m0}} = 1.0 \cdot \gamma_f \cdot \gamma_\beta \left( 4 - \frac{1.5}{\sqrt{\gamma_b \cdot \xi_{m-1,0}}} \right) \quad ; \quad \xi_{m-1,0} = \frac{\tan S_d}{\sqrt{H_{m0}/L_{m-1,0}}} \quad (2.1b)$$

where  $H_{m0}$  is wave height,  $\gamma_b$  is berm factor,  $\gamma_f$  is roughness factor,  $\gamma_\beta$  is oblique wave factor,  $\xi_{m-1,0}$  is surf similarity (breaker) parameter, and  $L_{m-1,0}$  is deepwater wavelength calculated from spectral wave period  $T_{m-1,0}$  and dispersion relation.

$$\frac{q}{\sqrt{g \cdot H_{m0}^3}} = \frac{0.023}{\sqrt{\tan S_d}} \gamma_b \cdot \xi_{m-1,0} \cdot \exp \left[ - \left( 2.7 \frac{R_c}{\xi_{m-1,0} \cdot H_{m0} \cdot \gamma_\beta \cdot \gamma_f \cdot \gamma_b \cdot \gamma_v} \right)^{1.3} \right] \quad (2.2a)$$

with a maximum of:

$$\frac{q}{\sqrt{g \cdot H_{m0}^3}} = 0.09 \cdot \exp \left[ - \left( 1.5 \frac{R_c}{H_{m0} \cdot \gamma_f \cdot \gamma_\beta \cdot \gamma^*} \right)^{1.3} \right] \quad (2.2b)$$

where  $q$  is mean overtopping discharge [l/m/s],  $S_d$  is dike slope,  $R_c$  is freeboard,  $\gamma_v$  is wall influence factor,  $\gamma^*$  is non-breaking waves for a storm wall on slope.

Vegetation provides a utility as surface projection for dikes as well. Run up and overtopping are used to defined the limit-state functions which depict failure, which in our case is flooding. Run-up greater than crest levels result in flooding or overtopping discharge greater than critical discharges results in flooding too. Vegetation provides a utility as surface projection for dikes as well. Critical overtopping discharges for surfaces with vegetation have been reported in the range from 0.1 to 10 l/m/s ([EurOtop, 2018](#)).

### 2.1.2. HYDRODYNAMIC FORCING

Hydrodynamic forcing greatly contributes to flood risk due to extremes getting more frequent ([Reguero et al., 2019](#); [Vitousek et al., 2017](#)) and severe ([Young et al., 2011](#); [Wang et al., 2009](#)). Climate change projections and indicators in terms of sea-level rise, global temperature rise, global wave power rise have direct effects on storm which results in surges. With the increasing hydrodynamic forcing, if adaptation measures are not adopted, a 30-fold increase in annual expected damages is projected by 2050, and a mounting 700-fold increase by 2100 ([Vousdoukas et al., 2018](#)). Furthermore, climate change is not just sea level rise, it's also a lot of uncertainty added to all other processes ([Niazi et al., 2018](#)).

### Storms

Storms in distant areas result in surges which increases water levels to significant degrees along the coasts. Propagation of these storms is mathematically described through a set of equations called *primitive equations*. These equations are based on conservation of mass, momentum and energy. Mass balance is solved by continuity equation, momentum balance is solved by Navier-Stokes equation and energy balance is solved by thermal equation.

Storms mainly occur due to various atmospheric processes like temperature and pressure gradients. Rise in global temperature due to climate change affect the frequency and intensity of storms. As storm surges in nearshore are merely fluctuations of water level due to distant storms, therefore the connection of rising temperatures and water level changes is critical for increasing hydrodynamic forcing and causing flooding.

Kim (2018) and Flather (2001) suggest that studying storm surges with waves in shallow water gives improved agreement with observations of water levels. This is so because wave orbital velocities fluctuates turbulence which gives rise to bottom shear stress. The combined study of storm surges and waves also bridges the gap between offshore and nearshore information. The exchange of surge information like ocean current and sea surface elevations and wave information like radiation stresses and wave-wind-induced drag leads to reliable predictions of water levels (Kim, 2018).

### Short & Long Waves

Wave attenuation by different types of vegetation and their response is different for short and long waves. For instance, the cospectral analysis of Bradley & Houser (2009) shows that submerged flexible vegetation attenuates waves with higher frequencies (short waves) more than the lower ones (long waves).

Infragravity waves are low frequency (high period) long waves which take energy from short sea waves. Mathematically, infragravity wave amplitude is related to energy of short waves mainly through radiation stress i.e. total wave averaged transport of x-momentum in x-direction (Longuet-Higgins & Stewart, 1962; Bosboom & Stive, 2012). These are called *bound long waves* when traveling in wave groups in deep water until reaching a breaker bar. In the nearshore, breaker bars disrupt the wave groupiness and waves are then *free long waves* which drastically change the wave motion and water levels during storms.

Bertin et al. (2018) summarizes infragravity waves generation into three mechanism: bound to free long wave transformation, wave superposition and merging of bores<sup>1</sup>. These processes makes it very likely for infragravity waves to have some connection to changing water levels. The source of changing water levels could be storm surges or sea level rise which, if, affects infragravity waves, could be important to the study.

Chang & Liu (2019); Zainali et al. (2018); Mei et al. (2011); Chang et al. (2017) studies long wave and vegetation interaction which results in both dissipation but harmonic generation as well (which can cause resonance). Tang et al. (2017) concludes that the vegetation reduced long wave run-up significantly and that the periodic long wave run-

<sup>1</sup>Bores: catching up of waves to form a hydraulic-jump-like breaking wave front

up on a rigid vegetation sloping beach is sensitive to frontal width ( $b_v$ ) and vegetation density ( $N_v$ ). More over incident wave period also affects the effectiveness of period long wave run-up which doesn't increase or decrease monotonically by varying wave periods (Tang et al., 2017).

## 2.2. VEGETATION HYDRODYNAMICS

Vegetated hydrodynamics revolves around flow-vegetation interaction, vegetation movement dynamics (for flexible vegetation), hydrodynamics – morphology– vegetation feedbacks, wave set-up, and wave attenuation. However, the scope of the study limits studying flexible vegetation and morphology feedbacks. Figure 2.2 presents the crux of vegetated hydrodynamics which indicates the effects on hydrodynamics like turbulence, changes in drag forces and velocities, and wave and energy attenuation by vegetation. (Paul, 2015).

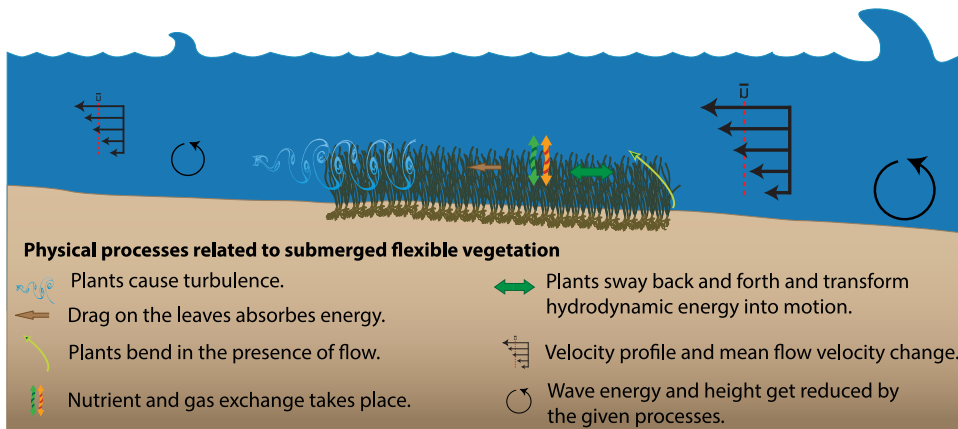


**Figure 2.2:** Interaction of seagrass-saltmarsh environment with hydrodynamics (Paul, 2015).

## CLASSIFICATIONS

Vegetation system are studied related to vegetation in coastal and river engineering have been undertaken based on various classifications. The domains of vegetation systems are summarized in Table 2.1 based on the most important criteria. Investigations of Wu & Cox (2015); Nepf & Vivoni (2000); K G & Bhaskaran (2017) leads to the conclusion that wave attenuation in most sensitive the classification based on relative water depth where relative depth is the ratio of vegetation height and depth of water column.

Deciding about which type of classification to adopt depends on scale and scope of the problem under consideration. In our case, the aim is to investigate the wave attenuation in vegetated environments on global scales and to make a prediction model for flood risk in such systems. The ultimate goal of studying vegetation hydrodynamics is to make sure that prediction model doesn't ignore the fundamental physics related to different types of flow-vegetation environments.

**Table 2.1:** Vegetation classifications

Criteria	Types		
Relative Depth	Benthic (Seagrass)	Submerged (Saltmarsh)	Emergent (Mangroves)
Spatial Density	Single blade	Meadow	Canopy
Movement Dynamics	Flexible (blade)	Rigid (sheath)	

After careful investigation and considering the scale under study, it was decided not to proceed with individual flexible vegetation blade elements since they might be more important for studying effect of hydrodynamics on vegetation rather than the other way around.

### Benthic Vegetation

A rooted vegetation with a vertical extent way less than the water depth is referred to as *benthic vegetation* (Nepf, 2012a). Sea grasses in reality have nearly infinite height to water depth ratio which makes it behave like a rough bed starting from deep water.

### Submerged Vegetation

*Submerged vegetation* approaches water depth therefore the relative depth is approximately 1 and characteristic blade width ranges from 0.1cm to 1cm (Nepf, 2012a). It can cover nearly the entire water column behaving as submerged or emergent based on the flow conditions like low or high tide. This classification type is to be dealt with care as it doesn't allow skimming flow to occur in submerged conditions and doesn't require vertical layers in emergent conditions.

### Emergent Vegetation

*Emergent vegetation* have heights larger than the water depth, with typical examples being mangroves and kelp forests. They affect both the both mean and turbulent flow while cascading the eddies larger than stem scale through generating stem-scale turbulence resulting in energy dissipation. Mangroves have rounded stems with mean trunk diameters of 4cm to 9cm resulting in relatively higher stiffness (Nepf, 2012a). The protective service of mangrove ecosystems is subject to coastal storms, sea-level rise, saline intrusion and erosion (Barbier, 2016) which can result in loss of mangroves and, eventually, in great reduction of it's protective potential.

#### 2.2.1. FLOW VARIATION

Velocity profile in the vertical column changes due to vegetation (Nepf & Vivoni, 2000). For submerged vegetation, the mean flow in most part of the water column follows a logarithmic follows which could be estimated through log-law of the wall (Nepf, 2012a).

$$\langle \overline{u(z)} \rangle = \frac{u_*}{\kappa} \ln \left( \frac{z - z_m}{z_0} \right) \quad (2.3)$$

where;  $\langle \overline{u(z)} \rangle$  is horizontally averaged mean velocity,  $\kappa = 0.4$  is von-Kármán constant,  $u_*$  is friction velocity,  $z$  is depth,  $z_m$  is displacement height, and  $z_0$  is roughness height.

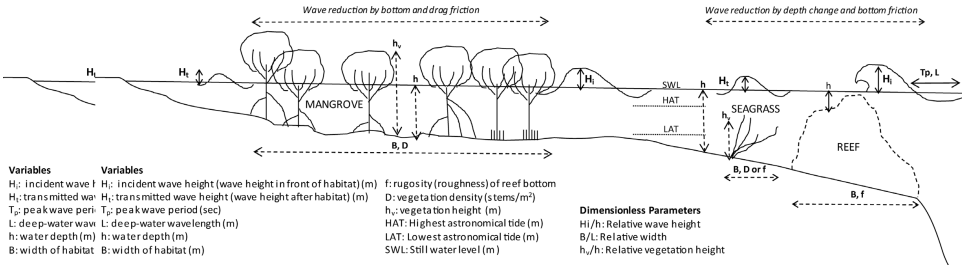


**Figure 2.3:** Summary of general mechanics of wave height reduction through habitats of seagrasses, salt-marshes and mangroves (Narayan et al., 2016).

### VEGETATION-INDUCED DRAG FORCES

The interaction of vegetation with the flow results in drag forces through which wave attenuation could be quantified. Vegetation is normally modeled as rigid cylinders which is inspired from studies related to forces on rigid cylinders in offshore (Sumer & Fredsøe, 1997). The behaviour of vegetation-induced drag is different under wave and currents due to effects like flow reversal.

#### UNDER CURRENTS

Under currents the flow is unidirectional which, when faces vegetation, experiences resistance resulting in change of flow. The boundary layer develops between the flow and the vegetation. This boundary layer is the source of exchange of momentum and causes loss of energy as the flow moves along. Assuming the velocity is small the energy dissipation happens due to viscous effects. However, if the velocity is high, turbulence might be produced which is another source of loss of energy from higher spatial scales to Kolmogorov scales.

Due to vegetation resistance flow separation occurs. In this situation a wake region is produced which depends on both vegetation parameters (e.g. frontal width) and hydrodynamic parameters (flow velocity). The flow separation and wake region induces different amount of forces at the rear of the vegetation than the ones experienced in the front. This develops a pressure gradient which induces a force referred to as *drag force*.

In case of the vegetation canopy the practice is to use the flow velocity outside the canopy for quantifying drag forces and wave attenuation. This approach is not the best way to reproduce drag forces during modeling as the flow changes inside the canopy. Many formulations including Dalrymple et al. (1984) assumes linear wave theory for deriving the expressions for wave decay. However, linear wave theory might not hold true inside the canopy which adds another source of uncertainty in the attenuation predictions.

The density of vegetation ( $N_v$ ) and spacing between elements ( $s$ ) in a canopy also determines the flow variations through what's called a *sheltering effect*. In the case where the vegetation elements are far from each other, the flow in the wake of a facing elements might have time to develop again and reproduce similar drag forces for the element next in line. However, if they are close enough to not allow this flow development, the assumption to use same velocity drifts the system away from realistic behaviour.

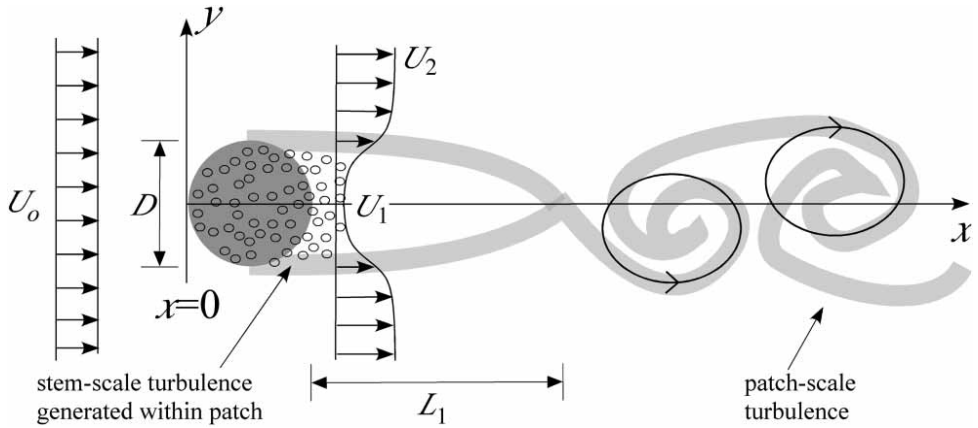


**Figure 2.4:** Flow variation in emergent vegetation.  $D$  is patch diameter,  $U_0$  is upstream velocity,  $U_1$  is downstream velocity, and  $U_2$  is edge velocity. Interaction between  $U_2$  is blocked by  $U_1$ . Turbulence is generated on stem-scale within the canopy and on patch-scale at a distance  $L_1$  from the patch revealing the von Karman vortex street (Nepf, 2012b).

The flow within submerged vegetation is affected by turbulence stress on top of the canopy, pressure gradients and bed slope (Nepf, 2012a). The relative dominance of these mechanisms depends on *submergence depth* defined as the ratio of water depth  $h$  to vegetation height  $h_v$  (Nepf & Vivoni, 2000).

$$\frac{\text{turbulent stress}}{\text{pressure gradient}} \sim \frac{h}{h_v} - 1 \quad (2.4)$$

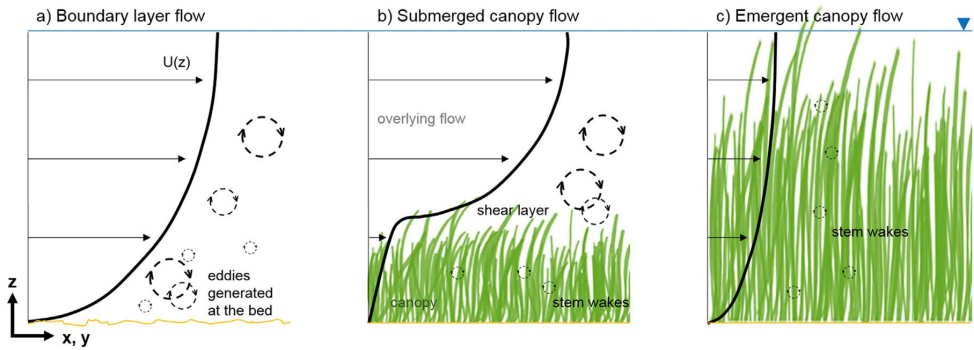


**Figure 2.5:** Regimes of flow variation in all types of vegetation where  $U(z)$  is flow velocity. In submerged vegetation canopy-scale turbulence is produced by shear layer due to skimming flow resembling like free shear layer and stem-scale turbulence is produced due to bed drag within the canopy (Beudin et al., 2017; Nepf, 2012a).

If the submergence depth is large, an unhindered flow region on top of the vegetation until water surface usually referred to as *skimming flow* develops a free shear layer. Due to the differences in the drag force on top of the canopy and the bed a discontinuity in

drag occurs (Nepf, 2012a). This discontinuity in canopy drag and bed drag introduces an inflection point in the velocity profile resulting in Kelvin-Helmholtz flow instability.

### UNDER WAVES

The waves have an orbital motion in the water column transforming the unidirectionality of the flow into *flow reversal*. This change of direction of the flow between crests and troughs of a wave induces forces on vegetation in opposite directions. Long waves have major contribution to this behavior as their orbital excursion is larger and stronger comparatively. However, in case of very low wave celerity it is possible that the flow starts developing and even inside the canopy it becomes similar to outside canopy flow.

Submerged vegetation under wind generated waves experiences mean mass drift inside the canopy due to drag-induced non-zero wave stresses (Nepf, 2012a) also referred to as *streaming* (Longuet-Higgins & Stewart, 1962). Furthermore, due to unsteady nature of waves inertial forces also become important along with drag forces. This reduces wave attenuation potential of vegetation under waves as compared to currents (Luhar et al., 2010; Nepf, 2012a).

### DRAG COEFFICIENT $C_D$ AS CALIBRATION FACTOR

Using drag coefficient  $C_D$  as a calibration factor in the model shows good agreement with data only in situation of rigid (no swaying) vegetation (Maza et al., 2013). Mainly because relative factors like relative velocity are only flow dependent since vegetation doesn't move. Also, viscous effects usually are ignored which results in wide ranges of  $C_d$  for calibration (Kobayashi et al., 1993).  $C_d$  also tends to vary with an indirect relation with vegetation Reynolds number  $Re_v$  in Equation 2.5.

$$Re_v = \frac{u_v b_v}{\nu} \quad (2.5)$$

$$u_v = \frac{kgH}{2\omega} \frac{\cosh kh}{\cosh[k(k+h)]}$$

where;  $u_v$  = characteristic fluid velocity acting on the vegetation,  $b_v$  = frontal width,  $H$  = wave height,  $h$  = water depth,  $\omega$  = angular frequency, and  $k$  = wave number.

Kobayashi et al. (1993) indicates that  $C_d$  decreases with the increase of  $Re_v$  on the order of 0.1 for large  $Re_v$ . This indirect relation is partly due ignoring of viscous effects which affect the skin friction offered by vegetation (Kobayashi et al., 1993).

Furthermore, in the analytical formulation where parameters represent properties on scales ranging from Kolmogorov scales for turbulence to the scales of largest dimension, drag coefficient has nature of a bulk parameter. Therefore, this approach is valid for applications in large scale flow-vegetation coupled systems. However, if the vegetation is spatially heterogeneous then the calibration through drag contribution isn't valid (Nepf, 2012b). Also, this approach is valid in situations where the vegetation is not swaying therefore the feedbacks between flow and individual vegetation elements, e.g. relative velocity, stand redundant. Rather, it must be preferred in the cases where effects on the changes in overall mean flow conditions are important.

Drag coefficient has been generalized to the extent that one can calibrate the same model for both rigid and flexible vegetation by merely changing the bulk drag coefficient values (Dalrymple et al., 1984; Mendez & Losada, 2004). Table 2.2 presents a review of experimental work in vegetated hydrodynamics. Lara et al. (2016); Maza et al. (2015) presents guidelines for large-scale 3-D experiments of wave and current interaction with real vegetation.

Extensive research other than the one collated in Table 2.2 has been published in which flow-vegetation interaction has been studied experimentally including (Fonseca & Cahalan, 1992; Nepf, 1999; Ghisalberti & Nepf, 2002; Möller, 2006; Lövstedt & Larson, 2010; Ali & Uijtewaal Wim, 2013; Luhar et al., 2013; Horstman et al., 2014; Uotani et al., 2014; John et al., 2015; Maza et al., 2016; Reidenbach & Thomas, 2018; Montgomery et al., 2019; Shan et al., 2019). However, these studies were excluded from Table 2.2 either because the datasets were old or they were not relevant enough to be used for validation of XBeach model runs. Some of the other studies were excluded because they were not primarily related to wave attenuation or deriving drag coefficients.

Despite the water depth and wave parameters, the hydrodynamic variations also include nature of conditions *e.g.* regular or irregular waves, wave only or combined wave-current conditions. Similarly, along with changing the vegetation parameters it's types has also been varied which changes characteristics like species, submergence or emergence of vegetation. Different drag coefficients and wave attenuation were reported as a result of the studies.

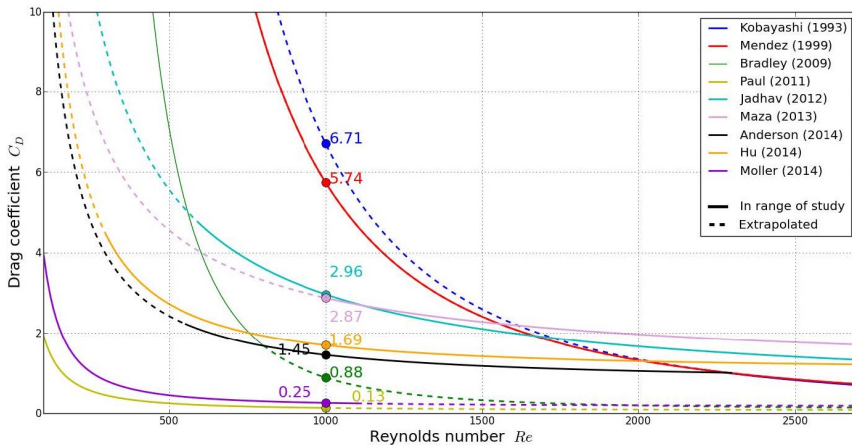


Figure 2.6: Drag Coefficients review (van Zelst, 2018).

**Table 2.2:** Review of experimental work presenting variety of hydrodynamic conditions, vegetation characteristics, bulk drag coefficients  $C_D$  and resulting wave attenuation. In the table,  $h$  = water depth,  $H_{m0}$  = wave height,  $h_v$  = vegetation height,  $b_v$  = frontal width,  $N_v$  = stem density,  $Re$  = Reynolds number,  $KC$  = Keulegan–Carpenter number. Inspired from [van Zelst \(2018\)](#); [H. Chen et al. \(2018\)](#); [Vuik et al. \(2016\)](#); [Henry et al. \(2015\)](#).

Study	Hydrodynamic Properties	Vegetation Characteristics	Drag Coefficient	Wave Attenuation
<a href="#">Asano et al. (1988)</a> Flume	Regular waves $h = 0.50m$ $H_{m0} = 0.036 - 0.19m$	Polypropylene strips as artificial kelp $h_v = 0.25m, 52 \times 0.03mm, N_v = 1110 - 1490m^{-2}$	–	–
<a href="#">Kobayashi et al. (1993)</a> Flume	Used <a href="#">Asano et al. (1988)</a>	Used <a href="#">Asano et al. (1988)</a>	$C_D = 0.08 + \left(\frac{2200}{Re}\right)^{2.4}$ $2200 < Re < 18000$	–
<a href="#">Méndez et al. (1999)</a> Flume	Used <a href="#">Asano et al. (1988)</a>	Used <a href="#">Asano et al. (1988)</a> and distinguished for rigid and flexible vegetation	Rigid $C_D = 0.08 + \left(\frac{2200}{Re}\right)^{2.2}$ $200 < Re < 15500$ Flexible $C_D = 0.40 + \left(\frac{4600}{Re}\right)^{2.9}$ $2300 < Re < 22000$	8–20% per 100m
<a href="#">Mendez &amp; Losada (2004)</a> Flume	Regular waves $h = 0.4 - 1.0m$ $H_{m0} = 0.045 - 0.17m$	L. hyperborea $h_v = 0.20m, b_v = 25mm, N_v = 1200m^{-2}$	$C_D = 0.47 \exp(-0.052KC)$ $3 < KC < 59$	–
<a href="#">Bradley &amp; Houser (2009)</a> Field (seagrass)	Irregular waves $h = 1 - 1.5m$ $H_{m0} \approx 0.09m$	Thalassia testudinum $h_v = 0.25 - 0.30m, b_v = 0.33mm, N_v = 1100m^{-2}$ Used relative velocity for drag calculation	$C_D = 0.10 + \left(\frac{925}{Re}\right)^{-3.16}$ $200 < Re < 800$ $C_D = 126.45KC^{-2.7}$ $0 < KC < 6$	–
<a href="#">Sánchez-González et al. (2011)</a> Flume	Both Regular & Irregular $h = 0.3 - 0.8m$ $H_{m0} = 0.05 - 0.13m$ (Reg.) $H_{m0} = 0.03 - 0.13m$ (Ir-reg.)	Posidonia oceanica $h_v = 0.1m, b_v = 3mm, N_v = 40000m^{-2}$	$C_D = 22.9KC^{-1.09}$ $15 < KC < 425$	Regular 75% Irregular 50%
<a href="#">Paul &amp; Amos (2011)</a> Field (seagrass)	Irregular waves $h \approx 0.75 - 3.5m$ $H_{m0} \approx 0.05 - 0.18m$	Zostera noltii $h_v = 0.13 \pm 0.030m, N_{v,avg} = 625 \pm 225m^{-2}$	$C_D = 0.06 + \left(\frac{153}{Re}\right)^{1.45}$ $100 < Re < 1000$	–
<a href="#">Jadhav &amp; Chen (2012)</a> Field (Salt marsh)	Irregular waves $h \approx 0.55m$ $H_{m0} = < 0.4m$	Spartina alterniflora $h_v \approx 0.63m, b_v \approx 8mm, N_v \approx 422m^{-2}$	$C_D = 0.36 + \left(\frac{2600}{Re}\right)^{1.0}$ $600 < Re < 3200$	–

**Table 2.2:** Review of experimental work presenting variety of hydrodynamic conditions, vegetation characteristics, bulk drag coefficients  $C_D$  and resulting wave attenuation. In the table,  $h$  = water depth,  $H_{m0}$  = wave height,  $h_v$  = vegetation height,  $b_v$  = frontal width,  $N_v$  = stem density,  $Re$  = Reynolds number,  $KC$  = Keulegan–Carpenter number. Inspired from [van Zelst \(2018\)](#); [H. Chen et al. \(2018\)](#); [Vuik et al. \(2016\)](#); [Henry et al. \(2015\)](#).

Study	Hydrodynamic Properties	Vegetation Characteristics	Drag Coefficient	Wave Attenuation
<a href="#">Infantes et al. (2012)</a> Field (Seagrass)	Irregular waves (Storms) $h = 6.5 - 16.5m$ $H_{m0} = 0.10 - 1.31m$	Posidonia oceanica $h_v = 0.8 \pm 0.1m, b_v \approx 4mm, N_v = 615 \pm 34m^{-2}$	Used <a href="#">Sánchez-González et al. (2011)</a>	30% – 60% Under 3 Storms
<a href="#">Maza et al. (2013)</a> : Flume	Regular waves	Posidonia oceanica (Polypropylene strips)	$C_D = 0.87 + \left(\frac{2200}{Re}\right)^{0.88}$	-
Rigid	$h = 1.8 - 2.4m$ $H_{m0} = 0.4 - 0.5m$	$h_v = 0.35, 0.55m, b_v = 1mm, N_v = 360, 180m^{-2}$	$C_D = 1.61 + \left(\frac{4600}{Re}\right)^{1.9}$	
Flexible	$h = 0.4 - 1.0m$ $H_{m0} = 0.045 - 0.17m$	Artificial seagrass (PVC strips) $h_v = 0.27, 0.45m, b_v = 1mm, N_v = 360, 180m^{-2}$	$1000 < Re < 3500$	
<a href="#">Jadhav et al. (2013)</a> Field (Salt marsh)	Irregular waves $h = 0.4 - 0.82m$ $H_{m0} = 0.15 - 0.4m$	Spartina alterniflora $h_v \approx 0.22m, b_v \approx 8mm, N_v \approx 422m^{-2}$	$C_D = 70KC^{-0.86}$ $25 < KC < 135$	-
<a href="#">Pinsky et al. (2013)</a>	Statistical evaluation of 35 studies	Statistical evaluation of kelp, seagrass, salt-marsh and mangroves	$\log_{10}(\mathbf{C}_{d,ijk}) = \beta_0 + \beta_1 \log(c \cdot Re) + \delta^2$ $17000 < Re < 350000$	Kelp 26%, Seagrass 98%, Saltmarsh 99%, Mangrove 87%
<a href="#">Ozeren et al. (2014)</a> Rigid (Flume)	Regular waves $h = 0.4 - 0.7m$ $H_{m0} = 0.03 - 0.15m$	Wooden cylinders (Rigid) $h_v = 0.48, 0.63m, b_v = 9.4mm, N_v = 156, 350, 623m^{-2}$	Rigid $C_D = 2.1 + \left(\frac{793}{Re}\right)^{2.39}$ $200 < Re < 4500$	Rigid 20 – 60% Flexible
Flexible (Flume)	Irregular waves $h = 0.5 - 0.7m$ $H_{m0} = 0.03 - 0.10m$	Spartina alterniflora (Flexible) $h_v = 0.59 \pm 0.21m, b_v = 6.5 \pm 0.9mm, N_v = 405m^{-2}$ Juncus roemerianus (Flexible) $h_v = 1.03 \pm 0.27m, b_v = 2.4 \pm 0.6mm, N_v = 2857m^{-2}$	$C_D = 1.5 + \left(\frac{6.785}{KC}\right)^{2.22}$ $5 < KC < 100$ Flexible $C_D = 0.683 + \left(\frac{12.07}{KC}\right)^{2.25}$ $5 < KC < 350$	10 – 50%

<sup>2</sup> $\mathbf{C}_{d,ijk}$  was the set of drag coefficients based on habitat  $i$ , location  $j$  and study  $k$ . Typical values for coefficients are  $c = 3 \cdot 10^{-4}$ ,  $\beta_0 = -1.72$ ,  $\beta_1 = -1.67$

**Table 2.2:** Review of experimental work presenting variety of hydrodynamic conditions, vegetation characteristics, bulk drag coefficients  $C_D$  and resulting wave attenuation. In the table,  $h$  = water depth,  $H_{m0}$  = wave height,  $h_v$  = vegetation height,  $b_v$  = frontal width,  $N_v$  = stem density,  $Re$  = Reynolds number,  $KC$  = Keulegan–Carpenter number. Inspired from [van Zelst \(2018\)](#); [H. Chen et al. \(2018\)](#); [Vuik et al. \(2016\)](#); [Henry et al. \(2015\)](#).

Study	Hydrodynamic Properties	Vegetation Characteristics	Drag Coefficient	Wave Attenuation
<a href="#">Anderson &amp; Smith (2014)</a> Flume	Irregular waves $h = 0.31 - 0.53m$ $H_{m0} = 0.05 - 0.19m$	<i>Spartina alterniflora</i> (Polyolefin tubes) $h_v = 0.41m, b_v = 6.4mm, N_v = 200,400m^{-2}$	$C_D = 0.76 + \left(\frac{744.2}{Re}\right)^{1.27}$ $553 < Re < 2296$ $C_D = 1.1 \left(\frac{27.4}{KC}\right)^{3.08}$ $26 < KC < 112$	-
<a href="#">Hu et al. (2014)</a> Flume	Regular waves & currents $h = 0.25, 0.50m$ $H_{m0} = 0.04 - 0.20m$	Vegetation mimics (Wooden rods) $h_v = 0.36m, b_v = 10mm, N_v = 62,139,556m^{-2}$	$C_D = 1.04 + \left(\frac{730}{Re}\right)^{1.37}$ $300 < Re < 4700$	-
<a href="#">Möller et al. (2014)</a> Flume	Irregular waves $h = 2m$ $H_{m0} = 0.2 - 0.7m$	<i>Puccinellia maritima</i> $h_v = 0.22 \pm 0.03m, b_v = 1.1 \pm 0.3mm$ <i>Elymus athericus</i> $h_v = 0.7 \pm 0.01m, b_v = 1.3 \pm 0.3mm$	$C_D = 0.16 + \left(\frac{227.3}{Re}\right)^{1.615}$ $100 < Re < 1100$	-
<a href="#">Losada et al. (2016)</a> Flume	Both Regular & Irregular waves & currents $h = 0.4, 0.6m$ $H_{m0} = 0.15, 0.2m$ (Regular) $H_{m0} = 0.12m$ (Irregular) Current vel. = $0.30ms^{-1}$	<i>Spartina anglica</i> $h_v = 0.284m, b_v = 6mm, N_v = 420,729m^{-2}$ <i>Puccinellia maritima</i> $h_v = 0.473m, b_v = 3mm, N_v = 877,1389,2436m^{-2}$	Irregular waves $C_D = 0.08 + \left(\frac{22000}{Re}\right)^{2.2}$ Irregular waves + current $C_D = 0.25 + \left(\frac{35000}{Re}\right)^9$ Irregular waves – current $C_D = 0.50 + \left(\frac{27000}{Re}\right)^9$ $25000 < Re < 60000$	-
<a href="#">Phan et al. (2019)</a> Flume (Mangroves)	Both Regular & Irregular $h = 0.65m$ $H_{m0} = 0.01 - 0.1m$ Regular $H_{m0} = 0.03 - 0.15m$ Irreg.	Wooden cylinders (Rigid mangroves) $h_v > 0.75m, b_v = 12mm, N_v = 200,400m^{-2}$	Used $C_D = 1.5$ from <a href="#">Hu et al. (2014)</a>	60% – 70%

## VEGETATION DYNAMICS

The flow on vegetation has effect on vegetation as well which are explained through combining flow equation like Navier-Stokes with dynamic equation of motion. [Asano et al. \(1993\)](#) first time presented coupled flow-vegetation model in which the expressions for flexible vegetation were derived and compared with the experimental data of swaying seaweeds.

In the flexible vegetation it is common to use relative velocity and effective height for explaining the flow-vegetation interaction because the vegetation is more streamlined due to an effect called *reconfiguration*<sup>3</sup>. Reconfiguration reduces the increase in drag force with flow velocity than predicted by the quadratic drag law ([Nepf, 2012b](#)).

The canopy-scale turbulence, as shown in [Figure 2.5](#), interacts with vegetation and produces an instantaneous drag ([Nepf, 2012a](#)). Usually this drag is large enough to overcome the rigidity and buoyancy of flexible blades resulting in a local depression ([Nepf, 2012a](#)) and an in-phase movement of the canopy with the vortex called *monami* ([Ackerman & Okubo, 1993](#); [Ikeda & Kanazawa, 1996](#); [Ikeda et al., 2001](#); [Ghisalberti & Nepf, 2002](#)). However, if instantaneous drag isn't large enough then monami is not present even if canopy-scale turbulence is present ([Nepf, 2012a](#)).

In varied hydrodynamic conditions monami and the hydrodynamically induced drag are not only relevant to each other but to wave attenuation as well. [Bradley & Houser \(2009\)](#) performed a cospectral analysis between wave orbital velocity and flexible blade velocity which showed that vegetation movement is in-phase with the currents of low frequencies and out of phase for high frequencies. This suggests that submerged flexible vegetation, e.g. seagrass, are wave energy attenuators along with a low-pass filter which attenuates higher frequencies more than the lower ones in the spectra ([Bradley & Houser, 2009](#)). In other words, seagrass 'goes with the flow' for long waves and generates minimum drag which results in no monami and lesser long-wave attenuation.

Drag force and flow around a rigid smooth cylinder in a steady current are represented through [Equation 2.6](#). [Morison et al. \(1950\)](#) equations are employed in order to neglect swaying motion and inertial force ([Mendez & Losada, 2004](#)).

$$F = F_D + F_I = \frac{1}{2} \rho C_D b_v h_v U_w |U_w| + \frac{1}{4} \rho C_M \pi h_v d^2 \frac{\partial U_w}{\partial t} \quad (2.6)$$

where;  $F$  is the total force and  $F_D$  is the drag force and  $F_I$  is the inertia force.  $\rho$  is the density of the fluid,  $d$  frontal width,  $h_v$  is the vegetation height immersed in the water.  $U_w$  is the characteristic velocity in oscillatory flow,  $C_d$  is the drag coefficient and  $C_M$  is the inertia coefficient.

<sup>3</sup>For flexible vegetation, flow velocity affects posture of the blade resulting in a phenomenon called *reconfiguration* ([Nepf, 2012b](#)).

### 2.2.2. WAVE ATTENUATION

Wave attenuation is subjected to both vegetation characteristics and hydrodynamic parameters. Vegetation parameters include geometry, buoyancy, density, stiffness, degrees of freedom and spatial configuration where as wave parameters include wave height, period and direction (Mendez & Losada, 2004).

#### ANALYTICAL FORMULATIONS

The elegance of understanding a system lies in being able to represent the underlying physical process of the system in the most unified and fundamental forms. More the formulations are, lesser the topic is understood. Representation flow-vegetation interaction is challenging because the system is dynamic in nature Mendez & Losada (2004) due to both time-dependent changes in the vegetation structure and the variable forcing offered by water flow (Koehl, 1984).

In a flow-vegetation system fundamental formulations explaining wave attenuation have evolved and are now converging towards a unified explanation. However, the element of correctly quantifying the drag coefficient is least understood (see Section 2.2.1).

The gradual evolution of mathematical sophistication in explaining the vegetated hydrodynamics has led us to represent reality of flow-vegetation systems in a better way. The elements in such systems which can categorizes these formulations are the conservation principle (mass, momentum, or energy), vegetation schematization (rigid or flexible), temporal resolution (phase-averaging or phase-resolving) and wave conditions (regular or random) (Suzuki et al., 2019).

Initially, vegetation was represented as an element parameterized through bottom friction causing wave energy dissipation. It was succeeded by representing vegetation as an entity affecting energy flux conservation. It was not too late until shallow water equation based formulations were presented but only for linear wave theory. Other models based on momentum conservation, stemming from Navier-Stokes equations and Boussinesq equations, are currently considered as the near-to-reality explanations.

#### ENERGY CONSERVATION

In the early formulations like in Hasselmann & Collins (1968); Camfield (1977) vegetation was assumed as a factor which just adds to bottom friction. This energy conservation based formulation only considered regular waves and was phase-averaging. Möller et al. (1999) extended the formulation and suggested that increase in bottom friction plays a primary role in increasing wave attenuation over a saltmarsh.

Early studies started treating vegetated environments as energy dissipation regions which were described through friction terms in energy balance equations (Camfield, 1977; Dean, 1978; Hasselmann & Collins, 1968; Dalrymple et al., 1984; Möller et al., 1999). For instance, Camfield (1977) used the Darcy-Weisbach friction factor, Möller et al. (1999) expressed it as bottom friction factor  $K_f$  (Equation 2.7), Dalrymple et al. (1984) developed a damping factor  $\omega_v$  (Equation 2.10) to account for vegetation-induced wave energy dissipation. Vegetation elements were idealized as rigid vertical cylinders which, later, in modern studies among many cases, resulted in a no-sway case (Maza et al., 2013). Other

cases included treating vegetation as flexible blades giving whip-like movements (Ikeda et al., 2001; Anderson & Smith, 2014; Luhar & Nepf, 2016; Mattis et al., 2019).

The analytical model initiated by Möller et al. (1999) and formulated by Möller et al. (1999) was based on theoretical wave energy dissipation. Equations of Putnam & Johson (1949) and Bretschneider (1954) formed the basis of the formulation but the constituting formulations were more focused on explaining wave energy dissipation due to shoaling, percolation or refraction and not due to vegetation.

$$H_f = H_i \cdot K_s \cdot K_v \cdot K_f \cdot K_p \quad (2.7a)$$

with the friction decay factor  $K_f$  and the friction factor  $f$  based on Putnam & Johson (1949); Bretschneider (1954); Horikawa (1978) is:

$$K_f = \left[ 1 + \frac{64\pi^3}{3g^2} \frac{fH_i\Delta x}{h^2} \frac{h^2}{T^4} \frac{K_s^2}{\sinh^3\left(\frac{2\pi h}{L}\right)} \right]^{-1} \quad ; \quad f = \frac{\tau_0}{\frac{1}{2}\rho a_u^2} \quad (2.7b)$$

where;  $H_f$  = final wave height at the end of vegetation,  $H_i$  = incident wave height at the start of vegetation, with vegetation over distance  $\Delta x$ ;  $K$  with the subscripts  $s$ ,  $v$ ,  $f$  and  $p$  are the shoaling coefficient, viscous friction, bottom friction and percolation decay factors, respectively;  $h$  = water depth,  $T$  = wave period,  $L$  = wave length and  $g$  = gravitational acceleration constant;  $\tau_0$  = bed shear stress,  $\rho$  = water density, and  $a_u$  = bottom orbital velocity.

Vegetation was represented in  $K_f$  term which was calculated from known values of other factors (Möller et al., 1999) because of difficulty in quantifying bottom friction initially without real-case calibration (Dalrymple et al., 1984). However, later in the same model  $K_f$  was calculated (see Equation 2.7) and results reported that friction factor  $f$  is one order higher than the other factors Möller et al. (1999) which means vegetation-induced wave attenuation is higher than all other wave energy dissipation processes.

### ENERGY FLUX CONSERVATION

Modeling vegetation merely as bottom friction was succeeded by the famous formulation of Dalrymple et al. (1984) which could be said to be the first attempt to mathematically express energy dissipation due to vegetation in a generalized manner. The generalization of Dalrymple et al. (1984) was a result of Dean (1978) work who studied the wave action effects associated with vegetation.

Energy flux conservation formulation of Dalrymple et al. (1984) assumed potential flow condition which means linear wave theory along with its all kinematic and dynamic boundary conditions held true. Wave dissipation due to vegetation was accounted in the model through the drag force exerted by vegetation. Morison et al. (1950) equations were used to represent drag force as vegetation was schematized to behave as a cluster of rigid cylinders present over the water column. This formulation is depth-integrated and time-averaged over a wave period and, also, does not include the wave reflection due to the plants (Mendez & Losada, 2004).

Time-averaged conservation of energy equation, where energy dissipation is based on drag force offered by vegetation, is formulated as:

$$\frac{\partial(Ec_g)}{\partial x} = -\epsilon_D = -F_D \cdot u = -\frac{1}{2} \rho C_D d N u |u| \cdot u \quad (2.8a)$$

The depth-integrated and time-averaged (over a wave period) energy dissipation  $\epsilon_D$  per horizontal area unit is given by integrating it over plant height which results in:

$$\epsilon_D = \int_{-h}^{s-h} (F_D u) \cdot dz = B a^3 \quad ; \quad B = 2\rho \frac{C_D}{3\pi} \frac{D}{k} \frac{(\sinh^3 ks + 3 \sinh ks)}{3 \cosh^3 kh} \left( \frac{gk}{\omega} \right)^3 \left( \frac{1}{b^2} \right) \quad (2.8b)$$

where;  $E$  = wave energy per unit area =  $\frac{1}{2} \rho g a^2$ ,  $\rho$  = fluid density;  $g$  = gravity;  $a$  = wave amplitude;  $c_g$  = wave group velocity =  $nc$ ;  $n = \frac{1}{2} \left( 1 + \frac{2kh}{\sinh 2kh} \right)$ ;  $c = \sqrt{\frac{g}{k} \tanh kh}$ ;  $k$  = wave number =  $\frac{2\pi}{L}$ ;  $L$  = wave length;  $h$  = water depth; and  $\epsilon_D$  = energy dissipation.  $F_D$  = drag force on the plant;  $C_D$  = drag coefficient;  $d$  = frontal width of plant (diameter);  $N$  = number of plants per unit area; and  $u$  = horizontal velocity due to the wave motion.  $s$  = elevation of the top of the plant relative to the bottom;  $b$  = spacing between plants;  $\omega$  = wave angular frequency =  $\frac{2\pi}{T}$ ;  $T$  = wave period.

Combining both expressions of energy dissipation  $\epsilon_D$  in Equation 2.8 and using initial energy equation  $\frac{\partial(Ec_g)}{\partial x} = -\epsilon_D$  gives an expression connecting differential of wave amplitude  $a$  to vegetation paramters:

$$\frac{dEc_g}{dx} = \frac{1}{2} \rho g c_g \frac{da^2}{dx} = -B a^3 \quad (2.9a)$$

Solution of which is what Dean (1978) showed as a wave amplitude decay relation:

$$a = a_0 \left( \frac{1}{1 + \frac{2B}{\rho g c_g} a_0 x} \right) \quad (2.9b)$$

where;  $a_0$  = incident wave amplitude before entering the vegetation field.

Dalrymple et al. (1984), inspired from Booij (1981), proposed a damping factor  $\omega_v$  to account for localized energy dissipation due to vegetation. He established that only the measure the energy loss, through  $\omega_v$ , is important to account for vegetation-induced wave damping.

$$\omega_v = 2n\omega \frac{k_i}{k} \sqrt{1 + \left( \frac{k_i}{k} \right)^2} \quad ; \quad k_i \approx \frac{2B}{\rho g c_g} a_0 \quad (2.10)$$

where;  $k_i$  = imaginary part of the complex wave number, including damping.

This factor was derived based on linear wave theory and Berkoff's equation:  $\nabla \cdot (nc^2 \nabla \Phi) + (n\omega^2 + 1\omega\omega_v)\Phi = 0$ , where  $\nabla = [(\partial/\partial x)\vec{i} + (\partial/\partial y)\vec{j}]$  and  $\Phi$  = wave velocity potential. This approach is different from the one from Dean (1978) however, for small values of  $k_i$ , the

decay factor of Dean (1978)  $k_i$  and Dalrymple et al. (1984)  $\omega_v$  are close enough and are related through Equation 2.10.

Similar conclusion of exponential decay was later on proposed by Kobayashi et al. (1993) as well. However, unlike Dean (1978); Dalrymple et al. (1984) where time-averaged wave energy balance was used and flow field was estimated through linear wave theory, Kobayashi et al. (1993) used mass and momentum balance.

Mendez & Losada (2004) advanced this formulation by including wave breaking and wave irregularity over vegetation fields at variable depths which was extended by to wave-current interaction by Losada et al. (2016). Wave breaking was included by splitting  $\epsilon_D$  into energy dissipation by wave breaking  $\epsilon_b$  and energy dissipation by vegetation  $\epsilon_v$  (see Equation 2.11). Wave irregularity was included using the probability density function of Rayleigh distributed wave heights which are described by the root-mean-square wave height  $H_{\text{rms},0}$ .

$$p(H_0) = \frac{2H_0}{H_{\text{rms},0}^2} \exp\left[-\left(\frac{H_0}{H_{\text{rms},0}}\right)^2\right] \quad ; \quad H_{\text{rms},0}^2 = \int_0^\infty H_0^2 p(H_0) dH_0 \quad (2.11a)$$

Through the assumption of linear summation of  $\epsilon_b$  and  $\epsilon_v$ , Equation 2.8 becomes:

$$\frac{\partial(Ec_g)}{\partial x} = -\epsilon_b - \epsilon_v \quad (2.11b)$$

The average energy dissipation rate per unit area

$$\epsilon_b = \frac{3\sqrt{\pi}}{16} \rho g \frac{B^3 f_p}{\gamma_b^4 h^5} H_{\text{rms}}^7 \quad ; \quad \epsilon_v = \frac{1}{2\sqrt{\pi}} \rho \tilde{C}_D b_v N \left(\frac{kg}{2\sigma}\right)^3 \times \frac{\sinh^3 kah + 3 \sinh kah}{3k \cosh^3 kh} H_{\text{rms}}^3 \quad (2.11c)$$

where;  $B$  and  $\gamma_b$  are calibration parameters and  $f_p$  is an average frequency corresponding to peak period  $T_p$

More action balance formulation include spectral action balance by Suzuki et al. (2012) and wave action balance for short waves by van Rooijen et al. (2016).

## MOMENTUM CONSERVATION

Momentum conservation formulations are mainly based on Naiver Stokes (NS) equations which through Reynolds decomposition results in Reynolds-averaged Navier–Stokes (RANS) based formulations (C. W. Li & Yan, 2007; Ma et al., 2013; Maza et al., 2013; X. Chen et al., 2016; Maza et al., 2016). Nonlinear Shallow Water equations (NSWE) based formulations are further simplified form of NS Kobayashi et al. (1993); Mei et al. (2011); Liu et al. (2015). Méndez et al. (1999) suggested that, while using NSWE, the correct quantification of the nonlinear drag force  $F_D$  should be done by using the relative velocity  $u_r$  between the plant and the fluid instead of flow velocity only.

Other formulations include Boussinesq based formulations (Augustin et al., 2009; Huang et al., 2011; Jadhav et al., 2013; Karambas et al., 2016; Yang et al., 2018) has an added

advantage of being able to include inertial force along with drag force. Moreover, Mild-slope equation [Cao et al. \(2015\)](#); [Tang et al. \(2015\)](#) based formulations also exist.

### PROBABILISTIC FORMULATIONS

In addition to analytics, experiments, and numerics, the effect of vegetation on wave attenuation has also been under researcher's microscopes for a probabilistic investigation ([Lövstedt & Larson, 2010](#); [Jadhav & Chen, 2013](#)). However, the results were mainly case-specific data-fitted probability distributions. [Jadhav & Chen \(2013\)](#), using wave decay relation of [Dalrymple et al. \(1984\)](#), proposed a model for vegetation-transformed wave height distribution based on measured data. It was two-parameter Weibull distribution.

$$p(H) = \frac{2H}{(1 - \beta_1 H)^3} \frac{1}{H_{rms,0}^2} \exp \left[ - \left( \frac{H}{(1 - \beta_1 H) H_{rms,0}} \right)^2 \right] \quad 0 \leq H < 1/\beta_1 \quad (2.12a)$$

Later improved the model for local conditions using ([Mendez & Losada, 2004](#)):

$$p(H) = \frac{2H}{\left(1 - \frac{\kappa}{H_{rms}} H\right)^3} \frac{\phi^2}{H_{rms}^2} \exp \left[ -\phi^2 \left( \frac{H}{\left(1 - \frac{\kappa}{H_{rms}} H\right) H_{rms}} \right)^2 \right] \quad 0 \leq H < H_{rms}/\kappa \quad (2.12b)$$

where,  $H$  is the wave height,  $H_{rms}$  is root mean squared wave height,  $p(H)$  is probability of wave height,  $\beta_1$  is the wave decay relation.

## 2.3. EXTREME BEHAVIOR MODELING: XBEACH

Extreme Beach Behavior Model (XBeach) was originally developed for hydro- morpho-dynamic modeling during extreme events ([Roelvink et al., 2009](#)), however, later on effects of vegetation were also added in the model ([van Rooijen et al., 2016](#)).

Storm impact model XBeach has three hydrodynamic modes to be chosen based on the choice of time-scales to solve. These modes include a wave phase-averaged stationary mode, a short wave-averaged long-wave resolving surfbeat mode, and a sea-swell wave phase-resolving non-hydrostatic mode. In surfbeat mode nonlinear wave-vegetation interaction processes are captured by a wave shape model solving short wave action. However, in non-hydrostatic mode intrawave effects are directly accounted through depth-averaged nonlinear shallow water equations with a non-hydrostatic pressure correction term ([van Rooijen et al., 2016](#)) as could be seen in Equation 2.19.

The choice of non-hydrostatic mode lies in the advantage of inclusion of short wave run-up which, beside the strength of the model on relatively flat beds, is important for steep slopes. This covers both dissipative and reflective foreshores giving us bigger range of systems to cover while modeling. Also, this mode resolves wave asymmetry and skewness casting aside the need for local model approximations or empirical formulations. Although in the non-hydrostatic mode short wave action is not solved but in order to solve the flow much higher spatial and temporal resolution is required making it more computationally expensive.

### 2.3.1. XBEACH FORMULATION

In non-hydrostatic mode the formulation is based on the conservation of mass and momentum rather than the energy conservation which is the case in the surfbeat mode.

#### GENERALIZED LAGRANGIAN MEAN (GLM) FORMULATION

Momentum balance together with continuity equation (2.13a) are referred to as *non-linear shallow water equations* (Equation 2.19) which are solved to account for low frequency waves and currents (mean flow). However, to account for the wave induced mass-flux and the resulting return flow, depth-averaged Generalized Lagrangian Mean (GLM) formulation is used (Andrews & McIntyre, 1978; Walstra et al., 2000) which in it's full 2DH<sup>4</sup> form are presented in Equation 2.13.

Continuity equation for mass balance can be written as

$$\frac{\partial \eta}{\partial t} + \frac{\partial hu^L}{\partial x} + \frac{\partial hv^L}{\partial y} = 0 \quad (2.13a)$$

Momentum balance in x-direction with explanation of terms is presented as

$$\begin{aligned} & \overbrace{\frac{\partial u^L}{\partial t}}^{\text{Temporal}} + \overbrace{u^L \frac{\partial u^L}{\partial x} + v^L \frac{\partial u^L}{\partial y}}^{\text{Convection}} - \overbrace{f v^L}^{\text{Coriolis}} - \overbrace{v_h \left( \frac{\partial^2 u^L}{\partial x^2} + \frac{\partial^2 u^L}{\partial y^2} \right)}^{\text{Diffusion}} \\ = & \underbrace{\frac{\tau_{sx}}{\rho h}}_{\text{Wind shear}} - \underbrace{\frac{\tau_{bx}^E}{\rho h}}_{\text{Bed shear}} - \underbrace{g \frac{\partial \eta}{\partial x}}_{\text{Pressure}} + \underbrace{\frac{F_x}{\rho h}}_{\text{Wave-induced}} + \underbrace{\frac{F_{v,x}}{\rho h}}_{\text{Vegetation-induced}} \end{aligned} \quad (2.13b)$$

Similarly the momentum balance in y-direction can be written as

$$\begin{aligned} & \frac{\partial v^L}{\partial t} + u^L \frac{\partial v^L}{\partial x} + v^L \frac{\partial v^L}{\partial y} + f u^L - v_h \left( \frac{\partial^2 v^L}{\partial x^2} + \frac{\partial^2 v^L}{\partial y^2} \right) \\ = & \frac{\tau_{sy}}{\rho h} - \frac{\tau_{by}^E}{\rho h} - g \frac{\partial \eta}{\partial y} + \frac{F_y}{\rho h} + \frac{F_{v,y}}{\rho h} \end{aligned} \quad (2.13c)$$

where;  $u^L$  and  $v^L$  are the Lagrangian velocities,  $x$  and  $y$  are the horizontal coordinates,  $t$  is the temporal coordinate,  $\rho$  is water density,  $h$  is water depth used for depth averaging,  $\tau_{sx}$  and  $\tau_{sy}$  are the wind shear stresses,  $\tau_{bx}$  and  $\tau_{by}$  are the bed shear stresses and superscript <sup>E</sup> shows Eulerian velocity influence on the bed and not the  $u^L$  influence,  $\eta$  is the water level,  $F_x$  and  $F_y$  are the wave-induced stresses,  $F_{v,x}$  and  $F_{v,y}$  are the vegetation-induced stresses,  $v_h$  is the horizontal viscosity and  $f$  is the Coriolis coefficient.

Flow through GLM formulation is solved in which Lagrangian velocities are solved and stoke drift is included to derive Eulerian velocities as depicted in Equation 2.14.  $u^L$  is instantaneous velocity within one wave period and  $u^E$  is the short-wave-averaged velocity

<sup>4</sup>2DH is two dimensional in horizontal plane (x and y direction) but averaged over the depth

calculated at a cell interface. Stokes drift  $u^S$  is calculated as a function short wave energy  $E_w$  varying over wave-group and direction  $\theta$  which are obtained from the wave-action balance (Equation 2.17).

$$u^L = u^E + u^S \quad ; \quad u^S = \frac{E_w \cos \theta}{\rho h c} \quad (2.14)$$

To account for the change from turbulent to viscous exchange of momentum Smagorinsky model (Smagorinsky, 1963) was used for horizontal momentum exchange. In Smagorinsky model horizontal viscosity  $\nu_h$  is calculated by Equation 2.15 for unresolved spatial scales smaller than cell grid size in which  $c_S$  is Smagorinsky constant set to 0.1.

$$\nu_h = c_S^2 2^{\frac{1}{2}} \sqrt{\left(\frac{\delta u}{\delta x}\right)^2 + \left(\frac{\delta v}{\delta y}\right)^2 + \frac{1}{2} \left(\frac{\delta u}{\delta x} + \frac{\delta v}{\delta y}\right)^2} \Delta x \Delta y \quad (2.15)$$

Bed shear stresses  $\tau_{bx}^E$  induced by long waves and mean currents are formulated through Equation 2.16 proposed by Ruessink et al. (2001). Among many ways to determine dimensionless bed friction coefficient  $c_f$  Chezy approach shows superiority because of its derivation procedure and in conveying physical meaning rather than merely being an empirical coefficient.

$$\tau_{bx}^E = c_f \rho u^E \sqrt{(1.16 u_{rms})^2 + (u^E + v^E)^2} \quad (2.16)$$

$$c_f = \sqrt{\frac{g}{C^2}} \quad ; \quad C = 55 m^{\frac{1}{2}} / s$$

### WAVE ACTION BALANCE

The non-linear shallow water equations through GLM formulation are forced by a time-dependent wave action balance (Smit et al., 2010). Wave action balance also which also accounts for various nearshore phenomenon like shoaling, refraction and breaking.

$$\frac{\partial A}{\partial t} + \frac{\partial c_x A}{\partial x} + \frac{\partial c_y A}{\partial y} + \frac{\partial c_\theta A}{\partial \theta} = - \frac{D_w + D_f + D_v}{\sigma} \quad (2.17a)$$

with A wave energy over radian wave frequency and sigma as:

$$A(x, y, t, \theta) = \frac{S_w(x, y, t, \theta)}{\sigma(x, y, t)} \quad ; \quad \sigma = \sqrt{g k \tanh kh} \quad (2.17b)$$

Roller energy balance accounts for energy sourced by the short wave energy dissipation and dissipated during roller propagation towards the coast.

$$\frac{\partial E_r}{\partial t} + \frac{\partial E_r c \cos \theta}{\partial x} + \frac{\partial E_r c \sin \theta}{\partial y} = D_w - D_r \quad (2.18)$$

### NON-HYDROSTATIC PRESSURE CORRECTION

The depth averaged dynamic pressure is computed from the mean of the dynamic pressure at the surface and at the bed by assuming the dynamic pressure at the surface to be zero and a linear change over depth (Roelvink et al., 2015). Non-hydrostatic pressure term is disabled after a defined wave steepness to control wave breaking process. During breaking and run-up the wave is modeled as a bore (Smit et al., 2010) and the pressure distribution under these breaking bores is considered as hydrostatic (Roelvink et al., 2015).

### 2.3.2. ABSTRACTIONS & SIMPLIFICATIONS

Certain terms are ignored in GLM formulation for these purpose to reach the final form of equation used for this study<sup>5</sup>. In order to make abstractions and still model realistically two of the most important questions are: (i) what processes are to be included and (ii) what scales should be resolved (Nepf, 2012b). In XBeach

$$\frac{\partial \eta}{\partial t} + \frac{\partial uh}{\partial x} = 0 \quad (2.19a)$$

$$\frac{\partial u}{\partial t} + u \frac{\partial u}{\partial x} - \nu_h \frac{\partial^2 u}{\partial x^2} = -g \frac{\partial \eta}{\partial x} - \frac{\partial \bar{q}}{\partial x} - \frac{\tau_{b,x}}{\rho h} + \frac{F_{v,nh}}{\rho h} \quad (2.19b)$$

where;  $x$  and  $t$  are the horizontal and temporal coordinates, respectively,  $\eta$  is the water surface elevation,  $u$  is the depth-averaged velocity,  $h$  is the local water depth,  $\nu_h$  is the horizontal viscosity,  $g$  is the gravitational acceleration,  $\bar{q}$  is the depth-averaged dynamic pressure,  $\tau_{b,x}$  is the bed shear stress, and  $F_{v,nh}$  is the vegetation force.

The diffusion term  $\nu_h \frac{\partial^2 u}{\partial x^2}$  represents the viscous stress related to the spatial variation in flow velocity  $u$  Nepf (2012a) and is negligible relative to vegetative-induced drag term  $\frac{F_{v,nh}}{\rho h}$  over most of the depth excluding the near-bed region (Nepf & Koch, 1999). Similarly, turbulent stresses in emergent vegetation are also negligible (2%) as the stem-scale eddy lengths are only 1%–3% of the water depth which restricts the turbulence flux of momentum (Nepf, 2012a; Nepf & Vivoni, 2000).

Fundamentally both cases of submerged and emergent vegetation are dealt through same formulation by not accounting for vegetation effects on bed shear stress and, infact, only in a depth-averaged vegetation force term. This force term is exactly the drag force in Equation 2.6 first proposed by Morison et al. (1950) and Dalrymple et al. (1984). Vertical layer systematization and defining different set of values for parameters like drag coefficient, frontal width and number of vegetation elements in equation 2.20 allows to obtain different drag force for each layer.

Wave module for solving non-linear shallow water equations for wave forcing and flow module for current, setup, and infragravity waves were employed to model the system under study. The information is shared between the modules for numerically updating

<sup>5</sup>All formulations are presented in one dimensional equivalent, except Equation 2.13 and 2.17 because of the 1D scope of the study.

the model to converge to solutions.

### 2.3.3. WAVE DISSIPATION BY VEGETATION

The formulation used in the model was first developed by [Mendez & Losada \(2004\)](#) and later improved by [Suzuki et al. \(2012\)](#) to include vertical variation of vegetation. The advantage of vertically heterogeneity gives the liberty to model both sea-grasses as vertically uniform and mangroves as vertically schematized systems.

$$F_v(t) = \sum_{i=1}^{n_v} F_{v,i}(t) \quad (2.20a)$$

The vegetation force per layer is given by:

$$F_{v,i}(t) = \frac{1}{2} \rho C_{D,i} b_{v,i} N_{v,i} h_{v,i} u^L(t) |u^L(t)| \quad (2.20b)$$

where  $F_{v,i}$  is the vegetation-induced force in vertical layer  $i$  and  $n_v$  is the number of vegetation layers.  $C_{D,i}$  is a (bulk) drag coefficient,  $b_{v,i}$  is the vegetation stem diameter,  $N_{v,i}$  is the vegetation density.

Limitation of the XBeach model lies in the inability to discretize in frequency space which means only one representative frequency is used for group velocity or orbital velocity calculation. Furthermore, while solving flow, it doesn't account for vertical variations as it's a depth averaged model. Regarding vegetation, although mangroves could be modeled by vertical layering but flow variations inside the canopy can't be studied. This limitation arises because modeling of porous in-canopy environments does not allow to schematize in vertical sections.

## 2.4. BAYESIAN NETWORKS

Bayesian Networks (BN) are one of the tools applied for predictive decision-making applications beside other methods like artificial neural network, analytic hierarchy process or fuzzy multiple-criteria decision making. Bayes' theorem of famous statistician Thomas Bayes forms the basis of BN functionality.

The choice of Bayesian network as a method for probabilistic modeling is made due its comparative perks over other classical methods of dependability and risk analysis. [Weber et al. \(2012\)](#) states those benefits as:

*“the capability to model complex systems, to make predictions as well as diagnostics, to compute exactly the occurrence probability of an event, to update the calculations according to evidences, to represent multi-modal variables and to help modeling user-friendly by a graphical and compact approach.”*  
~ [Weber et al. \(2012, p.671\)](#)

[Krzysztofowicz \(1999\)](#) introduced the first forecasting system using basic Bayesian inference principles and integrated quantification of uncertainties as well. However, the

system was restricted to forecasting river stages (as predictive Bayes density) using deterministic hydrological models (Han & Coulibaly, 2017).

### 2.4.1. BUILDING BLOCKS & THEORETICAL FRAMEWORK

Bayesian networks are the probabilistic models which are able to incorporate complex joint distributions in a modular way (Bae et al., 2016). There are many ways to build Bayesian network including by using copulas. Copulas being first introduced in 1959 by Sklar (1959), in the context of probabilistic metric spaces (Frees & Valdez, 1998), became a handy tool for understanding relationships in a multivariate system. One-parameter copulas include Gaussian, Clayton, Gumbel, see (Sadegh et al., 2017; Schweizer, 2007; Genest & Favre, 2007; Frees & Valdez, 1998; Genest & Mackay, 1986) for details. The text boxes about probability theory and Bayesian network builds on the background knowledge for non-parametric Bayesian networks.

#### Building Block # 1: Probability Theory

This block is built for the purpose of refreshing background knowledge. Introductory definition of terms related to probability theory are defined and special attention is paid in elaborating how these terms are used while describing the functionality of Bayesian networks.

– **Random variable**

A random variable  $X$  is like a random function that returns a value for a certain statistical experiment. In other words,  $X$  can take any value to quantify outcomes of a random occurrence.

– **Discrete & Continuous Random Variables**

Discrete random variables take finite number of distinct set of values. Continuous random variables can take any value within a continuous range therefore has infinite number of possible values.

– **Probability distribution (mass function)**

The probability distribution of a discrete random variable  $X$  is a function with all the probabilities for  $X$  and assigns a certain probability  $p_i$  to a possible value  $x_i$  of  $X$  (Morales Napoles et al., 2013).

$$p_i = P(X = x_i)$$

satisfying axioms of  $0 \leq p_i \leq 1$  and  $\sum p_i = 1$ .

– **Probability density (density function)**

Density function gives probabilities over an interval for a random variable

$$P(a \leq X \leq b) = \int_a^b f(x) dx$$

– **Cumulative distribution function (marginal distribution function)**

Continuous random variables can take infinite number of possible values.

The probability that random variable  $X$  is less than or equal to  $x$  (area so far of probability distribution)

– **Product moment correlation coefficient**

Product moment correlation coefficient determines the degree of linear relationship between random variables  $X$  and  $Y$ . It ranges from -1 to 1 and mathematically expressed as (Bedford & Cooke, 2001). It is also known as Pearson's  $\rho_p$  or linear correlation coefficient.

$$\rho(X, Y) = \frac{\text{Cov}(X, Y)}{(\sigma_X \sigma_Y)}$$

– **Rank Correlation coefficient (Spearman's  $r$ )**

Rank correlation is the product moment correlation of the inverse of the cumulative distribution function (quantile function) of two continuous random variables. When the rank correlation of two variables is too high, one of the variables should be defined as functional node to avoid numerical instabilities (Ababei et al., 2008).

Linear correlation and rank correlation could be inter-converted for normally distributed random variables  $X, Y$  by:

$$\rho(X, Y) = 2 \sin\left(\frac{\pi}{6} r(X, Y)\right)$$

– **Copula**

Copula of the two continuous random variables is the joint distribution of the cumulative distribution functions of those variables. Univariate marginals are linked to their full multivariate distributions through a function called *copula* (Frees & Valdez, 1998) which has a distribution on the unit square with uniform marginal distributions.

## BAYESIAN NETWORK

Bayesian Networks (BN) have a qualitative and a quantitative aspect to it steered by a directed acyclic graph (DAG). In DAG each random variable, which could be either discrete or continuous, is a node, and the direct influences between variables are arcs. The direction of arcs in DAG determines a non-unique order of variables giving a sampling order (Morales Napoles et al., 2013) in which preceding node is called *parent node* and succeeding node is called *child node*. DAG also conveys information about the dependence structure of a multidimensional distribution which could either be conditionally dependent or independent (Morales Napoles et al., 2013).

The quantitative part of the dependence modeling through BN is governed by either a dataset or an expert judgment. In either case conditional probability functions are associated with the random variables. In accordance with Bayes' rule once conditional distributions are determined and marginal distributions (without parents) are known, one can evaluate any conditional (posterior) probability (Morales Napoles et al., 2013).

This is done with the help of conditional probability tables (CPTs) in case of discrete BNs but through copulas in non-parametric Bayesian networks. For inference, if distributions are updated given the observations one can make what-if scenarios hence make predictions for hypothetical cases involving the same variables (Morales Napoles et al., 2013; A. Hanea et al., 2015).

### Building Block # 2: Bayesian Network

This block defines and elaborates terminology used while describing Bayesian networks. Major types of Bayesian networks considered before starting the study and their fundamental building principles are also described.

#### – *Bayesian Networks*

A Bayesian Network (BN) is a directed acyclic graph (DAG) consisting of random variables as nodes and the direct influences as arcs (Pearl, 1988). Conditional rank correlations are used to define probabilistic influence between parent and child nodes (Ababei et al., 2008). In order to account for the dependence relations bivariate copula is used (Mendoza-Lugo et al., 2019) to build the joint probability density for the probabilistic nodes. These joint distributions are either updated by analytical methods or Monte Carlo sampling could be used (Ababei et al., 2008).

#### – *Discrete Bayesian Networks*

In Discrete Bayesian Networks (DiBN) random variables have discrete distributions where nodes are assigned marginal distributions and child nodes are assigned a conditional probability table (CPT). DiBNs are only suitable for small networks because of their computational inefficiency for larger networks (Ababei et al., 2008).

#### – *Continuous Bayesian Networks*

Continuous Bayesian Networks are conceptually same as the discrete BN with the difference that the random variables are continuous on the nodes.

#### – *Hybrid Bayesian Networks*

In Hybrid Bayesian Networks (HBN) mixture of both discrete and continuous random variables are used resulting in a hybrid domain (A. Hanea et al., 2015).

#### – *Non-Parametric Bayesian Networks*

Non-Parametric Bayesian Networks (NPBN) are a form of hybrid BNs in which copulas are associated to the arcs (instead of conditional probabilities) and marginal probabilities are associated to the random variables i.e. nodes (A. Hanea et al., 2015).

NPBNs uses bivariate copulas (Mendoza-Lugo et al., 2019) which means that the nodes have uniform marginal distributions in a uniform interval (Genest & Mackay, 1986). NPBNs have the ability to incorporate all kinds of variables including discrete, continuous and functional (Mendoza-Lugo

et al., 2019).

- **Dynamic Bayesian Networks**

A Dynamic Bayesian Network (DBN) upgrades a Static Bayesian Network (SBN) by incorporating temporal dependencies of variables in the model. This possibly makes the model response closer to the natural response and therefore increases the credibility of predictions.

## BAYESIAN INFERENCE

The concept of prediction through a Bayesian network is based on the Bayes' rule (Bayes & Price, 1763). However, it is to be noted that Bayes' rule itself is not used in setting up the Bayesian network rather the whole idea of Bayesian modeling and inference is based on Bayes rule.

$$P(H|e) = \frac{P(e|H)P(H)}{P(e)} \quad (2.21)$$

where the meaning of four terms of the Bayes' rule as elaborated by Geller (2012) are:

- Prior  $P(H)$   
How probable was our hypothesis before observing the evidence?
- Marginal  $P(e)$   
How probable is the new evidence under all possible hypotheses?  
 $P(e) = \sum_{i=1}^n P(e|H_i)P(H_i)$  where  $n$  are the total number of hypothesis.
- Likelihood  $P(e|H)$   
How probable is the evidence given that our hypothesis is true?
- Posterior  $P(H|e)$   
How probable is our hypothesis given the observed evidence?

In the model built through Bayesian approach, the prior probability distribution  $P(H)$  contains all of the knowledge and expertise (Bedford & Cooke, 2001). By combining this prior distribution through Bayes' theorem in Equation 2.21 with the results of an experiment  $P(H|e)$  and a likelihood function  $P(e|H)$  one can obtain posterior probability distributions  $P(H|e)$  i.e. make predictions (Pearl, 1988; Bedford & Cooke, 2001). The limitation of Bayesian approach is that one has to be certain about the uncertainties in the prior knowledge (Bedford & Cooke, 2001).

### 2.4.2. NON-PARAMETRIC BAYESIAN NETWORKS

Non-Parametric Bayesian Networks (NPBNs) were first proposed by Kurowicka & Cooke (2004) and later improved by A. M. Hanea et al. (2006); Ababei et al. (2008); Morales Napoles et al. (2013); A. Hanea et al. (2015). Parametric marginal distributions for random variables are transformed to uniform marginals based on density of the data. Uniform marginals are linked with ranked correlations to form copulas. Hence, only dependence structure of two variables based on their ranks is considered. For NPBNs to be valid two conditions

should be fulfilled (Mendoza-Lugo et al., 2019).

- Underlying data has Gaussian copula. Bivariate data could not always be linked through Gaussian copula but they are preferred because these copulas are single parameter copulas and allows analytical updating.
- NPBN represents enough dependence where enough means that dependence is explained with as less influences as possible but still strong enough for the model to change when one observation is made.

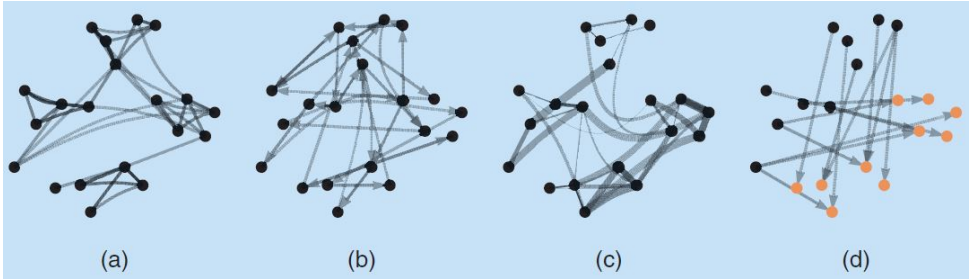


**Figure 2.7:** Types of BN structures: (a) Undirected graph: set of nodes and a set of edges, (b) directed graph: edges point from one node to another, (c) weighted graph: edges have an associated value representing the strength of the relation, and (d) bipartite graph: set of relations between two disjoint sets of nodes. Adapted from Schmidt & Morup (2013).

Non-parametric Bayesian models can be formulated for all of the network structure types in Figure 2.7 (Schmidt & Morup, 2013) but in this study directed graphs would be used. This choice was made to ensure that the Bayesian network captures and represents enough information for the prediction model to make sense without over-complicating it with subjectivity.

(Bedford & Cooke, 2001) classified the nodes into four generic categories: decision nodes (alternatives for the decision-maker); chance nodes (probabilistic quantities); deterministic nodes (functions); and value node (quantity of interest). All these nodes in a DAG have the same probabilistic function but delivers different values in the prediction models based on the interest of the user.

#### APPLICATIONS IN COASTAL ENGINEERING

Many Bayesian based studies for coastal problems have been published but nearly all of them uses discrete Bayesian networks (Plomaritis et al., 2018; Narayan et al., 2018; Jäger et al., 2018; Bolle et al., 2018; S. G. Pearson et al., 2017; Poelhekke et al., 2016; Den Heijer et al., 2012; Plant & Holland, 2011). Only very few and recent ones have used NPBNs (Terefenko et al., 2019; Mendoza-Lugo et al., 2019; Lee & Pan, 2018; Couasnon et al., 2018).

NPBNs are preferred for this study because discrete BNs require large amount of datasets in order to generate all the conditional probabilities. If the BN structure gets large or complicated it not only becomes computational expense but also inaccurate to work with discrete BNs. This is so because the conditional probability tables gets too large and

the calculations required to perform inference accurately becomes non-viable (Morales Napoles et al., 2013). In NPBN due to no marginal distribution assumption on nodes the number of simulation required reduces alot (A. Hanea et al., 2015) that give the comparative benefit as:

*“The quantification of NPBNs reduces to the quantification of a number of marginal distributions equal to the number of variables and a number of (conditional) dependence parameters equal to the number of arcs of the NPBN”*  
 ~ A. Hanea et al. (2015, p.271)

Furthermore, in discrete BNs many of the continuous variables are discretized into bins. The number of bins and the sizes of the bins both have to be correctly fine-tuned to make sure each bin represents a homogeneous information and has nearly similar impact on the child node. This introduces subjectivity as the decisions about bins could vary from person to person which adds another source of uncertainty in the modeling process.

### 2.4.3. DEPENDENCE MODELLING BY UNINET

UNINET is a state-of-the-art standalone program for multivariate stochastic modeling based on core principles of Bayesian Networks along with data mining for dependence modeling of high dimensional distributions (Ababei et al., 2008).

Bayesian methods are generally applied for predictive purposes because they have theoretical profundity along with the ability to quantify of all sources of uncertainties (Han & Coulibaly, 2017). This leads to reduction in predictive uncertainties and enables reliable and accurate forecasts (Han & Coulibaly, 2017). Another advantage of applying Bayesian approach is that it enables to assimilate new information from newer sources in the existing model (Han & Coulibaly, 2017).

While NPBNs could be expert-judgment based, they are mostly data-driven (Werner et al., 2017). The essential question is that can BNs represent and reproduce a dataset descriptively, or they need to have predictive skill to build on the dataset to make predictions about unprecedented events beyond the data (Beuzen et al., 2018).

UNINET qualifies to support all the kinds of Bayesian networks elaborated in Textbox 2.4.3 but in this study Non-Parametric Bayesian Network (NPBN) would be used. UNINET allows flexibility to assign arbitrary continuous or discrete distributions to the nodes which is important for NPBNs. Another advantage for NPBNs modeled in UNINET is that the nodes could be added even after quantification without reassessing all the previous children influences (Ababei et al., 2008). Stochastic modeling in UNINET follows the steps shown in Figure 2.8.

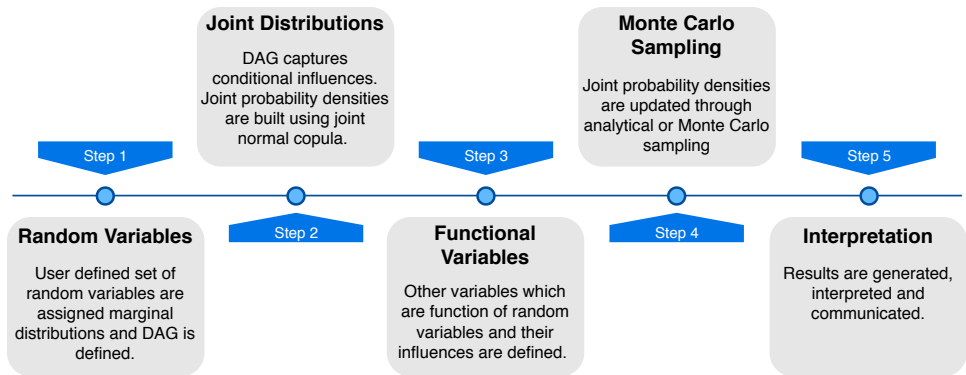


**Figure 2.8:** Steps for Stochastic modeling in UNINET. DAG stands from directed acyclic graph which reflects the graphical structure of a Bayesian network.

# II

## **PART II: MODELING ACTION, REACTION & PREDICTION**



# 3

## ACTION: GLOBAL VEGETATED HYDRODYNAMIC SYSTEM

*Truth is much too complicated,  
to allow anything but approximations.*

John von Neumann

### Abstract

Global vegetated hydrodynamic system of saltmarshes or mangroves could be parameterized through hydraulic and vegetation parameters. To study flood risk reduction, hybrid parameters related to dikes or dunes have been added. The schematized and parameterized systems have been represented through a multivariate stochastic model which caters underlying dependence among the parameters. Performing Monte Carlo sampling from the stochastic model generates realistic physical conditions which represent global vegetated hydrodynamic conditions to be used as an input for forthcoming numerical modelling.

**V**EGETATION interacts with local hydrodynamics which can have a mutual effect on both vegetation and hydrodynamics. This interaction produces effects on hydrodynamics like wave and energy attenuation which eventually reduces flood risk. Since the scope of the study is global, the vegetated hydrodynamic conditions had to be represented in a way which considers the dynamic interactions between vegetation and hydrodynamics through dependence modeling. Once the system is probabilistically interpreted, Monte Carlo sampling can then draw such vegetated hydrodynamic conditions.

Sampling of the parameters was critically important as it ensures global representation of vegetated hydrodynamic systems. For modelling purposes, parameters were identified from the system schematization characterizing vegetated hydrodynamic environments. The sampling results fed the global model runs in XBeach to prepare and simulate the conditions representing realistic global vegetated hydrodynamics.

Every parameter was quantified based on three-tier criteria of defining its range through the best representative distribution and the correlations between variables which can exist. The ranges guaranteed that the scope of input conditions is well-covered while the marginal distributions represented the significance of the most occurred values and the nature of variability of the parameter. In reality, certain values of a specific parameter coexist only for the certain windows of the other parameters. In order to make the physical relevance of the model to represent reality joint probability distributions from the marginal distributions of the correlated variables were defined by linking them through copulas. The three-tier parameter sampling criteria ensures that the:

- Range of a parameter covers global scope.
- Marginal distribution shows variability of a parameter individually.
- Ranked correlation coefficient builds copulas and, eventually, joint probability distributions with reference to correlated variables are defined.

The system was divided into three sets of parameters viz. hydraulic, vegetation and hybrid parameters. The same protocol of defining ranges, distributions and correlation was followed for every parameter.

### 3.1. SYSTEM IDEALIZATION

The system idealization constitutes simplifications through schematization and representation of the model through a set of parameters.

#### 3.1.1. SCHEMATIZATION

Vegetated hydrodynamics has a widespread variety of combinations as vegetation can be of all different types and can grow in many different places. The vegetation types and species along with hydrodynamic conditions could be varied by varying parameters which characterize them. Therefore, it was important to determine a schematization in which variation of components can reproduce most of the physical conditions observed across the world. As a result, the system was classified into segments, see Figure 3.1, which were designated based on the dominant physical and hydrodynamic processes. The segments of interest in the numerical modeling phase are: offshore ramp, foreshore,

vegetation forest and a dike.

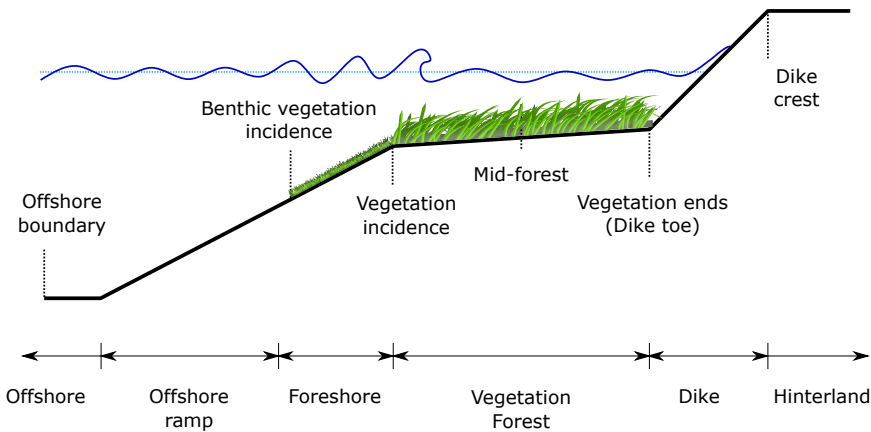


**Figure 3.1:** Idealized profile used for XBeach modeling including six output points

Hydraulic boundary conditions have been defined at offshore boundary which, through nearshore transformation, reach till the point where waves start to feel the bottom. At this point bottom friction kicks in and model starts mimicking as a benthic vegetation environment. *i.e.* seagrasses. This spatially-varying bottom friction prepares the waves to face the mature vegetation forest of a saltmarsh or mangroves. Following the philosophy, as suggested by (Spalding et al., 2014), to mitigate flood risk through cascade of defenses, a dike is introduced at the end of the vegetation forest. Figure 3.1 illustrates the idealized profile and system for all three types of vegetation systems viz. benthic, submerged, and emergent.

One of the important features of the schematized profile is the platform where the vegetation forest is placed. The platform was initially considered flat but due to concerns related to depth-induced wave breaking the idea was dropped. Another variant was the continuous slope extending from diketoe till offshore boundary. This was also dropped because of a major tradeoff between modeling big range of slopes or modeling realistically. Steeper slopes restricts vegetation growth and flatter slopes made the computational domain too large to be feasibly modeled. Although the adopted schematization adds another variable to be probabilistically investigated but it gives liberty to segregate offshore slope from vegetation slope, hence modeling complete ranges accurately.

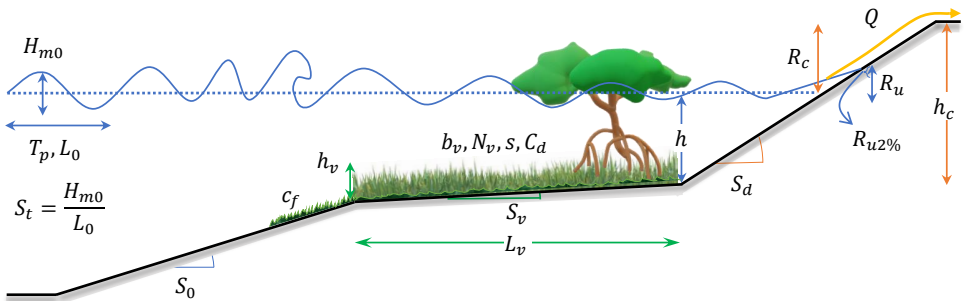
### SYSTEM RESOLUTION

Clearly from Chapter 2 we can conclude that vegetation affects the hydrodynamics from turbulent scales to the life-sized scales. Therefore, the resolution of the model in terms of considering the resolved processes and natural variability was a matter of choice. Whenever modeling global systems, scale and domain definition is always on the higher side, *i.e.* global, but the real question always stands about the detail which was taken into account while schematizing and modeling such dynamic systems.

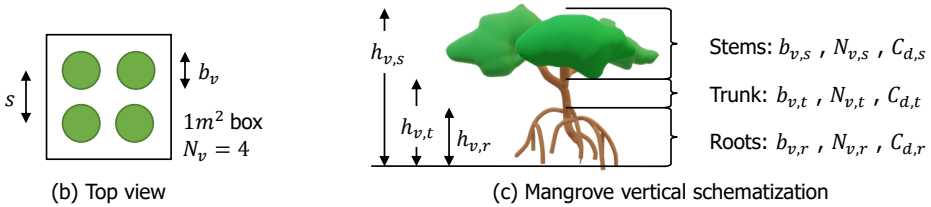
The variations related to hydrodynamics and vegetation exist on both spatial and temporal scales. Spatially hydrodynamics is different as is the vegetation. Table 3.3 summarizes the world wave climate which exhibits different means and variances of wave parameters based on where we are around the globe. On temporal scales there is a clear evidence of seasonal variation of forcing conditions (Young et al., 2011; Chu et al., 2010; Young, 1994). Not only that but even the water level takes a same value four times a day in semi-diurnal tidal conditions. In this work, the vegetated hydrodynamic conditions were differentiated based on spatial variation of the vegetation types, every other factor was varied accordingly. Explicitly, mangroves are assumed to be found in tropical areas and not coexist with saltmarshes and vice versa.

### 3.1.2. INPUT PARAMETERS

Choice of input parameters was made based on the criteria to define minimum parameters which can sufficiently describe hydrodynamic forcing, a vegetation field and a hybrid flood defence like a dike. Parameters were restricted to the ones shown in Figure 3.2 to avoid uncertainty yet establish wholeness. Each parameter is characterized probabilistically, therefore, more the parameters are more the uncertainty is in the prediction model. Wholeness is ensured as many other parameters used in vegetation modeling studies could be derived from combination of these primary parameters.



(a) Vegetated hydrodynamic system idealization



(b) Top view

(c) Mangrove vertical schematization

**Figure 3.2:** Idealized vegetated hydrodynamic system for input and (some) output parameters

A vegetated hydrodynamic system is parameterized through the variables in Figure 3.2 and together they form the distinct input conditions for the each global model run. The input conditions determined through primary input parameters have been varied based

on their probabilistic nature. A Bayesian network was created for stochastic modeling of these parameters where a stochastic process represents ordered set of random variables [Holthuijsen \(2010\)](#). The following section and Appendix A gives an in-depth explanation of the methodology followed to sample these input conditions.

Input parameters of the idealized system have been categorized into three families: hydraulic, vegetation and hybrid. Refer to Figure 3.2 for representation of all the parameters.

- Offshore wave height ( $H_{m0}$ ), peak wave period ( $T_p$ ), water depth ( $h$ ), offshore slope ( $S_0$ ) and offshore slope ( $S_0$ ) have been grouped as hydraulic parameters.
- Benthic vegetation has been represented through dimensionless bed friction coefficient ( $c_f$ ).
- Vegetation forest length ( $L_v$ ) and vegetation slope ( $S_v$ ) are general vegetation parameters which hold true for both saltmarshes and mangroves.
- Vegetation height ( $h_v$ ), frontal width ( $b_v$ ), vegetation density ( $N_v$ ), and drag coefficient ( $C_d$ ) are classified as parameters for submerged vegetation.
- Emergent vegetation has further three sub categories for each of the vertical layers.
  - Stem height ( $h_{v,s}$ ), stem frontal width ( $b_{v,s}$ ), stem density ( $N_{v,s}$ ), and stem drag coefficient ( $C_{d,s}$ ) are put in place for the top layer of mangroves.
  - Trunk height ( $h_{v,t}$ ), trunk frontal width ( $b_{v,t}$ ), trunk density ( $N_{v,t}$ ), and trunk drag coefficient ( $C_{d,t}$ ) are introduced to schematize the trunk.
  - Mangrove roots have height ( $h_{v,r}$ ), frontal width ( $b_{v,r}$ ), density ( $N_{v,r}$ ), and drag coefficient ( $C_{d,r}$ ).
- Lastly, dike slope ( $S_d$ ) and crest level ( $h_c$ ) have been labeled as hybrid parameters.

## HYDRAULIC PARAMETERS

Hydraulic parameters represents conditions related to flow boundary conditions.

### Offshore Wave Height ( $H_{m0}$ )

Wave heights are defined at the offshore boundary and transformed to nearshore on the vegetation and the dike by the model. ([Young et al., 2011](#); [Young, 1994](#)) presents global trends and distribution of wave height which has been used in this study. Generally, the wave heights are Rayleigh distributed for random sea but for long term they are Weibull distributed ([Chu et al., 2010](#); [Holthuijsen, 2010](#)). The wave heights encompass both mild and extreme conditions as the scope involves studying both wave attenuation and flooding. The range and distribution was based on both the literature and the global wave climate data collected for 10 cities around the world, see Table 3.3.

### Water Depth ( $h$ )

Water depth accounts for the mean sea level, storm surges, and sea level rise due to climate change. It has been defined as the vertical distance from the toe of the dike which is positive upwards. Water depth also defines the offshore water level ( $\eta_0$ ) if added to mean sea level. Ideally offshore water level should have been modeled as a reference

to mean sea level. However, water depth relative to the dike toe was taken as parameter which is more easy to be determined for design purposes.

Water depth is an important parameter as it controls many of the physical processes, *e.g.*, wave breaking, relative dominance of turbulent stresses (Nepf & Vivoni, 2000), and pressure gradients. Moreover, it is also used to derive other parameters, *e.g.*, vegetation submergence, offshore bed level, and freeboard. Wave attenuation corresponds to water depths and becomes frequency-dependent in shallower water (Wu & Cox, 2015).

### Peak Wave Period ( $T_p$ )

There are at least 10 different measures of wave periods including the zero up-crossing period, the average wave period, significant height period and peak of the energy density spectrum period (Manohar et al., 1976). Peak wave period have been used in this study because later on spectral analysis, for filtering wave components, uses peak frequency ( $f_p$ ) which could be directly calculated from  $T_p$ .

Furthermore, in early formulations, waves were usually considered as narrow-banded in order to use representative peak period  $T_p$  (Mendez & Losada, 2004). Also, wave steepness ( $S_t$ ) is linked to peak wave period ( $T_p$ ) and deepwater wavelength  $H_{m0}$ , see Equation 3.1.

$$S_t = \frac{H_{m0}}{L_0} \quad ; \quad L_0 = \frac{gT_p^2}{2\pi} \quad \Rightarrow \quad T_p = \sqrt{\frac{\left(\frac{H_{m0}}{H_{m0}/L_0}\right)}{g/2\pi}} \quad (3.1)$$

Wave steepness has a parameter has been used by (S. G. Pearson et al., 2017) to differentiate between the consistent sea states as it links both wave height and wave period. Wave steepness is also relevant because wave attenuation could double if wave steepness increases by a factor of two (Wu & Cox, 2015).

**Table 3.1:** Sea-state classification based on peak wave period  $T_p$  and peak frequency  $f_p$  inspired from S. G. Pearson et al. (2017).

Sea state	Frequency $f_p$ [Hz]	Period $T_p$ [s]
Sea-swell (SS)	1 – 0.04	1 – 25
Infragravity (IG)	0.04 – 0.004	25 – 250
Very low frequency (VLF)	0.004 – 0.001	250 – 1000

### Offshore Slope ( $S_0$ )

The offshore slope extends from offshore boundary to the vegetation forest incidence, see offshore ramp in Figure 3.1. It controls wave shoaling and wave breaking based on the wave height and water depth. Surf similarity parameter links foreshore slope to the wave height which could be used to know breaker types. Benthic vegetation, as bed friction, has been applied on this ramp.

### VEGETATION PARAMETERS

Vegetation parameters characterizes vegetation types (seagrasses, saltmarshes, and mangroves) and most of the species could be studied through the specified parameters. Vegetation parameters are of four types: general vegetation forest parameters, and for bethic, submerged and emergent vegetation. One vertical sections is being modeled for submerged vegetation and three for emergent vegetation.

The range of vegetataion parameters gathered from more than 25 studies as presented in Table 2.2 formed the basis of parametrization of global vegetaion. In addition to that, [van Zelst \(2018\)](#) has also collected parameter values related to saltmarshes found across the globe from more than 18 studies, see Figure 3.3. For mangroves, [Janssen \(2016\)](#) presents a detailed synthesis of vegetation parameters values published in more than 20 research papers, see Figure 3.4. [\(Reimann et al., 2019\)](#) was used for mangrove trunk parameters. [Janssen \(2016\)](#) was used for stems and roots parameters and also for deriving the correlations among mangrove parameters. Studies which are recent or cover global distribution of a certain parameter have been preferred over the aforementioned studies.

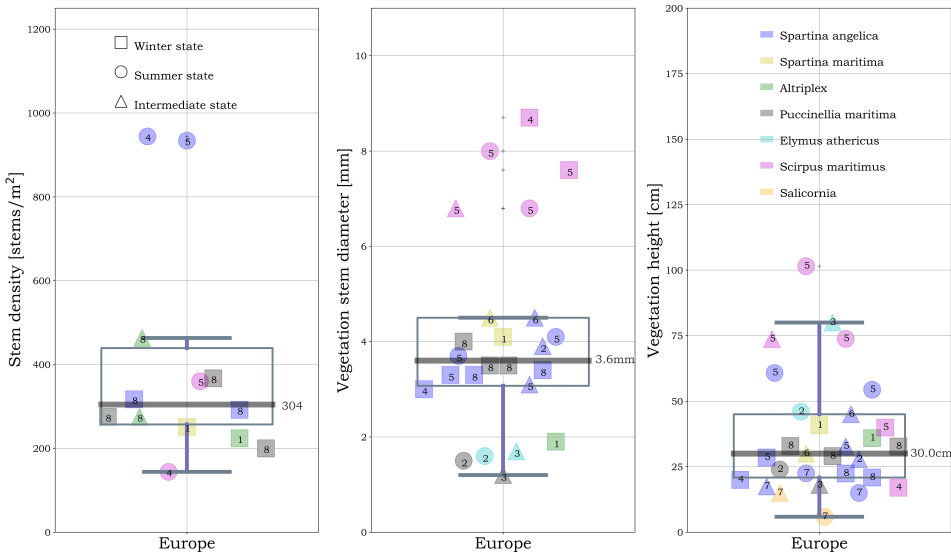


**Figure 3.3:** Saltmarsh parameter values for Europe, reproduced from [\(van Zelst, 2018\)](#). Refer to [\(van Zelst, 2018\)](#) for plots for North America and Asia.

#### Vegetation Forest Length ( $L_v$ )

Forest length represents the total cross shore extent where saltmarsh or mangroves are found. Although [\(Songy, 2016; Jadhav et al., 2013\)](#) report very large extents of forest lengths (upto 30km) however it has been curtailed keeping both the hazard and vulnerability in perspective.

#### Vegetation slope ( $S_v$ )

Vegetation slope is the slope of the platform where vegetation forest is place. It is an-

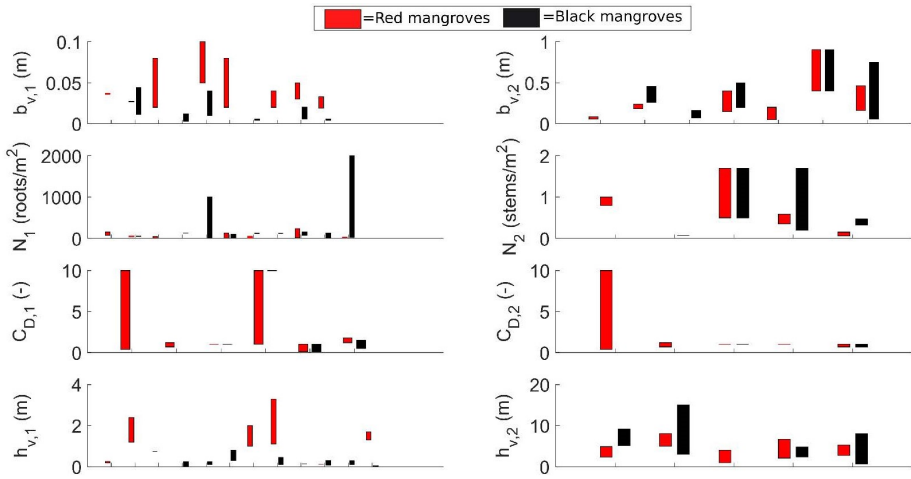


**Figure 3.4:** Vegetation parameters values for Mangroves collected from literature by (Janssen, 2016). Subscript <sub>1</sub> represents roots while subscript <sub>2</sub> represents stems. Figure has been reproduced from (Janssen, 2016).

other critical parameter as it affects the vegetation growth and wave dissipation. K G & Bhaskaran (2017) suggests that milder slopes have higher wave attenuation than steeper slopes.

#### Friction coefficient ( $c_f$ )

Bed roughness is introduced through dimensionless friction coefficient ( $c_f$ ) which mainly describes seagrass environments. Rahmeyer (1996) produced the range of ( $c_f$ ) transformed from Chow (1959). The friction was accounted as spatially varying until  $kh = 0.5$  and then constant value was used.

#### Vegetation Height ( $h_v$ )

Vegetation height is the vertical elevation that a plant takes in saltmarsh environment (stem height). For mangroves due to vertical schematization it was divided into three segments: roots, trunk and stems.

Simard et al. (2019) presents a global assessment of mangrove canopy height however many other parameters are overlooked in published scientific content. Maximum mangrove canopy height is less than 13.2m for more than half of the world (Simard et al., 2019). Root, trunk and stem heights have been inferred from the global distribution of maximum mangrove heights in a way that the combined height of all three segments sums upto to 14m and the distribution results in the same distribution as presented by Simard et al. (2019). Another source suggests that root heights can reach upto 6 meters (Marek, 2019).

#### Frontal Width ( $b_v$ )

Since vegetation is assumed to be rigid cylinder so frontal width is the diameter. Again,

for mangroves three different parameters were defined for three vertical layers. Mangrove root width started from 4mm for pencil roots reaching upto 6cm for cone roots (Marek, 2019).

**Vegetation Density ( $N_v$ )**

Spatial density of vegetation is the number of stems found in a unit meter square. ( $N_v$ ) plays an important role in the flow-vegetation interaction as in many models including vegetation is implemented as vegetation factor which is a function of  $N_v$ ,  $C_d$  and  $b_v$ . For mangroves three different values were used for roots, trunk and stems.

**Drag coefficient ( $C_d$ )**

The drag coefficient determines bulk drag introduced by the vegetation. For mangroves it was divided into three segments. It is a general practice to use drag coefficients as the calibration factor to validate the numerical models. Hu et al. (2012) presents values of drag coefficient ( $C_d$ ) in storm conditions which along with findings of Vuik et al. (2016); van Zelst (2018) and literature meta-analysis were used.

**HYBRID PARAMETERS****Crest level ( $h_c$ )**

Crest levels were defined as the maximum vertical distances relative to the toe of the dike. The levels as the top levels of the gray infrastructure are critical to determine the extents of run-up.

**Dike slope ( $S_d$ )**

Dike slope was used to determine horizontal distance of crest level from the toe of the dike. However, on the more flatter values this could be used as dune slope as well keeping in view that no bed change is assumed in this study.

Observations about many parameters might fall out of the ranges taken in this study but the curtailments were done keep flood risk reduction in perspective. Note that flood risk only prevails if there is hazard and vulnerability. A 20m wave height is irrelevant if there is no one living near the coast, similarly 30km marsh does deliver the service of hazard reduction but not flood risk reduction because of possibly the vulnerability would be negligible. The tallest mangrove forests observed in equatorial Africa are about 62.8m (Simard et al., 2019) but modeling 62.8m of mangroves isn't required because even combined level of storms, wave setup and run up won't reach 62.8m.

## 3.2. STOCHASTIC MODELING

System idealization was transformed to system schematization for implementing it into the numerical model. The set of input parameters had to be varied in order to simulate diverse states of the vegetated hydrodynamic systems around the globe. Monte-Carlo sampling of the forcing parameters along with the hybrid resistive components was carried out through a probabilistically correlated parameter framework.

Parameter sampling was one of the most critical aspects of the study because the sampling results not only delineates the scope of the study but also limits the applicability of the prediction model. Therefore attention was paid to prepare a sampling parameter framework which gives results that represent global systems in the most realistic way possible. Parameters were sampled based on three-tier criteria based on their ranges, distributions and correlations.

### – Ranges

Ranges of parameters were set to represent vegetated environments over global scales. Bayesian networks, as mostly implemented in software packages, can't extrapolate out of the minimum and maximum bounds defined. Hence, a suitable relaxation margin extending the minimum and maximum values found in literature was placed for most of the variables. However, this margin was never more than 10% of the respective parameter's mean value. An exception was made to vegetation forest length ( $L_v$ ) which was curtailed at 1500m to avoid high computational expense.

### – Distributions

Marginal distributions were defined to capture the variability of each parameter in the most realistic manner possible. These distributions might be different for local datasets but in order to cover the range of nature's variability across the globe, distributions were extended or modified for some of the variables. No change was made if they were determined from the data or literature.

### – Correlations

Correlations were estimated between parameters to stay in the window of physically realistic conditions. Initially these correlations were specified based on the bivariate dependence of parameters. However, due to the multivariate dependence, as presented in Figure 3.10, conditionality was introduced among parameters due to which partial rank correlations were calculated using Equation 3.3.

### 3.2.1. STOCHASTIC MODEL SETUP

The stochastic model was made in the user-defined mode of UNINET in order to sample input parameters for XBeach global runs.

#### Random Variables

Marginal distributions of the random variables were continuous and were selected from a range of parametric distributions available in UNINET. Ranges and distributions of all the random variables with their distributions were defined which have been summarized in Table 3.2.

### Probabilistic Nodes

Probabilistic nodes were created based on the defined random variables which later combined with arcs formed the directed acyclic graph (DAG) for the stochastic model.

### Influences

Influences were drawn and conditional rank correlations were designated based on conditional bivariate correlations determined through data or expert judgment, pursue detailed explanation in Section A.3. Some of the variables were conditionally dependent on the parent of the immediate parent node. These correlations were calculated by UNINET by using to Equation 3.3. Parent nodes and conditional rank correlations were reordered to make certain that these correlations are algebraically independent.

### Functional Nodes

Functional nodes were added to calculate the other commonly used notations for vegetated hydrodynamic systems *e.g.* vegetation factor, relative depth, wave steepness, breaker parameter etc. Functional nodes have parent nodes as the arguments of the function and are created only for purposes of better explanation of the model and comparison to other studies since they can't actively participate in the Bayesian network due to inability of rendering probabilistic child nodes.

### Sampling

Analytical conditioning of the network was performed by UNINET and Monte Carlo sampling was carried out to generate 300 samples establishing the inputs for vegetation modeling in XBeach.

## 3.2.2. MARGINAL DISTRIBUTIONS

Marginal distributions define the probability behaviour of a random variable without having any influence from other random variables. The choice of a marginal distribution is very sensitive to the available dataset in terms of where it was collected, how it was collected, what time scales does it represent etc. While determining the marginal distributions foremost preference was that the marginal distributions are derived from the data over multiple spatial domains and long temporal scales. However, when it was not possible local datasets at specific locations were used to derive the first best assessment of the distributions. As a last resort, in case of no data availability, literature was consulted to see if there are any formulations giving general trends of the parameter variability to infer distributions.

Some of the distributions which are common in hydraulic engineering are not available in UNINET like Rayleigh distribution. In the cases where distributions were unknown or the specific distributions had not been implemented in UNINET beta distribution, which belong to the family of Dirichlet distribution, was adopted. It was chosen for most of the variables because of its ability to handle fixed bounds and to function as a symmetric as well as a skewed distribution based on the values of its shape parameters  $\alpha, \beta$ .

Marginal distributions of wave height ( $H_{m0}$ ), peak wave period ( $T_p$ ), and water depth ( $h$ ), along with inter-parameter cross-scatter helped to define the input parameter joint distributions for the XBeach global runs and eventually the Bayesian network. In Figure 3.5, there is a clear correlation between wave height and water depth but there isn't much

**Table 3.2:** Input parameters for vegetated hydrodynamic system. Ranges and distributions along with correlations from Table 3.4 forms the foundation of stochastic modeling for parameter sampling. Refer to Table A.1 for complete distribution parameters.

Parameter	Symbol	Unit	Range	Distribution	Source
Offshore Wave Height	$H_{m0}$	m	0.1 to $\approx 8$	Weibull	<a href="#">Chu et al. (2010)</a>
Peak wave period	$T_p$	s	1 to $\approx 30$	Gamma	<a href="#">Xu et al. (2004)</a>
Water depth	$h$	m	0.01 to 5	Uniform	<a href="#">Hawkes et al. (2002)</a>
Offshore slope	$S_0$	–	$\frac{1}{10}$ to $\frac{1}{500}$	Beta	Experts
Veg. forest length	$L_v$	m	1 to 1500	Beta	<a href="#">Songy (2016)</a>
Vegetation slope	$S_v$	–	$\frac{1}{500}$ to $\frac{1}{1000}$	Beta	Expert
<b>Benthic</b>					
Friction coefficient	$c_f$	–	0.01 to 0.1	Beta	<a href="#">Rahmeyer (1996)</a>
<b>Submerged</b>					
Vegetation height	$h_v$	m	0.02 to 1.75	Beta	<a href="#">van Zelst (2018)</a>
Frontal width	$b_v$	m	0.0001 to 0.025	Beta	<a href="#">van Zelst (2018)</a>
Vegetation density	$N_v$	stems/m <sup>2</sup>	10 to 2000	Beta	<a href="#">van Zelst (2018)</a>
Drag coefficient	$C_d$	–	0.1 to 3	Beta	<a href="#">Hu et al. (2012)</a>
<b>Emergent</b>					
Stems height	$h_{v,s}$	m	0.1 to 5	Beta	<a href="#">Simard et al. (2019)</a>
Stems frontal width	$b_{v,s}$	m	0.01 to 0.25	Beta	<a href="#">Janssen (2016)</a>
Stems density	$N_{v,s}$	stems/m <sup>2</sup>	0.1 to 100	Beta	<a href="#">Janssen (2016)</a>
Stem drag coefficient	$C_{d,s}$	–	0.1 to 2.5	Beta	<a href="#">Hu et al. (2012)</a>
Trunk height	$h_{v,t}$	m	0.1 to 4	Beta	<a href="#">Simard et al. (2019)</a>
Trunk frontal width	$b_{v,t}$	m	0.1 to 0.8	Beta	<a href="#">Marek (2019)</a>
Trunk density	$N_{v,t}$	trunk/m <sup>2</sup>	0.5 to 5	Beta	<a href="#">Janssen (2016)</a>
Trunk drag coefficient	$C_{d,t}$	–	0.1 to 3	Beta	<a href="#">Hu et al. (2012)</a>
Roots height	$h_{v,r}$	m	0.2 to 6	Beta	<a href="#">Simard et al. (2019)</a>
Roots frontal width	$b_{v,r}$	m	0.004 to 0.1	Beta	<a href="#">Janssen (2016)</a>
Roots density	$N_{v,r}$	roots/m <sup>2</sup>	1 to 250	Beta	<a href="#">Janssen (2016)</a>
Roots drag coefficient	$C_{d,r}$	–	0.1 to 4	Beta	<a href="#">Hu et al. (2012)</a>
<b>Hybrid</b>					
Dike slope	$S_d$	–	$\frac{1}{2}$ to $\frac{1}{10}$	Beta	Experts
Crest level	$h_c$	m	1 to 20	Gaussian	Expert

dependence between wave period and water depth. Defining such correlations allows us to stay within realistic window while performing Monte Carlo sampling.

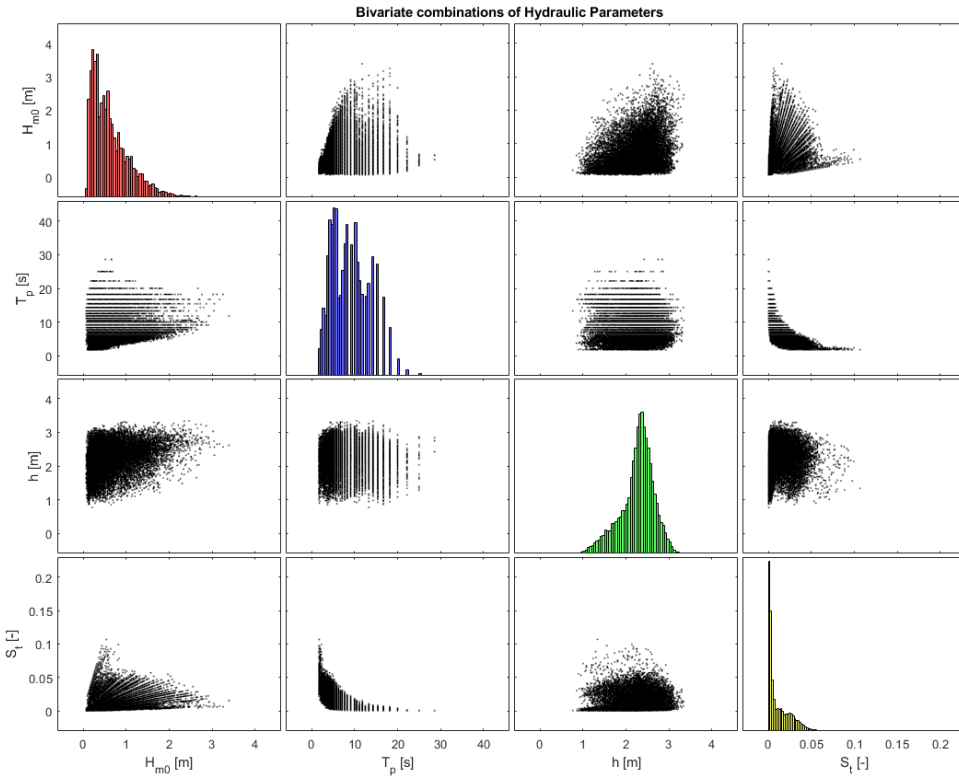


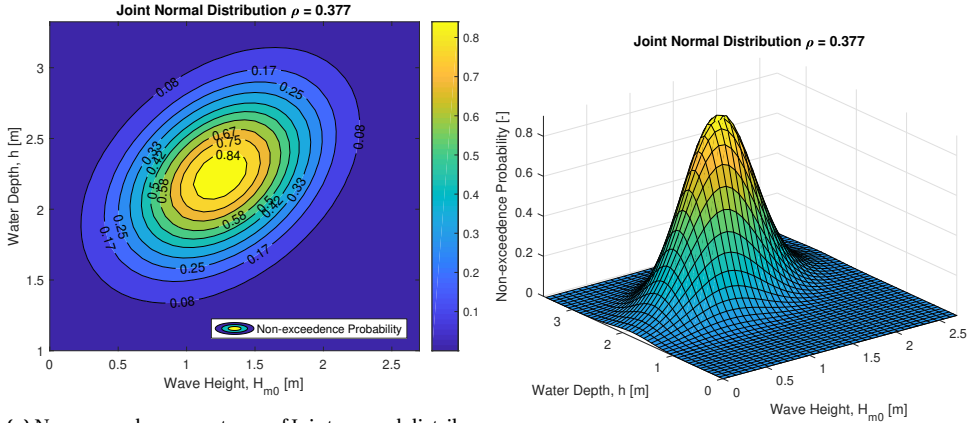
**Figure 3.5:** Bivariate matrix of hydraulic parameters obtained from field data from a wave buoy and a tidal gauge near Milford, UK. The data was taken for the entire year of 2018 to capture the seasonal variation and further quality controlled for the non realistic values, see Table A.2.

### 3.2.3. COPULAS & CORRELATIONS

Copulas are ranked correlations of the data which have uniform marginals (Genest & Favre, 2007). In order words, it's a joint distribution of the data which is ranked from 0 to 1 therefore making a joint density on unit square. The 'bonding' of the data is expressed through linear correlation coefficient also known as Pearson's correlation coefficient while the correlation for the copula is rank correlation coefficient also known as Spearman's correlation coefficient. Gaussian copula is presented in Equation 3.2 taken from (Sadegh et al., 2017; C. Li et al., 2013).

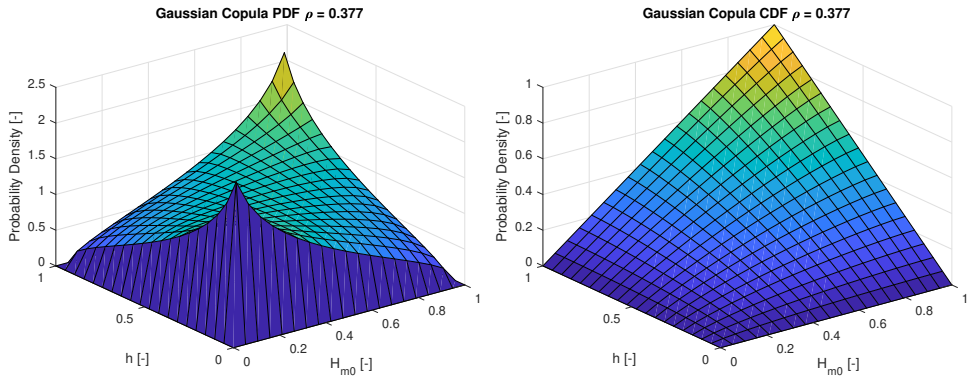
$$C = \int_{-\infty}^{\phi^{-1}(u)} \int_{-\infty}^{\phi^{-1}(v)} \frac{1}{2\pi\sqrt{1-\theta^2}} \exp\left(\frac{2\theta xy - x^2 - y^2}{2(1-\theta^2)}\right) dx dy^b ; \theta \in [-1, 1] \quad (3.2)$$

where;  $\phi$  is a standard Gaussian distribution presented in Equation A.1.



(a) Non-exceedance contours of Joint normal distribution

(b) Joint normal distribution



(c) Gaussian copula probability density function

(d) Gaussian copula cumulative density function

**Figure 3.6:** Gaussian copula and correlations from global wave climate data for offshore wave height ( $H_{m0}$ ) and water depth ( $h$ ). The linear correlation coefficient, Pearson's  $\rho$ , shows the strength of the correlation between bivariate realizations.

The case for wave heights ( $H_{m0}$ ) and water depths ( $h$ ) from the data specification presented in Table A.2 is introduced in Figure 3.6. Based on the mean, variance and covariance of both parameters the joint normal distribution could be constructed. Linear correlation coefficient Pearson's  $\rho$  could be determined from the bivariate data which is the only parameter required to build a Gaussian copula. Only in the case of a  $t$ -copula for wave heights ( $H_{m0}$ ) and peak wave period ( $T_p$ ), the degrees of freedom were determined from fitting the  $t$ -copula to the data.

The joint normal distribution in Figures 3.6a and 3.6b is valid if the two variables are normally distributed but for simplicity joint normal distribution is assumed. It builds on to Gaussian copula in Figures 3.6c and 3.6d which is the implemented in UNINET, therefore the assumption stays consistent in both parameter analysis and the Bayesian network.

### DATA PROCESSING

The correlations could be derived from the data if the data is reliable and caters natural variability along with statistical stability. Fortunately, for some of the parameters data was available but in different forms and from different parts of the world. The struggle was real to get homogeneous data which also could be globally representative. Scarcity of the literature on giving specific correlations used in this work led to determining the correlations through datasets available.

#### VEGETATION HEIGHT ( $h_v$ ) & FRONTAL WIDTH ( $b_v$ )

The data for vegetation was available for Chesapeake Bay in the north-eastern part of US<sup>1</sup>. The field data was acquired at four different stations along a transect mainly accommodating *Spartina alterniflora* and *Spartina patens* species. The measuring instruments were four sensors and 2 Acoustic Doppler current profilers (ADCPs).

Figure 3.7 illustrates the methodology used to sample the parameters through the copula fitted to the field data. The raw data in Figure 3.7a already shows the positive correlation between vegetation height ( $h_v$ ) and frontal width ( $b_v$ ) but to generate a copula the data must have uniform marginal distributions. Therefore, as in Figure 3.7b, the data was transformed on a unit square based on it's density over equal intervals of the data.

In Figure 3.7b, the two peaks in the uniform marginal of probability density of vegetation heights are representative of the two populations *i.e.* two saltmarsh species. The essence of the copulas lies in ranking the data which makes it possible to get rid of the peaks and form a generalized correlation of the same bivariate data. This is also one of the biggest reasons why copulas are more powerful and preferable than working with the real values of the non-homogeneous data.

The uniformly distributed data enables to fit any copula but Gaussain copula was used in this work as the Non-Parametric Bayesian network in UNINET uses Gaussain copulas. The copula in Figure 3.8a could be used to generate data for any range of parameters. Random sampling for both parameters has been transformed back to original scale of

<sup>1</sup>The author is highly obliged to Albrecht, A.M. (Alissa) and Lashley, C.H. (Christopher) for providing the vegetation data and making the much needed probabilistic analysis on vegetation parameters possible.

the data Figure 3.8b.

One must be careful to use the random sampling from the copula directly as an input to the numerical model because this is merely bivariate sampling. The same parameters could embrace dependence on other parameters as well which calls for a multivariate approach. This very reason formed the basis to not use these samples and carry out multivariate stochastic modeling.

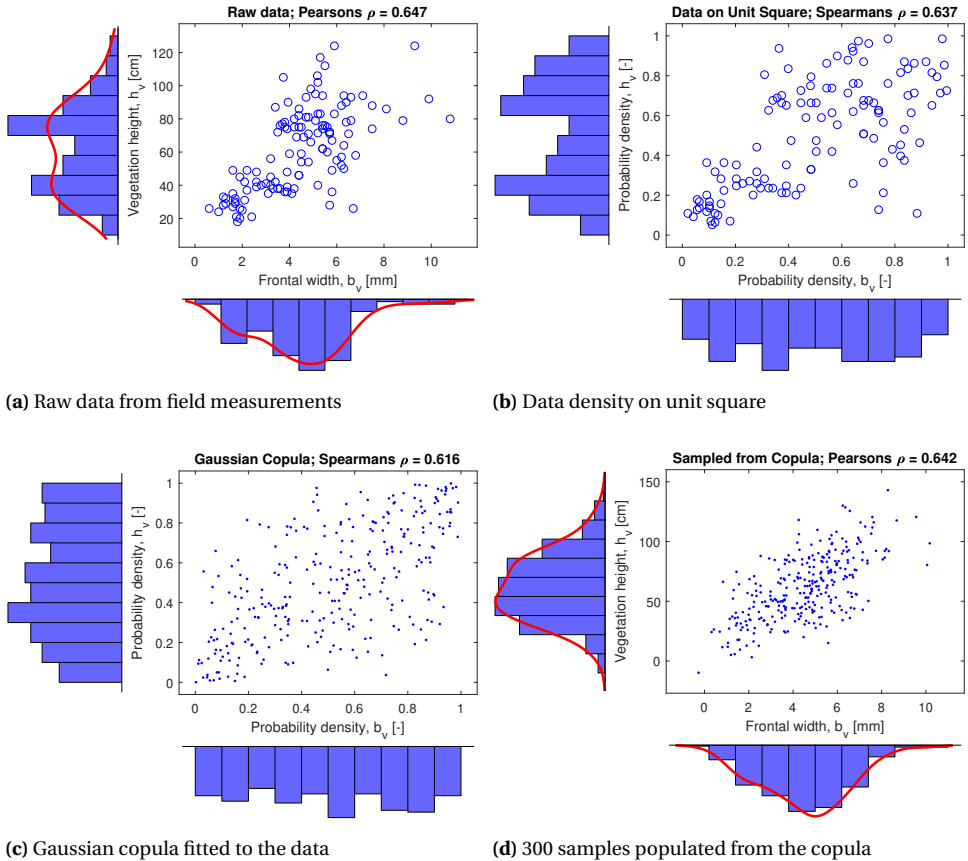


**Figure 3.7:** Copula and correlations from field data for vegetation height ( $h_v$ ) and frontal width ( $b_v$ ).

The analysis shows a strong positive correlation between vegetation height ( $h_v$ ) and frontal width ( $b_v$ ). The ranked correlation coefficient of 0.616 was calculated which was one of the input to the stochastic modeling for parameter sampling. Besides the copula, marginal distributions were also estimated which provided a good intuition about the type of distribution to be used. Nevertheless, it must be noted that this distribution and correlation coefficient is merely based on the data from one site. Further studies could use this as a first estimate but should prefer collecting more data to not standardize nature's variation from point scales to globe scales.

WAVE HEIGHT ( $H_{m0}$ ) & PEAK WAVE PERIOD ( $T_p$ )

The data for offshore wave heights and peak wave periods was collected from ©BMT ARGOSS website for ten cities of the world. 400km tile was specified as the size of the data area in the biggest deltas which have vegetated foreshore. The ball-park idea about which deltas to select was inspired from world vegetation map of Moffett et al. (2015), presented in Figure 1.6. The cities in Table 3.3 represent all continents and most types of vegetated hydrodynamic conditions in varied sea states<sup>2</sup>.

Table 3.3: World wave climate based on ten cities in biggest deltas having vegetated foreshores.

City, Country	Location	Vegetation	Wave Height ( $H_{m0}$ )		Wave Period ( $T_p$ )	
			Mean	Variance	Mean	Variance
Los Angeles, USA	33°N120°W	Saltmarsh	2.17	0.73	11.99	9.73
Mérida, Mexico	21°N090°W	Seagrass	0.44	0.07	4.13	2.55
São Luís, Brazil	01°S043°W	Mangroves	1.63	0.15	8.71	6.77
Texel, Netherlands	53°N005°E	Saltmarsh	0.82	0.46	5.91	5.03
Lagos, Nigeria	05°N003°E	Seagrass	1.34	0.13	12.69	4.30
Dubai, UAE	25°N054°E	Seagrass	0.60	0.18	4.99	1.14
Karachi, Pakistan	24°N067°E	Mangroves	1.35	1.38	10.39	11.50
Shanghai, China	32°N122°E	Saltmarsh	0.95	0.32	5.45	3.40
Surabaya, Indonesia	06°S113°E	Mangroves	0.63	0.17	4.32	1.44
Sydney, Australia	34°S152°E	Saltmarsh	2.15	0.87	9.29	8.99

Units for wave height are meters and wave period are seconds.

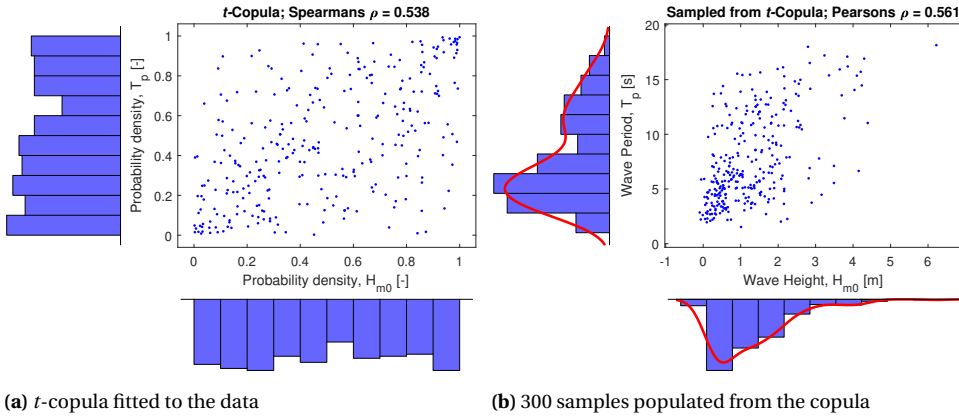


Figure 3.8:  $t$ -copula and correlations from global wave climate data for wave height ( $H_{m0}$ ) and peak wave period ( $T_p$ ).

Positive correlation is observed between offshore wave height ( $H_{m0}$ ) and peak wave pe-

<sup>2</sup>For some locations like in Mérida, Mexico tropical storms are likely to occur but these were not properly represented in the data. Therefore, while using the values from Table 3.3 for case studies it is advised to perform peak over threshold for calculating wave parameters during storms.

riod ( $T_p$ ) with the rank correlation coefficient of 0.538. Jäger & Nápoles (2017) reported the rank correlation of 0.78 based on a vine-copula model. However, this value was restricted to North Sea and wave period parameter was mean zero-crossing period.

### EXPERT JUDGMENT

Utilizing the merits of non-parametric Bayesian networks and avoiding the computational expense, limited number of input conditions which are representative of global vegetated hydrodynamic systems have been modeled. These input conditions are Monte Carlo sampled from a multivariate stochastic model. Every parameter is probabilistically defined through ranges, distributions, and correlations. For some of the parameters data was available but for some a well-known classical model of expert judgment was being used (R. Cooke, 1991; Kurowicka & Cooke, 2004; Morales Napoles et al., 2008; R. M. Cooke & Goossens, 2008; Morales-Nápoles et al., 2014; Werner et al., 2017).

The classical model could not be implemented in its true letter and spirit due to limited number of responses from the expert panel. However based on verbal communication from experts, following the approach in Figure 3.9 was carried out.

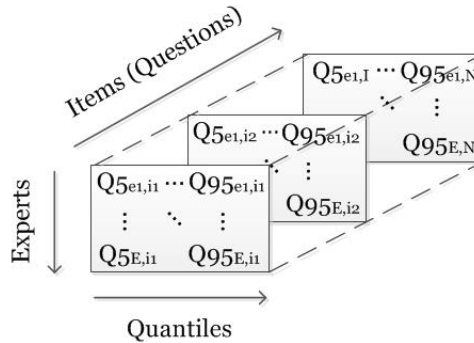


**Figure 3.9:** Three-dimensional arrays of item questions about quantiles assessments from experts for structured expert judgment based on ANDURIL (Leontaris & Morales-Nápoles, 2018). ANDURIL is abbreviated form of 'ANalysis and Decisions with Uncertainty: Learning from expert judgments'.

Ten members of the scientific community researching about vegetation as a flood defense formed the panel of experts who were consulted for their judgment. Table 3.2 and Table 3.4 was shared and following questions were asked:

- Are the ranges representative of vegetated-hydrodynamic system on global scale?
  - Could you propose your own minimum, mean and maximum value?
- Could you propose distributions?
- Do you agree with the correlations defined between parameters?
  - Do you think they exist?
  - If yes, what do you think the correlation coefficient would be?

The reason to carry out expert judgment was the scarcity of data and literature about the dependence information of specific variables that seemed inevitable to exist. The correlations defined based on expert judgment were mainly for vegetation and hybrid parameters. These were important to be defined because while Monte Carlo sampling any value could have been picked with any other value which meant that either some input control had to be defined or the sampling the sampled input conditions had to be tweaked.

It was exactly this reason, to avoid such tweaks, that the correlations through expert judgment were defined to make the method more reliable right from the start. This assured that in one iteration all the parameters are sampled in such a way that they represent a realistic system somewhere in the world.

### CORRELATIONS

Copulas were computed for the parameters with the data availability and for the rest expert judgment was used. The resulting rank correlations are summarized in Table 3.4.

**Table 3.4:** Rank correlations between global saltmarsh system. See Figure 3.11 for correlation of global mangrove system.

Correlations	Nature	Coefficient	Source
$H_{m0} \leftrightarrow T_p$	+	0.54	Data
$H_{m0} \leftrightarrow h$	+	0.37	Data
$S_v \leftrightarrow H_{m0}$	+	0.41	Expert Judgment
$S_v \leftrightarrow L_v$	-	0.33	Expert Judgment
$S_v \leftrightarrow N_v$	-	0.57	Expert Judgment
$h_v \leftrightarrow b_v$	+	0.62	Data
$N_v \leftrightarrow h_v$	-	0.38	Data
$N_v \leftrightarrow b_v$	-	0.48	Data
$N_v \leftrightarrow L_v$	-	0.12	Expert Judgment
$b_v \leftrightarrow C_d$	+	0.55	Expert Judgment
$h \leftrightarrow h_c$	+	0.31	Expert Judgment
$S_d \leftrightarrow h_c$	+	0.43	Expert Judgment

The rank correlations coefficients in Table 3.4 only show bivariate dependence. Since, the Bayesian network in Figure 3.10 is a multivariate stochastic model, there is a possibility of multivariate dependence when a child node has two parents. For instance, rank correlation for vegetation density has been determined from data for vegetation height ( $N_v \leftrightarrow h_v$ ) and frontal width ( $N_v \leftrightarrow b_v$ ) but frontal width could only be correlated to vegetation density given vegetation height. Therefore, conditional rank correlation coefficient were calculated using recursive formula (Yule, 1919; A. M. Hanea et al., 2006).

$$\rho_{12|3,\dots,n} = \frac{\rho_{12|4,\dots,n} - \rho_{13|4,\dots,n} \cdot \rho_{23|4,\dots,n}}{\sqrt{(1 - \rho_{13|4,\dots,n}^2) \cdot (1 - \rho_{23|4,\dots,n}^2)}} \quad (3.3a)$$

However, in the very model conditionality is only imposed by one parameter, therefore the formula reduces to:

$$\rho_{12|3} = \frac{\rho_{12} - \rho_{13} \cdot \rho_{23}}{\sqrt{(1 - \rho_{13}^2) \cdot (1 - \rho_{23}^2)}} \quad (3.3b)$$

where  $\rho_{12|3,\dots,n}$  is the conditional rank correlation coefficient (partial correlation) of random variables  $X_1$  and  $X_2$  given  $X_3, \dots, X_n$ .

**Table 3.5:** Conditional (partial) rank correlations between input parameters. To define partial correlations additional rank correlation were specified in order to apply recursive formula in Equation 3.3.

Correlations	Nature	Coefficient	Constituents
$\rho_{b_v, N_v   h_v}$	–	0.37	$N_v \leftrightarrow b_v, h_v \leftrightarrow b_v, N_v \leftrightarrow h_v$
$\rho_{L_v, S_v   N_v}$	–	0.49	$L_v \leftrightarrow S_v, L_v \leftrightarrow N_v, N_v \leftrightarrow S_v$

A Bayesian network in Figure 3.10 was created for multivariate stochastic modeling of input parameter. This BN was used to carry out Monte Carlo sampling which formed input conditions for XBeach global model runs. Parameters in Figure 3.2 and Table 3.2 were defined as nodes. Arcs were drawn based on the rank correlations presented in Table 3.4 and partial rank correlations from Table 3.5. Detailed methodology employed to determine these correlation from data and expert judgment is presented in Appendix A.

### 3.3. RESULTS & DISCUSSION: GLOBAL VEGETATED HYDRODYNAMICS

The aim of the stochastic modelling was to represent vegetated hydrodynamic system probabilistically and generate physically realistic input conditions for numerical modelling. The resulting Bayesian network representing global saltmarsh environments is presented in Figure 3.10. The BN captures underlying dependence of the system in which the feedbacks between vegetation and hydrodynamic are covered. Dike or dune parameters are also in the network which enables to study run-up and eventually flood risk mitigation. The multivariate-dependent model in Figure 3.10 has been used to generate Monte Carlo samples of parameters which constitutes input conditions for XBeach global model runs of seagrass-saltmarsh environments. All parameters families, including hydraulic, dike and vegetated parameters, are interconnected through Gaussian copulas calculated at the back end using marginal distributions (nodes) and rank correlation coefficients (arcs).

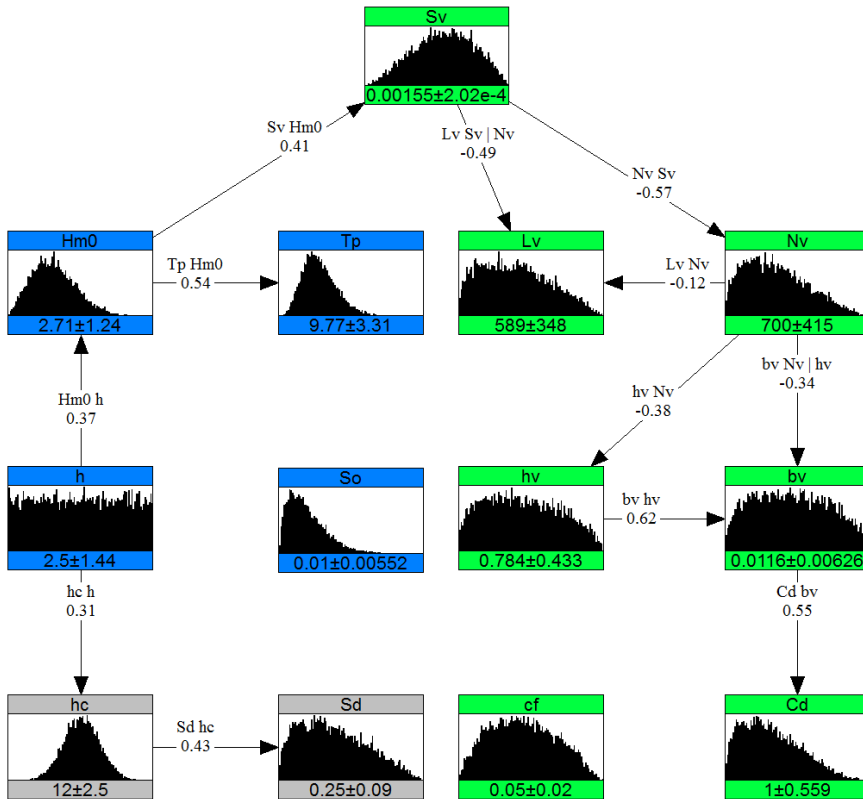


**Figure 3.10:** Bayesian network for stochastic modeling of saltmarsh input parameters. The boxes represent nodes (parameters with their marginal distributions) and lines represent influences (correlations). Color coding could be followed to identify different components in the system: blue for hydrodynamics, gray for dike, light green for seagrass-saltmarsh parameters.

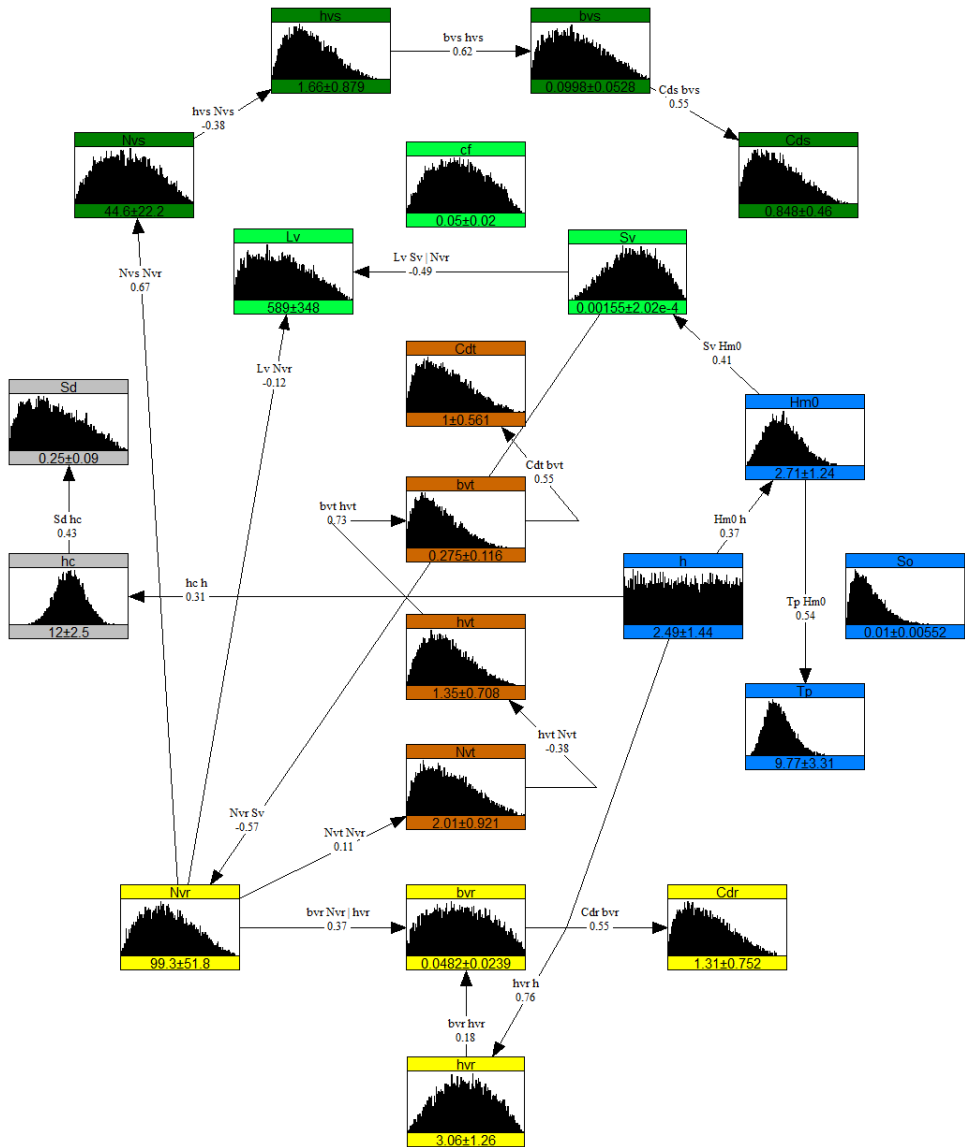


**Figure 3.11:** Bayesian network for stochastic modeling of mangroves input parameters. The boxes represent nodes (parameters with their marginal distributions) and lines represent influences (correlations). Color coding could be followed to identify different components in the system: blue for hydrodynamics, gray for dike, light green for general vegetation parameters, dark green for stems, brown for trunk, and yellow for roots of mangroves.

Similarly, for the seagrass-mangroves environments another BN was developed and is presented in Figure 3.11. The sampling from this BN would form running conditions for seagrass-mangroves environments modeling in XBeach. Carving out the major con-

nections reveal the connections between parameter families like hydraulic parameters influence overall vegetation forest parameters, dike parameters and mangrove root parameters. This, for instance, in case of relatively extreme hydraulic conditions makes sure we get samples of reflective beaches, higher and steeper dikes or dunes with higher mangrove roots. Similarly, root parameters influence trunk and stem parameters as root structure categorizes mangroves and could be used in differentiating mangroves types like juvenile or mature mangroves.

### 3.3.1. CORRELATIONS MATRICES

More correlations are calculated from the ones that have already been defined which are presented through a correlation matrix. UNINET itself determines multivariate dependence among variables beyond the correlations already defined which results in a symmetric correlation matrix. The results could be seen in Table 3.6 in for the correlation matrix of saltmarsh system. Correlations have been drawn out based on the network beyond the the ones which were already defined. The partial correlations have been calculated by the model using Equation 3.3.

**Table 3.6:** Correlation matrix of stochastic model for saltmarshes, also see Figure 3.12. Highest correlation is 1.00, lowest is 0.00. Positive and negative values show positive and negative correlations. The correlations other than the ones in Figure 3.10 have been calculated using Equation 3.3.

	$H_{m0}$	$h$	$T_p$	$c_f$	$S_d$	$h_c$	$L_v$	$N_v$	$C_d$	$h_v$	$b_v$	$S_v$	$S_0$
$H_{m0}$	1.00	0.37	0.54	0.00	0.05	0.12	-0.14	-0.24	0.07	0.09	0.12	0.41	0.00
$h$	0.37	1.00	0.20	0.00	0.14	0.31	-0.05	-0.09	0.03	0.04	0.05	0.16	0.00
$T_p$	0.54	0.20	1.00	0.00	0.03	0.07	-0.08	-0.13	0.04	0.05	0.07	0.23	0.00
$c_f$	0.00	0.00	0.00	1.00	0.00	0.00	0.00	0.00	0.00	0.00	0.00	0.00	0.00
$S_d$	0.05	0.14	0.03	0.00	1.00	0.43	-0.01	-0.01	0.00	0.01	0.01	0.02	0.00
$h_c$	0.12	0.31	0.07	0.00	0.43	1.00	-0.02	-0.03	0.01	0.01	0.01	0.05	0.00
$L_v$	-0.14	-0.05	-0.08	0.00	-0.01	-0.02	1.00	-0.12	0.03	0.05	0.06	-0.32	0.00
$N_v$	-0.24	-0.09	-0.13	0.00	-0.01	-0.03	-0.12	1.00	-0.27	-0.38	-0.48	-0.57	0.00
$C_d$	0.07	0.03	0.04	0.00	0.00	0.01	0.03	-0.27	1.00	0.35	0.55	0.16	0.00
$h_v$	0.09	0.04	0.05	0.00	0.01	0.01	0.05	-0.38	0.35	1.00	0.62	0.22	0.00
$b_v$	0.12	0.05	0.07	0.00	0.01	0.01	0.06	-0.48	0.55	0.62	1.00	0.28	0.00
$S_v$	0.41	0.16	0.23	0.00	0.02	0.05	-0.32	-0.57	0.16	0.22	0.28	1.00	0.00
$S_0$	0.00	0.00	0.00	0.00	0.00	0.00	0.00	0.00	0.00	0.00	0.00	0.00	1.00

The correlation matrices generated by UNINET were transformed to adjacency matrices. The adjacency matrices takes absolute values of correlations have been plotted as could be seen in Figure 3.12 for both the saltmarsh and mangrove models. The dependence, for instance in Figure 3.12c in complex enough to be dealt with deterministic methods. The strength of copulas and dependence modeling allows to learn the influences which are not perceived initially.

### 3.3.2. MONTE CARLO SAMPLING

Monte Carlo sampling is a process of picking up random values from a probabilistically interpreted system. Table 3.7 shows the results of Monte Carlo sampling which form the running conditions for seagrass-saltmarsh environments. The essence of dependence

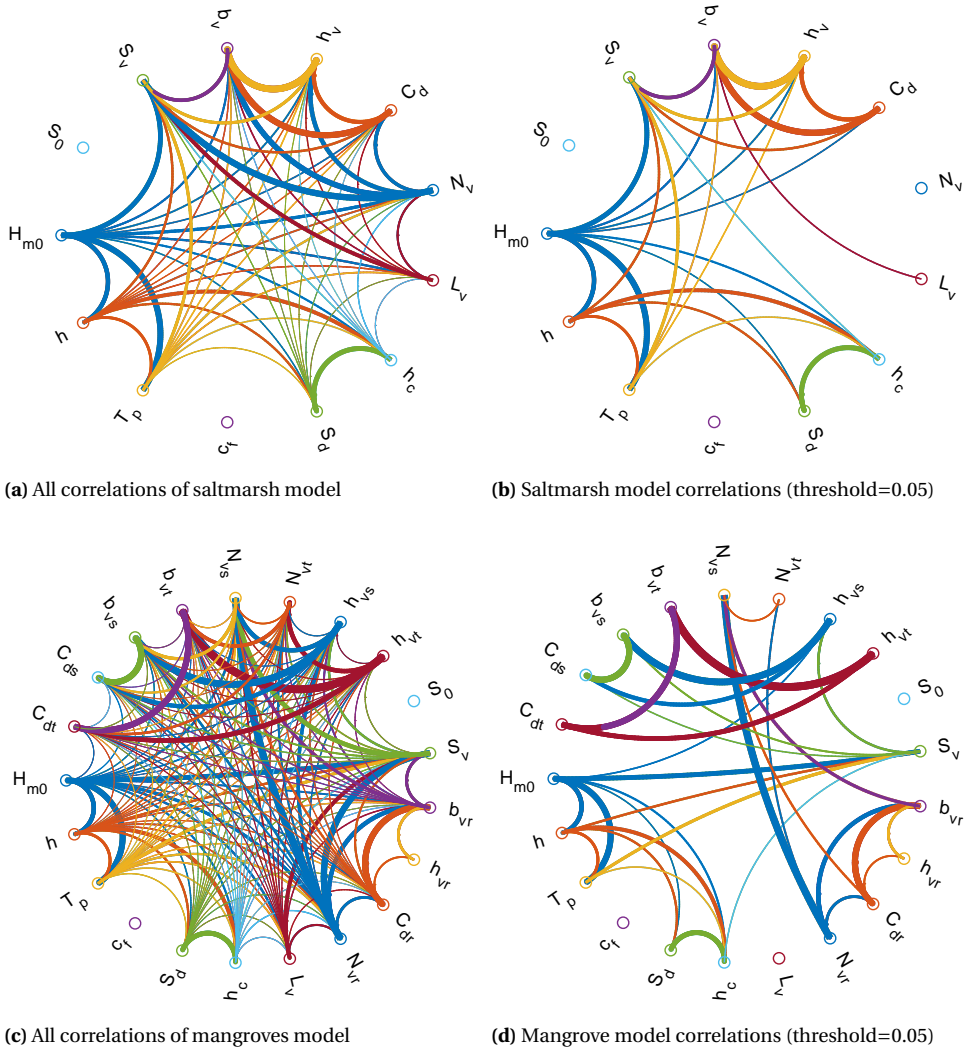


**Figure 3.12:** Correlations in global vegetated hydrodynamic conditions in saltmarshes (a-b) and mangroves (c-d). The circles represent nodes (parameters), lines represent the correlations in the network, and thickness of the lines represents strength of the correlation. Plots (b) and (d) have minimum correlation threshold of 0.05 to distinguish dominant correlations.

modeling has greatly reduced the number of simulations required to feed prediction models. The number of simulations done by (S. G. Pearson et al., 2017; Songy, 2016; van Zelst, 2018) are in the order of  $(O)^4$  to  $(O)^5$ . The number of simulations required by the methodology are a function of number of parameters and the number of permutations per parameter. If any of the two things are increased the number of simulations required increases like a geometric series.

$$\text{Number of simulations} = \prod_{i=1}^n v_i \tag{3.4}$$

where,  $n$  is number of parameters,  $i$  is a given parameter, and  $v$  is the number of variations for a given parameter (S. Pearson, 2016).

With 13 parameters of seagrass-saltmarshes system even if only 13 permutations per parameter are to be numerically modeled, the number of simulation required goes to  $3.2 \cdot 10^{14}$  which is computationally near to impossible. Therefore, extracting the value of copulas and dependence modeling through non-parametric Bayesian networks allows to model all 13 variables as many times as the computational capacity permits. In this study 300 permutations per variable would be modeled.

**Table 3.7:** Monte Carlo samples from stochastic model to be used as input conditions for XBeach global model runs

Run	$H_{m0}$	$T_p$	$h$	$S_0$	$h_v$	$b_v$	$N_v$	$S_v$	$L_v$	$C_d$	$c_f$	$S_d$	$h_c$
1	2.32	11.5	0.39	0.024	0.259	0.006	417	0.00156	309.1	1.63	0.03	0.27	11.18
2	6.63	20.0	3.58	0.011	0.404	0.007	759	0.00165	342.7	1.52	0.072	0.29	13.05
3	3.37	14.2	4.86	0.006	0.911	0.012	1217	0.00131	1075.2	0.91	0.057	0.36	12.04
4	4.69	8.2	2.99	0.007	0.109	0.002	651	0.00175	478.2	0.72	0.061	0.3	14.8
5	0.15	5.1	0.53	0.007	0.667	0.013	1464	0.00118	168.3	1.73	0.079	0.12	12.69
6	1.29	8.5	0.81	0.021	0.653	0.021	372	0.00179	1310.3	1.98	0.052	0.15	11.63
7	1.95	8.9	0.84	0.021	0.147	0.010	125	0.00174	1224.4	1.37	0.093	0.16	13.17
8	7.14	13.0	2.23	0.005	1.625	0.024	504	0.00199	4.4	1.56	0.074	0.29	11.42
9	1.37	5.6	0.78	0.014	0.219	0.001	1311	0.00164	676.5	0.35	0.062	0.16	10.31
10	1.72	8.3	0.56	0.011	0.462	0.017	1086	0.00174	123.91	1.52	0.065	0.25	9.79
⋮	⋮	⋮	⋮	⋮	⋮	⋮	⋮	⋮	⋮	⋮	⋮	⋮	⋮
300	1.30	8.2	0.84	0.012	0.731	0.008	140	0.00164	1200.97	0.71	0.08	0.26	9.92

An example of the sampling result could be seen in Figure 3.13. These show combinations of foreshore slope, vegetation forest length, crest level, and dike slope. Implicitly, the sampled profiles also caters changes in hydraulic characteristics as the offshore bed level is calculated through  $kh$  criterion. Based on varying water depth and wave length offshore bed level is different is every permutation however the boundary condition stays the same *i.e.*  $kh = 1$  therefore making is more of a dynamic boundary condition. Due to changed offshore bed level and other varying parameters like offshore slope and forest length whole profile changes making every run distinct.

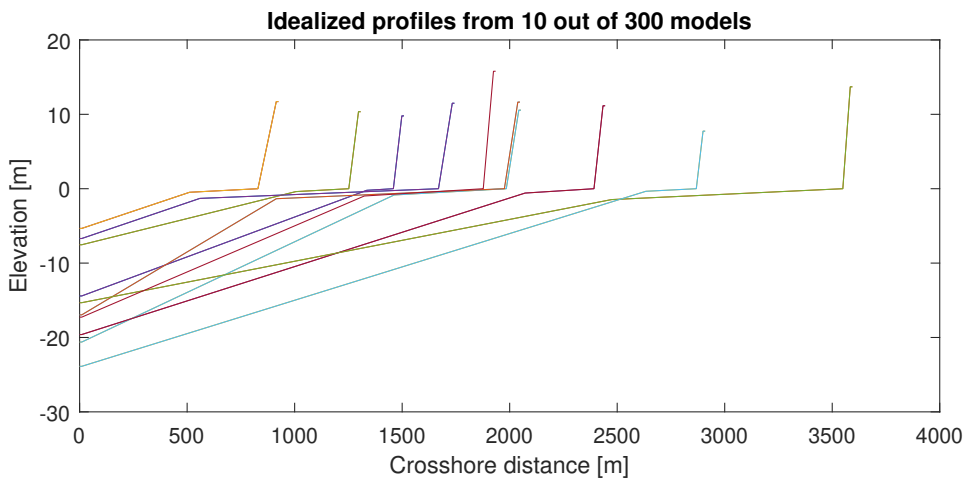


**Figure 3.13:** Profile samples from 10 random models. Shows the variation of slopes  $S_0$ ,  $S_V$ ,  $S_d$ , vegetation forest length  $L_V$ , crest level  $h_c$  and the effect of water depth and wave number (local  $kh$  criteria) which determines offshore bed level ( $z_{b,0}$ ) relative to the dike toe ( $z = 0$  m).

# 4

## REACTION: NUMERICAL MODEL & VEGETATION RESPONSE

*All models are wrong,  
but some are useful.*

George E. P. Box

### Abstract

Numerical implementation of global vegetated hydrodynamic system in XBeach Non-Hydrostatic mode has been presented. The coupled system of seagrasses-saltmarshes and seagrasses-mangroves was modeled with former as one and latter as three vertical layer schematizations. Wave attenuation, wave set-up and wave run-up has been analyzed through spectral evolution of short wind, infragravity and very low frequency waves. The global model runs form the large synthetic dataset for the prediction tool.

NUMERICAL modeling was carried out primarily to develop a large synthetic dataset to feed the Bayesian network and quantify vegetation-induced wave attenuation, wave set-up and wave run-up.

To carry out numerical simulations system idealization and parameterization was required in a way that we can grasp reality of vegetated hydrodynamic systems along with keeping the model as simple as possible to curtail the computational expense, see Chapter 3. Before moving on to running model multiple times for dataset preparation through global model runs, it was made sure through case model runs that the model behaviour is correct and reliable.

Numerical modeling was carried out through an open source numerical model: XBeach. Besides XBeach, other models developed indigenously at TUDelft and Deltares like SWAN and SWASH were also under consideration. SWASH is equally capable as XBeach in terms of computational efficiency and modeling freedom but XBeach was selected due to limited amount of vegetation modeling done using XBeach. The idea was to contribute not only to nature-based solutions but also to advocate for more and more tools, like this open-source numerical model, helping to improve the understanding about such systems.

Furthermore, XBeach Non-Hydrostatic mode was chosen over surfbeat or stationary modes because of its ability to:

- Transform and resolve short wave height and period
- Include long infragravity and low-frequency waves
- Perform vegetation interaction with short and long infragravity waves
- Compute run-up and overtopping directly

The scales and processes involved in wave-flow-vegetation interaction are relatively small which makes spectrally averaged models insufficient to explain complete vegetated hydrodynamics (S. Pearson, 2016). Bed changes along with variation through the vertical water column affects wave breaking, setup, reflection, bottom friction, percolation, wave induced currents, and wave-current interaction (S. Pearson, 2016) and Nwogu & Demirbilek (2010) suggests to resolve low-frequency process as well.

Furthermore, while attenuation of long infragravity waves in vegetated environments has been reported (Mei et al., 2011; Chang et al., 2017; Tang et al., 2017; Zainali et al., 2018; Chang & Liu, 2019), it has also been reported that long wave run-up varies significantly based on local bathymetry and vegetation characteristics (Tang et al., 2017). On the higher frequency side in the spectrum, incident short waves contribution to run-up is also well reported therefore, it is important to use a phase-resolving model for both high and low frequency waves.

## 4.1. GLOBAL MODEL SETUP

Global models represent the modeling exercise done multiple times for the range of input parameters over a schematization that represent the vegetated hydrodynamic systems around the globe. Different combinations of hydrodynamics, physical conditions, sea states, vegetation types, vegetation characteristics, and flood defence extents have been modelled to cover the entire space of variations. The numerical model architecture in Figure 4.1 gives an overview of how the modeling was carried out.

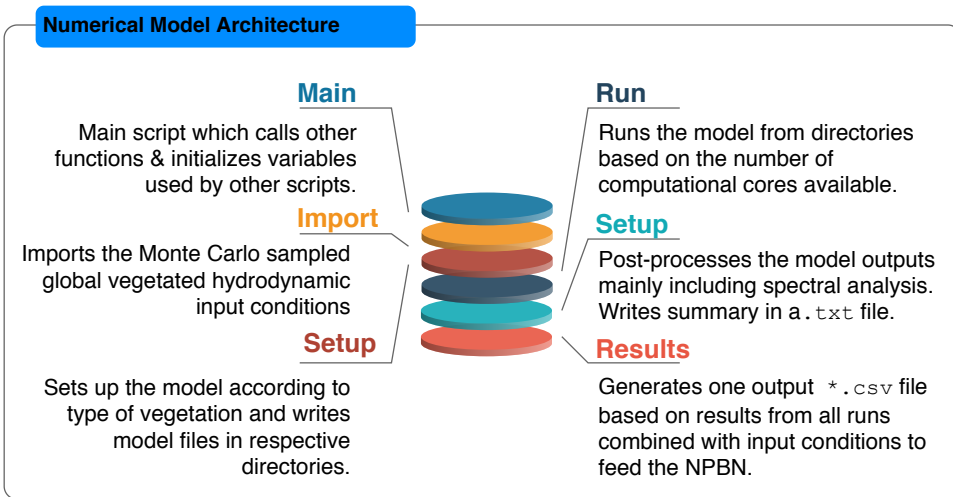


**Figure 4.1:** Scripts overview for vegetation modeling in XBeach using MATLAB

Following the idealized profile in Figure 3.1, the bathymetry was defined starting from the maximum offshore depth  $z_{b,0}$  which was a function of local- $kh$ . Model running time, including spin-up time, was calculated based on the number of cross-shore grid points. Spectral wave boundary conditions were specified at the offshore boundary. Model spin-up time ensures that the model has reached to stationary condition before the output is generated. Further to grid definition, vegetation was implemented along with general model settings related to physics of the model. Specific model settings were defined including a spatially varying bed friction to account for growing effect of seagrasses towards the shore and hotstart water level to avoid completely dry vegetation bed. The flowchart of the model setup could be followed in Figure 4.3 for sequential overview of model setup.

### 4.1.1. MODEL SETTINGS

General and specific model settings include defining boundary conditions (BC) and initial conditions (IC) necessary for numerical modeling of any convection-advection equation. Apart from general model settings, two specific model setting were introduced namely: spatially varying friction and hotstart water level, both explained hereunder.

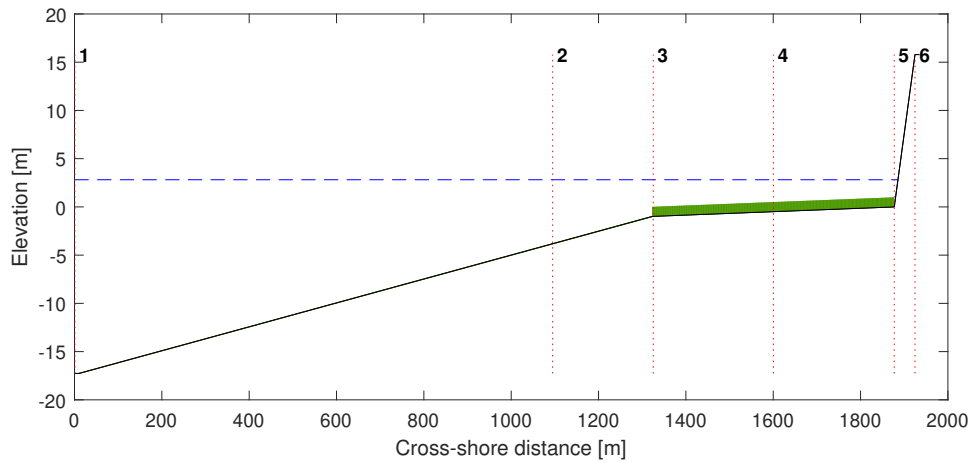


**Figure 4.2:** Numerical model setup based on system idealization of vegetated hydrodynamic system. Black full line shows the bed, blue dash shows still water level, green shows vegetation, and red dotted lines (Points 1-6) show output locations, see Figure 3.1 for details.

### General Model Settings

Morphology and sediment transport modules were turned off as change in bed state was not scoped in this study. Active reflective compensation (ARC) was activated to absorb secondary waves being developed in the numerical domain due to reflection from the boundaries or the dike. If ARC is not applied water would keep piling up in the model resulting in continuous increase in mean water level. Second order corrections in numerical discretization of shallow water equations related to advective non-linear terms were applied for increased accuracy. To control the wave shoaling and breaking process, maximum ratio of wave height to water depth was fixed at 2 and maximum wave steepness was fixed at 0.4.

### Waves

Waves boundary condition was defined through spectral description at the seaward boundary for the period equal to the simulation duration. Parametric spectral input using JONSWAP spectrum was defined for irregular waves *i.e.* spectral shape, wave period and directional spreading were defined. Not only that the waves were irregular for a burst period of maximum 3 hours but also the randomness was introduced by varying next wave timeseries. After performing preliminary sensitivity analysis, and observing no significant difference in results, first order primary wave interaction with its sub-harmonics was specified for computational ease.

### Wave Direction

Wave incidence was kept shore-normal which allowed using one wave direction for all simulations. Due to normal wave incidence the system response would result in conservative values *i.e.* higher run-up and eventually higher overtopping. Secondly, it reduces the computational effort required to extract meaningful results for the schematized system. Changing the wave direction would be appreciated in case coastal erosion or long-

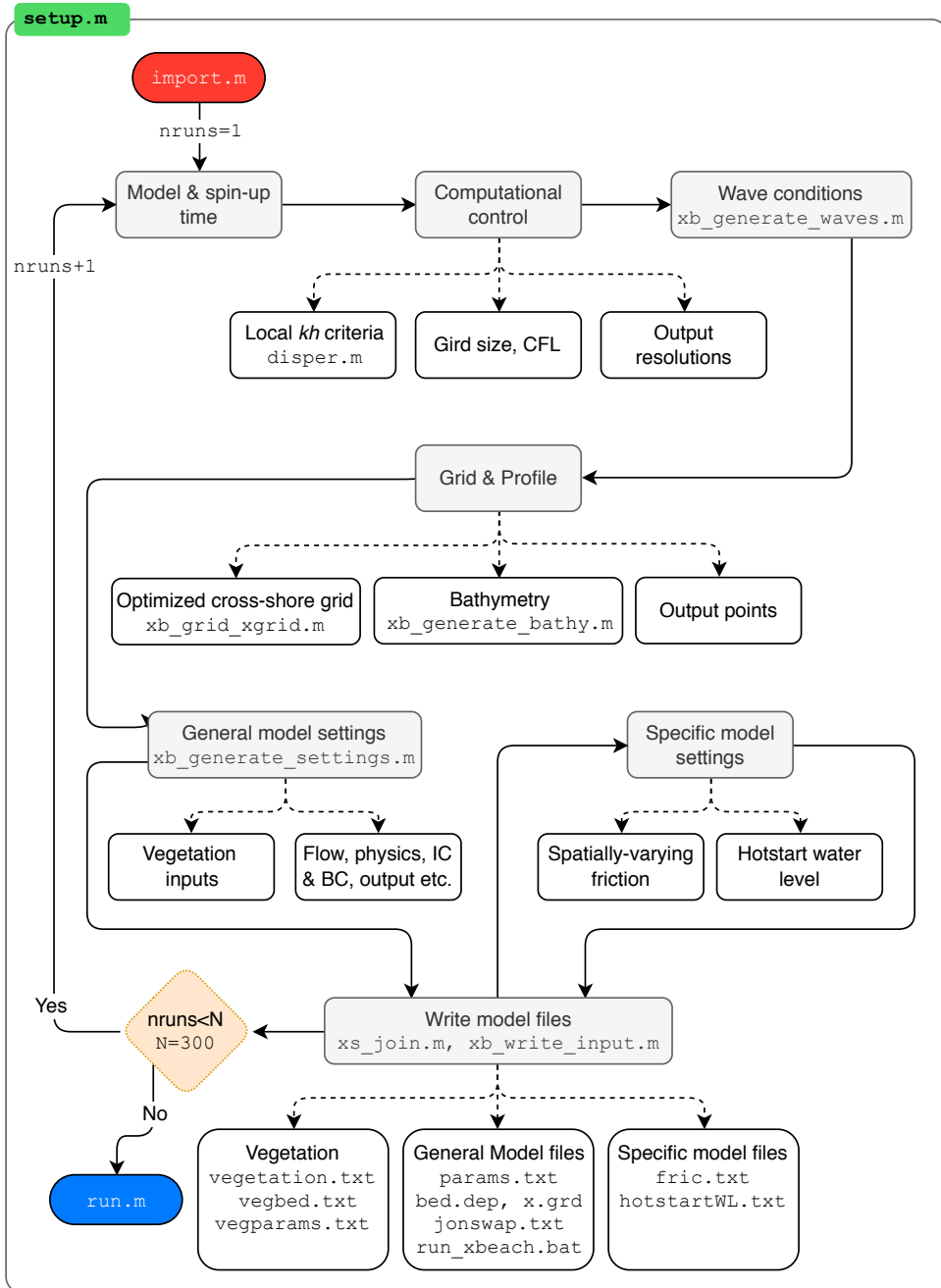


**Figure 4.3:** Pseudocode `setup.m` for XBeach model setup. Full lines could be followed to see major steps whereas dashed lines represent sub-steps of the major step. Special thanks to Pearson, S.G. (Stuart) and van Ormondt, M. (Maarten) from Deltares whose scripts formed the basis of `setup.m`.

shore sediment transport is also studied along with coastal flooding. Nevertheless, keeping wave direction constant gave two-front advantage which is why it outweighed the alternative.

### Computational Grid

Grid size directly corresponds to numerical convergence of solution and hence to the accuracy of the results but at the cost of computational power. Finer grid would yield relatively accurate results but will take more time to run as simulation run time is proportional to number of grid points. Grid sizing was determined through number of grid points per wavelength ( $np=100$ ) and  $CFL=0.7$ . However, XBeach calculated optimized grid size within the user-defined minimum (0.01m) and maximum (1m) grid spacing. Furthermore, variable grid size was allowed to across the cross-shore domain to decrease grid spacing where local wave length was shorter and increase grid size where wave length was longer.

### Temporal Control

Model spin-up time is the time required for the model to reach stationary condition. One way to observe it to see evolution of mean water level; *i.e.* water level timeseries should get stable with time. Therefore, spin-up time was defined based on cross-shore grid points after a sensitivity analysis for the quartiles of cross-shore grid points from all runs. Figure B.3 shows the histogram of all number of grid points and simulation running durations.

### Local- $kh$ criteria

Diketoe was fixed at  $z_{toe} = 0m$  and rest of the depths were calculated positive upwards from this reference. Offshore bed level  $z_{b,0}$  was calculated based on  $kh = 1$  where  $k = \frac{2\pi}{L}$  and  $L$  is local wave length calculated from dispersion relation. Local  $kh$  was used to segregate deep  $kh > 1$ , intermediate  $kh = 0.5$  and shallow water  $kh << 1$ .

Water depth and wavelength affects the dispersion relation  $\omega^2 = gk \tanh(kh)$  which is mainly controlled by  $\tanh(kh)$ . Shallow water has  $kh \ll 1$  and deep water  $kh \gg 1$  which makes  $\tanh(kh) = kh$  for shallow and  $\tanh(kh) = 1$  for deep water. But  $\tanh(kh)$  versus  $kh$  becomes linear from  $kh = 0.3$  (shallow) and becomes flat from  $kh = 2$  (deep) therefore a value of intermediate water is justified between  $kh = 0.3$  and  $kh = 2$ . Now, since XBeach doesn't work for  $kh > 1$  therefore our deep water is  $kh = 1$ , intermediate  $1 > kh > 0.3$  and shallow  $kh < 0.3$  so seagrass was introduced just before shallow water starts at  $kh = 0.5$ .

### Specific Model Settings

Spatially varying friction file was created to account for varying bed roughness of seagrasses due to differential growth. Bed experienced no friction until  $kh = 0.5$  after which bed friction was specified by dimensionless bed friction coefficient  $c_f$  till the diketoe. Moreover, hotstart water level was also introduced as a specific model setting which puts a thin film of water when the still water level was lower than the vegetation bed. It was done for both numerical stability purposes and to make the model more realistic.

### 4.1.2. VEGETATION IMPLEMENTATION

The vegetation systems in this study have been defined by following the classification based on the relative depth between water and vegetation height from Table 2.1. Seagrasses are idealized as benthic vegetation systems, saltmarshes as submerged which means that the water depth approaches vegetation height and mangroves are emergent vegetation systems with multiple vertical layers.

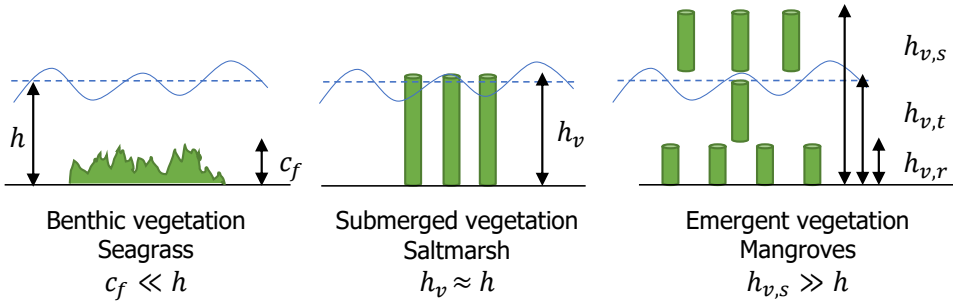


**Figure 4.4:** Implementation of all three types of vegetation in XBeach. Benthic vegetation (seagrasses) was modeled as bottom friction, submerged vegetation (saltmarshes) as rigid cylinders and emergent (mangroves) as rigid cylinder with 3 vertical layer schematizations.

Vegetation models have been implemented in XBeach based on physical significance of height of the vegetation related to the water depth. Benthic vegetation is observed to have minimal influence on the wave traveling on top of mean water level therefore it has been modeled as bed roughness only. This roughness has been parameterized through the friction coefficient  $c_f$ . A spatially varying friction file was created as an input to the models containing seagrass. Saltmarshes and mangroves have been modeled as rigid cylinders in XBeach which are implemented through vegetation height (stem height), drag coefficient, frontal width (stem diameter), and vegetation density.

In reality seagrasses were modeled together with saltmarshes and mangroves to make seagrass-saltmarsh and seagrass-mangrove coupled models. Seagrass was placed before the vegetation forest of saltmarsh or mangrove, as could be seen in Figure 3.2, and was extended till the diketoe. The coupled models were created to avoid unnecessary simulations as the effect of seagrass could be quantified without the influence of other vegetation.

## 4.2. ANALYSIS & POST-PROCESSING

The outputs of XBeach Non-Hydrostatic mode were obtained mainly in the form of water-level timeseries. Spectral analysis on the waterlevel time-series generated at 6 output points for all 300 simulations (global model runs) was carried out separately for saltmarshes and mangroves. Refer to Figure 4.2 to see output locations and to Figure 4.5 to follow the analysis procedure about how each output variable was calculated.

### 4.2.1. OUTPUTS

Bearing in mind the scope of the study, the output from XBeach was generated for water level ( $h$ ), bed level ( $z_b$ ), horizontal velocity ( $u$ ), overtopping ( $Q$ ) and run-up ( $R_{u2\%}$ ). After due analysis, these outputs are enough to explain wave attenuation and flooding in vegetated environments.

For all types of outputs explained hereunder, the results were recorded after the spin up time was completed which means that the flow has developed and waves have reached the dike. Time-averaged spatial output (mean output) is given at intervals of  $t_{intm}$  and instantaneous spatial output (global output) is given at intervals of  $t_{intp}$ . In other words,  $t_{intp}$  determines the sampling resolution of time-series of the water level ( $h$ ), horizontal velocity ( $u$ ), overtopping ( $Q$ ) and run-up ( $R_{u2\%}$ ). For time-averaged outputs like water levels first output is generated at one mean interval step after  $t_{start}$  which is identified by tapering the simulation duration at spin up time. The types of outputs utilized in the model are:

- Instantaneous spatial output referred to as global output  
Global output is generated for water levels  $zs$  and bed levels  $zb$  to have results for instantaneous state of these parameters across the entire model domain at various points in time.
- Time-averaged spatial output referred to as mean output  
Mean output for water levels  $zs$ , bed levels  $zb$  and overtopping discharge  $qx$  is generated to get time-averaged state of variables across the entire model domain at various points in time. The averaging period is described by  $t_{intm}$  which was specified in a way that it divides the model domain in four equal intervals each containing 250 waves.
- Fixed point output referred to as point output  
Time series of water levels  $zs$ , bed levels  $zb$  and overtopping discharge  $qx$  are generated at the observation points shown in 3.1. The points are identified in horizontal plane and are called by XBeach for the nearest computational grid point.
- Run-up gauge output  
Run-up gauge is specified at a location near the vegetation incidence but XBeach moves it to the waterline along the cross-shore transect. It generates a time-series of local coordinates ( $x_w, y_w$ ) and water levels  $zs$  at the moving waterline.

The time-series output starts with the offshore point which is added to get a reference for initial conditions. Benthic vegetation incidence and vegetation incidence points helps to compare wave dissipation due to seagrass. Mid-forest points gives a good reference of the flow-wave-vegetation interaction inside the forest along with an additional reference value for describing wave attenuation as a function of forest length. The point at the vegetation end is also the point identifying dike toe. Conditions at this point helps to study wave attenuation due to vegetation and also describes the design conditions for the dike. Last point at the dike crest gives output only when run-up has exceeded the crest level and overtopping has started to occur.

### 4.2.2. ANALYSIS METHODS

Timeseries of water levels were extracted for all observation points. To avoid miscalculations, in case of a long spin-up time, first time instance was indexed from the timeseries at the diketoe where toe of the dike was submerged and hence waves had arrived. For all frequency splitting in the spectral analysis infragravity waves were split at  $f_{split,IG} = f_p/2$  where  $f_p = 1/T_p$  and very low frequency waves were split at  $f_{split,VLF} = 0.004Hz$ .

#### Run-up, Water Levels & Set-up

Run-up gauge results were extracted using Delft3D Quickplot at the maximum landward point of the water surface. The water level timeseries at this point was sorted to calculate top 2% value as  $R_{u2\%}$ . Energy density spectrum was calculated and frequency splitting was carried out to determine effect of different frequencies on run-up. Swash was calculated based on filtering the timeseries based on high pass and low pass to determine different high or low frequency run-up components. Setup was calculated by taking the mean of this timeseries. Means of the 6 timeseries at observation points resulted in mean water levels. Timeseries at the diketoe was ranked and extreme water level ( $h_{2\%}$ ) was calculated as the top 2% value.

#### Wave Heights & Spectral Period

Water level timeseries was detrended linearly and split into a high and low frequencies using fast Fourier transformation, see Figure 4.6 for the wave components. Variance-conserving smoothed power spectrum was calculated for the different frequency components and root mean squared wave heights ( $H_{rms}$ ) from these wave spectrums were calculated at observation points. Overall root mean squared wave height and the infragravity and very low frequency wave heights ( $H_{rms,Swash}$ ,  $H_{rms,IG}$ ,  $H_{rms,VLF}$ ) were calculated based on the variance of the water level series from run-up gauge. Spectral period ( $T_{m-1,0}$ ) was calculated by taking moments of the total spectrum.

#### Coefficients

Energy density spectrums were determined at all 6 output location and root mean square wave heights were calculated. Using these wave heights four kinds of coefficients were calculated as found in the literature for comparison purposes.

- Attenuation Coefficient ( $K_r$ ): Ratio of difference in wave heights at forest ends to the incident wave height at the forest start  $((H_{rms,start} - H_{rms,end})/H_{rms,start})$ . Attenuation coefficient for saltmarshes ( $K_{r,SM}$ ) and mangroves ( $K_{r,M}$ ) were calculated from their respective global runs.
- Transmission Coefficient ( $K_t$ ): The  $K_t$  is the ratio of the wave height ( $H_{rms,x}$ ) at distance  $x$  inside the forest, which is mid-forest in this study, as compared to the wave height at the start ( $H_{rms,start}$ ).
- Reduction Coefficient ( $R$ ): Reduction of values like velocities and drag forces at the end of forest relative to the start of the forest. Mean langrangian velocity was used to calculate drag forces using Equation 2.20.
- Reflection Coefficient ( $Gr$ ): Ratio of outgoing to incoming waves near the offshore boundary. Guza et al. (1984) method was used to calculate reflection coefficient.

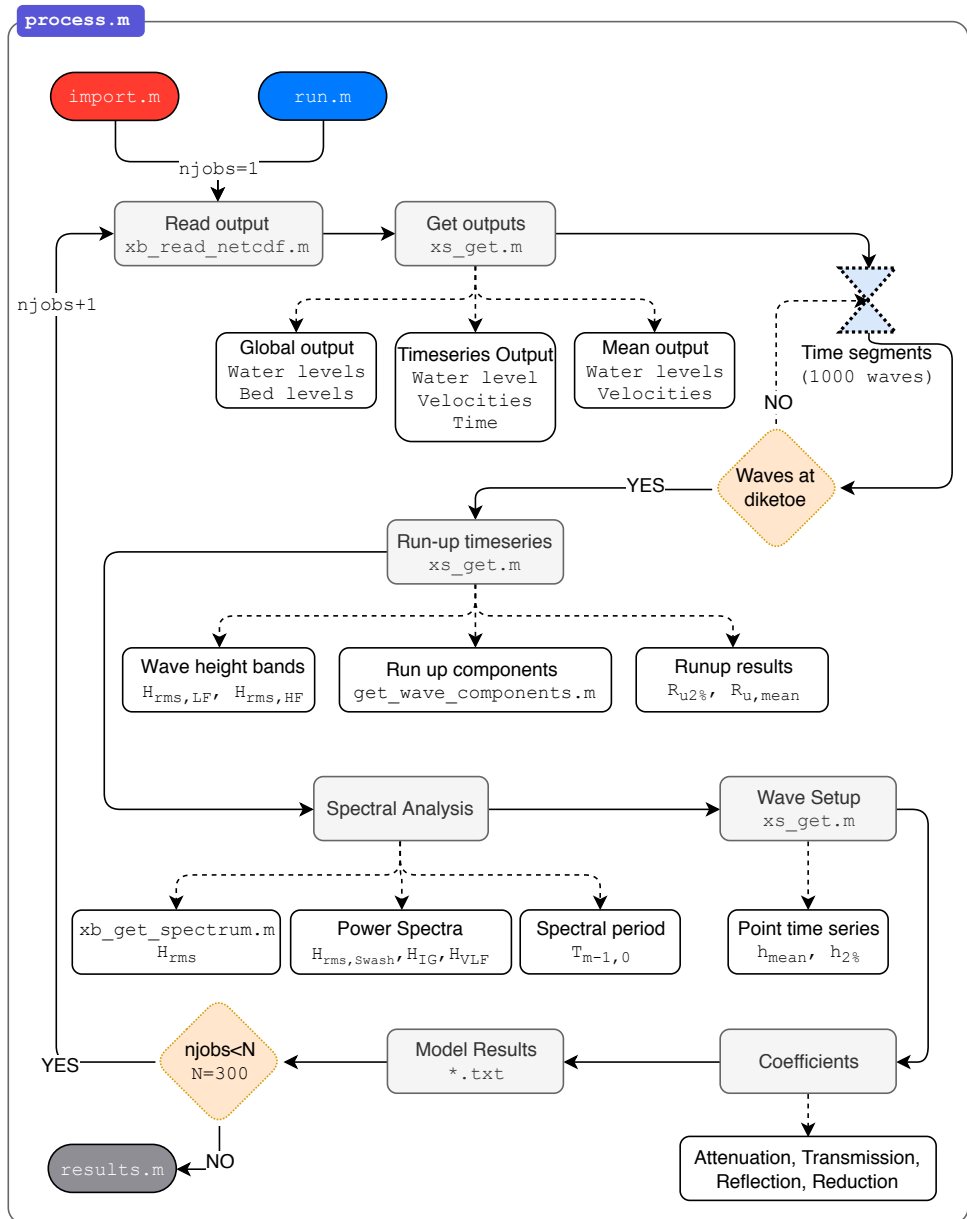


**Figure 4.5:** Pseudocode `process.m` for processing the XBeach results. Full lines could be followed to see major steps whereas dashed lines represent sub-steps of the major step. Special thanks to Pearson, S.G. (Stuart) and van Ormondt, M. (Maarten) from Deltares whose scripts formed the basis of `process.m`.

### 4.3. RESULTS & DISCUSSION: VEGETATION RESPONSE

Numerical model results are presented as case model results which establish wave attenuation, wave set-up and run-up for one of the runs. Global model results which synthesis the bulk results from all simulations reveal mean, quartiles, and distributions of the resulting parameters.

#### 4.3.1. CASE MODEL RESULTS

Model results have been presented after the spectral analysis of one of the runs. Spectral analysis was conceptually the same however, instead of determining wave heights at the 6 observation locations they were determined at every grid point. The input specifications for the case run are tabulated in Table 4.1.

**Table 4.1:** Input conditions for a sample XBeach case model run. All case model results are based on this simulation.

$H_{m0}$ m	$T_p$ s	$h$ m	$S_0$ -	$h_v$ m	$b_v$ m	$N_v$ stems/m <sup>2</sup>	$S_v$ -	$L_v$ m	$C_d$ -	$c_f$ -	$S_d$ -	$h_c$ m
4.34	9.92	3.82	$\frac{1}{80}$	0.99	0.0128	101	$\frac{1}{564}$	553.34	1.25	0.057	$\frac{1}{3}$	15.79

Figure 4.6 depicts the evidence of different wave frequency components occurring at the same time in vegetated hydrodynamic environments. Exchange of energy and momentum between the components takes place which can cause constructive interference resulting in resonance. Resonant waves are typically low frequency waves and are critical for flooding, therefore separate effect of wave frequencies on run-up and eventually flooding was important to investigate.

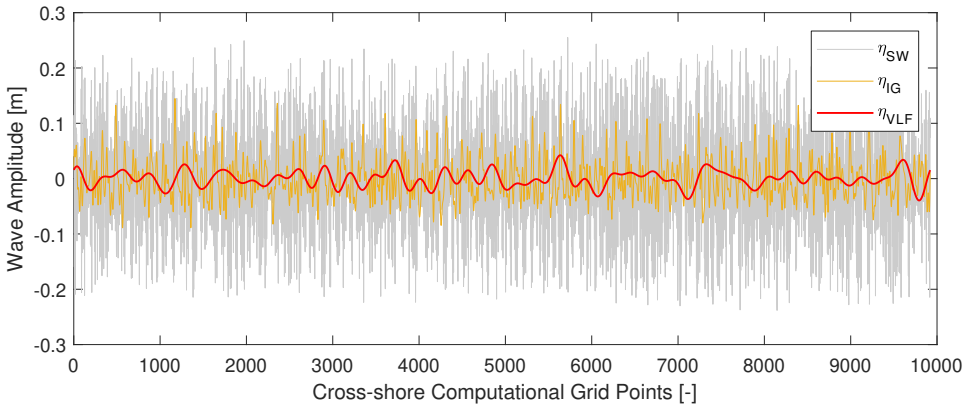


**Figure 4.6:** Wave amplitude timeseries showing short wind (SW) waves, infragravity (IG) waves and very low frequency (VLF) waves occurring simultaneously. The timeseries has been generated by detrending the wave level timeseries and frequency splitting. The same series have been used to calculate power spectra for all model runs which results in incident SW, IG and VLF wave heights at the dike toe.

Vegetation-induced wave attenuation could be expressed through energy around different wave frequencies forming wave energy spectrums. Figure 4.7 shows spectral evolution with and without vegetation. The energy is introduced at the offshore boundary based on the JONSWAP wave boundary condition. Gradually the energy propagates on-shore and results in some losses due to bottom friction or wave breaking. Delta-like peaks or uni-modal spectrum shows that the sea state is relatively homogeneous as the energy is concentrated around waves of similar frequency.

Higher frequencies start to diminish once the offshore ramp is over and the platform has started resulting in relative dominance of the infragravity component. At mid-forest, on the platform, the spectrum becomes bi-modal showing simultaneous occurrence of very low frequency, infragravity and sea-swell components which forms the basis of increased complexity in making run-up predictions.

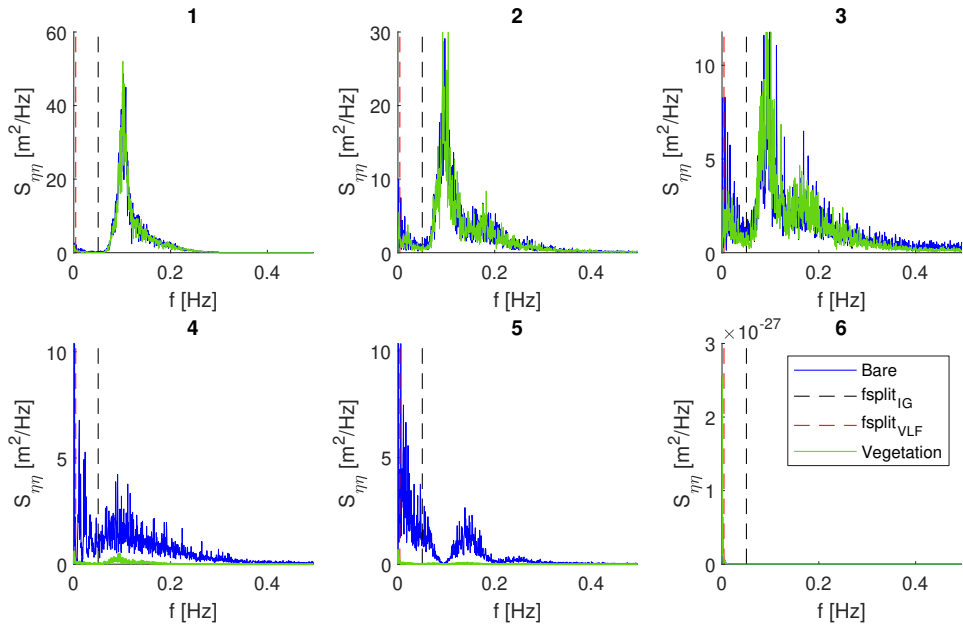


**Figure 4.7:** Comparison of spectral evolution across 6 output points in the scenario of vegetation and without vegetation (bare-bed). Black dash lines represent splitting frequency between short-wind waves and infragravity while red dash lines represent splitting frequency between infragravity and very low frequency waves.

The comparison between spectra at mid-forest (observation point 4) in Figure 4.7 shows that significant amount of energy has been dissipated due to vegetation as the energy near peak frequency has dropped nearly by 90%. Similar effect could be seen at the dike toe (observation point 5) with a difference that more energy has been concentrated around low frequency waves than short waves. This clearly reaffirms the wave attenuation potential of vegetation and that the design load for the dike design has been greatly reduced. In other words, if there is already a dike there, the flood risk for the system has been decreased due to inclusion of vegetation in the flood defence system.

Furthermore, the detailed comparison between spectra, presented in Figure C.1, also reveal that the high frequency waves get attenuated quicker than the low frequency waves. The deduction is based on the observation that, while moving into the forest, the wave energy dissipation of frequencies higher than  $f_p/2$  is more than the wave energy dissipation of frequencies lower than  $f_p/2$ . The deduction is critical for flooding because if the vegetation forest length is not sufficient long the infragravity waves might be successful in surviving the forest and result in major contribution to the wave run-up and overtopping.

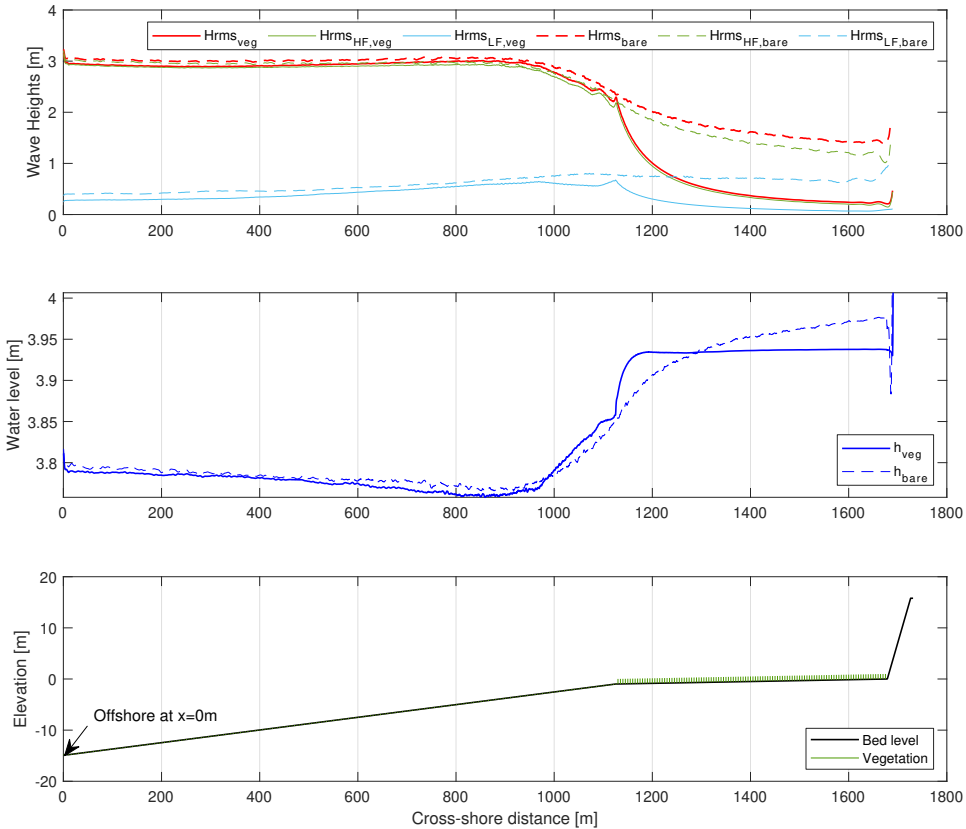


**Figure 4.8:** Case model results showing wave height evolution (top panel), water levels and wave setup (middle panel) along with bed levels (bottom panel). The depth of the diketoe was used as a reference ( $z_{toe} = 0$ ) and offshore boundary was taken as the start of cross-shore distance. Input conditions for the case model are presented in Table 4.1 for reference.

The results of the case model with cross-shore domain of nearly 2km and vegetation forest of 550m are presented Figure 4.8. The beach is more of a reflective beach than dissipative so relatively high waves of about 4.3m on water depth of 3.8m were forced on the offshore boundary with bed depth of about ( $z_{b,0} = 15m$ ), see Table 4.1 for all input conditions.

The comparison of wave heights and water levels on a vegetated and bare bed is shown in Figure 4.8. Comparison with bare bed explicitly establishes wave attenuation due to vegetation. The root mean squared wave height ( $H_{rms}$ ) increases as it approaches shallow region exhibiting effects of wave shoaling process. The decrease in wave heights start even before the start of vegetation forest due to wave breaking process but breaking point might vary from case to case as the wave height to water depth ratio is different in different case models. However,  $H_{rms}$  reduces sharply once the vegetation starts and most of the attenuation takes place within initial 100m of the vegetation forest.

Due to bi-modal wave spectra at the start of the vegetation forest the model output was analyzed for different frequency components. The results show that the high frequency component of the wave height ( $H_{rms,HF}$ ) has major contribution to the total wave height and both show similar attenuation behavior. On the other hand, low frequency infragravity wave show resonance and increase in wave heights ( $H_{rms,LF}$ ) on bare-bed which is in agreement with conclusions of Chang & Liu (2019); Zainali et al. (2018); Tang et al. (2017); Chang et al. (2017); Mei et al. (2011). Moreover, vegetation also catalyzes harmonic interaction which results in infragravity generation but both low and high frequency waves attenuates due to vegetation. Similar conclusion was made by the analysis of wave energy spectra from Figure C.1.

Based on the results, water level increases due to vegetation causing wave set-up which is the difference of mean water level and still water level. The water level in the scenario of vegetated bed is comparatively sharper due to higher resistance faced by the flow. The effect is due to increase in radiation stresses in cross-shore direction resulting in accumulation of momentum causing wave set-up. Although the phenomenon exists in both situations and the increase in water level with vegetation is a sharper increase but it is still lesser than the bare bed case and stabilizes as well.

The reduction of wave set-up in comparison to bare bed also establishes the attenuation of storm surges due to vegetation which is in agreement with the findings of (Montgomery et al., 2019; Rupprecht et al., 2017; Möller et al., 2014; McIvor et al., 2012). The increase in water level directly corresponds to increase in flooding therefore wave set-up reduction is also of paramount importance. Conclusively the set-up due to vegetation is lesser than the bare-bed therefore it corresponds to reduced flood risk due to vegetation.

#### 4.3.2. GLOBAL MODEL RESULTS

Global model results are the bulk results from all the simulations which are presented through violin plots. The violin plot is a combination of frequency-density and box and whiskers plot, see Figure 4.9. It has the ability to show complete statistical description of a parameter including its frequency variation, quartiles, and outliers. Every simulation result, along with input conditions, would form a realization while making continuous distributions in the Bayesian networks.

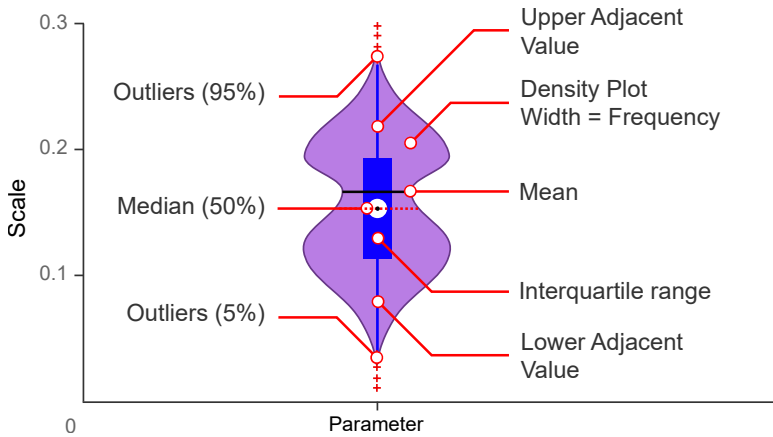


**Figure 4.9:** Violin Plot combining box and whiskers plot and probability density plots.

### WAVE HEIGHTS

Output wave heights are quadratically weighted averaged from energy spectrum as energy is proportional to  $H_{rms}$  (Holthuijsen, 2010). A general reduction in overall wave heights ( $H_{rms,Swash}$ ) is observed in Figure 4.10 due to vegetation as compared to initial offshore wave height ( $H_{rms} = 0.707 \cdot H_{m0}$ ). Most of attenuated wave heights fall under  $0.5m$  for saltmarshes and under  $0.15m$  for mangroves in the swash region. However, some extreme wave heights have also been observed which, in comparison to offshore wave height, have not reduced with the same proportion. This concludes that vegetation is less effective in reducing extreme wave heights as it is in reducing relatively smaller or less extreme wave heights.

Incident wave heights at the dike toe are relevant for designers which have also decreased to a mean around  $0.3m$  for saltmarshes and  $0.1m$  for mangroves. Wave heights at the toe of the dike don't go beyond  $2.5m$  for saltmarshes and  $0.4m$  for mangroves. Surprisingly, wave heights in the swash region are higher relative to the wave heights at the dike toe possibly due to amplification due to reflective waves or due to secondary depth-induced shoaling while moving up the dike ramp.

Furthermore, the individual high and low frequency components of wave height have also been presented and fall in the range  $0$  to  $0.5m$  for saltmarshes and between  $0$  to  $0.2m$  for mangroves. As concluded from the case result in Figure 4.8 that most of the high frequency waves contribute to total wave height, similar trend is observed in the bulk model results in Figure 4.10. The conclusion is deduced based on the observation that high frequency waves have nearly same range of values as total wave height and low frequency waves are relatively very small in the swash region. Moreover, both saltmarshes and mangroves have same effect on very low frequency waves rather both vegetation types help in forming sub and super harmonics of waves therefore resulting in similar magnitudes of attenuated wave heights.

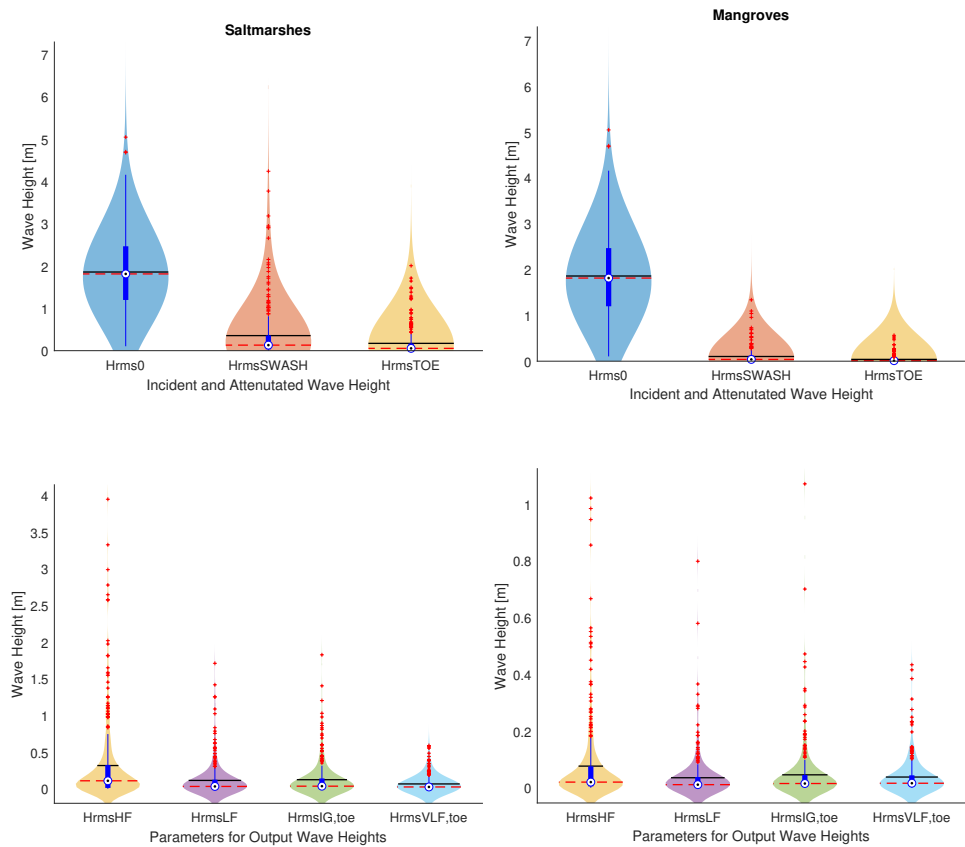


**Figure 4.10:** Comparison from bulk model results between offshore wave heights and attenuated wave heights at diketoe ( $*_{Toe}$ ) and swash region ( $*_{Swash}$ ) for both saltmarsh and mangrove environments. Subscript  $*_{HF}$  stands for high frequency,  $*_{LF}$  for low frequency,  $*_{IG}$  for infragravity, and  $*_{VLF}$  for very low frequency waves.

### WATER DEPTHS & SET-UP

Water depths were initially interpreted as uniformly distributed vertical distances relative to diketoe ( $z_{toe} = 0m$ ). The bulk results of water depths have been compared based on the mean water levels at different cross-shore locations, extreme water level ( $h_{2\%}$ ), and set-up. The output locations were seagrass incidence ( $h_{SG}$ ), vegetation incidence ( $h_{VEG}$ ), and toe of the dike ( $h_{toe}$ ) labeled as observation point 2, 3 and 5 respectively in Figure 4.2. However, for flooding  $h_{2\%}$  and set-up are more relevant which have been calculated based on water depths in swash region.

Water depths at the seagrass incidence ( $kh = 0.5$ ) are higher than the water depths at vegetation incidence possibly due to wave shoaling at former and wave breaking at latter location. Both mean and median water depths at the diketoe and in the swash region are greater than still water level due to vegetation. Mean wave set-up in the swash region is around  $0.3m$  and goes as high as  $1m$  in extreme cases.

Deceptively, the additional set-up due to nonlinear transfer of energy in vegetation is a matter of concern for flooding (Dean & Bender, 2006). However, this study concludes that undoubtedly vegetation causes wave set-up but the mean water levels in vegetation scenario don't go higher than the mean water levels in bare-bed scenario provided sufficient forest length. Therefore, inclusion of vegetation in the flood defense system would provide an effective buffer for mitigating surges and increase in water levels as well. Additionally, as the water levels were initially described as uniform distributions, the resulting densities also show uniform behavior within the interquartile range.

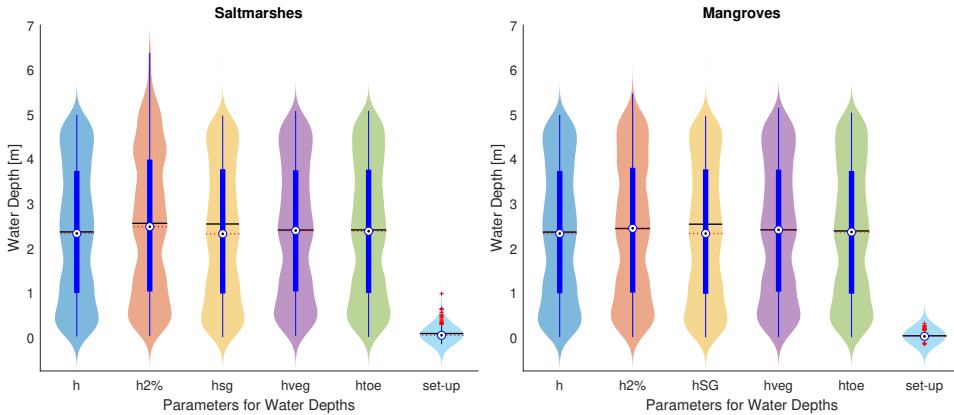


**Figure 4.11:** Bulk model results showing comparison between still water level and mean water levels at observation points across cross-shore profile. The parameter  $h_{2\%}$  is extreme water level in the swash region, and  $h_{SG}$ ,  $h_{VEG}$ ,  $h_{toe}$  are mean water levels at seagrass incidence, vegetation incidence, and toe of the dike respectively. All water depths are relative to dike toe ( $z_{toe} = 0m$ ).

## RUN-UP

Wave run-up ( $R_{u2\%}$ ) is the most relevant parameter in this study for flooding along with wave heights. In the bulk mode results, in Figure 4.12, the run-up shows a wide range of variability in terms of its range of values. The interquartile range exceeds  $3m$  which means that with the change in hydrodynamic and by changing the vegetation characteristics a variation of  $3m$  in  $R_{u2\%}$  could be obtained. Maximum run-up has been observed around  $10m$  with mean and median around  $3m$ . Tail with higher values of  $R_{u2\%}$  is extended as compared to still water level distribution which depicts more higher values of  $R_{u2\%}$  exist than the lower values making the systems more prone to flooding.

Run-up was also calculated using Gent Marcel (2001) method which seems to over-predict run-up values as both the mean and median values are slightly higher than the ones calculated directly through XBeach. As concluded earlier that most of the wave energy contribution to total wave energy comes from high frequency waves and simultaneously the higher frequency waves are attenuated more than low frequency waves, the conclusion has been reconfirmed through ( $R_{uVG, VLF}$ ) calculation from Gent Marcel (2001) method. It has been deduced that most of the run-up contribution comes from low frequency wave components.

Results also show that mangroves are not only more effective in reducing the mean run-up but also the extreme values of run-up. Outliers show extreme run-up values and more outliers have been noticed for saltmarshes than mangroves. It could be concluded that saltmarshes do let through some of the extreme waves, potentially more low frequency waves, which result in higher wave run-up.

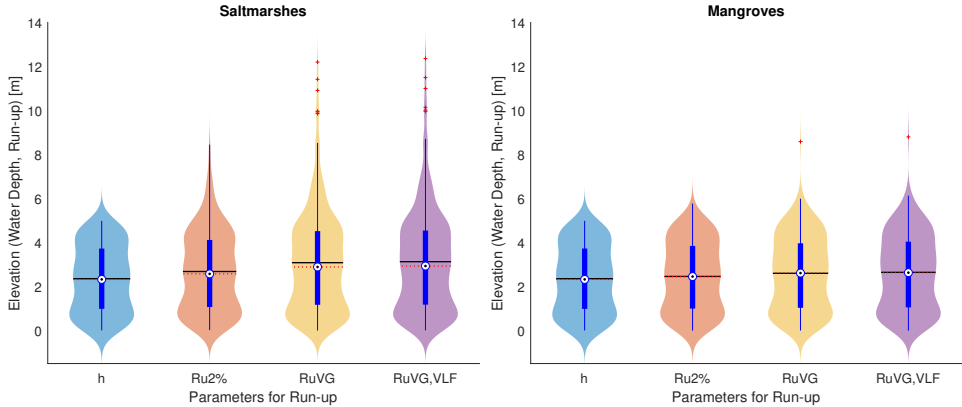


**Figure 4.12:** Bulk model results of run-up ( $Ru_{2\%}$ ) calculated directly through XBeach and by Gent Marcel (2001) method ( $Ru_{VG}$ ) to investigate role of very low frequency waves contribution to run-up ( $Ru_{VG,VLF}$ ) in comparison to still water level  $h$ .

## COEFFICIENTS

The attenuation and transmission coefficients help to predict wave heights and other parameters like velocities and drag forces in relevance to most widely known input parameters. For instance, if offshore wave height is known transmission coefficient ( $K_{t,OD}$ ) could be used to determine wave height at the toe of the dike. If incidence wave height at the vegetation incidence is known wave height in the mid-forest could be calculated by  $K_{t,VM}$ . Similarly, the wave attenuation coefficient  $K_{r,SM}$  for saltmarshes and  $K_{r,M}$  for mangroves could be used to calculate and compare wave height reduction due to vegetation.

The attenuation coefficients of saltmarshes are lower than mangroves which means they attenuate waves lesser than mangroves. Mean value of  $K_{r,SM}$  is 0.87 (87% mean energy dissipation due to saltmarshes) and  $K_{r,M}$  is 0.94 (94% mean energy dissipation due to mangroves). Also, there are more lower values of  $K_{r,SM}$  as compared to  $K_{r,M}$  making attenuation of saltmarshes less effective for extreme conditions as compared to mangroves. Similar trends have been observed by comparing wave transmission coefficients  $K_{t,OD}$  and  $K_{t,VM}$ .

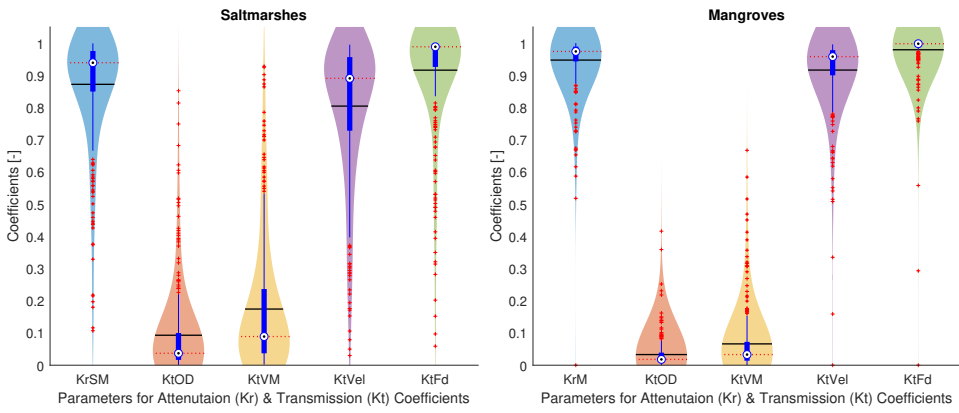


**Figure 4.13:** Bulk model results of attenuation and transmission coefficients. Wave attenuation coefficients for saltmarshes is  $K_{r,SM}$  and mangroves is  $K_{r,M}$  where as  $K_{t,OD}$ ,  $K_{t,VM}$ ,  $K_{t,Vel}$ ,  $K_{t,Fd}$  are transmission coefficients of waves from offshore to dike, wave from vegetation incidence to mid-forest, streamwise velocities and drag forces from vegetation incidence to mid-forest respectively.



# 5

## PREDICTION: PROBABILISTIC MODEL AND BAYESIAN NETWORK

*We make to ourselves pictures of facts.  
The picture presents the facts in logical space,  
the existence and non-existence of atomic facts.  
The picture is a model of reality.*

Ludwig Wittgenstein

*Fate laughs at probabilities.*

Edward Bulwer-Lytton

### Abstract

The chapter presents non-parametric Bayesian network (NPBN) for seagrass-saltmarshes, and seagrass-mangroves coupled environments. These environments have been modelled through the dependence structure based on Gaussian copulas. The NPBN serves as the flood risk prediction tool in vegetated environments which aids decision makers in making quick assessments about flood risk reduction potential of vegetation. Primary results of vegetation-induced wave attenuation, run-up and set-up has been well-predicted through the developed tool. Infact, the model also shows good predictive skill for secondary parameters like attenuation rate. The model also carves out most influential parameters affecting the complex dynamics of vegetated hydrodynamic system.

**D**YNAMICS and complexity of vegetated hydrodynamic system stems from natural variation in both the constituting components of vegetation and hydrodynamics. Studying such a system in depth necessitates methodologies that have the ability to embrace the complex system dynamics. Only by doing so the obtained results could be explained in relevance to near-to-reality situations otherwise the information would be fragmented and only a few isolated aspects could be investigated.

## 5.1. NON-PARAMETRIC BAYESIAN NETWORK

The core part of this thesis lies in probabilistic modeling of vegetated hydrodynamic system with the aim to make flood risk predictions in vegetated environments. The approach of Bayesian networks (BN) was adopted which are directed acyclic graphs (DAG) having parameters of interest as marginal distributions on nodes and the correlations among the nodes on arcs. The BNs were instrumental in capturing the complex system dynamics through a dependence structure. Particularly, the non-parametric Bayesian networks (NPBN) have been used which uses Gaussian copula – a ranked (bi- or even multivariate) joint normal distribution.

5

Non-parametric Bayesian networks are the form of hybrid Bayesian networks which can deal with both discrete and continuous random variables. The marginal distributions and ranked correlations were determined from the synthetic dataset. With the results of input conditions (Chapter 3), the results of numerical modeling (Chapter 4) were combined to form this synthetic dataset in order to train the NPBN. As presented in Chapter 4, a complete timeseries of water levels comprising of 1000 waves was analyzed to calculate wave heights, run-up and attenuation parameters. The number of data points for each of the NPBNs are equal to the number of global model simulations done.

Multivariate density model was generated from the dataset which devises joint distributions using joint Gaussian copula based on the empirical rank correlations (Ababei et al., 2008). The input data was in the form of a \*.csv file with parameter names in the first row and the parameter values in the following rows. The pseudocode `results.m` was created to write this file directly after the global model runs. Marginal distributions were directly mined from the data which formed empirical multivariate distribution related through a Gaussian copula.

### 5.1.1. VEGETATED SYSTEMS

Two coupled systems of seagrass-saltmarsh and seagrass-mangroves were modeled in XBeach. However, since the seagrasses were modelled as bottom friction, they don't take any effect from the coupling vegetation. For wave attenuation three different vegetation types could have been probabilistically modeled but it wasn't possible to study the effect of seagrasses on run-up so only two prediction models were developed. This section presents the background of modelled vegetated system in terms of its parameterization and the outputs that have been generated to address flood risk assessment.

Most of the input and output parameters were common for both the models like hydraulic and hybrid parameters. To differentiate the systems only the vegetation parameters which are related to the plant itself had to change. The common input parameters

are:

- **Hydraulic parameters:** Offshore wave height ( $H_{m0}$ ), peak wave period ( $T_p$ ), water depth relative to diketoe ( $h$ ), and offshore slope ( $S_0$ ) were specified as hydraulic parameters.
- **Benthic vegetation parameter:** Dimensionless bed friction coefficient ( $c_f$ ) accounts for benthic vegetation like seagrasses.
- **Vegetation forest parameters:** Vegetation forest length ( $L_v$ ) and vegetation slope ( $S_v$ ) represents overall vegetation forest characteristics in the prediction model.
- **Hybrid parameters:** Dike slope ( $S_d$ ) and crest level ( $h_c$ ) would characterize the dike or a dune present at the landward end of the system domain.

Based on the scope of the study, to quantify the wave attenuation potential of vegetation and predict flood risk, the outputs for both the system were kept the same.

- **Primary outputs:** Wave run-up ( $R_{u2\%}$ ) and set-up were generated as output for flooding predictions. For wave attenuation, the attenuation coefficient ( $K_r$ ), overall root mean squared wave height in the swash region ( $H_{rms,Swash}$ ), high frequency wave height ( $H_{rms,HF}$ ), low frequency wave height ( $H_{rms,LF}$ ) were output child nodes. Attenuation coefficient varies according to the vegetation system *i.e.*  $K_{r,SM}$  for saltmarshes and  $K_{r,M}$  for mangroves. Wave set-up ( $\eta = setup$ ) has also been added to the output to see the effect on mean water level due to vegetation.
- **Additional outputs:** A probability distribution of flooding damages was determined based on the future flood losses in 136 major coastal cities (Hallegatte et al., 2013). This world wide estimation of flooding damages was imperative to determine flood risk. Additionally, freeboard ( $R_c$ ) was also put in the network to make overtopping calculation.
- **Functional outputs:** Offshore root mean squared wave height ( $H_{rms,0}$ ) was calculated for comparison purposes to the predicted  $H_{rms,Swash}$ . Wave overtopping was calculated using Equation 2.2. Flooding criteria was defined and flood risk was calculated by combining probability of flooding and damages.

#### BENTHIC & SUBMERGED VEGETATION: SEAGRASS-SALTMARSH

Seagrasses were parameterized through bed friction ( $c_f$ ) which contributes to wave attenuation and hence flood risk reduction. It was not hypothesized that benthic vegetation like seagrasses would have solitary existence and would result in significant run-up reduction. Therefore, benthic seagrass was put along with saltmarsh or mangroves to make a coupled system of seagrass-saltmarsh or seagrass-mangroves.

The flood risk prediction model for coupled seagrass-saltmarsh or seagrass-mangroves system predicts attenuated wave heights, attenuation coefficient, wave run-up, and set-up as primary output variables. However, secondary output parameters could also be generated from the model which are a function of input and primary output parameters. A common metric for attenuation is wave attenuation rate ( $K_r/L_v$ ) which, as a secondary parameter, could be calculated for consistent comparison with literature.

The generic parameters used to form this model were hydraulic, benthic vegetation, vegetation forest and hybrid parameters. Specifically, the submerged vegetation parameters were added to characterize saltmarshes:

- **Submerged vegetation parameters:** Vegetation height ( $h_v$ ), frontal width ( $b_v$ ), vegetation density ( $N_v$ ), and drag coefficient ( $C_d$ ).
- **Outputs:** Wave attenuation coefficient for saltmarsh ( $K_{r,SM}$ ) was specific output along with all other generic outputs.

#### BENTHIC & EMERGENT VEGETATION: SEAGRASS-MANGROVES

Mangroves were schematized in three vertical layers keeping in view the difference in roots, trunk and stems. The schematization resulted in different parameterization of each layer. The parameters related to layers are:

- **Emergent vegetation parameters:** For the roots layers height ( $h_{v,r}$ ), frontal width ( $b_{v,r}$ ), density ( $N_{v,r}$ ), and drag coefficient ( $C_{d,r}$ ) were defined. Trunk height ( $h_{v,t}$ ), trunk frontal width ( $b_{v,t}$ ), trunk density ( $N_{v,t}$ ), and trunk drag coefficient ( $C_{d,t}$ ) characterized the middle layer. Stem height ( $h_{v,s}$ ), stem frontal width ( $b_{v,s}$ ), stem density ( $N_{v,s}$ ), and stem drag coefficient ( $C_{d,s}$ ) were used to model top layer of mangroves.
- **Outputs:** Wave attenuation coefficient for mangroves ( $K_{r,M}$ ) was specific output along with all other generic outputs.

#### 5.1.2. FLOOD RISK

Flood risk is a product of both hazard accounted through flooding probability and vulnerability accounted through damages due to flooding. The current model can predict hazard based on a two-level flooding criteria and damages through a probability distribution of future flood losses based on Hallegatte et al. (2013) data about losses in 136 major coastal cities.

For hazard, a two-level flooding criteria was defined based on run-up and overtopping rate. First level criteria was based on run-up which gives flooding if run-up ( $R_{U2\%}$ ) exceeds the dike crest level ( $h_c$ ). Once there is evidence of water reaching the dike crest second level criteria kicks in which is based on overtopping rate ( $Q$ ). Flooding happens when the overtopping rate exceeds critical overtopping rate ( $Q_{cr}$ ) in a given scenario. The logical relation of flooding criteria is formulated in Equation 5.1.

$$\text{Flooding} = \text{if}(Ru_{2\%} \geq h_c) \quad \& \quad \text{if}(Q \geq Q_{cr}) \quad (5.1)$$

For damages, Hallegatte et al. (2013) has presented the results of the loss analysis for the 136 major coastal cities for different sea level rise (SLR) and socio-economic growth scenarios in different years in future. The results for the year 2050 have been used in this study to account for future losses and yet not include too much uncertainty of the damage predictions in far-future. In 2050, sea level rise and subsidence of 40cm was used in the cities under consideration which is the pessimistic limit of SLR. To account for

the socio-economic change, maximum city population was limited to 35 million inhabitants and the optimistic bound of flood protection level was assumed (maximum flood defence protection). With the pessimistic bound of SLR and optimistic bound of protection level, the damages would be over-predicted resulting in conservative predictions. The table about all city results in 2050 in supplementary information of [Hallegatte et al. \(2013\)](#) could be consulted as a reference for the losses in the major cities.

## 5.2. RESULTS & DISCUSSION: FLOOD RISK PREDICTION

The exercise of system parameterization followed by the XBeach numerical modelling resulted in the synthetic dataset. The input conditions through the stochastic model and the outputs, as a result of numerical simulations, were collated to feed the Bayesian network. The Bayesian network consists of nodes and arcs which form a directed acyclic graph (DAG). As a result, a DAG is used to explain inter-connectedness among various parameters of interest. This section present DAGs of seagrasses-saltmarshes and seagrasses-mangroves coupled models and unveils the underlying dependence of output parameters like attenuated wave height, run-up, and set-up to the input parameters.

### 5.2.1. PREDICTION TOOL

The final aim of the thesis was to develop a flood risk prediction tool which predicts flooding in vegetated environments and wave attenuation potential of vegetation. The developed tool is a non-parametric Bayesian network for two distinct vegetated environments namely seagrass-saltmarshes and seagrass-mangroves coupled environments.

The resulting NPBN for seagrass-saltmarshes is presented in Figure 5.1 which has 13 nodes of input parameters, 6 nodes of primary output parameters and 6 nodes of secondary outputs (including functional nodes) forming a DAG of 25 parameters in total. The number of parameters goes to 32 for seagrass-mangrove model. Handling multivariate joint distributions of 32 parameters is an acceptable number for a non parametric Bayesian networks. However, if other approaches, like discrete BN approach, were applied then the size of conditional probability table would have been unfeasible to handle.

The NPBN for seagrass-mangroves is presented in Figure 5.2 with same output parameters as the saltmarsh model. Minimum correlation value was specified as 0.1 to unsaturate the DAG in both models. The direction of arcs was optimized in a way to reduce partial correlations. Partial correlation exist if a child node has two parents which makes both the parents conditionally dependent. Therefore, due to existence of partial correlations, the values on the arcs are not entirely bivariate rank correlations but some of them have conditional dependence.

The NPBN for seagrass-saltmarsh predicts vegetation induced wave attenuation with a mean of about 0.87 (87% mean wave attenuation) whereas seagrass-mangroves model predicts mean wave attenuation coefficient of 0.95 which is 95% of energy dissipation due to mangroves. Mean run-up value is higher in saltmarsh environments than in mangroves and same goes for a setup making mangroves more effective for flood risk reduction. It must be noted that both the models were forced with the same hydrodynamic forcing therefore the comparison of output parameters is only dependent on vegetation.

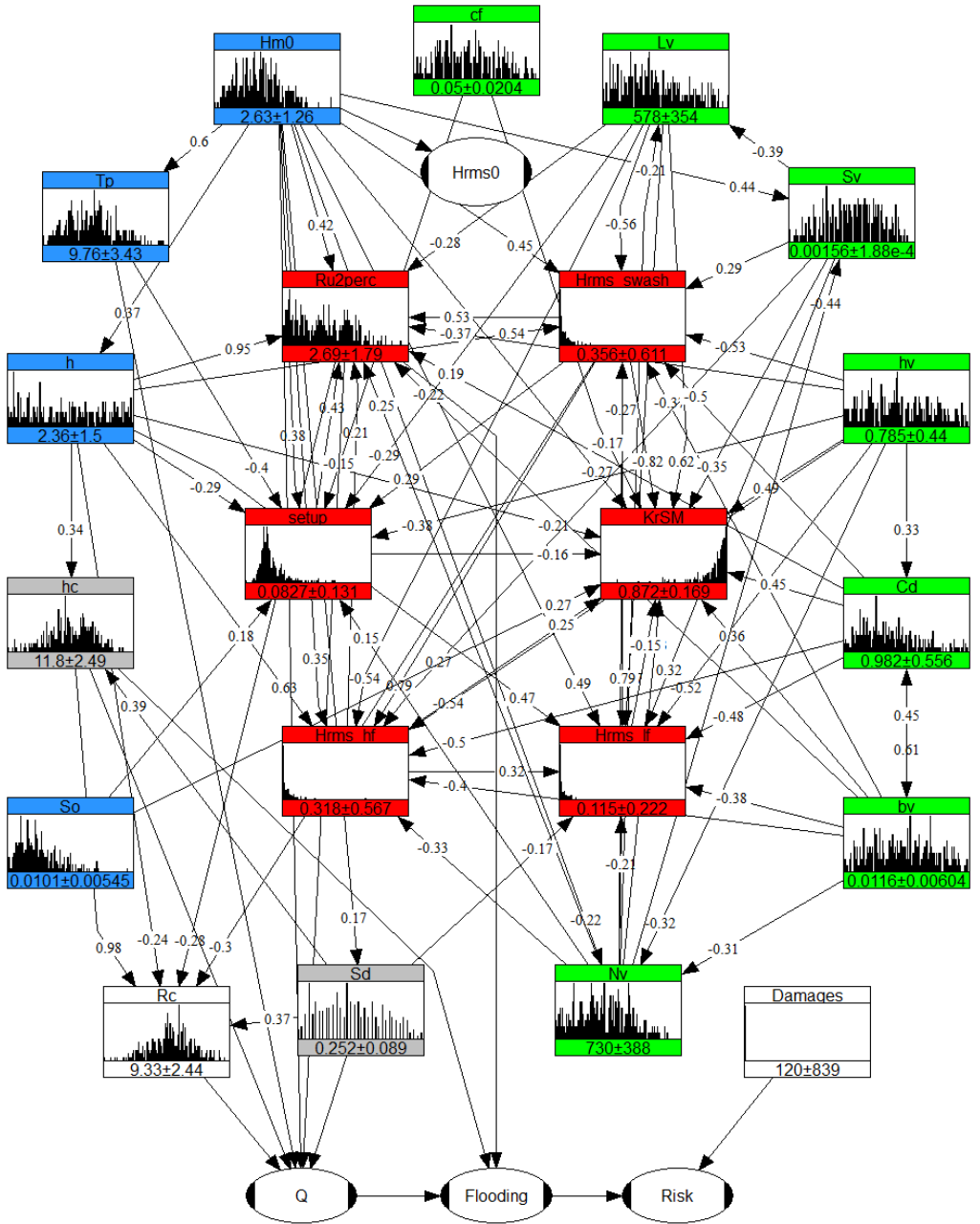


**Figure 5.1:** Flood risk prediction tool (non-parametric Bayesian network for seagrass-saltmarsh environment. The boxes represents nodes (parameters with their marginal distributions) and lines represents influences (rank correlations). Color coding could be followed to identify different components in the system: blue for hydrodynamics, gray for dike, light green for seagrass-saltmarsh parameters and primary outputs have been presented in red with white eclipses as functional nodes.



### 5.2.2. DEPENDENCE

The biggest advantage of Bayesian networks, as compared to other predictive models like neural networks, is that they can, along with making predictions, unveil the dependence among the system components. The system components in this study are the input and output parameters. The results in this section mainly focus on the dependence between output and the input parameters while the dependence between input parameters is presented in Chapter 3.

The hidden dependence among parameters in the NPBN could be revealed based on the rank correlation and partial correlations. The correlations values also represent the strength of copula while positive or negative values show the direct or indirect relation between two parameters. Higher the rank correlation is, higher the dependence between respective parameters is which, for a correlation of 1.0, makes them change with similar proportions. Figure 5.3 presents all the dependence relations between all the parameters in both saltmarshes and mangroves models. The relations have been obtained by fixing the absolute value of correlation to a minimum of 0.1.

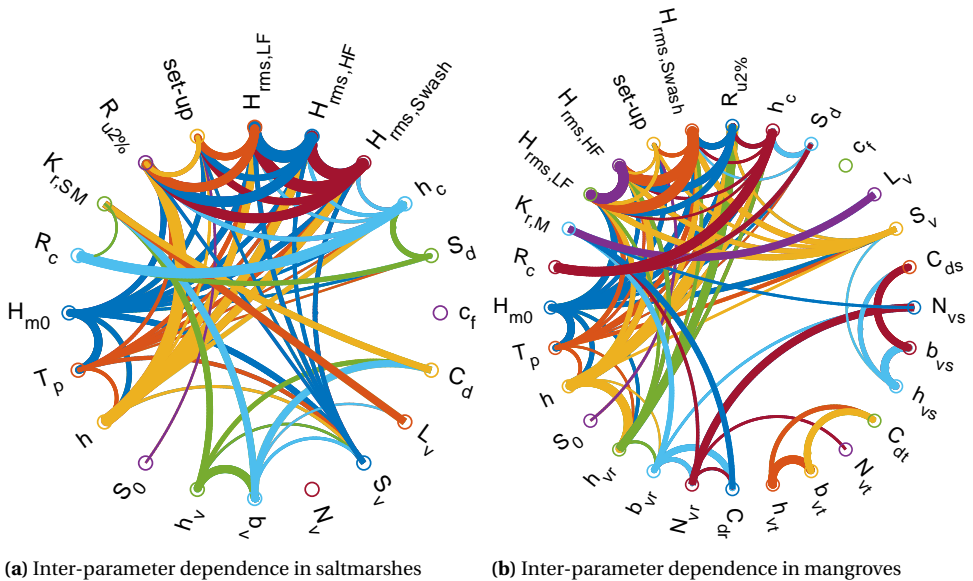


**Figure 5.3:** Inter-parameter dependence in saltmarshes and mangroves based on the rank correlations among parameters. The circles represent nodes (parameters), lines represent the correlations in the network, and thickness of the lines represents strength of the correlation with minimum correlation threshold of 0.1 used to unsaturate the graph.

Maximum dependence of the attenuation coefficient is on wave height in the swash region followed by the length of the forest which is consistent with the theoretical basis. Higher wave height in the swash region or smaller forest length means less waves have been attenuated which yields lower value of attenuation coefficient. Among the vegetation parameters, next to length of the forest, attenuation coefficient has the maximum dependence on the drag coefficient and vegetation height for the salt marshes. Water

depth also plays an important role as increased water depth doesn't allow waves to feel the bottom. Therefore, higher water depth results in lower the attenuation coefficient which means the wave height at the end of the vegetation would be closer to the value at the start.

Run-up could also be directly predicted from the prediction models which has the highest dependence on water depth and then to offshore wave height from input parameters. Similar trend continues for output variables where water depth is replaced by set-up and offshore height is replaced by the wave height in swash region. Vegetation parameters show negative correlations to the run-up which is also consistent with the theory as more vegetation would reduce the run-up. Run-up has a highest negative correlation with vegetation height among vegetation parameters which means it is one of the critical parameters in flood risk reduction.

### 5.2.3. EMPIRICAL PARAMETERIZATION

At the backend of the developed prediction models there is huge framework of joint multivariate rank distributions which in other words are known as copulas. Based on the finalized NPBNs, sensitivity could be performed on the network's copulas. The sensitivity is performed by running simulations which predict the desired variable based on the conditionalization of the base variable. The results of sensitivity forms the basis of empirical parameterization of the predicted parameters. Hence, an empirical relation for expected value of predicted variable could be proposed as a function of base variable.

Results were analyzed and are presented by taking a step back from probabilistic approach to deterministic approach. Empirical parameterization was obtained by determining the joint distribution of predicted and base variable followed by conditionalization of base variable. Importance of base variables was determined from the correlation matrix, see Figure 5.4. Predicted variables were narrowed down to run-up ( $R_{12\%}$ ) and wave attenuation coefficient ( $K_{r,SM}; K_{r,M}$ ) keeping flood risk reduction in perspective. Flooding in this study directly corresponds to run-up and reduction of flooding is quantified by wave attenuation across the vegetation forest.

For empirical parameterization, most important correlations for run-up and attenuation coefficient were screened-out by fixing the minimum correlation value to 0.4. The resulting relations have been presented in Figure 5.4. As expected, the run-up is highly related to hydrodynamic parameters and the wave attenuation is mostly dependent on vegetation parameters. However, in mangroves run-up is also a highly dependent on mangroves root height in addition to hydrodynamic parameters.

The empirical formulas for conditional expectation of run-up and wave attenuation coefficient for salt marshes have been presented in Equation 5.2 and for mangroves in Equation 5.3 as second-order polynomials. Although these formulas are only single parameter formulas but these have been generated from the NPBN sensitivity simulations by conditionalizing base variables. Therefore, explicitly the formulas don't cater other parameters than base variables but implicitly the predicted variables does have effect from other parameters because of possible conditional dependence among predicted, base and other parameters.

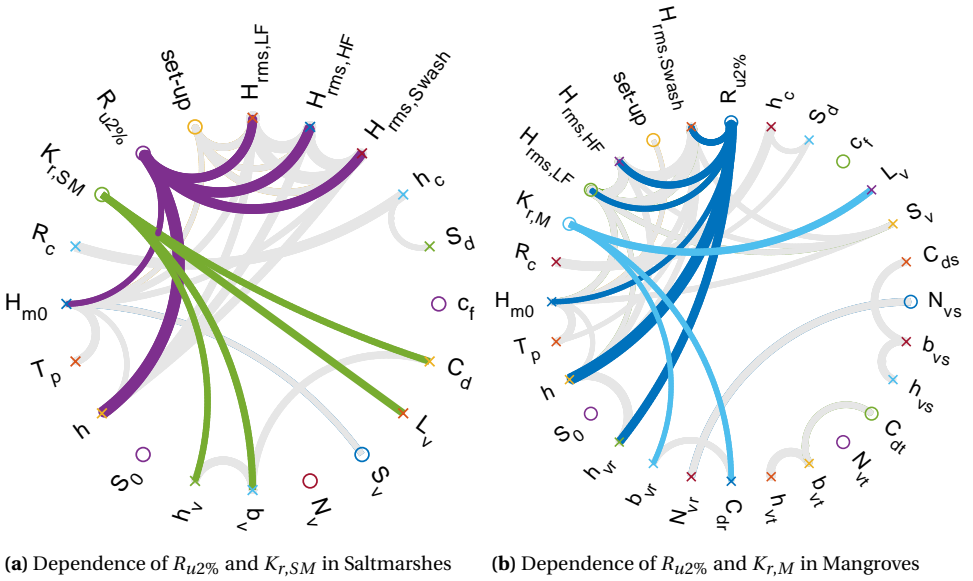


**Figure 5.4:** Maximum dependence of Run-up ( $R_{u2\%}$ ) and Attenuation coefficients ( $K_{r,SM}; K_{r,M}$ ) on other parameters for empirical parameterization of  $R_{u2\%}$  and  $K_{r,SM}; K_{r,M}$  in both saltmarshes and mangroves environments. The arc lines shown have ranked correlations higher than 0.4 while the coloured ones shows ranked correlation of only  $R_{u2\%}$  and  $K_{r,SM}; K_{r,M}$ .

Empirical parameterization of conditional expectation of run-up for saltmarshes:

$$E[R_{u2\%}|H_{m0}] = 0.994 + 0.704H_{m0} - 0.019H_{m0}^2 \quad (5.2a)$$

$$E[R_{u2\%}|h] = 0.290 + 0.792h + 0.067h^2 \quad (5.2b)$$

Empirical parameterization of conditional expectation of wave attenuation coefficient for saltmarshes:

$$E[K_{r,SM}|C_d] = 0.665 + 0.325C_d - 0.088C_d^2 \quad (5.2c)$$

$$E[K_{r,SM}|L_v] = 0.667 + 0.001L_v - 0.0001L_v^2 \quad (5.2d)$$

$$E[K_{r,SM}|b_v] = 0.661 + 27.937b_v - 662.104b_v^2 \quad (5.2e)$$

$$E[K_{r,SM}|h_v] = 0.700 + 0.335h_v - 0.113h_v^2 \quad (5.2f)$$

where;  $R_{u2\%}$  is run-up,  $K_{r,SM}$  is wave attenuation coefficient for saltmarshes,  $H_{m0}$  is offshore wave height,  $h$  is water depth,  $C_d$  is drag coefficient,  $L_v$  is vegetation forest length,  $b_v$  is frontal width, and  $h_v$  is vegetation height.

Run up has positive (relatively) linear behaviour with offshore wave height and water depth in both saltmarshes and mangroves. However, it does show different behaviour for higher values of water depth, see Figure 5.5b and 5.6b. In saltmarshes it shows a lot of variation for higher values of water depth which in other words means that there is a higher tail dependence between run-up and water depth in saltmarshes. Based on this

observation it could be concluded that saltmarshes are not as effective as mangroves in attenuating storm surges.

Wave attenuation coefficient highly depends on vegetation parameters and the coefficient also exhibit tail dependence on vegetation parameters. Maximum tail dependence was observed for vegetation forest length which could be seen in Figure 5.5f and 5.6f. Attenuation coefficient increases rapidly for initial increase in vegetation forest length but becomes relatively constant as the forest length increases after a certain limit. It concludes that effectively vegetation forest does not have a linear relationship with wave damping. The forest length has the potential to be optimized in a way that maximum utility of wave damping could be achieved within the optimal forest length limit and then other vegetation parameters could be changed to produce maximum wave attenuation.

Empirical parameterization of conditional expectation of run-up in mangroves environment:

$$E[R_{u2\%}|H_{m0}] = 0.920 + 0.684H_{m0} - 0.029H_{m0}^2 \quad (5.3a)$$

$$E[R_{u2\%}|h] = 0.101 + 0.992h + 0.003h^2 \quad (5.3b)$$

$$E[R_{u2\%}|h_{vr}] = -0.016 + 0.764h_{vr} + 0.018h_{vr}^2 \quad (5.3c)$$

Empirical parameterization of conditional expectation of wave attenuation coefficient in mangroves:

$$E[K_{r,M}|b_{vr}] = 0.886 + 1.930b_{vr} - 10.197b_{vr}^2 \quad (5.3d)$$

$$E[K_{r,M}|L_v] = 0.862 + 0.001L_v - 0.0001L_v^2 \quad (5.3e)$$

$$E[K_{r,M}|C_{dr}] = 0.880 + 0.083C_{dr} - 0.017C_{dr}^2 \quad (5.3f)$$

where;  $R_{u2\%}$  is runup,  $K_{r,M}$  is wave attenuation coefficient for mangroves,  $H_{m0}$  is offshore wave height,  $h$  is water depth,  $C_{dr}$  is mangroves root drag coefficient,  $L_v$  is vegetation forest length,  $b_{vr}$  is mangroves root width, and  $h_{vr}$  is mangroves root height.

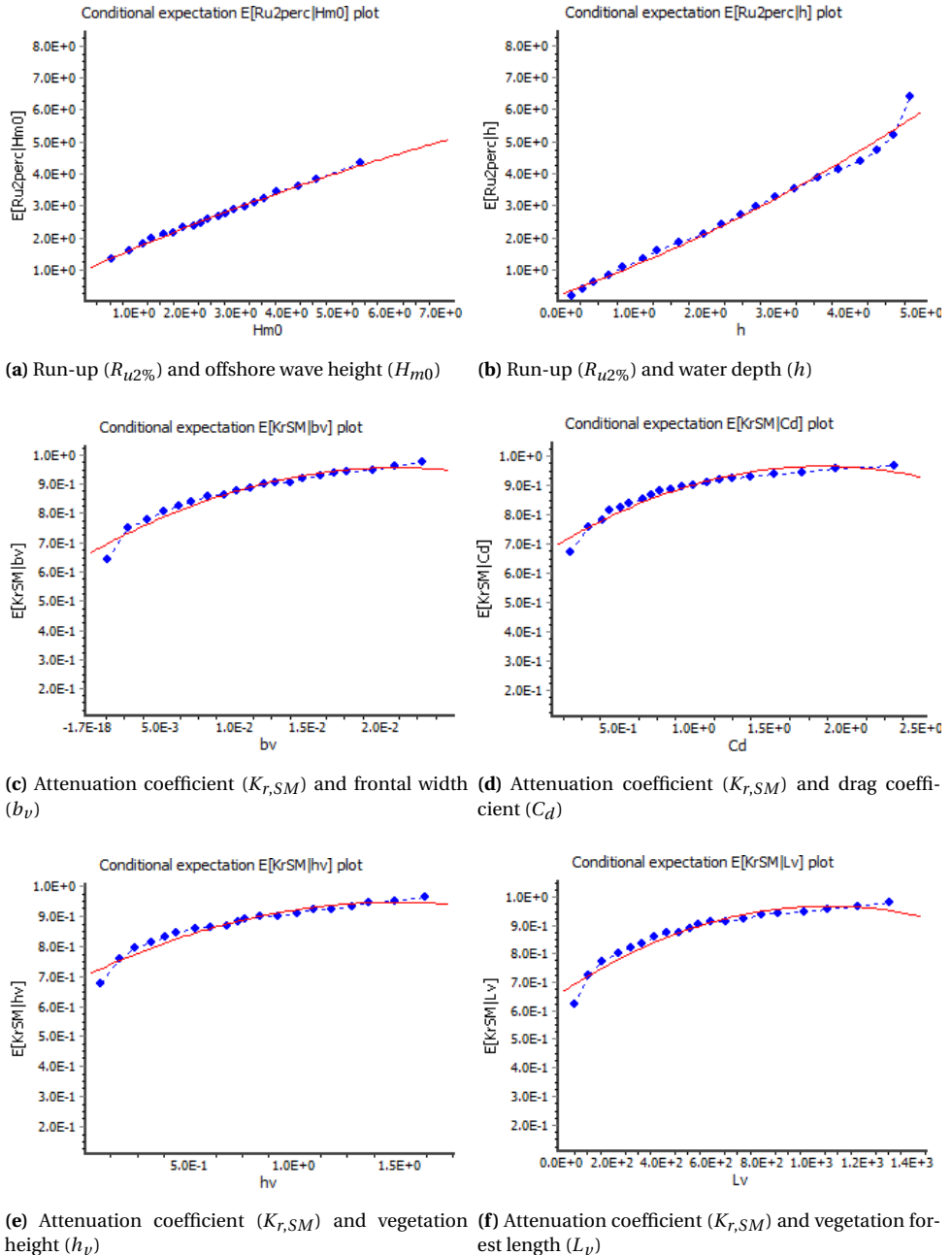


**Figure 5.5:** Empirical parameterization of conditional expectations of run-up and wave attenuation coefficient for saltmarshes. The plots have been generated by multiple conditionalizations (20) of base variables and observing the predicted variables through their joint distributions. The best fit line functions for conditional expectations could be seen in Equation 5.2.

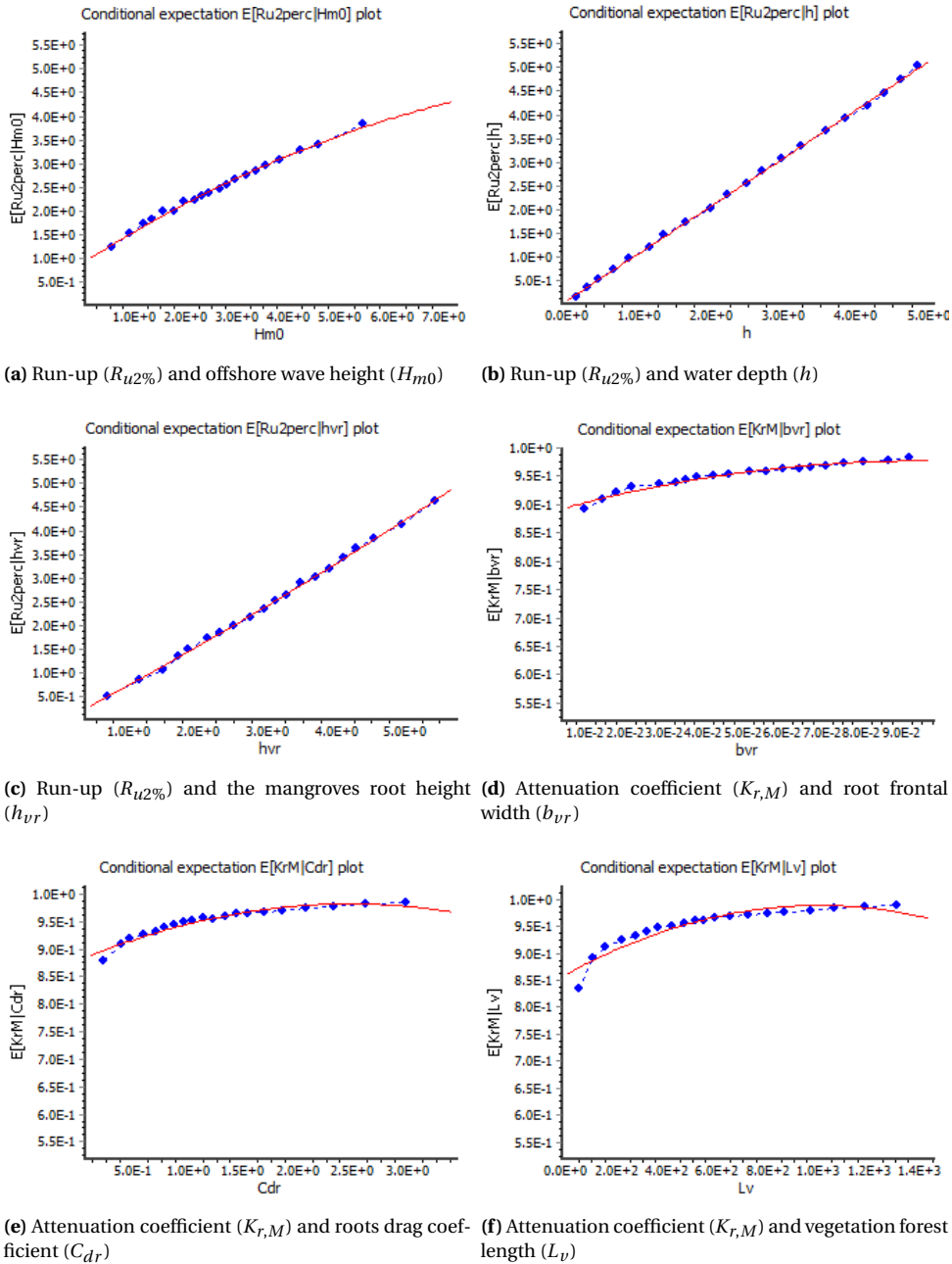


**Figure 5.6:** Empirical parameterization of run-up and wave attenuation coefficient for mangroves through conditional expectations. The plots have been generated by multiple conditionalizations (20) of base variables and observing the predicted variables through their joint distributions. The best fit line functions for conditional expectations could be seen in Equation 5.3.

### 5.3. VALIDATION

The validation was immensely vital to confirm if the complete progression of modelling steps work and the developed tool is successful in making reliable predictions. The complete approach of predicting flood risk through non-parametric Bayesian networks, feeding NPBN through synthetic dataset from XBeach simulations, and running XBeach simulation through Monte Carlo sampled vegetated hydrodynamic conditions from a stochastic model is relatively a long methodological progression.

With such a large number of steps involved to reach to the prediction tool, there was uncertainty involved at every step. However, if the final validation to field cases is successful the quantum of uncertainty could be considered within acceptable limit.

Therefore, detailed validation was carried out for both the statistical behaviour and predictive skill of the tool. Validation of NPBN was done on the lines of validating the dependence structure (Gaussian copula) and comparison of the model to the full saturated form by comparing the determinants of the correlation matrices. Furthermore, case validations through field studies was also done for both the saltmarshes and mangroves to check the predictive skill of the developed models.

5

#### 5.3.1. DOES THE MODEL REPRESENT REALITY?

In reality, on way or the other, everything has an explicit or implicit connection to everything. However, if we attempt to comprehend the reality the way it is, the complexity we start to deal with goes beyond the human capacity to fathom. Therefore, the need for knowledge development becomes important which, in Bayesian networks, is introduced through representing the same reality but only through dominant connections.

A non-parametric Bayesian network having all inter-parameter connections is a representation of a saturated directed acyclic graph (DAG) and the dependence structure is based on empirical normal rank correlations. For the NPBN where only dominant parameters are inter-connected, it has an unsaturated DAG and the dependence structure is calculated based on the correlations of unsaturated DAG. Calculation of rank correlations from data and partial rank correlations through recursive formula of Equation 3.3 results in a empirical normal rank correlation matrix for saturated DAG and BN rank correlation matrix for unsaturated DAG. The determinants of these matrices could be calculated and compared to validate the model to reality.

As determinants of the correlation matrices could be compared to validate the prediction model (A. Hanea et al., 2015), so, in order to assess the adequacy of the model, determinants of the BN rank correlation matrix and empirical normal rank correlation matrix were compared as a part of statistical validation. The statistical test gives an indication whether the developed NPBN is a good representation of the normal data as it compares the dependence structure of the NPBN with the dependence structure of the empirical normal data. In other words, the determinant of the correlation matrix of user-defined Bayesian network DAG is compared to the determinant of the correlation matrix of a DAG in which every variable is influencing every other variable. Having the hypothesis unrejected, that the multivariate dependence is significantly explained through the reduced influences, the UNINET model stands acceptable (Ababei et al., 2008).

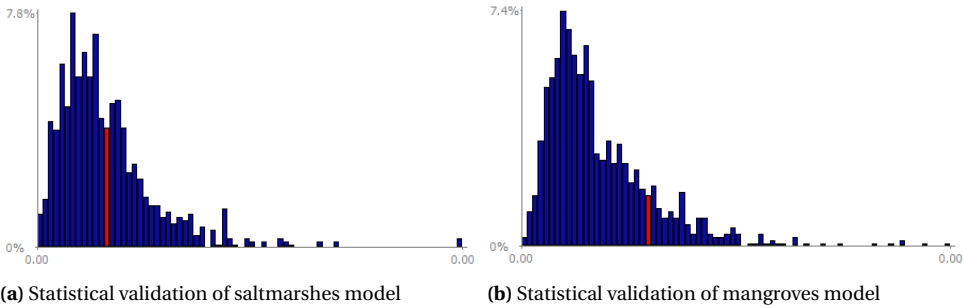


**Figure 5.7:** Statistical validation of developed non-parametric Bayesian networks for seagrass-saltmarshes and seagrass-mangroves environments based on the determinant of the correlation matrix is presented. The blue bars show probability distribution of determinants of BN rank correlation matrix while the red bar shows the determinant of normal rank correlation matrix. The determinant of normal rank correlation matrix falls in the distribution so the models stand statistically validated.

1000 simulations were run to sample joint normal distributions and calculate a probability distribution of the determinant of the BN rank correlation matrix, refer to Figure 5.7. The model validation was successful as the determinant of the empirical normal rank correlation matrix was within the 90% central confidence band of the determinant of the model rank correlation matrix. For saltmarshes, the determinant of the normal rank correlation matrix,  $1.963 \times 10^{-9}$ , falls between the 0.6 and 0.65 quantiles of the aforementioned probability distribution of determinants of the BN rank correlation matrices. For mangroves, the determinant of the normal rank correlation matrix,  $2.291 \times 10^{-10}$ , falls between the 0.85 and 0.9 quantiles of the aforementioned distribution so the mangroves model was also successfully validated.

The validation of the model was done as compared to the reality. Bayesian network introduce knowledge from the data if one can express the system with as less relations as possible. If a saturated DAG is created, where every parameters is connected to every other parameter, the segregation between dominant and less important influences isn't expressed. Therefore, the correlations which were more than 0.1 were obtained and the rank correlation of the model were compared with the empirical rank correlations. As a conclusion, the secret of a better model lies in representing reality with only the most dominant influences. Also, the utility of reducing the influences is also the identification of most significant parameters which are affecting the system response.

### 5.3.2. DEPENDENCE STRUCTURE VALIDATION

In UNINET the dependence is modelled by Gaussian copula (Ababei et al., 2008) however not every set of parameters are meant to be related through Gaussian copula. For instance, offshore wave height ( $H_{m0}$ ) and peak wave period ( $T_p$ ) are related through a skewed- $t$  copula to preserve the limiting wave steepness condition (Jäger & Nápoles, 2017). Therefore, the question arises if Gaussian copula was the appropriate dependence structure for the parameters under consideration?

The results of dependence structure show that Gaussian copula is not the best depen-

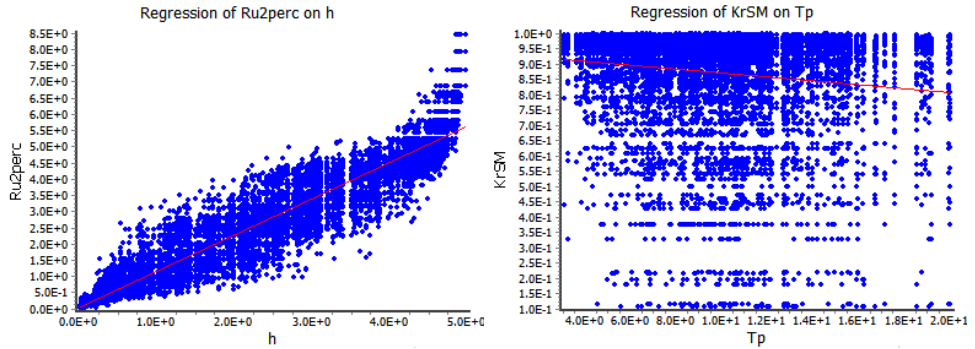


**Figure 5.8:** Dependence structure validation of developed non-parametric Bayesian network presented from seagrass-saltmarshes model. The Gaussian copula as could be seen in Figure 3.6 is not validated for these models. This requires extension of the work to advanced dependence modeling like vines which caters a wide variety of copulas other than Gaussian.

## 5

dence for many of the output parameters. In the statistical test the dependence structure of the synthetic dataset developed from XBeach simulations was compared with the dependence structure of the dataset transformed to Gaussian distribution. As a result, the determinant of the empirical rank correlation matrix didn't fall in the 90% central confidence band of the determinant of the rank correlation matrix of Gaussian data. Hence, in future studies the dependence modelling should be extended from NPBN possibly to vines for application of other copulas than Gaussian copulas.

### 5.3.3. PREDICTIVE SKILL VALIDATION

The way how Bayesian networks are implemented in software packages like Netica or UNINET they can not make prediction beyond the ranges defined at input stage. The model then only infers the posterior distributions based on the prior distributions and the conditionalizations in the defined ranges. This raises the question that is the model making predictions or just reproducing the XBeach results?

The predictive skill of the tool was validated for the parameters in the NPBN and also for the derived parameters. Field studies of [Infantes et al. \(2012\)](#); [van Zelst \(2018\)](#) were considered for validating the tool for saltmarshes and [Montgomery et al. \(2019\)](#); [Horstman et al. \(2014\)](#) for mangroves. Cases were validated by conditionalizing those parameters from field studies which had highest correlations in the NPBNs. If more parameters are conditionalized with lesser correlation values to the output there wasn't significant change in the outputs. Also, more the parameters were added to conditionalization the error between the field results and the model prediction was reduced.

Two cases from [van Zelst \(2018\)](#) were validated including one from Tillingham, United Kingdom and the other from Paulina, Netherlands. The values for input conditions were directly taken from [FAST Project](#) webservice and mean value of predicted wave height was compared. The error was lesser than 10% therefore the prediction tool is considered validated.

**Table 5.1:** Validation of flood risk prediction tool *i.e.* non-parametric Bayesian networks for seagrass-saltmarshes and seagrass-mangroves. All validation cases are from published field studies for realistic comparison to the developed model. Sample validated NPBN has been presented in Figure 5.9 for reference. All length units are in meters.

Study	Reference		Output	Model			
	Input Conditions			Prediction	Error	Validated	
	Hydraulic	Vegetation					
<b>Saltmarshes</b>							
van Zelst (2018) (England)	$H_{m0} = 2.16$ $h = 4.21$	$L_v = 780$	$H_{m0} = 0.42$	$H_{m0} = 0.45$	6.67%	Yes	
van Zelst (2018) (Netherlands)	$H_{m0} = 2.82$ $h = 4.47$	$L_v = 100$	$H_{m0} = 1.71$	$H_{m0} = 1.68$	1.79%	Yes	
Infantes et al. (2012) (Spain)	$H_{m0} = 1.85$ $h = 4.95$	$h_v = 0.8$ , $b_v = 4\text{mm}$ $N_v = 615$	$K_r = 0.45$	$K_r = 0.43$	4.65%	Yes	
<b>Mangroves</b>							
Horstman et al. (2014) (Vietnam)	$H_{m0} = 0.2$ $h = 1.0$	$L_v = 500$	$K_{r,M/m} = 0.0018$	$K_{r,M/m} = 0.00196$	8.16%	Yes	
Montgomery et al. (2019) (New Zealand)	$H_{m0} = 0.5$ $h = 2.5$ $T_p = 20\text{s}$	$L_v = 812$ , $h_v = 2.75$	$\eta = -0.17$	$\eta = -0.158$	7.59%	Yes	

For Infantes et al. (2012), rather than the wave height, wave attenuation coefficient was compared which was also successfully validated as the error was less than 5%. The conditionalizations of input conditions done in the saltmarsh NPBN, as presented in Table 5.1, have also been presented in Figure 5.9 as a reference. Infantes et al. (2012) used the drag coefficient ( $C_d$ ) formulation of Sánchez-González et al. (2011) which is based on  $KC$  number, see Table 2.2, so the  $C_d = 0.15$  was calculated based on  $KC = 100$ . The wave heights were not validated from Infantes et al. (2012) because the field measurements were done in the absence of the dike. Also, Infantes et al. (2012) reported water depths based on bed level, and not relative to the dike toe, therefore maximum water depth in NPBN was taken as a worst case scenario to validate.

For Montgomery et al. (2019) a derived parameter wave attenuation rate ( $K_{r,M/m}$ ) was validated. In the NPBN for mangroves a functional node was created by dividing mangrove wave attenuation coefficient  $K_{r,M}$  and the length of the forest  $L_v$  giving  $K_{r,M/m}$ . Surprisingly, this derived parameter was also validated which extended the tools ability to not just predict the primary variables which have been generated from XBeach

but also predict derived variables. For [Horstman et al. \(2014\)](#) wave set-up was validated because the study was about potential of mangroves in attenuation surges. Maximum value of peak wave period in the NPBN was used as the storm surges are very low frequency waves with high periods, see [Figure 1.8](#). The results of the predictive skill validation have been presented in [Table 5.1](#).

Although the errors of the predictive skill of mangroves tool are lower than 10% but they are higher than the saltmarshes tool. The statistical validation presented in [Figure 5.7](#) gave the similar indication as the determinant of the mangroves empirical normal correlations matrix (red bar in [Figure 5.7b](#)) was in higher quantile range (85-90 quantile) of the determinant of the mangroves BN correlation matrix. Simultaneously, for the saltmarshes model the determinant of the empirical normal correlations matrix was relatively closer (60-65 quantile) to the the median of the determinant distribution of the saltmarshes BN correlation matrix ([Figure 5.7a](#)). The NPBN for the mangroves still stands validated but it could be improved by increasing the modelled vegetated hydrodynamic conditions and revisiting the influences.

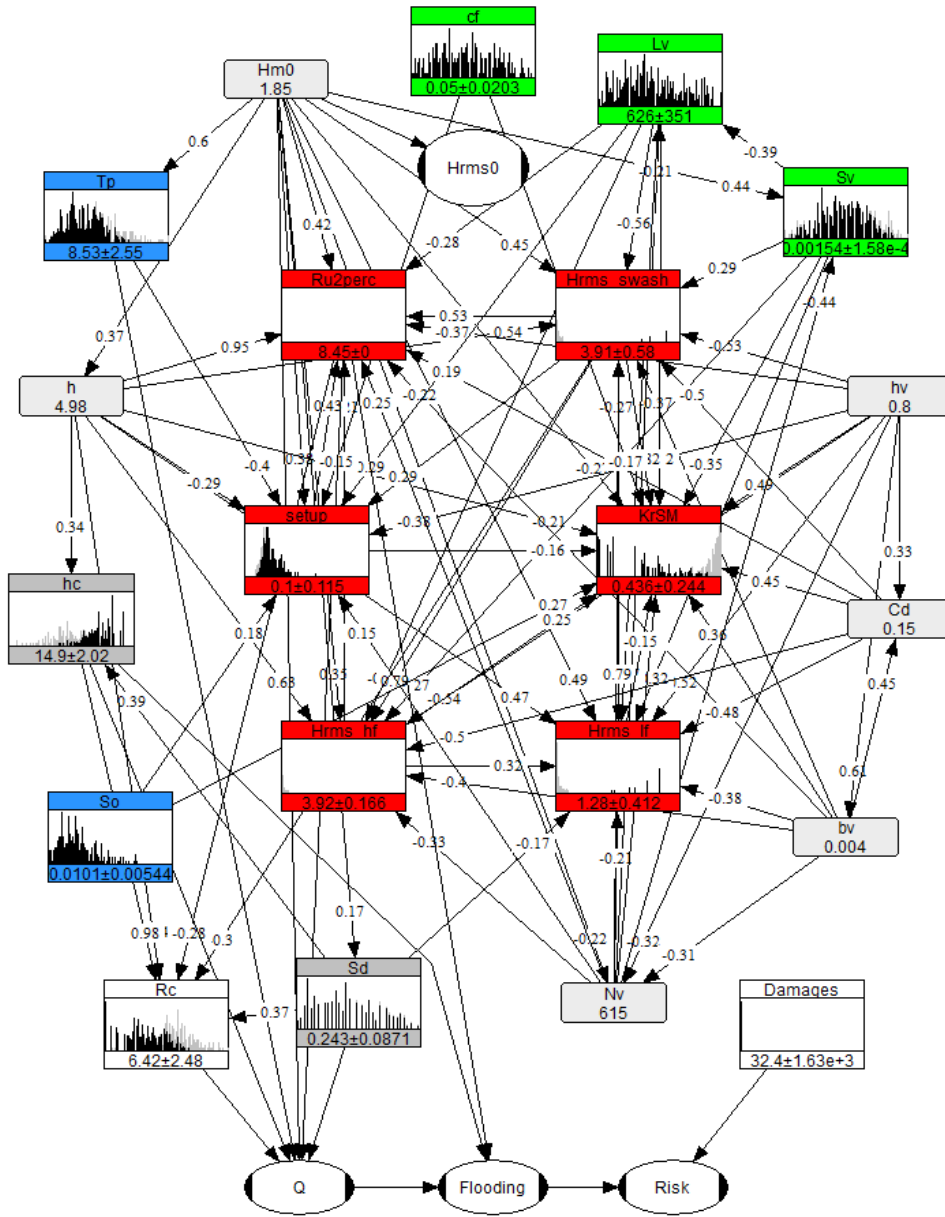


**Figure 5.9:** Predictive skill validation of seagrass-saltmarshes non-parametric Bayesian network based on a the measurements of Infantes et al. (2012) in Spain under storm conditions. The gray boxes with one value have been conditionalized based on site characteristics and mean values of output parameters have been compared for validation. See Table 5.1 for the results of validation.



# 6

## CONCLUSIONS & WAY FORWARD

*In the end, we will conserve only what we love;  
we will love only what we understand.*

Baba Dioum

### Abstract

The chapter concludes the thesis with major conclusions based on the research questions, highlights the novelty of this thesis provides recommendations to improve the current work, and proposes emerging research questions as a way forward for the extension of the current topic.

THE chapter concludes the thesis with major conclusions based on the research questions, highlights the novelty of this thesis, provides recommendations to improve the current work, and proposes emerging research questions as a way forward for the extension of the current topic.

### 6.1. NOVELTY

The thesis was successful in introducing some novel aspects to the scientific areas of research about potential of vegetation in attenuating hydrodynamic forcing in a range of conditions and flood risk prediction in global vegetated hydrodynamic environments.

- System idealization, parameterization and stochastic modeling of global vegetated hydrodynamic systems using Gaussian copulas.
- Vegetation response modelling to quantify effects of vegetation on wave attenuation, set-up and run-up in a global range of conditions using XBeach non-hydrostatic mode.
- Flood risk predictions under global vegetated hydrodynamics using non-parametric Bayesian networks.

### 6.2. CONCLUSIONS

The conclusions based on the results and discussion of the thesis are presented in this section according to the research questions drafted in Chapter 1.

#### OBJECTIVE # 1: GLOBAL VEGETATED HYDRODYNAMIC SYSTEM

##### **How can the global vegetated hydrodynamic system be idealized and probabilistically parameterized for seagrasses, saltmarshes and mangroves?**

Global vegetated hydrodynamic system could be idealized based on slopes of offshore ramp and vegetation platform. Hydrodynamics could be represented through offshore wave height, wave period and water depth where as vegetation as rigid cylinders could be parameterized through its height, frontal width, density, drag coefficient, roughness coefficient and length of the forest. Mangroves have to be schematized in vertical layers. Hybrid parameters are case dependent but for the case of dikes and dunes the crest level and sea-facing slope should be sufficient. Probabilistic parameterization could be done by defining the ranges and distributions of the aforementioned parameters along with the correlations among them.

##### **Does carrying out stochastic modelling add any value to the process of preparing synthetic dataset to feed the prediction tool?**

Yes, stochastic modelling does add value in the development of prediction tool both qualitatively and quantitatively. Quantitatively, due to stochastic modelling through Gaussian copulas, the required number of simulations were reduced from an nearly impossible order of magnitude ( $O$ )<sup>32</sup> for 300 variations of 13 saltmarsh model parameters and ( $O$ )<sup>52</sup> for 300 variations of 21 mangroves model parameters to a computationally feasible order of magnitude ( $O$ )<sup>2</sup>. Qualitatively, the Monte Carlo sampling from the stochastic model resulted in the global vegetated hydrodynamic conditions within physically real-

istic windows which makes every simulation more useful and meaningful as it'd be a physically realistic case somewhere in the world.

### OBJECTIVE # 2: VEGETATION RESPONSE MODELLING

#### **What is the degree of effectiveness of vegetation in attenuating hydrodynamic forcing in a range of conditions?**

Saltmarshes attenuates waves by 87% as a mean value and mangroves attenuates waves by 94% as a mean value. The mean values are based on difference in wave heights at the seaward and landward end of the vegetation forest. Vegetation also reduces wave set-up *i.e.* relative set-down as compared to bare-bed scenario which establishes the attenuation of storm surges. Moreover, mean water levels in vegetation scenario don't go higher than the mean water levels in bare-bed scenario provided sufficient forest length. However, vegetation is less effective in reducing extreme wave heights as it is in reducing relatively smaller or less extreme wave heights.

#### **Is vegetation more effective in attenuating high frequency (sea-swell) waves or low frequency (infragravity) waves?**

Both saltmarshes and mangroves catalyzes formation of sub and super harmonics of waves causing resonance. Although the high frequency (sea-swell) component of the wave height has major contribution to the total wave height but fortunately it is the high frequency waves that get attenuated more and quicker than the low frequency (infragravity) waves. Most of the high frequency waves gets attenuated more than 60% within initial 100 to 150m of the vegetation forest while some of the infragravity waves can still maintain same wave height after 100m of the forest.

#### **Which vegetation type, saltmarshes or mangroves, is more effective in wave run-up reduction?**

Mangroves are more effective in wave run-up reduction as compared to saltmarshes. Wave run-up is more dependent on low frequency waves than high frequency waves. Therefore, the question comes down to which vegetation type better attenuates low frequency waves? The answer is mangroves as it results in reduction of both mean and extreme wave run-up as compared to saltmarshes.

### OBJECTIVE # 3: FLOOD RISK PREDICTION TOOL

#### **What are the critical parameters that govern the wave attenuation and wave run-up processes in a vegetated hydrodynamic system?**

Wave attenuation has highest positive dependence on vegetation height, frontal width, drag coefficient and length of the forest. For mangroves the same vegetation parameters are critical but only for the roots layer. Wave run-up has highest positive dependence on offshore wave height and water depth in saltmarshes but in mangroves it also have significant negative dependence on mangroves root height. Other than the input parameters, wave run-up has equally important positive dependence on wave heights in the swash region. Offshore slope is the least significant and vegetation density is the relatively less significant parameter in the vegetated hydrodynamic system for both wave attenuation and wave run-up.

### **How accurate is a non-parametric Bayesian network as a probabilistic model for predicting flood risk in a vegetated hydrodynamic system?**

While the non-parametric Bayesian networks as predictive models definitely have an edge over other predictive techniques like neural network but they are still not enough. NPBNs employ Gaussian copulas which are insufficient for complete dependence modelling of output parameters like wave attenuation coefficient and run-up. The Gaussian copula was not validated based on the synthetic dataset from XBeach simulations which necessitates the extension of current work to more copulas and possibly to vines. It is hypothesized that extension to vines will resolve the matter and result in accurate and precise multivariate dependence structure.

### **How accurate is the developed flood risk prediction tool in predicting reality?**

The flood risk prediction tool can predict reality statistically within the 90% confidence band and generally with less than 10% error. The successful prediction of 'reality' is statistically connotated as a comparison of developed NPBN to an NPBN with a saturated graph and generally connotated as a comparison to field studies in vegetated hydrodynamic environments. The developed NPBNs for both saltmarshes and mangroves fall within the 90% confidence band of their respective saturated graphs and the tool predictions doesn't have error more than 10% compared to 5 of the field studies in various parts of the world for both saltmarshes and mangroves.

### **How can the developed model help decision makers in implementing nature-based solutions involving vegetation for flood risk mitigation?**

The flood risk prediction tool can make quick assessments about wave attenuation potential of vegetation globally. For implementing vegetation as a nature-based solution for flood risk mitigation the tool could be used to assess the utility acquired through different vegetation types and species. The tool has also skimmed out the most critical parameters affecting the vegetated hydrodynamic system which will help decision makers to focus their efforts and efficiently allocate the limited resources to achieve optimal results. Various design scenarios could also be assessed without rigorous and cumbersome numerical modelling as the tool is user-friendly and requires just a basic understanding of the meaning of various parameters. The tool could also be used as an early warning system and the effect of climate change or extreme conditions could also be predicted well ahead of time which will increase the chances of evacuation and hence reduce the flood risk.

## **6.3. RECOMMENDATIONS**

The recommendations are suggested as possible improvements which are mainly linked with the scoping and limitations of the current study. Certain aspects in this study which were scoped out or were not addressed in greater detail forms the basis of recommendations. Future studies could pick up from here to improve and add value to the current research topic.

- Extend the numerical modeling to two dimensional study by taking both cross-shore and long-shore domain into consideration. Morphological changes could also be added to modelling list to make the model more realistic.

- Increases the number of simulations *i.e.* increase Monte Carlo samples from the stochastic model because for some of the distributions the tails get curtailed and usually the extreme values are not included in the sampling. For some of the variables like extreme wave heights it makes the model less conservative and also limits the applicability.
- Field data or data from global models could be obtained to expand the domain and scale of hydrodynamic and vegetation parameters both spatially and temporally. Distributions of the parameters and the correlations among them could be determined from more real field data at different spatial locations with longer temporal scales than 3 years.
- Second order wave interaction could be included as a part of wave boundary conditions in XBeach simulations. It would add sub-harmonics on top of primary waves which changes wave steering and making the boundary conditions more realistic.
- Better dependence structure should be explored since the Gaussian copula was not validated for most of the output parameters. Extension to vines is suggested to improve the dependence modeling.
- Real bathymetry could be generated based on geographic information system (GIS) processing or even from Google Earth. The real bathymetry would be complex for the numerical model but accounting for variations in bed will make the system realistic.
- Carry out similar numerical simulations for bare bed scenarios for the same hydrodynamic and physical boundary conditions. Wave attenuation was calculated based on the reduction on the ends of vegetation but the better way to compare attenuation is to compare vegetation scenario with bare-bed scenario. By doing so another very valuable conclusion about dike crest level reduction could also be made which was not possible in this study.
- Detailed damage modelling should be done to quantify vulnerability which is the equally important half of the flood risk. The damage model could be based on the inundation depth or directly on the volume of water transmitted to the landward end of the dike.
- The prediction tool could be geo-tagged with global models for instance the ones giving wave data. Wave heights could be conditionalized in every spatial grid cell along with vegetation height (from GIS module) and a database of local scale predictions could be prepared. The database could be made available as more post-processed form of the developed tool which will require minimal user-input.

## 6.4. WAY FORWARD

Due to acute scarcity of global vegetation data next study about global vegetation modeling should start from collecting field data. Collecting vegetation data is not a complicated task, all one needs is to measure in length units or count number of plant's in a

square meter. As a starting point, collaborations could be made in places based on the locations in Table 3.3 to collect in-situ hydraulic and vegetation parameters. Also, GIS could be used with high resolution digital elevation models to extract plant heights and high resolution raster data to determine vegetation extents.

XBeach model needs improvements in how it has implemented vegetation in the model. For instance, drag coefficient could be internally calculated based on the vegetation parameters, see Equation 6.1. Vegetation Reynolds number ( $Re_v$ ) could be calculated at every time step based on Lagrangian flow velocities using Equation 2.5 and drag coefficient could be updated using Equation 6.1. It is hypothesized that it will increase accuracy of model results as compared to using one bulk value of drag coefficient for the entire simulation.

$$C_D = a + \left( \frac{b}{Re_v} \right)^c \quad (6.1)$$

Moreover, extensive research has been done in modeling vegetation as flexible blades and so it is about time to implement vegetation as flexible blades in models like XBeach, SWAN, SWASH and more that implement vegetation as rigid vegetation.

It is also highly recommended that global distributions of the parameters taken in this study, especially vegetation parameters, are researched. Global distributions of hydrodynamic parameters are available but very scarce knowledge is available for vegetation parameters. To the author's knowledge one very recent study (Simard et al., 2019) has published global distribution of mangroves height but the trend should be continued for all the vegetation parameters.

As flood risk is a likelihood of damages there are many aspects to it. In this study dike was assumed to be kept in a way that doesn't change the risk level *i.e.* the protection level was maximum. However, it is vital to include the contribution of dikes to the likelihood of increasing damages in case of not coping up with extreme conditions or climate change. Therefore, the conventional solution part of the hybrid flood defences should also be investigated in combination with nature-based solutions.

Future research should also investigate the long term sustainability of the vegetation. Long term sustainability should be researched in context of vegetation strength and resilience under storm conditions and in context of climate change. Seasonal variation of both hydrodynamic and vegetation characteristics should also be taken into account while making prediction models and evaluating wave damping effect of vegetation. With climate change intensity and frequency of extreme events is increasing and so over the long term scales the restive capacity of vegetation would be tested like never before.

Only recently guidelines about implementation of nature-based solutions have surfaced. Although, this thesis has contributed in elucidating the system dynamics of vegetated hydrodynamic environments and has pointed critical parameters to focus on but more should be investigated and standardized possibly based on the famous SMART (Specific, Measurable, Attainable, Relevant and Timely) criteria.

# BIBLIOGRAPHY

- Ababei, D., Lewandowski, D., Hanea, A., Napoles, O. M., Kurowicka, D., & Cooke, R. (2008). *Uninet help documentation* (Report). Delft University of Technology. Retrieved from <http://www.lighttwist.net/wp/wp-content/doc/UninetHelp.pdf>
- Ackerman, J. D., & Okubo, A. (1993). Reduced mixing in a marine macrophyte canopy [Journal Article]. *Functional Ecology*, 7(3), 305-309. Retrieved from <https://www.jstor.org/stable/pdf/2390209.pdf> doi: Doi10.2307/2390209
- Ali, S., & Uijtewaal Wim, S. J. (2013). Flow resistance of vegetated weirlike obstacles during high water stages [Journal Article]. *Journal of Hydraulic Engineering*, 139(3), 325-330. Retrieved from [https://doi.org/10.1061/\(ASCE\)HY.1943-7900.0000671](https://doi.org/10.1061/(ASCE)HY.1943-7900.0000671) doi: 10.1061/(ASCE)HY.1943-7900.0000671
- Anderson, M. E., & Smith, J. M. (2014). Wave attenuation by flexible, idealized salt marsh vegetation [Journal Article]. *Coastal Engineering*, 83, 82-92. Retrieved from <https://www.sciencedirect.com/science/article/pii/S0378383913001609> doi: <https://doi.org/10.1016/j.coastaleng.2013.10.004>
- Andrews, D. G., & McIntyre, M. E. (1978). An exact theory of nonlinear waves on a lagrangian-mean flow [Journal Article]. *Journal of Fluid Mechanics*, 89(4), 609-646. Retrieved from <https://www.cambridge.org/core/article/an-exact-theory-of-nonlinear-waves-on-a-lagrangian-mean-flow/BEAD9C3B8EC53E14CED92577EC58DECB> doi: 10.1017/S0022112078002773
- Asano, T., Deguchi, H., & Kobayashi, N. (1993). Interaction between water waves and vegetation [Book Section]. In *Coastal engineering 1992* (p. 2709-2723). Retrieved from <https://ascelibrary.org/doi/abs/10.1061/9780872629332.206> doi: doi:10.1061/9780872629332.206
- Asano, T., Tsutsui, S., & Sakai, T. (1988). Wave damping characteristics due to seaweed [Conference Proceedings]. In *Proceedings of 35th conference on coastal engineering (in japanese)*. Retrieved from <https://ci.nii.ac.jp/naid/10021137137/en/>
- Augustin, L. N., Irish, J. L., & Lynett, P. (2009). Laboratory and numerical studies of wave damping by emergent and near-emergent wetland vegetation [Journal Article]. *Coastal Engineering*, 56(3), 332-340. Retrieved from <http://www.sciencedirect.com/science/article/pii/S037838390800152X> doi: <https://doi.org/10.1016/j.coastaleng.2008.09.004>
- Bae, H., Monti, S., Montano, M., Steinberg, M. H., Perls, T. T., & Sebastiani, P. (2016). Learning bayesian networks from correlated data [Journal Article]. *Scientific Reports*, 6, 25156. Retrieved from <https://doi.org/10.1038/srep25156><https://www.ncbi.nlm.nih.gov/pmc/articles/PMC4857179/pdf/srep25156.pdf> doi: 10.1038/srep25156<https://www.nature.com/articles/srep25156#supplementary-information>

- Barbier, E. B. (2016). The protective service of mangrove ecosystems: A review of valuation methods [Journal Article]. *Marine Pollution Bulletin*, 109(2), 676-681. Retrieved from <https://www.sciencedirect.com/science/article/pii/S0025326X16300224?via%3Dihub> doi: <https://doi.org/10.1016/j.marpolbul.2016.01.033>
- Bayes, T., & Price, R. (1763). Lii. an essay towards solving a problem in the doctrine of chances. by the late rev. mr. bayes, f. r. s. communicated by mr. price, in a letter to john canton, a. m. f. r. s [Journal Article]. *Philosophical Transactions of the Royal Society of London*, 53, 370-418. Retrieved from <https://royalsocietypublishing.org/doi/10.1098/rstl.1763.0053> doi: 10.1098/rstl.1763.0053
- Bedford, T., & Cooke, R. (2001). *Probabilistic risk analysis: foundations and methods* [Book]. Cambridge University Press. Retrieved from [http://www.cambridge.org/catalogue/catalogue.asp?isbn=0521773202&utm\\_source=DOI&utm\\_medium=MultiLink&utm\\_content=0521773202&utm\\_campaign=CDI](http://www.cambridge.org/catalogue/catalogue.asp?isbn=0521773202&utm_source=DOI&utm_medium=MultiLink&utm_content=0521773202&utm_campaign=CDI) doi: 10.2277/0521773202
- Bertin, X., de Bakker, A., van Dongeren, A., Coco, G., André, G., Arduin, F., ... Tissier, M. (2018). Infragravity waves: From driving mechanisms to impacts [Journal Article]. *Earth-Science Reviews*, 177, 774-799. Retrieved from <http://www.sciencedirect.com/science/article/pii/S0012825217303239> doi: <https://doi.org/10.1016/j.earscirev.2018.01.002>
- Beudin, A., Kalra, T. S., Ganju, N. K., & Warner, J. C. (2017). Development of a coupled wave-flow-vegetation interaction model [Journal Article]. *Computers and Geosciences*, 100, 76-86. Retrieved from <http://www.sciencedirect.com/science/article/pii/S0098300416308184> doi: <https://doi.org/10.1016/j.cageo.2016.12.010>
- Beuzen, T., Splinter, K. D., Marshall, L. A., Turner, I. L., Harley, M. D., & Palmsten, M. L. (2018). Bayesian networks in coastal engineering: Distinguishing descriptive and predictive applications [Journal Article]. *Coastal Engineering*, 135, 16-30. Retrieved from <http://www.sciencedirect.com/science/article/pii/S0378383917303678> doi: <https://doi.org/10.1016/j.coastaleng.2018.01.005>
- Bolle, A., das Neves, L., Smets, S., Mollaert, J., & Buitrago, S. (2018). An impact-oriented early warning and bayesian-based decision support system for flood risks in zeebrugge harbour [Journal Article]. *Coastal Engineering*, 134, 191-202. Retrieved from <http://www.sciencedirect.com/science/article/pii/S0378383917300236> doi: <https://doi.org/10.1016/j.coastaleng.2017.10.006>
- Booij, N. (1981). *Gravity waves on water with non-uniform depth and current* (Thesis). Retrieved from <https://repository.tudelft.nl/islandora/object/uuid%3A05f9b2b1-b237-491f-927a-2a470e0808f3>
- Bosboom, J., & Stive, M. J. F. (2012). *Coastal dynamics 1: Lecture notes cie4305* (4th ed.) [Book]. Netherlands: Delft Academic Press (DAP) of the Vereniging voor Studie- en Studentenbelangen te Delft (VSSD).
- Bradley, K., & Houser, C. (2009). Relative velocity of seagrass blades: Implications for wave attenuation in low-energy environments [Journal Article]. *Journal of Geophysical Research: Earth Surface*, 114(F1). Retrieved from <https://agupubs.onlinelibrary.wiley.com/doi/pdf/10.1029/2007JF000951> doi: 10.1029/2007JF000951

- Bretschneider, C. L. (1954). Modification of waveheight due to bottom friction, percolation and refraction [Journal Article]. *BEB Tech. Memo.*, 45, 1-36. Retrieved from <https://ci.nii.ac.jp/naid/10003518134/>
- Brown, S., Nicholls, R. J., Woodroffe, C. D., Hanson, S., Hinkel, J., Kebede, A. S., ... Vafeidis, A. T. (2013). Sea-level rise impacts and responses: A global perspective [Book Section]. In C. W. Finkl (Ed.), *Coastal hazards* (p. 117-149). Dordrecht: Springer Netherlands. Retrieved from [https://doi.org/10.1007/978-94-007-5234-4\\_5](https://doi.org/10.1007/978-94-007-5234-4_5) [https://link.springer.com/content/pdf/10.1007/978-94-007-5234-4\\_5.pdf](https://link.springer.com/content/pdf/10.1007/978-94-007-5234-4_5.pdf) doi: 10.1007/978-94-007-5234-4\_5
- Camfield, F. E. (1977). *Wind-wave propagation over flooded, vegetated land* (Report). Coastal Engineering Research Center Fort Belvoir VA. Retrieved from <https://apps.dtic.mil/dtic/tr/fulltext/u2/a048747.pdf>
- Cao, H., Feng, W., Hu, Z., Suzuki, T., & Stive, M. J. F. (2015). Numerical modeling of vegetation-induced dissipation using an extended mild-slope equation [Journal Article]. *Ocean Engineering*, 110, 258-269. Retrieved from <http://www.sciencedirect.com/science/article/pii/S0029801815005375> doi: <https://doi.org/10.1016/j.oceaneng.2015.09.057>
- Carrick, J., Abdul Rahim, M. S. A. B., Adjei, C., Ashraa Kalee, H. H. H., Banks, S. J., Bolam, F. C., ... Stewart, G. (2018). Is planting trees the solution to reducing flood risks? [Journal Article]. *Journal of Flood Risk Management*, 0(0). Retrieved from <https://doi.org/10.1111/jfr3.12484> <https://onlinelibrary.wiley.com/doi/pdf/10.1111/jfr3.12484> doi: 10.1111/jfr3.12484
- Chang, C.-W., & Liu, P. L.-F. (2019). Long waves dissipation and harmonic generation by coastal vegetation [Journal Article]. *Applied Ocean Research*, 82, 210-224. Retrieved from <http://www.sciencedirect.com/science/article/pii/S014111871830275X> doi: <https://doi.org/10.1016/j.apor.2018.10.001>
- Chang, C.-W., Liu, P. L. F., Mei, C. C., & Maza, M. (2017). Modeling transient long waves propagating through a heterogeneous coastal forest of arbitrary shape [Journal Article]. *Coastal Engineering*, 122, 124-140. Retrieved from <http://www.sciencedirect.com/science/article/pii/S0378383916301806> doi: <https://doi.org/10.1016/j.coastaleng.2017.01.010>
- Chen, H., Ni, Y., Li, Y., Liu, F., Ou, S., Su, M., ... Suzuki, T. (2018). Deriving vegetation drag coefficients in combined wave-current flows by calibration and direct measurement methods [Journal Article]. *Advances in Water Resources*, 122, 217-227. Retrieved from <http://www.sciencedirect.com/science/article/pii/S030917081830112X> doi: <https://doi.org/10.1016/j.advwatres.2018.10.008>
- Chen, X., Chen, Q., Zhan, J., & Liu, D. (2016). Numerical simulations of wave propagation over a vegetated platform [Journal Article]. *Coastal Engineering*, 110, 64-75. Retrieved from <http://www.sciencedirect.com/science/article/pii/S0378383916000041> doi: <https://doi.org/10.1016/j.coastaleng.2016.01.003>
- Chow, V. T. (1959). *Open-channel hydraulics* (Vol. 1) [Book]. McGraw-Hill New York. Retrieved from <https://www.worldcat.org/title/open-channel-hydraulics/oclc/4010975>
- Chu, P. C., Kuo, Y., & Galanis, G. (2010). Statistical structure of the global significant wave heights [Conference Proceedings]. In *20th conference on probability and statistics in the atmospheric sciences*. Retrieved from <https://ams.confex.com/ams/pdfpapers/159792.pdf>

- Cohen-Shacham, E., Andrade, A., Dalton, J., Dudley, N., Jones, M., Kumar, C., ... Walters, G. (2019). Core principles for successfully implementing and upscaling nature-based solutions [Journal Article]. *Environmental Science and Policy*, 98, 20-29. Retrieved from <http://www.sciencedirect.com/science/article/pii/S1462901118306671> doi: <https://doi.org/10.1016/j.envsci.2019.04.014>
- Cooke, R. (1991). *Experts in uncertainty: opinion and subjective probability in science* [Book]. Oxford University Press on Demand. Retrieved from <https://global.oup.com/academic/product/experts-in-uncertainty-9780195064650>
- Cooke, R. M., & Goossens, L. L. H. J. (2008). Tu delft expert judgment data base [Journal Article]. *Reliability Engineering and System Safety*, 93(5), 657-674. Retrieved from <http://www.sciencedirect.com/science/article/pii/S0951832007000944> doi: <https://doi.org/10.1016/j.res.2007.03.005>
- Costanza, R., d'Arge, R., de Groot, R., Farber, S., Grasso, M., Hannon, B., ... van den Belt, M. (1997). The value of the world's ecosystem services and natural capital [Journal Article]. *Nature*, 387(6630), 253-260. Retrieved from <https://www.nature.com/articles/387253a0.pdf> doi: [10.1038/387253a0](https://doi.org/10.1038/387253a0)
- Couason, A., Sebastian, A., & Morales-Nápoles, O. (2018). A copula-based bayesian network for modeling compound flood hazard from riverine and coastal interactions at the catchment scale: An application to the houston ship channel, texas [Journal Article]. *Water*, 10(9), 1190. Retrieved from <http://www.mdpi.com/2073-4441/10/9/1190>
- Dalrymple, R. A., Kirby, J. T., & Hwang, P. A. (1984). Wave diffraction due to areas of energy dissipation [Journal Article]. *Journal of Waterway, Port, Coastal, and Ocean Engineering*, 110(1), 67-79. Retrieved from [https://doi.org/10.1061/\(ASCE\)0733-950X\(1984\)110:1\(67\)](https://doi.org/10.1061/(ASCE)0733-950X(1984)110:1(67)) doi: [10.1061/\(ASCE\)0733-950X\(1984\)110:1\(67\)](https://doi.org/10.1061/(ASCE)0733-950X(1984)110:1(67))
- Davies, C., & Lafortezza, R. (2019). Transitional path to the adoption of nature-based solutions [Journal Article]. *Land Use Policy*, 80, 406-409. Retrieved from <http://www.sciencedirect.com/science/article/pii/S026483771830872X><https://www.sciencedirect.com/science/article/pii/S026483771830872X?via%3Dihub> doi: <https://doi.org/10.1016/j.landusepol.2018.09.020>
- Dean, R. G. (1978). Effects of vegetation on shoreline erosional processes [Conference Proceedings]. In *National symposium on wetlands* (p. 415-426).
- Dean, R. G., & Bender, C. J. (2006). Static wave setup with emphasis on damping effects by vegetation and bottom friction [Journal Article]. *Coastal Engineering*, 53(2), 149-156. Retrieved from <http://www.sciencedirect.com/science/article/pii/S0378383905001316> doi: <https://doi.org/10.1016/j.coastaleng.2005.10.005>
- Den Heijer, C., Knipping, D. T. J. A., Plant, N. G., Van Thiel De Vries, J. S. M., Baart, F., & Van Gelder, P. H. A. J. M. (2012). Impact assessment of extreme storm events using a bayesian network [Conference Proceedings]. In *International conference on coastal engineering*. Retrieved from [https://journals.tdl.org/icce/index.php/icce/article/view/6677/pdf\\_654](https://journals.tdl.org/icce/index.php/icce/article/view/6677/pdf_654)
- Donelan, M. A., Drennan, W. M., & Katsaros, K. B. (1997). The air-sea momentum flux in conditions of wind sea and swell [Journal Article]. *Journal of Physical Oceanography*, 27(10), 2087-2099. Retrieved from [https://doi.org/10.1175/1520-0485\(1997\)027<2087:TASMF1>2.0.CO;2](https://doi.org/10.1175/1520-0485(1997)027<2087:TASMF1>2.0.CO;2) doi: [10.1175/1520-0485\(1997\)027<2087:TASMF1>2.0.CO;2](https://doi.org/10.1175/1520-0485(1997)027<2087:TASMF1>2.0.CO;2)

- EurOtop, I. (2018). *Manual on wave overtopping of sea defences and related structures. an overtopping manual largely based on european research, but for worldwide application* (Report).
- Flather, R. A. (2001). Storm surges [Book Section]. In J. H. Steele (Ed.), *Encyclopedia of ocean sciences (second edition)* (p. 530-540). Oxford: Academic Press. Retrieved from <http://www.sciencedirect.com/science/article/pii/B9780123744739001247> doi: <https://doi.org/10.1016/B978-012374473-9.00124-7>
- Fonseca, M. S., & Cahalan, J. A. (1992). A preliminary evaluation of wave attenuation by four species of seagrass [Journal Article]. *Estuarine, Coastal and Shelf Science*, 35(6), 565-576. Retrieved from <http://www.sciencedirect.com/science/article/pii/S0272771405800393> doi: [https://doi.org/10.1016/S0272-7714\(05\)80039-3](https://doi.org/10.1016/S0272-7714(05)80039-3)
- Frees, E. W., & Valdez, E. A. (1998). Understanding relationships using copulas [Journal Article]. *North American Actuarial Journal*, 2(1), 1-25. Retrieved from <https://www.tandfonline.com/doi/abs/10.1080/10920277.1998.10595667> doi: 10.1080/10920277.1998.10595667
- Geller, E. H. (2012). Bayes' rule and bomb threats [Journal Article]. *Psychology In Action*, 14(14 April 2019). Retrieved from <https://www.psychologyinaction.org/psychology-in-action-1/2012/10/22/bayes-rule-and-bomb-threats>
- Genest, C., & Favre, A. C. (2007). Everything you always wanted to know about copula modeling but were afraid to ask [Journal Article]. *Journal of Hydrologic Engineering*, 12(4), 347-368. Retrieved from <https://ascelibrary.org/doi/pdf/10.1061/%28ASCE%291084-0699%282007%2912%3A4%28347%29> doi: 10.1061/(ASCE)1084-0699(2007)12:4(347)
- Genest, C., & Mackay, J. (1986). The joy of copulas: Bivariate distributions with uniform marginals [Journal Article]. *The American Statistician*, 40(4), 280-283. Retrieved from <https://www.tandfonline.com/doi/abs/10.1080/00031305.1986.10475414> doi: 10.1080/00031305.1986.10475414
- Gent Marcel, R. A. v. (2001). Wave runup on dikes with shallow foreshores [Journal Article]. *Journal of Waterway, Port, Coastal, and Ocean Engineering*, 127(5), 254-262. Retrieved from <https://ascelibrary.org/doi/10.1061/%28ASCE%290733-950X%282001%29127%3A5%28254%29> doi: 10.1061/(ASCE)0733-950X(2001)127:5(254)
- Ghisalberti, M., & Nepf, H. M. (2002). Mixing layers and coherent structures in vegetated aquatic flows [Journal Article]. *Journal of Geophysical Research-Oceans*, 107(C2). Retrieved from <https://agupubs.onlinelibrary.wiley.com/doi/pdf/10.1029/2001JC000871> doi: Artn301110.1029/2001jc000871
- Green, E. P., & Short, F. T. (2003). *World atlas of seagrasses* [Book]. Univ of California Press.
- Guza, R., Thornton, E., & Holman, R. (1984). Swash on steep and shallow beaches [Conference Proceedings]. In 1984. Retrieved from <https://icce-ojs-tamu.tdl.org/icce/index.php/icce/article/view/3829> doi: 10.9753/icce.v19.%p
- Hallegatte, S., Green, C., Nicholls, R. J., & Corfee-Morlot, J. (2013). Future flood losses in major coastal cities [Journal Article]. *Nature Climate Change*, 3, 802. Retrieved from <https://doi.org/10.1038/nclimate1979> doi: 10.1038/nclimate1979 <https://www.nature.com/articles/nclimate1979#supplementary-information>

- Han, S., & Coulibaly, P. (2017). Bayesian flood forecasting methods: A review [Journal Article]. *Journal of Hydrology*, 551, 340-351. Retrieved from <http://www.sciencedirect.com/science/article/pii/S0022169417304031> doi: <https://doi.org/10.1016/j.jhydrol.2017.06.004>
- Hanea, A., Morales Napoles, O., & Ababei, D. (2015). Non-parametric bayesian networks: Improving theory and reviewing applications [Journal Article]. *Reliability Engineering and System Safety*, 144, 265-284. Retrieved from <http://www.sciencedirect.com/science/article/pii/S0951832015002331> doi: <https://doi.org/10.1016/j.res.2015.07.027>
- Hanea, A. M., Kurowicka, D., & Cooke, R. M. (2006). Hybrid method for quantifying and analyzing bayesian belief nets [Journal Article]. *Quality and Reliability Engineering International*, 22(6), 709-729. Retrieved from <https://onlinelibrary.wiley.com/doi/pdf/10.1002/qre.808> doi: 10.1002/qre.808
- Hasselmann, K., & Collins, J. I. (1968). Spectral dissipation of finite-depth gravity waves due to turbulent bottom friction [Journal Article]. *Journal of Marine Research*, 26(1), 1-12.
- Hawkes, P. J., Gouldby, B. P., Tawn, J. A., & Owen, M. W. (2002). The joint probability of waves and water levels in coastal engineering design [Journal Article]. *Journal of Hydraulic Research*, 40(3), 241-251. Retrieved from <https://doi.org/10.1080/00221680209499940><https://www.tandfonline.com/doi/abs/10.1080/00221680209499940> doi: 10.1080/00221680209499940
- Henry, P.-Y., Myrhaug, D., & Aberle, J. (2015). Drag forces on aquatic plants in nonlinear random waves plus current [Journal Article]. *Estuarine, Coastal and Shelf Science*, 165, 10-24. Retrieved from <http://www.sciencedirect.com/science/article/pii/S0272771415300767> doi: <https://doi.org/10.1016/j.ecss.2015.08.021>
- Holthuijsen, L. H. (2010). *Waves in oceanic and coastal waters* [Book]. Cambridge university press. Retrieved from [http://www.cambridge.org/gb/knowledge/isbn/item112254/?site\\_locale=en\\_GB](http://www.cambridge.org/gb/knowledge/isbn/item112254/?site_locale=en_GB)
- Horikawa, K. (1978). Coastal engineering: an introduction to ocean engineering [Journal Article]. *Publ. by: University of Tokyo Press*.
- Horstman, E. M., Dohmen-Janssen, C. M., Narra, P. M. F., van den Berg, N. J. F., Siemerink, M., & Hulscher, S. J. M. H. (2014). Wave attenuation in mangroves: A quantitative approach to field observations [Journal Article]. *Coastal Engineering*, 94, 47-62. Retrieved from <http://www.sciencedirect.com/science/article/pii/S0378383914001574> doi: <https://doi.org/10.1016/j.coastaleng.2014.08.005>
- Hu, Z., Stive, M., Zitman, T., & Suzuki, T. (2012). Drag coefficient of vegetation in flow modeling [Conference Proceedings]. In *International conference on coastal engineering*. Retrieved from <https://journals.tdl.org/icce/index.php/icce/article/view/6405> doi: 10.9753/icce.v33.posters.4
- Hu, Z., Suzuki, T., Zitman, T., Uittewaal, W., & Stive, M. (2014). Laboratory study on wave dissipation by vegetation in combined current-wave flow [Journal Article]. *Coastal Engineering*, 88, 131-142. Retrieved from <http://www.sciencedirect.com/science/article/pii/S0378383914000416> doi: <https://doi.org/10.1016/j.coastaleng.2014.02.009>

- Huang, Z., Yao, Y., Sim, S. Y., & Yao, Y. (2011). Interaction of solitary waves with emergent, rigid vegetation [Journal Article]. *Ocean Engineering*, 38(10), 1080-1088. Retrieved from <http://www.sciencedirect.com/science/article/pii/S0029801811000448> doi: <https://doi.org/10.1016/j.oceaneng.2011.03.003>
- Hugo, G. (2011). Future demographic change and its interactions with migration and climate change [Journal Article]. *Global Environmental Change*, 21, S21-S33. Retrieved from <http://www.sciencedirect.com/science/article/pii/S0959378011001439> doi: <https://doi.org/10.1016/j.gloenvcha.2011.09.008>
- Ikeda, S., & Kanazawa, M. (1996). Three-dimensional organized vortices above flexible water plants [Journal Article]. *Journal of Hydraulic Engineering-Asce*, 122(11), 634-640. Retrieved from <https://ascelibrary.org/doi/pdf/10.1061/%28ASCE%290733-9429%281996%29122%3A11%28634%29> doi: [Doi10.1061/\(ASCE\)0733-9429\(1996\)122:11\(634\)](https://doi.org/10.1061/(ASCE)0733-9429(1996)122:11(634))
- Ikeda, S., Yamada, T., & Toda, Y. (2001). Numerical study on turbulent flow and honami in and above flexible plant canopy [Journal Article]. *International Journal of Heat and Fluid Flow*, 22(3), 252-258. Retrieved from <http://www.sciencedirect.com/science/article/pii/S0142727X0100087X> doi: [https://doi.org/10.1016/S0142-727X\(01\)00087-X](https://doi.org/10.1016/S0142-727X(01)00087-X)
- Infantes, E., Orfila, A., Simarro, G., Terrados, J., Luhar, M., & Nepf, H. (2012). Effect of a seagrass (*Posidonia oceanica*) meadow on wave propagation [Journal Article]. *Marine Ecology Progress Series*, 456, 63-72. Retrieved from <https://www.int-res.com/articles/meps2012/456/m456p063.pdf> doi: [10.3354/meps09754](https://doi.org/10.3354/meps09754)
- IPCC, Parry, M., Parry, M. L., Canziani, O., Palutikof, J., Van der Linden, P., & Hanson, C. (2007). *Climate change 2007-impacts, adaptation and vulnerability: Working group ii contribution to the fourth assessment report of the ipcc* (Vol. 4) [Book]. Cambridge University Press. Retrieved from [https://www.ipcc.ch/site/assets/uploads/2018/03/ar4\\_wg2\\_full\\_report.pdf](https://www.ipcc.ch/site/assets/uploads/2018/03/ar4_wg2_full_report.pdf)
- Jadhav, R. S., & Chen, Q. (2012). Field investigation of wave dissipation over saltmarsh vegetation during tropical cyclone [Conference Proceedings]. In *Coastal engineering proceedings; proceedings of 33rd conference on coastal engineering*. Retrieved from <https://journals.tdl.org/icce/index.php/icce/article/view/6575> doi: <https://doi.org/10.9753/icce.v33.waves.41>
- Jadhav, R. S., & Chen, Q. (2013). Probability distribution of wave heights attenuated by salt marsh vegetation during tropical cyclone [Journal Article]. *Coastal Engineering*, 82, 47-55. Retrieved from <http://www.sciencedirect.com/science/article/pii/S0378383913001348> doi: <https://doi.org/10.1016/j.coastaleng.2013.08.006>
- Jadhav, R. S., Chen, Q., & Smith, J. M. (2013). Spectral distribution of wave energy dissipation by salt marsh vegetation [Journal Article]. *Coastal Engineering*, 77, 99-107. Retrieved from <http://www.sciencedirect.com/science/article/pii/S0378383913000537> doi: <https://doi.org/10.1016/j.coastaleng.2013.02.013>
- Jaeger, W. (2018). *Multivariate methods for coastal and offshore risks* (Thesis). Retrieved from <https://repository.tudelft.nl/islandora/object/uuid:4be7ac1d-8232-457c-8ad6-73ec23baf9ce?collection=research>
- Janssen, M. (2016). *Flood hazard reduction by mangroves* (Thesis). Retrieved from <https://repository.tudelft.nl/islandora/object/uuid:b3cfe9b0-c8d3-4eb6-aad2-977d879430b5?collection=education>

- Jäger, W. S., Christie, E. K., Hanea, A. M., den Heijer, C., & Spencer, T. (2018). A bayesian network approach for coastal risk analysis and decision making [Journal Article]. *Coastal Engineering*, 134, 48-61. Retrieved from <http://www.sciencedirect.com/science/article/pii/S0378383917300625> doi: <https://doi.org/10.1016/j.coastaleng.2017.05.004>
- Jäger, W. S., & Nápoles, O. M. (2017). A vine-copula model for time series of significant wave heights and mean zero-crossing periods in the north sea [Journal Article]. *ASCE-ASME Journal of Risk and Uncertainty in Engineering Systems, Part A: Civil Engineering*, 3(4), 04017014. Retrieved from <https://ascelibrary.org/doi/10.1061/AJRUA6.0000917> doi: 10.1061/AJRUA6.0000917
- John, B. M., Shirlal, K. G., & Rao, S. (2015). Effect of artificial vegetation on wave attenuation – an experimental investigation [Journal Article]. *Procedia Engineering*, 116, 600-606. Retrieved from <http://www.sciencedirect.com/science/article/pii/S18777058151019864> doi: <https://doi.org/10.1016/j.proeng.2015.08.331>
- Karambas, T., Koftis, T., & Prinos, P. (2016). Modeling of nonlinear wave attenuation due to vegetation [Journal Article]. *Journal of Coastal Research*, 32(1), 142-152, 11. Retrieved from <https://doi.org/10.2112/JCOASTRES-D-14-00044.1>
- Kellens, W., Terpstra, T., & De Maeyer, P. (2013). Perception and communication of flood risks: A systematic review of empirical research [Journal Article]. *Risk Analysis*, 33(1), 24-49. Retrieved from <https://doi.org/10.1111/j.1539-6924.2012.01844.x> <https://onlinelibrary.wiley.com/doi/pdf/10.1111/j.1539-6924.2012.01844.x> doi: 10.1111/j.1539-6924.2012.01844.x
- K G, P., & Bhaskaran, P. K. (2017). Wave attenuation in presence of mangroves: A sensitivity study for varying bottom slopes [Journal Article]. *The International Journal of Ocean and Climate Systems*, 8(3), 126-134. Retrieved from <https://doi.org/10.1177/1759313117702919> doi: 10.1177/1759313117702919
- Kim, S. (2018). Storm surges [Book Section]. In *Reference module in earth systems and environmental sciences*. Elsevier. Retrieved from <http://www.sciencedirect.com/science/article/pii/B9780124095489108498> doi: <https://doi.org/10.1016/B978-0-12-409548-9.10849-8>
- Kobayashi, N., Raichle, A. W., & Asano, T. (1993). Wave attenuation by vegetation [Journal Article]. *Journal of Waterway, Port, Coastal, and Ocean Engineering*, 119(1), 30-48. Retrieved from [https://ascelibrary.org/doi/abs/10.1061/\(ASCE\)0733-950X\(1993\)119:1\(30\)-950X%281993%29119%3A1%2830%29](https://ascelibrary.org/doi/abs/10.1061/(ASCE)0733-950X(1993)119:1(30)-950X%281993%29119%3A1%2830%29) doi: doi:10.1061/(ASCE)0733-950X(1993)119:1(30)
- Koehl, M. A. R. (1984). How do benthic organisms withstand moving water? [Journal Article]. *American Zoologist*, 24(1), 57-70. Retrieved from <https://doi.org/10.1093/icb/24.1.57> doi: 10.1093/icb/24.1.57
- Kourgialas, N. N., Dokou, Z., & Karatzas, G. P. (2015). Statistical analysis and ann modeling for predicting hydrological extremes under climate change scenarios: The example of a small mediterranean agro-watershed [Journal Article]. *Journal of Environmental Management*, 154, 86-101. Retrieved from <http://www.sciencedirect.com/science/article/pii/S0301479715001097> doi: <https://doi.org/10.1016/j.jenvman.2015.02.034>
- Krzysztofowicz, R. (1999). Bayesian theory of probabilistic forecasting via deterministic hydrologic model [Journal Article]. *Water Resources Research*, 35(9), 2739-2750. Retrieved from

- <https://agupubs.onlinelibrary.wiley.com/doi/abs/10.1029/1999WR900099> doi: 10.1029/1999wr900099
- Kurowicka, D., & Cooke, R. (2004). Non-parametric continuous bayesian belief nets with expert judgement [Journal Article]. *Probabilistic Safety Assessment and Management*, 2784-2790. Retrieved from [https://link.springer.com/chapter/10.1007/978-0-85729-410-4\\_446](https://link.springer.com/chapter/10.1007/978-0-85729-410-4_446)
- Lafortezza, R., & Sanesi, G. (2019). Nature-based solutions: Settling the issue of sustainable urbanization [Journal Article]. *Environmental Research*, 172, 394-398. Retrieved from <http://www.sciencedirect.com/science/article/pii/S0013935118306984><https://www.sciencedirect.com/science/article/pii/S0013935118306984?via%3Dihub> doi: <https://doi.org/10.1016/j.envres.2018.12.063>
- Lara, J. L., Maza, M., Ondiviela, B., Trinogga, J., Losada, I. J., Bouma, T. J., & Gordejuela, N. (2016). Large-scale 3-d experiments of wave and current interaction with real vegetation. part 1: Guidelines for physical modeling [Journal Article]. *Coastal Engineering*, 107, 70-83. Retrieved from <http://www.sciencedirect.com/science/article/pii/S0378383915001696> doi: <https://doi.org/10.1016/j.coastaleng.2015.09.012>
- Lashley, C. H., Roelvink, D., van Dongeren, A., Buckley, M. L., & Lowe, R. J. (2018). Nonhydrostatic and surfbeat model predictions of extreme wave run-up in fringing reef environments [Journal Article]. *Coastal Engineering*, 137, 11-27. Retrieved from <https://www.sciencedirect.com/science/article/pii/S0378383917305926?via%3Dihub> doi: 10.1016/j.coastaleng.2018.03.007
- Lee, D., & Pan, R. (2018). A nonparametric bayesian network approach to assessing system reliability at early design stages [Journal Article]. *Reliability Engineering and System Safety*, 171, 57-66. Retrieved from <http://www.sciencedirect.com/science/article/pii/S0951832017305033> doi: <https://doi.org/10.1016/j.ress.2017.11.009>
- Lei, J., & Nepf, H. (2019a). Blade dynamics in combined waves and current [Journal Article]. *Journal of Fluids and Structures*, 87, 137-149. Retrieved from <http://www.sciencedirect.com/science/article/pii/S0889974618306996> doi: <https://doi.org/10.1016/j.jfluidstructs.2019.03.020>
- Lei, J., & Nepf, H. (2019b). Wave damping by flexible vegetation: Connecting individual blade dynamics to the meadow scale [Journal Article]. *Coastal Engineering*, 147, 138-148. Retrieved from <http://www.sciencedirect.com/science/article/pii/S0378383918300905> doi: <https://doi.org/10.1016/j.coastaleng.2019.01.008>
- Leontaris, G., & Morales-Nápoles, O. (2018). Anduril — a matlab toolbox for analysis and decisions with uncertainty: Learning from expert judgments [Journal Article]. *SoftwareX*, 7, 313-317. Retrieved from <http://www.sciencedirect.com/science/article/pii/S2352711018300608> doi: <https://doi.org/10.1016/j.softx.2018.07.001>
- Li, C., Singh, V. P., & Mishra, A. K. (2013). A bivariate mixed distribution with a heavy-tailed component and its application to single-site daily rainfall simulation [Journal Article]. *Water Resources Research*, 49(2), 767-789. Retrieved from <https://doi.org/10.1002/wrcr.20063><https://agupubs.onlinelibrary.wiley.com/doi/pdf/10.1002/wrcr.20063> doi: 10.1002/wrcr.20063

- Li, C. W., & Yan, K. (2007). Numerical investigation of wave–current–vegetation interaction [Journal Article]. *Journal of Hydraulic Engineering*, 133(7), 794–803. Retrieved from [https://doi.org/10.1061/\(ASCE\)0733-9429\(2007\)133:7\(794\)](https://doi.org/10.1061/(ASCE)0733-9429(2007)133:7(794)) doi: 10.1061/(ASCE)0733-9429(2007)133:7(794)
- Liu, P. L. F., Chang, C.-W., Mei, C. C., Lomonaco, P., Martin, F. L., & Maza, M. (2015). Periodic water waves through an aquatic forest [Journal Article]. *Coastal Engineering*, 96, 100–117. Retrieved from <http://www.sciencedirect.com/science/article/pii/S0378383914002002> doi: <https://doi.org/10.1016/j.coastaleng.2014.11.002>
- Longuet-Higgins, M. S., & Stewart, R. W. (1962). Radiation stress and mass transport in gravity waves, with application to ‘surf beats’ [Journal Article]. *Journal of Fluid Mechanics*, 13(4), 481–504. Retrieved from [https://www.cambridge.org/core/services/aop-cambridge-core/content/view/CEE23C7B7F6776AA78150426A67B98BB/S0022112062000877a.pdf/radiation\\_stress\\_and\\_mass\\_transport\\_in\\_gravity\\_waves\\_with\\_application\\_to\\_surf\\_beats.pdf](https://www.cambridge.org/core/services/aop-cambridge-core/content/view/CEE23C7B7F6776AA78150426A67B98BB/S0022112062000877a.pdf/radiation_stress_and_mass_transport_in_gravity_waves_with_application_to_surf_beats.pdf) doi: <https://doi.org/10.1017/S0022112062000877>
- Losada, I. J., Maza, M., & Lara, J. L. (2016). A new formulation for vegetation-induced damping under combined waves and currents [Journal Article]. *Coastal Engineering*, 107, 1–13. Retrieved from <http://www.sciencedirect.com/science/article/pii/S0378383915001684> doi: <https://doi.org/10.1016/j.coastaleng.2015.09.011>
- Luhar, M., Coutu, S., Infantes, E., Fox, S., & Nepf, H. (2010). Wave-induced velocities inside a model seagrass bed [Journal Article]. *Journal of Geophysical Research-Oceans*, 115. Retrieved from <https://agupubs.onlinelibrary.wiley.com/doi/pdf/10.1029/2010JC006345> doi: ArtnC1200510.1029/2010jc006345
- Luhar, M., Infantes, E., Orfila, A., Terrados, J., & Nepf, H. M. (2013). Field observations of wave-induced streaming through a submerged seagrass (*posidonia oceanica*) meadow [Journal Article]. *Journal of Geophysical Research-Oceans*, 118(4), 1955–1968. Retrieved from <https://agupubs.onlinelibrary.wiley.com/doi/pdf/10.1002/jgrc.20162> doi: 10.1002/jgrc.20162
- Luhar, M., & Nepf, H. M. (2016). Wave-induced dynamics of flexible blades [Journal Article]. *Journal of Fluids and Structures*, 61, 20–41. Retrieved from <http://www.sciencedirect.com/science/article/pii/S0889974615002613> doi: <https://doi.org/10.1016/j.jfluidstructs.2015.11.007>
- Lövstedt, C. B., & Larson, M. (2010). Wave damping in reed: Field measurements and mathematical modeling [Journal Article]. *Journal of Hydraulic Engineering*, 136(4), 222–233. Retrieved from <https://ascelibrary.org/doi/abs/10.1061/%28ASCE%29HY.1943-7900.0000167> doi: doi:10.1061/(ASCE)HY.1943-7900.0000167
- Ma, G., Kirby, J. T., Su, S.-E., Figlus, J., & Shi, F. (2013). Numerical study of turbulence and wave damping induced by vegetation canopies [Journal Article]. *Coastal Engineering*, 80, 68–78. Retrieved from <http://www.sciencedirect.com/science/article/pii/S0378383913001063> doi: <https://doi.org/10.1016/j.coastaleng.2013.05.007>
- Manohar, M., Mobarek, I., & El Sharaky, N. (1976). Characteristics of wave period [Conference Proceedings]. In *International conference on coastal engineering*. Retrieved from <https://journals.tdl.org/icce/index.php/icce/article/view/3064> doi: 10.9753/icce.v15.15

- Marek, P. (2019). *Mangroves* (Vol. 2003) (Web Page No. 11 May 2019). Retrieved from <http://www.mangrove.at/mangrove.html>
- Marsooli, R., & Wu, W. (2014). Numerical investigation of wave attenuation by vegetation using a 3d rans model [Journal Article]. *Advances in Water Resources*, 74, 245-257. Retrieved from <http://www.sciencedirect.com/science/article/pii/S030917081400195X> doi: <https://doi.org/10.1016/j.advwatres.2014.09.012>
- Mattis, S. A., Kees, C. E., Wei, M. V., Dimakopoulos, A., & Dawson, C. N. (2019). Computational model for wave attenuation by flexible vegetation [Journal Article]. *Journal of Waterway, Port, Coastal, and Ocean Engineering*, 145(1), 04018033. Retrieved from [https://doi.org/10.1061/\(ASCE\)WW.1943-5460.0000487](https://doi.org/10.1061/(ASCE)WW.1943-5460.0000487) doi: 10.1061/(ASCE)WW.1943-5460.0000487
- Maza, M., Lara, J. L., & Losada, I. J. (2013). A coupled model of submerged vegetation under oscillatory flow using navier-stokes equations [Journal Article]. *Coastal Engineering*, 80, 16-34. Retrieved from <http://www.sciencedirect.com/science/article/pii/S0378383913000914> doi: <https://doi.org/10.1016/j.coastaleng.2013.04.009>
- Maza, M., Lara, J. L., & Losada, I. J. (2016). Solitary wave attenuation by vegetation patches [Journal Article]. *Advances in Water Resources*, 98, 159-172. Retrieved from <http://www.sciencedirect.com/science/article/pii/S0309170816302196> doi: <https://doi.org/10.1016/j.advwatres.2016.10.021>
- Maza, M., Lara, J. L., Losada, I. J., Ondiviela, B., Trinogga, J., & Bouma, T. J. (2015). Large-scale 3-d experiments of wave and current interaction with real vegetation. part 2: Experimental analysis [Journal Article]. *Coastal Engineering*, 106, 73-86. Retrieved from <http://www.sciencedirect.com/science/article/pii/S0378383915001581> doi: <https://doi.org/10.1016/j.coastaleng.2015.09.010>
- McIvor, A., Spencer, T., Möller, I., & Spalding, M. (2012). *Storm surge reduction by mangroves. natural coastal protection series: Report 2* (Report). Retrieved from <http://www.torbenpjensen.dk/13/07-vestindiske-oer/25-kajaktur/pdf/storm-surge-reduction-by-mangroves-report.pdf>
- Mei, C. C., Chan, I. C., Liu, P. L. F., Huang, Z., & Zhang, W. (2011). Long waves through emergent coastal vegetation [Journal Article]. *Journal of Fluid Mechanics*, 687, 461-491. Retrieved from <https://www.cambridge.org/core/article/long-waves-through-emergent-coastal-vegetation/4AEB4110327F4FF3DBC143C1F679AB03> doi: 10.1017/jfm.2011.373
- Mendez, F. J., & Losada, I. J. (2004). An empirical model to estimate the propagation of random breaking and nonbreaking waves over vegetation fields [Journal Article]. *Coastal Engineering*, 51(2), 103-118. Retrieved from <http://www.sciencedirect.com/science/article/pii/S0378383903001182> doi: <https://doi.org/10.1016/j.coastaleng.2003.11.003>
- Mendoza-Lugo, M. A., Delgado-Hernández, D. J., & Morales-Nápoles, O. (2019). Reliability analysis of reinforced concrete vehicle bridges columns using non-parametric bayesian networks [Journal Article]. *Engineering Structures*, 188, 178-187. Retrieved from <http://www.sciencedirect.com/science/article/pii/S014102961833565X> doi: <https://doi.org/10.1016/j.engstruct.2019.03.011>

- Möller, I. (2006). Quantifying saltmarsh vegetation and its effect on wave height dissipation: Results from a uk east coast saltmarsh [Journal Article]. *Estuarine, Coastal and Shelf Science*, 69(3), 337-351. Retrieved from <http://www.sciencedirect.com/science/article/pii/S027277140600182X> doi: <https://doi.org/10.1016/j.ecss.2006.05.003>
- Möller, I., Kudella, M., Rupprecht, F., Spencer, T., Paul, M., van Wesenbeeck, B. K., ... Schimmels, S. (2014). Wave attenuation over coastal salt marshes under storm surge conditions [Journal Article]. *Nature Geoscience*, 7, 727. Retrieved from <https://www.nature.com/articles/ngeo2251>, <https://www.nature.com/articles/ngeo2251#supplementary-information> doi: <https://doi.org/10.1038/ngeo2251>
- Möller, I., Spencer, T., French, J. R., Leggett, D. J., & Dixon, M. (1999). Wave transformation over salt marshes: A field and numerical modelling study from north norfolk, england [Journal Article]. *Estuarine, Coastal and Shelf Science*, 49(3), 411-426. Retrieved from <http://www.sciencedirect.com/science/article/pii/S0272771499905097> doi: <https://doi.org/10.1006/ecss.1999.0509>
- Méndez, F. J., Losada, I. J., & Losada, M. A. (1999). Hydrodynamics induced by wind waves in a vegetation field [Journal Article]. *Journal of Geophysical Research: Oceans*, 104(C8), 18383-18396. Retrieved from <https://agupubs.onlinelibrary.wiley.com/doi/pdf/10.1029/1999JC900119> doi: 10.1029/1999JC900119
- Moffett, K. B., Nardin, W., Silvestri, S., Wang, C., & Temmerman, S. (2015). Multiple stable states and catastrophic shifts in coastal wetlands: Progress, challenges, and opportunities in validating theory using remote sensing and other methods [Journal Article]. *Remote Sensing*, 7(8), 10184-10226. Retrieved from [https://res.mdpi.com/remotesensing/remotesensing-07-10184/article\\_deploy/remotesensing-07-10184.pdf?filename=&attachment=1](https://res.mdpi.com/remotesensing/remotesensing-07-10184/article_deploy/remotesensing-07-10184.pdf?filename=&attachment=1) doi: 10.3390/rs70810184
- Montgomery, J. M., Bryan, K. R., Mullarney, J. C., & Horstman, E. M. (2019). Attenuation of storm surges by coastal mangroves [Journal Article]. *Geophysical Research Letters*, 46(5), 2680-2689. Retrieved from <https://agupubs.onlinelibrary.wiley.com/doi/pdf/10.1029/2018GL081636> doi: 10.1029/2018GL081636
- Morales Napoles, O., Kurowicka, D., & Roelen, A. (2008). Eliciting conditional and unconditional rank correlations from conditional probabilities [Journal Article]. *Reliability Engineering and System Safety*, 93(5), 699-710. Retrieved from <http://www.sciencedirect.com/science/article/pii/S095183200700097X> doi: <https://doi.org/10.1016/j.j.res.2007.03.020>
- Morales Napoles, O., Worm, D., Haak, P. v. d., Hanea, A., Courage, W., & Miraglia, S. (2013). *Reader for course: Introduction to bayesian networks* (Report). Retrieved from <https://brightspace.tudelft.nl>
- Morales-Nápoles, O., Delgado-Hernández, D. J., De-León-Escobedo, D., & Arteaga-Arcos, J. C. (2014). A continuous bayesian network for earth dams' risk assessment: methodology and quantification [Journal Article]. *Structure and Infrastructure Engineering*, 10(5), 589-603. Retrieved from <https://www.tandfonline.com/doi/abs/10.1080/15732479.2012.757789> doi: 10.1080/15732479.2012.757789
- Morison, J. R., Johnson, J. W., & Schaaf, S. A. (1950). The force exerted by surface waves on piles [Journal Article]. *Journal of Petroleum Technology*, 2(05), 149-154. Retrieved from <https://doi.org/10.2118/950149-G> <https://www.onepetro.org/443/download/>

- [journal-paper/SPE-950149-G?id=journal-paper%2FSPE-950149-G](#) doi: 10.2118/950149-G
- Munk, W. H. (1950). Origin and generation of waves [Conference Proceedings]. In *International conference on coastal engineering*. Retrieved from <https://icce-ojs.tamu.tdl.org/icce/index.php/icce/article/view/904/1> doi: 10.9753/icce.v1.1
- Narayan, S., Beck, M. W., Reguero, B. G., Losada, I. J., van Wesenbeeck, B., Pontee, N., ... Burks-Copes, K. A. (2016). The effectiveness, costs and coastal protection benefits of natural and nature-based defences [Journal Article]. *PLOS ONE*, 11(5), e0154735. Retrieved from <https://www.ncbi.nlm.nih.gov/pmc/articles/PMC4852949/pdf/pone.0154735.pdf> doi: <https://doi.org/10.1371/journal.pone.0154735>
- Narayan, S., Simmonds, D., Nicholls, R. J., & Clarke, D. (2018). A bayesian network model for assessments of coastal inundation pathways and probabilities [Journal Article]. *Journal of Flood Risk Management*, 11(S1), S233-S250. Retrieved from <https://doi.org/10.1111/jfr3.12200><https://onlinelibrary.wiley.com/doi/pdf/10.1111/jfr3.12200> doi: 10.1111/jfr3.12200
- Nepf, H. M. (1999). Drag, turbulence, and diffusion in flow through emergent vegetation [Journal Article]. , 35(2), 479-489. Retrieved from <https://agupubs.onlinelibrary.wiley.com/doi/abs/10.1029/1998WR900069><https://agupubs.onlinelibrary.wiley.com/doi/pdf/10.1029/1998WR900069> doi: doi:10.1029/1998WR900069
- Nepf, H. M. (2012a). Flow and transport in regions with aquatic vegetation [Journal Article]. *Annual Review of Fluid Mechanics*, 44(1), 123-142. Retrieved from <https://www.annualreviews.org/doi/pdf/10.1146/annurev-fluid-120710-101048> doi: 10.1146/annurev-fluid-120710-101048
- Nepf, H. M. (2012b). Hydrodynamics of vegetated channels [Journal Article]. *Journal of Hydraulic Research*, 50(3), 262-279. Retrieved from <https://doi.org/10.1080/00221686.2012.696559><https://www.tandfonline.com/doi/pdf/10.1080/00221686.2012.696559?needAccess=true> doi: 10.1080/00221686.2012.696559
- Nepf, H. M., & Koch, E. W. (1999). Vertical secondary flows in submersed plant-like arrays [Journal Article]. *Limnology and Oceanography*, 44(4), 1072-1080. Retrieved from <https://aslopubs.onlinelibrary.wiley.com/doi/pdf/10.4319/lo.1999.44.4.1072> doi: DOI10.4319/lo.1999.44.4.1072
- Nepf, H. M., & Vivoni, E. R. (2000). Flow structure in depth-limited, vegetated flow [Journal Article]. , 105(C12), 28547-28557. Retrieved from <https://agupubs.onlinelibrary.wiley.com/doi/pdf/10.1029/2000JC900145> doi: doi:10.1029/2000JC900145
- Neumann, B., Vafeidis, A. T., Zimmermann, J., & Nicholls, R. J. (2015). Future coastal population growth and exposure to sea-level rise and coastal flooding - a global assessment [Journal Article]. *PLOS ONE*, 10(3), e0118571. Retrieved from <https://www.ncbi.nlm.nih.gov/pmc/articles/PMC4367969/pdf/pone.0118571.pdf> doi: 10.1371/journal.pone.0118571
- Niazi, M. H. K., Sigalas, N., Scott, E., Grossmann, E., & Damdam, K. (2018). *Robust flood defence in response to climate change* (Report). Delft University of Technology. Retrieved from <https://repository.tudelft.nl/islandora/object/uuid%3A7140327a-17e8-4218-b7ad-a63193044d4e>

- Nicholls, R. J., & Cazenave, A. (2010). Sea-level rise and its impact on coastal zones [Journal Article]. *Science*, 328(5985), 1517. Retrieved from <http://science.sciencemag.org/content/328/5985/1517.abstract><https://science.sciencemag.org/content/sci/328/5985/1517.full.pdf> doi: 10.1126/science.1185782
- Nicholls, R. J., Hoozemans, F. M. J., & Marchand, M. (1999). Increasing flood risk and wetland losses due to global sea-level rise: regional and global analyses [Journal Article]. *Global Environmental Change*, 9, S69-S87. Retrieved from <http://www.sciencedirect.com/science/article/pii/S0959378099000199> doi: [https://doi.org/10.1016/S0959-3780\(99\)00019-9](https://doi.org/10.1016/S0959-3780(99)00019-9)
- Nwogu, O., & Demirbilek, Z. (2010). Infragravity wave motions and runup over shallow fringing reefs [Journal Article]. *Journal of Waterway, Port, Coastal, and Ocean Engineering*, 136(6), 295-305. Retrieved from [https://doi.org/10.1061/\(ASCE\)WW.1943-5460.0000050](https://doi.org/10.1061/(ASCE)WW.1943-5460.0000050) doi: 10.1061/(ASCE)WW.1943-5460.0000050
- Ozeren, Y., Wren, D. G., & Wu, W. (2014). Experimental investigation of wave attenuation through model and live vegetation [Journal Article]. *Journal of Waterway Port Coastal and Ocean Engineering*, 140(5). Retrieved from <https://ascelibrary.org/doi/10.1061/%28ASCE%29WW.1943-5460.0000251> doi: Artn0401401910.1061/(Asce)Ww.1943-5460.0000251
- Paul, M. (2015). *Interaction of seagrass and hydrodynamics* [Figure]. Retrieved from <https://doi.org/10.5281/zenodo.16406> doi: 10.5281/zenodo.16406
- Paul, M., & Amos, C. L. (2011). Spatial and seasonal variation in wave attenuation over zostera noltii [Journal Article]. *Journal of Geophysical Research: Oceans*, 116(C8). Retrieved from <https://doi.org/10.1029/2010JC006797><https://agupubs.onlinelibrary.wiley.com/doi/pdf/10.1029/2010JC006797> doi: 10.1029/2010JC006797
- Pearl, J. (1988). Bayesian inference [Book Section]. In J. Pearl (Ed.), *Probabilistic reasoning in intelligent systems* (p. 29-75). San Francisco (CA): Morgan Kaufmann. Retrieved from <https://www.elsevier.com/books/probabilistic-reasoning-in-intelligent-systems/pearl/978-0-08-051489-5> doi: <https://doi.org/10.1016/B978-0-08-051489-5.50008-4>
- Pearson, S. (2016). *Predicting wave-induced flooding on low-lying tropical islands using a bayesian network* (Thesis). doi: <http://resolver.tudelft.nl/uuid:c3988f4b-99f8-4936-9504-261b32bb0cd1>
- Pearson, S. G., Storlazzi, C. D., van Dongeren, A. R., Tissier, M. F. S., & Reniers, A. J. H. M. (2017). A bayesian-based system to assess wave-driven flooding hazards on coral reef-lined coasts [Journal Article]. *Journal of Geophysical Research: Oceans*, 122(12), 10099-10117. Retrieved from <https://agupubs.onlinelibrary.wiley.com/doi/pdf/10.1002/2017JC013204> doi: 10.1002/2017JC013204
- Phan, K. L., Stive, M. J. F., Zijlema, M., Truong, H. S., & Aarninkhof, S. G. J. (2019). The effects of wave non-linearity on wave attenuation by vegetation [Journal Article]. *Coastal Engineering*, 147, 63-74. Retrieved from <http://www.sciencedirect.com/science/article/pii/S0378383918303600> doi: <https://doi.org/10.1016/j.coastaleng.2019.01.004>
- Pinsky, M. L., Guannel, G., & Arkema, K. K. (2013). Quantifying wave attenuation to inform coastal habitat conservation [Journal Article]. *Ecosphere*, 4(8), art95. Retrieved from <https://esajournals.onlinelibrary.wiley.com/doi/pdf/10.1890/ES13-00080.1> doi: 10.1890/es13-00080.1

- Plant, N. G., & Holland, K. T. (2011). Prediction and assimilation of surf-zone processes using a bayesian network: Part i: Forward models [Journal Article]. *Coastal Engineering*, 58(1), 119-130. Retrieved from <http://www.sciencedirect.com/science/article/pii/S0378383910001353> doi: <https://doi.org/10.1016/j.coastaleng.2010.09.003>
- Plomaritis, T. A., Costas, S., & Ferreira, s. (2018). Use of a bayesian network for coastal hazards, impact and disaster risk reduction assessment at a coastal barrier (ria formosa, portugal) [Journal Article]. *Coastal Engineering*, 134, 134-147. Retrieved from <http://www.sciencedirect.com/science/article/pii/S0378383917300972> doi: <https://doi.org/10.1016/j.coastaleng.2017.07.003>
- Poelhekke, L., Jäger, W. S., van Dongeren, A., Plomaritis, T. A., McCall, R., & Ferreira, s. (2016). Predicting coastal hazards for sandy coasts with a bayesian network [Journal Article]. *Coastal Engineering*, 118, 21-34. Retrieved from <http://www.sciencedirect.com/science/article/pii/S0378383916302034> doi: <https://doi.org/10.1016/j.coastaleng.2016.08.011>
- Putnam, J., & Johson, J. (1949). The dissipation of wave energy by bottom friction [Journal Article]. *Eos, Transactions American Geophysical Union*, 30(1), 67-74. Retrieved from <https://agupubs.onlinelibrary.wiley.com/doi/pdf/10.1029/TR030i001p00067>
- Rahmeyer, D., William Werth. (1996). *The study of the resistance and stability of vegetation ecosystem plant groupings in flood control channels: Vol. 1* (Report No. 148). UtahState Univeristy. Retrieved from [https://digitalcommons.usu.edu/water\\_rep/148/](https://digitalcommons.usu.edu/water_rep/148/)
- Reguero, B. G., Losada, I. J., & Méndez, F. J. (2019). A recent increase in global wave power as a consequence of oceanic warming [Journal Article]. *Nature Communications*, 10(1), 205. Retrieved from <https://doi.org/10.1038/s41467-018-08066-0><https://www.nature.com/articles/s41467-018-08066-0.pdf> doi: 10.1038/s41467-018-08066-0
- Reidenbach, M. A., & Thomas, E. L. (2018). Influence of the seagrass, *zostera marina*, on wave attenuation and bed shear stress within a shallow coastal bay [Journal Article]. *Frontiers in Marine Science*, 5(397). Retrieved from <https://www.frontiersin.org/article/10.3389/fmars.2018.00397> doi: 10.3389/fmars.2018.00397
- Reimann, S., Husrin, S., Strusińska, A., & Oumeraci, H. (2019). *Damping tsunami and storm waves by coastal forests – parameterisation and hydraulic model tests* [Book]. Retrieved from [https://www.researchgate.net/publication/266879770\\_DAMPING\\_TSUNAMI\\_AND\\_STORM\\_WAVES\\_BY\\_COASTAL\\_FORESTS\\_-\\_PARAMETERISATION\\_AND\\_HYDRAULIC\\_MODEL\\_TESTS/download](https://www.researchgate.net/publication/266879770_DAMPING_TSUNAMI_AND_STORM_WAVES_BY_COASTAL_FORESTS_-_PARAMETERISATION_AND_HYDRAULIC_MODEL_TESTS/download)
- Roelvink, D., McCall, R., Mehvar, S., Nederhoff, K., & Dastgheib, A. (2018). Improving predictions of swash dynamics in xbeach: The role of groupiness and incident-band runup [Journal Article]. *Coastal Engineering*, 134, 103-123. Retrieved from <http://www.sciencedirect.com/science/article/pii/S0378383917301321> doi: <https://doi.org/10.1016/j.coastaleng.2017.07.004>
- Roelvink, D., Reniers, A., Van Dongeren, A., Van Thiel de Vries, J., Lescinski, J., & McCall, R. (2015). *Xbeach model description and manual: Kingsday release* (Report). UNESCO-IHE Institute for Water Education, Deltares and Delft University of Technology. Retrieved from [https://oss.deltares.nl/documents/48999/2022076/Documentation\\_XBeach-v1.23.5527-XBeachX\\_FINAL.pdf/d366edea-db7c-1c2e-4295-a7222c8970bc?version=1.0&download=true](https://oss.deltares.nl/documents/48999/2022076/Documentation_XBeach-v1.23.5527-XBeachX_FINAL.pdf/d366edea-db7c-1c2e-4295-a7222c8970bc?version=1.0&download=true)

- Roelvink, D., Reniers, A., van Dongeren, A., van Thiel de Vries, J., McCall, R., & Lescinski, J. (2009). Modelling storm impacts on beaches, dunes and barrier islands [Journal Article]. *Coastal Engineering*, 56(11), 1133-1152. Retrieved from <http://www.sciencedirect.com/science/article/pii/S0378383909001252> doi: <https://doi.org/10.1016/j.coastaleng.2009.08.006>
- Ruessink, B. G., Miles, J. R., Feddersen, F., Guza, R. T., & Elgar, S. (2001). Modeling the alongshore current on barred beaches [Journal Article]. *Journal of Geophysical Research: Oceans*, 106(C10), 22451-22463. Retrieved from <https://agupubs.onlinelibrary.wiley.com/doi/abs/10.1029/2000JC000766> doi: 10.1029/2000jc000766
- Rupprecht, F., Möller, I., Paul, M., Kudella, M., Spencer, T., van Wesenbeeck, B. K., ... Schimmels, S. (2017). Vegetation-wave interactions in salt marshes under storm surge conditions [Journal Article]. *Ecological Engineering*, 100, 301-315. Retrieved from <http://www.sciencedirect.com/science/article/pii/S0925857416307443> doi: <https://doi.org/10.1016/j.ecoleng.2016.12.030>
- Sadegh, M., Ragno, E., & AghaKouchak, A. (2017). Multivariate copula analysis toolbox (mvmcat): Describing dependence and underlying uncertainty using a bayesian framework [Journal Article]. *Water Resources Research*, 53(6), 5166-5183. Retrieved from <https://doi.org/10.1002/2016WR020242><https://agupubs.onlinelibrary.wiley.com/doi/pdf/10.1002/2016WR020242> doi: 10.1002/2016WR020242
- Saleh, F., & Weinstein, M. P. (2016). The role of nature-based infrastructure (nbi) in coastal resiliency planning: A literature review [Journal Article]. *Journal of Environmental Management*, 183, 1088-1098. Retrieved from <http://www.sciencedirect.com/science/article/pii/S0301479716307484> doi: <https://doi.org/10.1016/j.jenvman.2016.09.077>
- Schmidt, M. N., & Morup, M. (2013). Nonparametric bayesian modeling of complex networks: an introduction [Journal Article]. *IEEE Signal Processing Magazine*, 30(3), 110-128. Retrieved from <https://ieeexplore.ieee.org/ielx7/79/6494646/06494690.pdf?tp=&arnumber=6494690&isnumber=6494646> doi: 10.1109/MSP.2012.2235191
- Schuerch, M., Spencer, T., Temmerman, S., Kirwan, M. L., Wolff, C., Lincke, D., ... Brown, S. (2018). Future response of global coastal wetlands to sea-level rise [Journal Article]. *Nature*, 561(7722), 231-234. Retrieved from <https://www.nature.com/articles/s41586-018-0476-5.pdf> doi: <https://doi.org/10.1038/s41586-018-0476-5>
- Schweizer, B. (2007). Introduction to copulas [Journal Article]. *Journal of Hydrologic Engineering*, 12(4), 346-346. Retrieved from <https://ascelibrary.org/doi/pdf/10.1061/%28ASCE%291084-0699%282007%2912%3A4%28346%29> doi: Doi10.1061/(Asce)1084-0699(2007)12:4(346)
- Shan, Y., Liu, C., & Nepf, H. (2019). Comparison of drag and velocity in model mangrove forests with random and in-line tree distributions [Journal Article]. *Journal of Hydrology*, 568, 735-746. Retrieved from <http://www.sciencedirect.com/science/article/pii/S0022169418308588> doi: <https://doi.org/10.1016/j.jhydrol.2018.10.077>
- Simard, M., Fatoyinbo, L., Smetanka, C., Rivera-Monroy, V. H., Castañeda-Moya, E., Thomas, N., & Van der Stocken, T. (2019). Mangrove canopy height globally related to precipitation, temperature and cyclone frequency [Journal Article]. *Nature Geoscience*, 12(1), 40-45. Retrieved from <https://www.nature.com/articles/s41561-018-0279-1.pdf> doi: 10.1038/s41561-018-0279-1

- Sklar, A. (1959). Random variables (fonctions de répartition à n dimensions et leurs marges.) [Journal Article]. *Joint Distribution Functions and Copulas*. Retrieved from [https://www.scirp.org/\(S\(i43dyn45teexjx455qlt3d2q\)\)/reference/ReferencesPapers.aspx?ReferenceID=1545355](https://www.scirp.org/(S(i43dyn45teexjx455qlt3d2q))/reference/ReferencesPapers.aspx?ReferenceID=1545355)<https://pdfs.semanticscholar.org/feed/9337c89730250b11ab722742cf27e94c335a.pdf>
- Smagorinsky, J. (1963). General circulation experiments with the primitive equation i the basic experiment [Journal Article]. *Monthly Weather Review*, 91(3), 99-164. Retrieved from [https://doi.org/10.1175/1520-0493\(1963\)091<0099:GCEWTP>2.3.CO;2](https://doi.org/10.1175/1520-0493(1963)091<0099:GCEWTP>2.3.CO;2) doi: 10.1175/1520-0493(1963)091<0099:GCEWTP>2.3.CO;2
- Small, C., & Nicholls, R. J. (2003). A global analysis of human settlement in coastal zones [Journal Article]. *Journal of Coastal Research*, 19(3), 584-599. Retrieved from <http://www.jstor.org/stable/4299200>
- Smit, P., Stelling, G., Roelvink, J., Van Thiel de Vries, J., McCall, R., Van Dongeren, A., ... Jacobs, R. (2010). *Xbeach: Non-hydrostatic model: Validation, verification and model description* (Report). Retrieved from [https://oss.deltares.nl/documents/48999/49476/non-hydrostatic\\_report\\_draft.pdf](https://oss.deltares.nl/documents/48999/49476/non-hydrostatic_report_draft.pdf)
- Sánchez-González, J. F., Sánchez-Rojas, V., & Memos, C. D. (2011). Wave attenuation due to posidonia oceanica meadows [Journal Article]. *Journal of Hydraulic Research*, 49(4), 503-514. Retrieved from <https://www.tandfonline.com/doi/full/10.1080/00221686.2011.552464> doi: 10.1080/00221686.2011.552464
- Songy, G. (2016). *Wave attenuation by global coastal salt marsh habitats* (MSc). Retrieved from <https://repository.tudelft.nl/islandora/object/uuid%3Af00e7416-f330-4d99-90fe-bf54367da78b?collection=education>
- Spalding, M. D., McIvor, A. L., Beck, M. W., Koch, E. W., Möller, I., Reed, D. J., ... Woodroffe, C. D. (2014). Coastal ecosystems: A critical element of risk reduction [Journal Article]. *Conservation Letters*, 7(3), 293-301. Retrieved from <https://onlinelibrary.wiley.com/doi/pdf/10.1111/conl.12074> doi: 10.1111/conl.12074
- Sperotto, A., Molina, J.-L., Torresan, S., Critto, A., & Marcomini, A. (2017). Reviewing bayesian networks potentials for climate change impacts assessment and management: A multi-risk perspective [Journal Article]. *Journal of Environmental Management*, 202, 320-331. Retrieved from <http://www.sciencedirect.com/science/article/pii/S0301479717307211> doi: <https://doi.org/10.1016/j.jenvman.2017.07.044>
- Sterl, A., & Caires, S. (2005). Climatology, variability and extrema of ocean waves: the web-based knmi/era-40 wave atlas [Journal Article]. *International Journal of Climatology*, 25(7), 963-977. Retrieved from <https://doi.org/10.1002/joc.1175><https://rmets.onlinelibrary.wiley.com/doi/pdf/10.1002/joc.1175> doi: 10.1002/joc.1175
- Stockdon, H. E., Holman, R. A., Howd, P. A., & Sallenger, A. H. (2006). Empirical parameterization of setup, swash, and runup [Journal Article]. *Coastal Engineering*, 53(7), 573-588. Retrieved from <http://www.sciencedirect.com/science/article/pii/S0378383906000044> doi: <https://doi.org/10.1016/j.coastaleng.2005.12.005>
- Sumer, B. M., & Fredsøe, J. r. (1997). *Hydrodynamics around cylindrical structures* (Vol. Volume 12) [Book]. WORLD SCIENTIFIC. Retrieved from <https://doi.org/10.1142/3316> doi: 10.1142/3316

- Suzuki, T., Hu, Z., Kumada, K., Phan, L. K., & Zijlema, M. (2019). Non-hydrostatic modeling of drag, inertia and porous effects in wave propagation over dense vegetation fields [Journal Article]. *Coastal Engineering*, 149, 49-64. Retrieved from <http://www.sciencedirect.com/science/article/pii/S0378383917304179> doi: <https://doi.org/10.1016/j.coastaleng.2019.03.011>
- Suzuki, T., Zijlema, M., Burger, B., Meijer, M. C., & Narayan, S. (2012). Wave dissipation by vegetation with layer schematization in swan [Journal Article]. *Coastal Engineering*, 59(1), 64-71. Retrieved from <http://www.sciencedirect.com/science/article/pii/S0378383911001347> doi: <https://doi.org/10.1016/j.coastaleng.2011.07.006>
- Tang, J., Shen, S., & Wang, H. (2015). Numerical model for coastal wave propagation through mild slope zone in the presence of rigid vegetation [Journal Article]. *Coastal Engineering*, 97, 53-59. Retrieved from <http://www.sciencedirect.com/science/article/pii/S0378383914002233> doi: <https://doi.org/10.1016/j.coastaleng.2014.12.006>
- Tang, J., Shen, Y., Causon, D. M., Qian, L., & Mingham, C. G. (2017). Numerical study of periodic long wave run-up on a rigid vegetation sloping beach [Journal Article]. *Coastal Engineering*, 121, 158-166. Retrieved from <http://www.sciencedirect.com/science/article/pii/S0378383916304562> doi: <https://doi.org/10.1016/j.coastaleng.2016.12.004>
- Terefenko, P., Paprotny, D., Giza, A., Morales-Nápoles, O., Kubicki, A., & Walczakiewicz, S. (2019). Monitoring cliff erosion with lidar surveys and bayesian network-based data analysis [Journal Article]. *Remote Sensing*, 11(7), 843. Retrieved from <http://www.mdpi.com/2072-4292/11/7/843>
- UNISDR. (2018). *Disaster statistics - undrr* (Web Page No. 29 October 2018). Retrieved from <https://www.unisdr.org/we/inform/disaster-statistics>
- United Nations, H. (2017). Factsheet: People and oceans [Conference Proceedings]. In U. Nations (Ed.), *The ocean conference: Our oceans, our future: partnering for the implementation of sustainable development goal 14*. Retrieved from <https://www.un.org/sustainabledevelopment/wp-content/uploads/2017/05/Ocean-fact-sheet-package.pdf>
- Uotani, T., Kanda, K., & Michioku, K. (2014). Experimental and numerical study on hydrodynamics of riparian vegetation [Journal Article]. *Journal of Hydrodynamics*, 26(5), 796-806. Retrieved from <https://link.springer.com/article/10.1016%2FS1001-6058%2814%2960088-3> doi: 10.1016/S1001-6058(14)60088-3
- Uppala, S. M., Kållberg, P. W., Simmons, A. J., Andrae, U., Bechtold, V. D. C., Fiorino, M., ... Woollen, J. (2005). The era-40 re-analysis [Journal Article]. *Quarterly Journal of the Royal Meteorological Society*, 131(612), 2961-3012. Retrieved from <https://doi.org/10.1256/qj.04.176><https://rmets.onlinelibrary.wiley.com/doi/pdf/10.1256/qj.04.176> doi: 10.1256/qj.04.176
- van Rooijen, A., Lowe, R., Ghisalberti, M., Conde-Frias, M., & Tan, L. (2018). Predicting current-induced drag in emergent and submerged aquatic vegetation canopies [Journal Article]. *Frontiers in Marine Science*, 5(449). Retrieved from <https://www.frontiersin.org/article/10.3389/fmars.2018.00449> doi: 10.3389/fmars.2018.00449
- Van Rooijen, A. A., De Vries, J. S. M. V. T., Mccall, R. T., Van Dongeren, A. R., Roelvink, J. A., & Reniers, A. J. H. M. (2015). Modeling of wave attenuation by vegetation with xbeach [Conference Proceedings]. In *Proceedings of the 36th iahr world congress* (p. 6749-6755). Retrieved

- from <https://www.semanticscholar.org/paper/MODELING-OF-WAVE-ATTENUATION-BY-VEGETATION-WITH-Rooijen-Vries/d18c866094439f0a0ca2ab14b939024a322a70c6>
- van Rooijen, A. A., McCall, R. T., de Vries, J. S. M. V., van Dongeren, A. R., Reniers, A. J. H. M., & Roelvink, J. A. (2016). Modeling the effect of wave-vegetation interaction on wave setup [Journal Article]. *Journal of Geophysical Research-Oceans*, 121(6), 4341-4359. Retrieved from <https://agupubs.onlinelibrary.wiley.com/doi/pdf/10.1002/2015JC011392> doi: 10.1002/2015jc011392
- van Wesenbeeck, B. K., Ijff, S., Jongman, B., Balog-Way, S. A. B., Kaupa, S. M., Bosche, L. V., ... Meliane, I. (2017). *Implementing nature based flood protection : principles and implementation guidance* (Report). World Bank Group. Retrieved from <http://documents.worldbank.org/curated/en/739421509427698706/Implementing-nature-based-flood-protection-principles-and-implementation-guidance>
- van Zelst, V. (2018). *Global flood hazard reduction by foreshore vegetation* (Report). Delft University of Technology. Retrieved from <https://repository.tudelft.nl/islandora/object/uuid:524dcd46-f697-4e85-ae6a-18a1eb4db710>
- Vitousek, S., Barnard, P. L., Fletcher, C. H., Frazer, N., Erikson, L., & Storlazzi, C. D. (2017). Doubling of coastal flooding frequency within decades due to sea-level rise [Journal Article]. *Scientific Reports*, 7(1), 1399. Retrieved from [https://www.ncbi.nlm.nih.gov/pmc/articles/PMC5437046/pdf/41598\\_2017\\_Article\\_1362.pdf](https://www.ncbi.nlm.nih.gov/pmc/articles/PMC5437046/pdf/41598_2017_Article_1362.pdf) doi: 10.1038/s41598-017-01362-7
- Vousdoukas, M. I., Mentaschi, L., Voukouvalas, E., Bianchi, A., Dottori, F., & Feyen, L. (2018). Climatic and socioeconomic controls of future coastal flood risk in europe [Journal Article]. *Nature Climate Change*, 8(9), 776-780. Retrieved from <https://www.nature.com/articles/s41558-018-0260-4.pdf> doi: <https://doi.org/10.1038/s41558-018-0260-4>
- Vuik, V., Jonkman, S. N., Borsje, B. W., & Suzuki, T. (2016). Nature-based flood protection: The efficiency of vegetated foreshores for reducing wave loads on coastal dikes [Journal Article]. *Coastal Engineering*, 116, 42-56. Retrieved from <http://www.sciencedirect.com/science/article/pii/S0378383916301004> doi: <https://doi.org/10.1016/j.coastaleng.2016.06.001>
- Vuik, V., Jonkman, S. N., Borsje, B. W., Suzuki, T., Kratzer, I., & Bouma, T. J. (2015). Nature-based flood protection: The efficiency of vegetated foreshores in reducing wave run-up [Conference Proceedings]. In *Proceedings of the 36th iahr world congress* (p. 6716-6722).
- Walstra, D. J. R., Roelvink, J. A., & Groeneweg, J. (2000). Calculation of wave-driven currents in a 3d mean flow model [Conference Proceedings]. In *International conference on coastal engineering 2000* (p. 1050-1063). Retrieved from <https://ascelibrary.org/doi/abs/10.1061/40549%28276%2981> doi: [doi:10.1061/40549\(276\)81](https://doi.org/10.1061/40549(276)81)
- Wang, X. L., & Swail, V. R. (2001). Changes of extreme wave heights in northern hemisphere oceans and related atmospheric circulation regimes [Journal Article]. *Journal of Climate*, 14(10), 2204-2221. Retrieved from [https://doi.org/10.1175/1520-0442\(2001\)014<2204:COEWHI>2.0.CO;2](https://doi.org/10.1175/1520-0442(2001)014<2204:COEWHI>2.0.CO;2) doi: 10.1175/1520-0442(2001)014<2204:COEWHI>2.0.CO;2
- Wang, X. L., Swail, V. R., Zwiers, F. W., Zhang, X., & Feng, Y. (2009). Detection of external influence on trends of atmospheric storminess and northern oceans wave heights [Journal Article]. *Climate Dynamics*, 32(2), 189-203. Retrieved from <https://link.springer.com/content/pdf/10.1007%2Fs00382-008-0442-2.pdf> doi: 10.1007/s00382-008-0442-2

- Weber, P., Medina-Oliva, G., Simon, C., & Iung, B. (2012). Overview on bayesian networks applications for dependability, risk analysis and maintenance areas [Journal Article]. *Engineering Applications of Artificial Intelligence*, 25(4), 671-682. Retrieved from <http://www.sciencedirect.com/science/article/pii/S095219761000117X> doi: <https://doi.org/10.1016/j.engappai.2010.06.002>
- Werner, C., Bedford, T., Cooke, R. M., Hanea, A. M., & Morales-Nápoles, O. (2017). Expert judgement for dependence in probabilistic modelling: A systematic literature review and future research directions [Journal Article]. *European Journal of Operational Research*, 258(3), 801-819. Retrieved from <http://www.sciencedirect.com/science/article/pii/S0377221716308517> doi: <https://doi.org/10.1016/j.ejor.2016.10.018>
- Wittgenstein, L. (1922). *Tractatus logico-philosophicus* [Book]. London and New York: Routledge and Kegan Paul. Retrieved from <https://www.gutenberg.org/files/5740/5740-pdf.pdf>
- Wu, W.-C., & Cox, D. T. (2015). Effects of wave steepness and relative water depth on wave attenuation by emergent vegetation [Journal Article]. *Estuarine, Coastal and Shelf Science*, 164, 443-450. Retrieved from <http://www.sciencedirect.com/science/article/pii/S0272771415300664> doi: <https://doi.org/10.1016/j.ecss.2015.08.009>
- Wu, W.-C., Ma, G., & Cox, D. T. (2016). Modeling wave attenuation induced by the vertical density variations of vegetation [Journal Article]. *Coastal Engineering*, 112, 17-27. Retrieved from [http://www.sciencedirect.com/science/article/pii/S0378383916300199https://ac.els-cdn.com/S0378383916300199/1-s2.0-S0378383916300199-main.pdf?\\_tid=d5be9365-c740-4d1c-b71f-635afabfd70&acdnat=1545666637\\_f3217a700710a2682ec873cf210e80f0](http://www.sciencedirect.com/science/article/pii/S0378383916300199https://ac.els-cdn.com/S0378383916300199/1-s2.0-S0378383916300199-main.pdf?_tid=d5be9365-c740-4d1c-b71f-635afabfd70&acdnat=1545666637_f3217a700710a2682ec873cf210e80f0) doi: <https://doi.org/10.1016/j.coastaleng.2016.02.004>
- Xu, D., Li, X., Zhang, L., Xu, N., & Lu, H. (2004). On the distributions of wave periods, wavelengths, and amplitudes in a random wave field [Journal Article]. *Journal of Geophysical Research: Oceans*, 109(C5). Retrieved from <https://doi.org/10.1029/2003JC002073https://agupubs.onlinelibrary.wiley.com/doi/pdf/10.1029/2003JC002073> doi: 10.1029/2003JC002073
- Yang, Z., Tang, J., & Shen, Y. (2018). Numerical study for vegetation effects on coastal wave propagation by using nonlinear boussinesq model [Journal Article]. *Applied Ocean Research*, 70, 32-40. Retrieved from <http://www.sciencedirect.com/science/article/pii/S0141118717301013> doi: <https://doi.org/10.1016/j.apor.2017.09.001>
- Yi, S., Sun, W., Heki, K., & Qian, A. (2015). An increase in the rate of global mean sea level rise since 2010 [Journal Article]. *Geophysical Research Letters*, 42(10), 3998-4006. Retrieved from <https://agupubs.onlinelibrary.wiley.com/doi/pdf/10.1002/2015GL063902> doi: 10.1002/2015GL063902
- Young, I. R. (1994). Global ocean wave statistics obtained from satellite observations [Journal Article]. *Applied Ocean Research*, 16(4), 235-248. Retrieved from <http://www.sciencedirect.com/science/article/pii/014111879490023X> doi: [https://doi.org/10.1016/0141-1187\(94\)90023-X](https://doi.org/10.1016/0141-1187(94)90023-X)
- Young, I. R., Zieger, S., & Babanin, A. V. (2011). Global trends in wind speed and wave height [Journal Article]. *Science*, 332(6028), 451. Retrieved from <https://science.sciencemag.org/content/sci/332/6028/451.full.pdf> doi: 10.1126/science.1197219

- Yule, G. U. (1919). *An introduction to the theory of statistics* [Book]. C. Griffin, limited. Retrieved from [http://cda.psych.uiuc.edu/Wallace/yule\\_1911.pdf](http://cda.psych.uiuc.edu/Wallace/yule_1911.pdf)
- Zainali, A., Marivela, R., Weiss, R., Yang, Y., & Irish, J. L. (2018). Numerical simulation of nonlinear long waves in the presence of discontinuous coastal vegetation [Journal Article]. *Marine Geology*, 396, 142-149. Retrieved from <http://www.sciencedirect.com/science/article/pii/S0025322717303717> doi: <https://doi.org/10.1016/j.margeo.2017.08.001>



# III

## PART III: SUPPLEMENTARY



**A**

## **PARAMETER SAMPLING**

PARAMETERS sampling was the result of a stochastic model which was a crucial part in preparing global vegetated hydrodynamic conditions. This chapter presents some of the background decisions and some extended results which formed the stochastic model.

### A.1. ALTERNATIVE SYSTEM IDEALIZATIONS

One of the important features of the schematized profile was the horizontal platform where the vegetation forest is placed. Two alternatives other than the finalized one were considered including the one with slope extending from the diketoe to the offshore boundary and the other with flat vegetation platform. The inflexion point at the vegetation incidence in case of flat forest existed which resulted in most of the depth induced wave breaking right in the start of the vegetation forest. For the case when the slope was continuous the schematizations were computationally unfeasible.

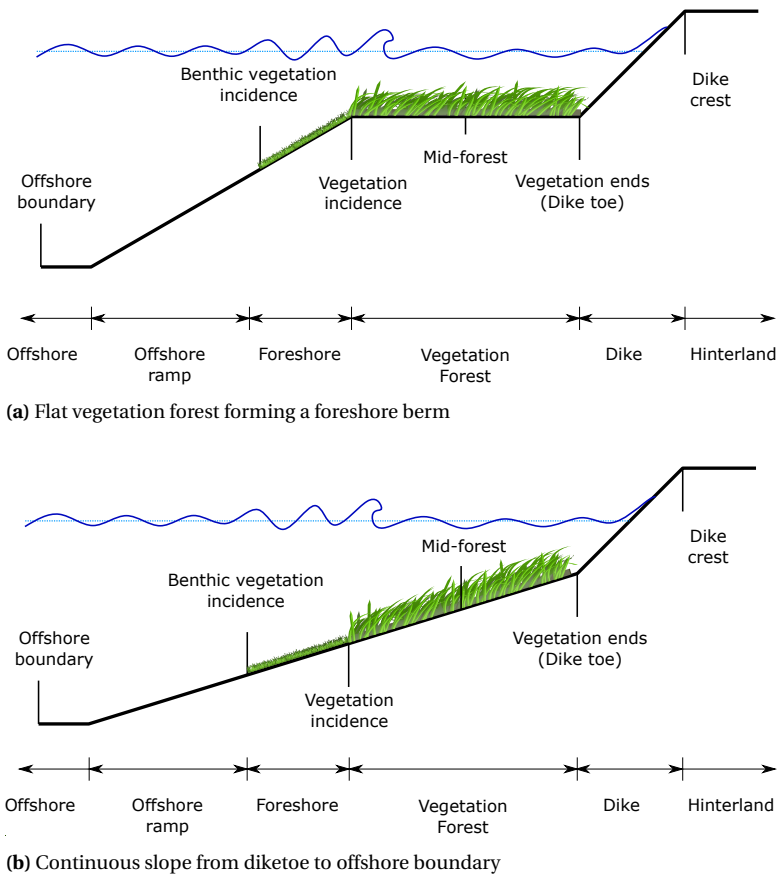


Figure A.1: Alternative System Idealizations based on vegetation forest platform.

The following factors were critical and formed the basis of the decision about finalized schematization.

- Avoid large variations in relative depth  
The large variations in the ratio between the vegetation height and water depth would have made the model inconsistent in terms of the classification of the vegetation systems (submerged or emergent). The front (offshore side) of the vegetation could have been submerged and, in the same model, it could have been emergent at the rear end which would change the model behavior within the vegetation forest making the wave attenuation coefficient incomparable and irrelevant. Therefore, a schematization with very mild slopes was adopted.
- Limitation of vegetation growth  
Vegetation like saltmarshes have growth restriction on slopes steeper than 1 in 50. Where as literature about vegetation modeling have quoted foreshore slopes of 1 in 10 as well which advocates for differentiating between foreshore slope and placement of vegetation forest.
- Avoid larger spatial domain  
To avoid modeling very large cross-shore domain, foreshore (vegetation) slope should have been different from offshore slope which had introduced another variable to be included in the model.
- Energy dissipation is mainly by vegetation  
The vegetation on the flat would have resulted in the maximum energy dissipation at the starting point of the vegetation flat. To make sure that the wave attenuation is mainly due to vegetation, and not due to bottom friction or depth-induced wave breaking the vegetation slope was introduced.

## A.2. MARGINAL DISTRIBUTIONS

The stochastic model was made in the user-defined mode of UNINET in order to sample input parameters for XBeach global runs. The model was made based on range, distribution and correlations of the parameters. This section presents the background on the ranges and distributions of the parameters. Probability density functions  $f(x)$  for the distributions used in the probabilistic models have been presented in Equation A.1 with detailed distribution parameters in Table A.1.

Weibull distribution with  $\alpha > 0$  as the scale parameter and  $\beta > 0$  as the shape parameter

$$f(x) = \frac{\beta}{\alpha} \left( \frac{x-b}{\alpha} \right)^{\beta-1} \exp \left( - \left( \frac{x-b}{\alpha} \right)^{\beta} \right) \quad ; \quad \text{for } x \geq b \quad (\text{A.1a})$$

Gamma distribution with  $\alpha > 0$  as the inverse scale parameter,  $\beta > 0$  as the rate parameter and  $\Gamma(\beta)$  as the gamma function

$$f(x) = \frac{1}{\alpha^{\beta} \Gamma(\beta)} (x-b)^{\beta-1} \exp \left( - \left( \frac{x-b}{\alpha} \right) \right) \quad ; \quad \text{for } x \geq b \quad (\text{A.1b})$$

A

Uniform distribution

$$f(x) = \begin{cases} \frac{1}{b-a} & ; \quad \text{for } x \leq x \leq b \\ 0 & ; \quad \text{for } x < a \text{ or } x > b \end{cases} \quad (\text{A.1c})$$

Beta distribution with shape parameters as  $\alpha, \beta > 0$ 

$$f(x) = \frac{(x-a)^{\alpha-1}(b-x)^{\beta-1}}{B(\alpha, \beta)(b-a)^{\alpha+\beta+1}} \quad ; \quad \text{for } a \leq x \leq b \quad (\text{A.1d})$$

Gaussian distribution with expected value  $\mu$  and variance  $\sigma^2$ 

$$f(x) = \frac{1}{\sigma \cdot \sqrt{2\pi}} \exp\left(-\frac{(x-\mu)^2}{2\sigma^2}\right) \quad ; \quad \text{for } x \in R \quad (\text{A.1e})$$

Discrete distribution with realization  $x$  having probability  $p$ 

$$P(X = x) = p \quad ; \quad \text{for } x \in R \quad (\text{A.1f})$$

$$(\text{A.1g})$$

where  $x$  is a realization,  $a$  and  $b$  are lower and upper bounds, therefore, range is  $b - a$ .

**Table A.1:** Random variables in stochastic modeling for parameter sampling

Parameter	Symbol	Units	Distribution	Parameters	Bounds		Mean	Std. Dev	Percentiles		
					Min	Max			5%	50%	95%
Wave Height	$H_{m0}$	m	Weibull	$\alpha = 2.93; \beta = 2.21$	0.1	$\approx 8$	2.69	1.24	0.86	2.58	4.91
Peak wave period	$T_p$	s	Gamma	$\alpha = 1.25; \beta = 7.02$	1	$\approx 30$	9.77	3.31	5.12	9.36	15.83
Water depth	$h$	m	Uniform	$a = 0.01; b = 5$	0.01	5	2.5	1.44	0.25	2.5	4.75
Offshore slope	$S_0$	–	Beta	$\alpha = 1.86; \beta = 20.9$	$\frac{1}{10}$	$\frac{1}{1000}$	$\frac{1}{180}$	$\frac{1}{350}$	$\frac{1}{90}$	$\frac{1}{200}$	$\frac{1}{500}$
Friction coefficient	$c_f$	–	Beta	$\alpha = 1.75; \beta = 2.18$	0.01	0.1	0.05	0.02	0.018	0.049	0.084
Vegetation slope	$S_v$	–	Beta	$\alpha = 2.85; \beta = 2.33$	$\frac{1}{500}$	$\frac{1}{1000}$	$\frac{1}{660}$	$\frac{1}{5000}$	$\frac{1}{530}$	$\frac{1}{660}$	$\frac{1}{830}$
Vegetation length	$L_v$	m	Beta	$\alpha = 1.35; \beta = 2.10$	1	1500	587	346	86	553	1205
Vegetation height	$h_v$	m	Beta	$\alpha = 1.30; \beta = 1.64$	0.02	1.75	0.79	0.43	0.13	0.76	1.52
Frontal width	$b_v$	m	Beta	$\alpha = 1.36; \beta = 1.60$	0.0001	0.025	0.011	0.006	0.002	0.011	0.022
Vegetation density	$N_v$	$\frac{\text{stems}}{\text{m}^2}$	Beta	$\alpha = 1.45; \beta = 2.75$	10	2000	697	415	115	645	1458
Drag coefficient	$C_d$	–	Beta	$\alpha = 1.47; \beta = 3.26$	0.1	3	1	0.56	0.24	0.91	2.04
Dike slope	$S_d$	–	Beta	$\alpha = 1.38; \beta = 2.30$	$\frac{1}{2}$	$\frac{1}{10}$	$\frac{1}{4}$	$\frac{1}{112}$	$\frac{1}{2.5}$	$\frac{1}{4}$	$\frac{1}{8}$
Crest level	$h_c$	m	Gaussian	$\mu = 12; \sigma = 2.5$	1	20	12	2.5	7.88	12	16.11

See Equation A.1 for the probability density functions  $f(x)$  and the meaning of distribution parameters.

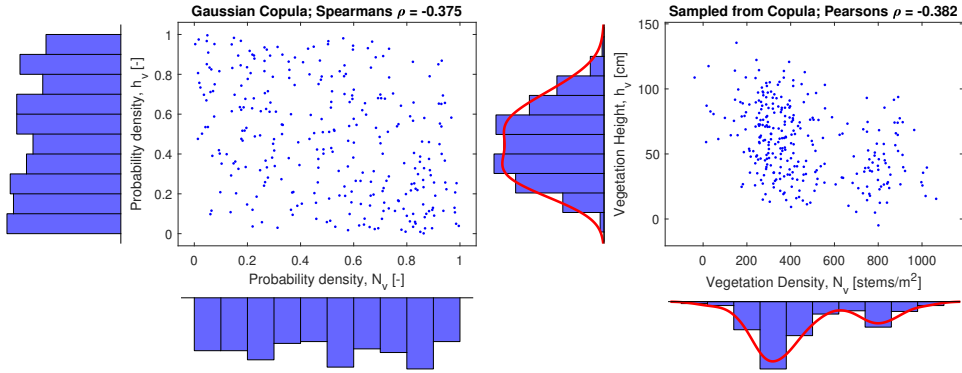
### A.3. COPULAS & CORRELATIONS

Copulas are a joint distribution based on ranked correlations of the data which has uniform marginals. In addition to details about copulas this section presented extended results about copulas and ranked correlation determined from the data for various parameters.

#### VEGETATION DENSITY ( $N_v$ ) WITH VEGETATION HEIGHT ( $h_v$ ) & FRONTAL WIDTH ( $b_v$ )

Both the vegetation height ( $h_v$ ) and frontal width ( $b_v$ ) show negative correlation to vegetation density ( $N_v$ ), refer to Figure A.2 and A.3.

#### Vegetation Density ( $N_v$ ) & Vegetation Height ( $h_v$ )

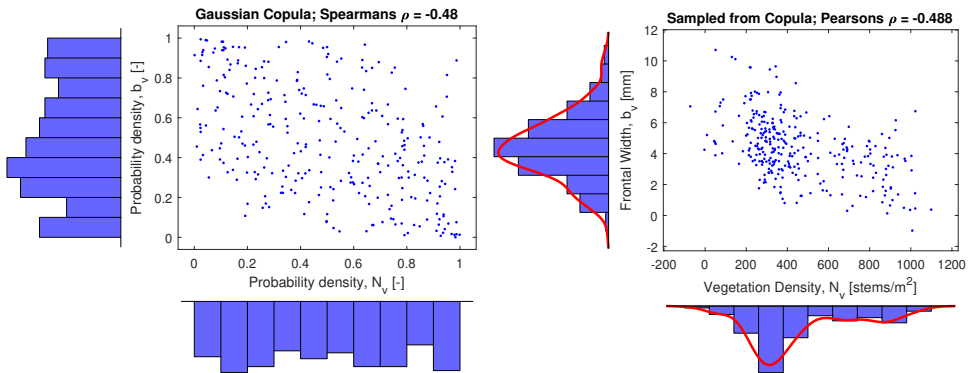


(a) Gaussian copula fitted to the data

(b) 300 samples populated from the copula

**Figure A.2:** Copula and correlations from field data for vegetation density  $N_v$  and vegetation height ( $h_v$ ).

#### Vegetation Density ( $N_v$ ) & Frontal Width ( $b_v$ )



(a) Gaussian copula fitted to the data

(b) 300 samples populated from the copula

**Figure A.3:** Copula and correlations from field data for vegetation density  $N_v$  and frontal width ( $b_v$ ).

WAVE STEEPNESS ( $S_t$ ) WITH WAVE HEIGHT ( $H_{m0}$ ) & WAVE PERIOD ( $T_p$ )

Although peak wave period was used instead of wave steepness but correlation were calculated because initially the idea was to use wave steepness as a parameter which could also be used as sea-state classification parameter. Later on, sea-states were classified based on frequency splitting. Wave steepness show positive correlation to wave height as seen in Figure A.4 and negative correlation to wave period as seen in Figure A.5.

Wave Height ( $H_{m0}$ ) and Wave Steepness ( $S_t$ )

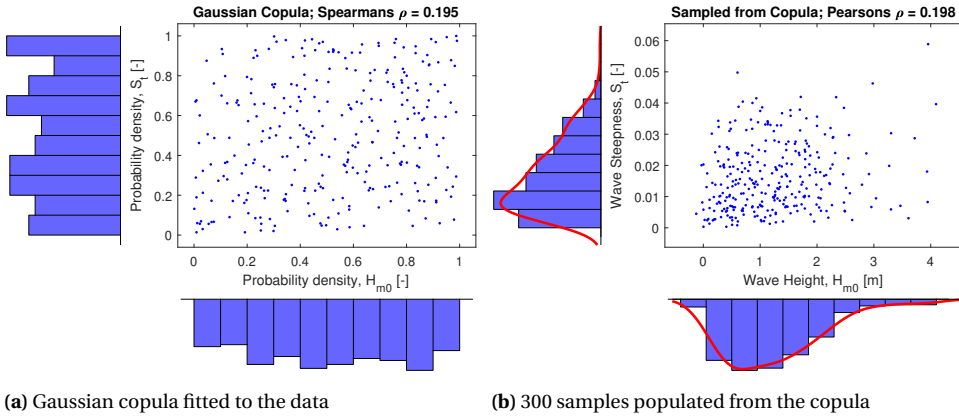


Figure A.4: Gaussian copula and correlations from global wave climate data for offshore wave height ( $H_{m0}$ ) and wave steepness ( $S_t$ ).

Wave Period ( $T_p$ ) & Wave Steepness ( $S_t$ )

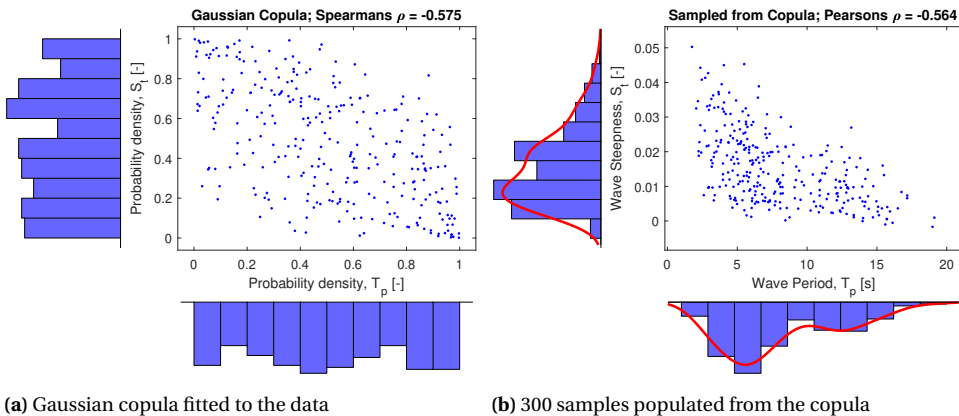
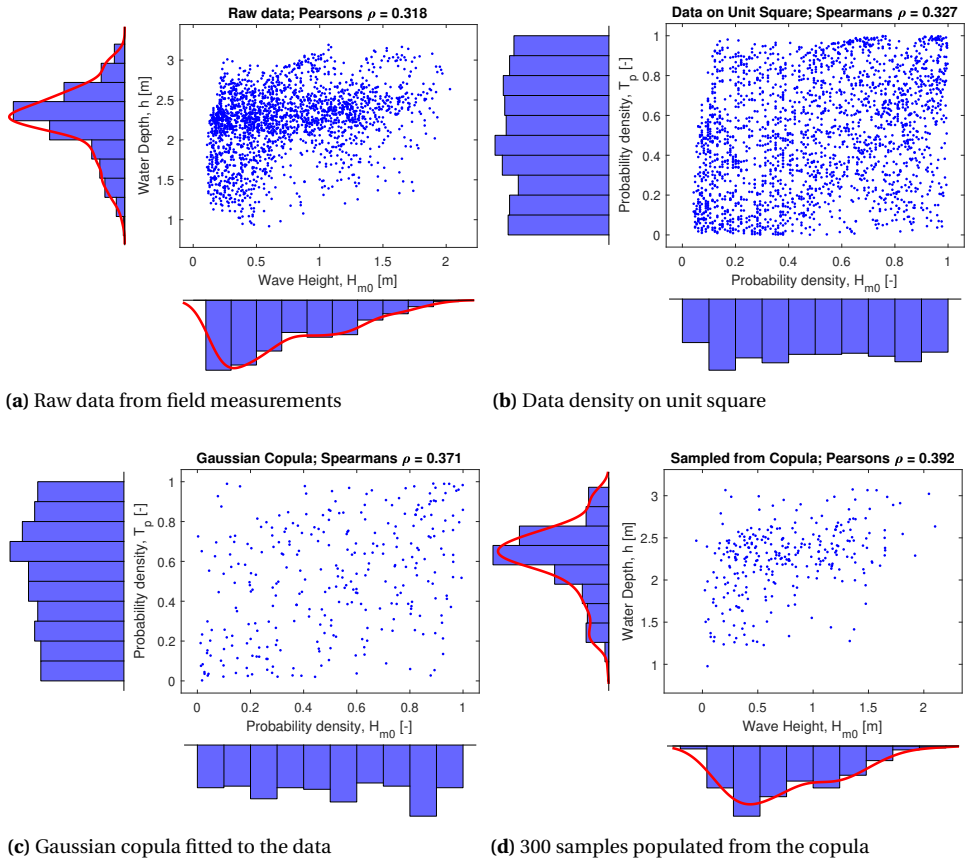


Figure A.5: Gaussian copula and correlations from global wave climate data for peak wave period ( $T_p$ ) and wave steepness ( $S_t$ ).

### WAVE HEIGHT ( $H_{m0}$ ) & WATER DEPTH ( $h$ )

The waves and tides data was acquired from Channel Coastal Observatory (CCO) [website](#) and shown in Table A.2. The data was then quality controlled to rule out spurious values in the database. The CoastalTools, a MATLAB-based GUI, was used to process and manipulate the data. The wave time-series generate by `getwavedata.m` function was the same as the one acquired from CCO with an addition of water levels which means wave climate is the actual wave time-series from the buoy and not a synthetic data which making the correlations more reliable.



**Figure A.6:** Gaussian copula and correlations from field data for wave height ( $H_{m0}$ ) and water depth ( $h$ ).

<sup>1</sup>CoastalTools didn't have the option to quality control for minimum  $T_p$ . So it was done separately in MATLAB.

**Table A.2:** Data sources and specifications used to create the database for bivariate dependence matrix of hydraulic parameters. However, this dataset was only used to determine the correlation between offshore wave height and water depth. Rest of the hydraulic parameters are analyzed through the global dataset based on the details in Table 3.3.

Type	Duration	Location	Quality Control	Explanation
Waves	2013-2018	Milford	Max $T_p = 28.6\text{s}$ Min $T_p = 1\text{s}$	The data had spurious values for $T_p > 28.6\text{s}$ and $T_p < 1\text{s}^1$ .
Tides	2008-2018	Swanage	Water level= 1.5 to -1.3m	Minimum and maximum water levels were selected by qualitative observation.



# B

## MODEL SETUPS & PRE-PROCESSING

THE chapter builds on the modeling methodology in greater detail in order to ensure reproducibility. Elaboration on the decisions taken during both numerical and probabilistic modeling phases which were not addressed in Chapters 1, 2, and 3 are provided in the forthcoming sections.

## B

### B.1. PSEUDOCODES

The architecture of the numerical model was structured through scripts written in MATLAB which uses most of the functions available through Open Earth Tools (OET).

The pseudocode `main.m`, as seen in Figure B.1, was used to initialize the model settings which were consistent through out the numerical modeling process *e.g.* spatial and temporal grid sizes. Grid resolution *i.e.*, grid size and number of grid points, and simulation running duration were defined after a detailed XBeach sensitivity tests.

The pseudocode `import.m`, also seen in Figure B.1 used to collect and store input conditions sampled from the stochastic model for saltmarshes and mangroves as column vectors to be used as a part model setup.

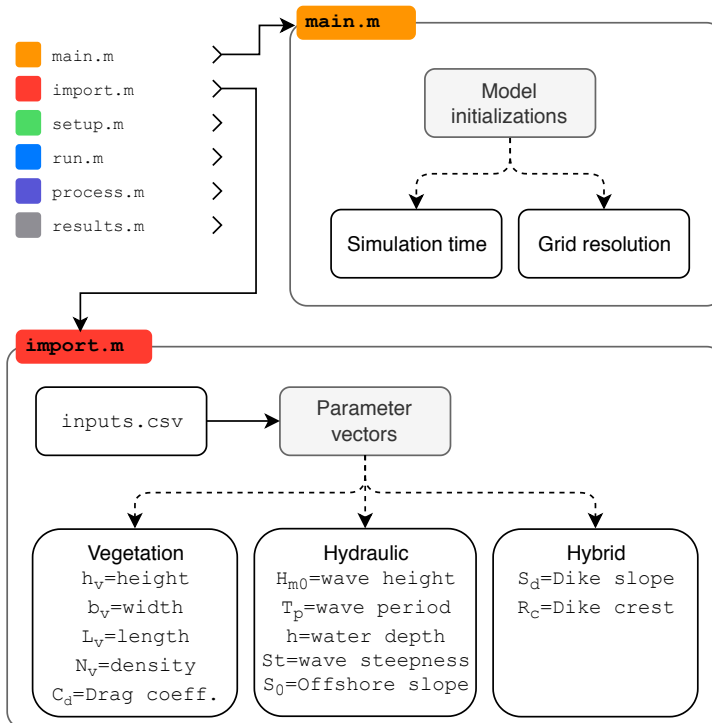


**Figure B.1:** Parent files calling all the functions to run the XBeach simulations through `main.m` and to import all the Monte Carlo sampled input conditions through `import.m`.

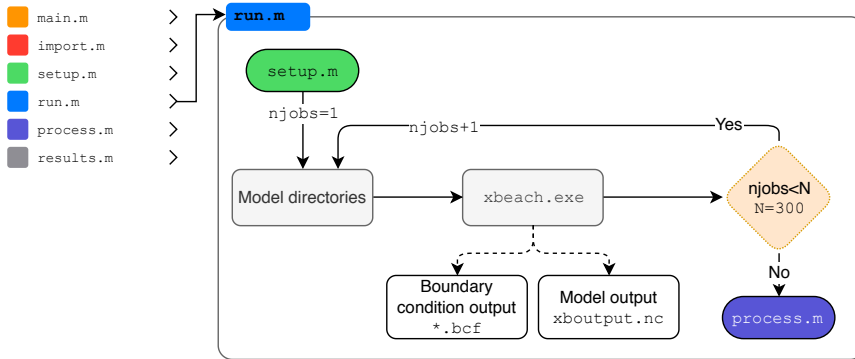


Figure B.2: The pseudocode run.m to run XBeach global model simulations.

## B.2. XBEACH INPUT FILES

XBeach is software without a user interface so a pre-compiled version of XBeach could be downloaded from (OET) and used instantly without any installation. All the relevant input files should be placed in one folder and the pre-compiled version of XBeach should be called in the same directory. List of files to be generated in one folder for running the model are hereunder.

- bed.dep: Bed morphology file.
- x.grd: Cross-shore profile definition with grid points
- jonswap.txt: Spectral input wave boundary condition wbctype=jonstable.
- params.txt: All input parameters and running conditions for simulations.
- veggiefile.txt: Vegetation characteristics based on vegetation parameters.
- veggiemapfile.txt: Vegetation locations on the cross-shore grid points.

### PARAMS.TXT

Sample params.txt from a case model run specifying model specifications for XBeach is presented in this section. The comments explain how and why the parameter was selected. Flagged variables changes in every simulation based on how they are defined to vary with varying wave, flow or vegetation characteristics.

Non-hydrostatic mode is used because of the interests in resolving both short and long waves and eventually see the effect of vegetation on both short and infragravity waves. Waves were specified through JONSWAP spectrum and vegetation module was turned on. The latest XBeach model version which wrote NetCDF output files was used. Point output of water level timeseries was the most important output for post-processing.

```

1  %%%%%%%%%%%%%%%%%%%%%%%%%%%%%%%%%%%%%%%%%%%%%%%%%%%%%%%%%%%%%%%%%%%%%%%%%%
2  %% XBeach Parameter Settings Input file                                %%
3  %%                                                                    %%
4  %% Date:      16-May-2019 19:45:27                                    %%
5  %% Function:  setup.m -> xb_write_params.m                            %%
6  %%%%%%%%%%%%%%%%%%%%%%%%%%%%%%%%%%%%%%%%%%%%%%%%%%%%%%%%%%%%%%%%%%%%%%%%%%
7
8  %% Flow boundary condition (BC) parameters %%%%%%%%%%%%%%%%%%%%%%%%%%%
9  front        = nonh_ld        % Non-hydrostatic BC on offshore end
10 left         = wall           % No flux wall BC on left side
11 right        = wall           % No flux wall BC on right side
12 back         = abs_ld         % Weakly-reflective BC on landward end
13 ARC          = 0              % Active reflection compensation
14 order        = 1              % Short wave steering
15 epsi         = -1            % Ratio of mean to time varying current
16
17 %% Flow numerics parameters %%%%%%%%%%%%%%%%%%%%%%%%%%%
18 secorder     = 1              % 2-order corrections to nonlinear terms
19
20 %% Flow parameters %%%%%%%%%%%%%%%%%%%%%%%%%%%
21 bedfriction  = cf             % Bed friction coefficient for seagrass
22 bedfricfile  = fric.txt       % Spatially-varying friction (seagrass)
23
24 %% General %%%%%%%%%%%%%%%%%%%%%%%%%%%
25 maxbrsteep  = 0.40           % Maximum wave steepness criterium
26 vegetation   = 1              % Waves-flow-vegetation interaction=true
27 veggiefile   = vegetation.txt % Vegetation characteristics file
28 veggiemapfile = vegbed.txt    % Vegetation location file
29 wavemodel    = 2              % Non-hydrostatic mode activated
30
31 %% Grid parameters %%%%%%%%%%%%%%%%%%%%%%%%%%%
32 depfile     = bed.dep         % Bathymetry file from optimized grid
33 posdwn      = -1             % Bathymetry is positive upwards
34 nx          = 6229 (FLAGGED) % Cross-shore computational cell corners
35 ny          = 0              % Along-shore computational cell corners
36 alfa        = 0              % Angle of shoreline from east
37 vardx       = 1              % Variable grid spacing = True
38 xfile       = x.grd          % Cross-shore grid points file
39 xori        = 0              % X-coordinate of origin of axis [deg]
40 yori        = 0              % Y-coordinate of origin of axis [deg]
41 thetamin    = -90            % Lower wave directional limit [deg]
42 thetamax    = 90             % Higher wave directional limit [deg]
43 dtheta      = 180            % Wave directional resolution [deg]
44
45 %% Initial conditions %%%%%%%%%%%%%%%%%%%%%%%%%%%
46 zs0         = 3.817 (FLAGGED) % Initial water level from veg. bed [m]
47
48 %% Model time %%%%%%%%%%%%%%%%%%%%%%%%%%%
49 tstop       = 11904 (FLAGGED) % Simulation stop time [s]
50 CFL         = 0.70           % Maximum courant-friedrichs-lewy number
51
52 %% Physical constants %%%%%%%%%%%%%%%%%%%%%%%%%%%
53 rho         = 1025           % Seawater density [kg/m^3]
54 depthscale  = 50             % Depth scale of lab tests validation
55
56 %% Physical processes %%%%%%%%%%%%%%%%%%%%%%%%%%%

```

```

57 swave          = 0           % Short wave action balance turned off
58 sedtrans       = 0           % Sediment transport turned off
59 morphology     = 0           % Morphological processes turned off
60 nonh           = 1           % Non-hydrostatic pressure activated
61
62 %%% Wave boundary condition parameters %%%%%%%%%%%%%%%%%%%%%%%%%%%%%%%
63 instat         = jons_table   % Wave boundary condition type
64 taper          = 1200 (FLAGGED) % Spin-up time of wave BC [s]
65
66 %%% Wave breaking parameters %%%%%%%%%%%%%%%%%%%%%%%%%%%%%%%
67 gammax         = 2           % Max. wave height to water depth ratio
68
69 %%% Wave-spectrum boundary condition parameters %%%%%%%%%%%%%%%%%%%%%%%%%%%
70 bcfile         = jonswap.txt   % JONSWAP spectrum file
71 random         = 1           % Random incident wave time-series=True
72 rt             = 11904 (FLAGGED) % Duration of wave time-series [s]
73 dtbc           = 1           % Resolution of wave time-series [s]
74
75 %%% Output variables %%%%%%%%%%%%%%%%%%%%%%%%%%%%%%%
76 outputformat   = netcdf       % Output file format
77 rugdepth       = 0.10        % Run-up gauge depth [m]
78 tintm         = 3968 (FLAGGED) % Interval time of mean output [s]
79 tintp         = 1.0          % Interval time of point output [s]
80 tintg         = 1            % Interval time of global output=10Hz[s]
81 tstart        = 0 (FLAGGED)  % Start time of output [s]
82
83 nglobalvar     = 2           % Number of global output variables
84 zs             % Water level
85 zb             % Bed level
86
87 nmeanvar       = 3           % Number of mean output variables
88 zs             % Mean water level
89 uu             % Mean horizontal GLM velocity
90 qx             % Mean overtopping discharge
91
92 npointvar      = 3           % Number of point output variables
93 zs             % Water level time-series
94 uu             % Horizontal GLM velocity time-series
95 qx             % Overtopping discharge time-series
96
97 npoints        = 6           % Number of point output locations (x,y)
98 0.3 1.         (FLAGGED) % Offshore point kh=1.0
99 4984.2 1.      (FLAGGED) % Benthic vegetation incidence kh=0.5
100 5840.3 1.     (FLAGGED) % Vegetation forest incidence
101 5979.9 1.     (FLAGGED) % Mid-forest
102 6120.0 1.     (FLAGGED) % Vegetation endpoint (dike toe)
103 6166.0 1.     (FLAGGED) % Crest point
104
105 nrugauge       = 1           % Number of output runup gauge locations
106 6120.0 1.     (FLAGGED) % Initial location of runup gauge

```

Lateral flow boundary conditions on left and right sides doesn't really matter since it's a 1D model but these defined to avoid the partial reflectiveness that can possibly occur. The model becomes conservative as the energy is then concentrated and enforced on the vegetation system without absorption on right and left model boundaries. Similarly

thetamin, thetamax and dtheta have little significance due to one dimensionality of the model.

Due to the depth-averaging  $kh > 1$  isn't recommended for XBeach which means the model is only valid for shallow water (Roelvink et al., 2015). Therefore, the offshore depth at the offshore boundary was calculated based on  $kh = 1$ . Maximum courant-friedrichs-lewy CFL number defines the time step used to stabilize the scheme with respect to spatial grid for convective terms. The depth scale of the lab tests `depthscale` sets different cut-off values for parameters defining vertical limits. It was only used while performing case model runs for validation purposes.

Initial water levels `zs0` are sampled from the Monte Carlo simulations as a result of the stochastic modeling of input parameters. The maximum ratio of wave height to water depth `gammamax` determines how waves will break in shallow water. Higher value of  $\gamma_{max} = 2$  than the standard value  $\gamma \approx 0.55$  was used to avoid forced wave breaking in case if the larger wave heights are being modeled on top of the vegetation forest with limited water depth. Furthermore, the positive correlation coefficient of wave height and water depth encourages in Monte Carlo simulations to sample higher wave heights with higher water levels.

#### JONSWAP.TXT

Waves, which had to be defined as a boundary condition, form the forcing mechanism for the model. Spectral wave boundary conditions were defined at the offshore end using a series of parametric spectra. The spectral shape `gammajsp`, peak wave period `Tp` and the directional spreading `s` determines the shape of the JONSWAP spectrum. These spectra are used to generate a time-series of random waves for duration `rt`, usually equal to simulation time, on specified resolution `dtbc`. The resolution of the time-series is determined in a way that it maintains a balance between a value accurately representing bound long wave and the model time step.

```

1  % <Hm0> <Tp> <mainang> <gammajsp> <s> <duration> <dtbc>
2
3  4.339 9.92 270.00 3.30 100000.00 11904.00 1.00
4
5  % Hm0      -      Hm0 of the wave spectrum, significant wave height [m]
6  % Tp       -      Peak wave period [s]
7  % mainang  -      Main wave angle (nautical convention) [deg]
8  % gammajsp -      Peak enhancement factor in the JONSWAP expression [-]
9  % s        -      Directional spreading coefficient, cos^2s law [-]
10 % duration -      Simulation duration [s]
11 % dtbc     -      Boundary condition time step [s]

```

#### VEGPARAMS.TXT

Vegetation was incorporated in the model through parameters described in `vegparams.txt` file. The typical file hereunder is for a case run which models seagrass-saltmarsh environment. For mangroves all the parameters are a vector containing three values characterizing each of the three vertical layers: roots, trunk and stems as illustrated in Figure 3.2.

1	nsec = 1	% No. of vertical sections 1=Saltmarsh, 3=Mangroves
2	ah = 0.81893	(FLAGGED) % Vegetation Height [m]
3	bv = 0.015648	(FLAGGED) % Frontal width [m]
4	N = 478.4331	(FLAGGED) % Vegetation density [stems/m <sup>2</sup> ]
5	Cd = 0.94296	(FLAGGED) % Drag coefficient

### B.3. XBEACH SENSITIVITY TESTS

XBeach sensitivity tests were performed for the non-hydrostatic mode based on many numerical parameters. The results for the most significant sensitivity results were obtained by varying active reflective compensation (ARC) and maximum grid spacing (dxmax) which have been presented in Figure B.4. Sensitivity of np number of points per wave length, and CFL doesn't have significant effect on mean water levels since most of the grid spacing is controlled by dxmax.

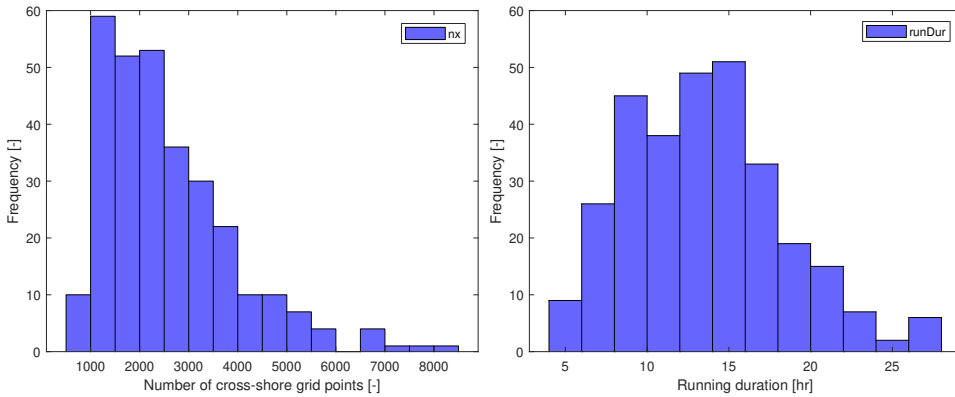


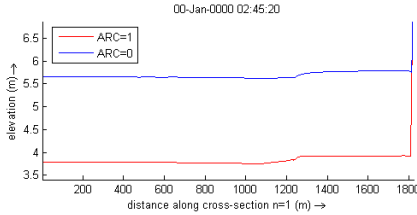
Figure B.3: Bins of grid points for total simulation running duration.

Simulation times were greatly dependent on number of grid points, see Figure B.3 for the histograms of number of grid points and running duration. Grid size was controlled by number of points per wavelength and the maximum and minimum grid spacing. Mostly the maximum bound of the grid spacing was the controlling factor in deciding grid spacing. Sensitivity tests were performed for range of parameters and have been reported hereunder.

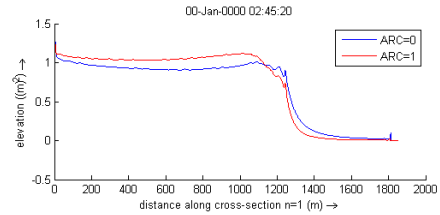
- Number of points per wavelength np from 40 to 150 with an increment of 20 - No significant difference in mean water levels was observed.
- CFL was varied from 0.3 to 0.7 with an increment on 0.1 - No difference in mean water levels was observed.
- Upper limit of grid spacing dxmax 0.1 to 1m - Significant difference in mean water levels was observed. The simulation with dxmax=0.1m was very long (73 hours) therefore more finer grid was not tested.

- Wave boundary condition were defined through `wbctype=jonswap` instead of the `wbctype=jonstable` to check the effect of maximum `rt=3600` - No difference in mean water levels was observed.
- Taper was taken out and set to zero - No difference in mean water levels was observed.

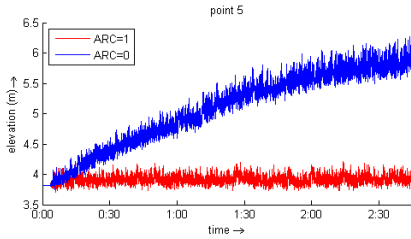
B



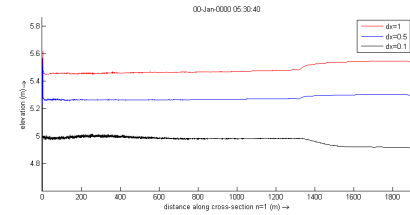
(a) Sensitivity of mean water level to ARC



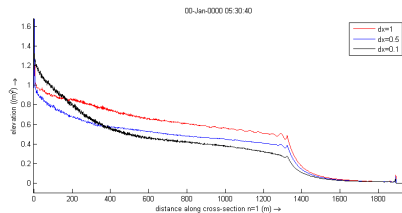
(b) Sensitivity of water level variance to ARC



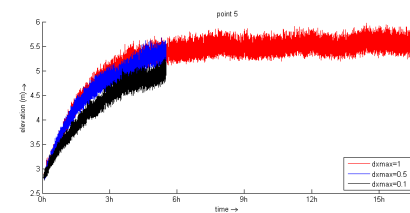
(c) Sensitivity of water level timeseries to ARC



(d) Sensitivity of mean water level to dxmax



(e) Sensitivity of water level variance to dxmax



(f) Sensitivity of water level timeseries to dxmax

**Figure B.4:** XBeach sensitivity tests of mean water levels, water levels variance, and water timeseries based on dxmax and ARC.

## B.4. STOCHASTIC MODEL

Probabilistic model was setup up in two phases; both setting up a Bayesian network. First part was the stochastic modeling based on user-defined probabilistic framework used to describe input parameters. Appendix A reports the details for parameter sampling and Figure 2.8 outlines the methodology used to implement it in UNINET.

Second part of setting up the flood risk prediction model was executed through ordinal data mining for multivariate density modeling. Magnitude and ordering of the values of

the variables are important in an ordinal dataset (Ababei et al., 2008) e.g. run-up ( $R_{u2\%}$ ) is ordinal data while locations of a saltmarsh are not. XBeach-generated dataset containing output variables along with the output of the first part containing sampled input parameters was the input to prediction tool.

Multivariate density model was generated from the synthetic dataset developed based on XBeach global model runs. The input data to the prediction tool was in the form of a \*.csv file with parameter names in the first row and the parameter values in the following rows. Marginal distributions were directly mined from the data which formed multivariate distributions related through a normal copula.



# C

## EXTENDED RESULTS

THE scope of the research going on in the field of vegetated hydrodynamics is extensive and stretches in all direction beyond the scope of this study. However, in this study during the two modeling phases, numerical and probabilistic, some on the analysis was extensive. The analysis yielded results which also extend our understanding in the areas which have been addressed through the research questions defined in Section 1.2.

## C.1. SPECTRAL EVOLUTION

The sample output file generated by `process.m` after post-processing the model runs is as presented hereunder. The processing techniques used in the script are explained as analysis methods in Chapter 4.

```

1      0.497 % Hrms_hf      [m] High frequency wave height
2      0.112 % Hrms_lf     [m] Low frequency wave height
3      0.521 % Hrms_swash  [m] Wave height in swash region
4      0.133 % setup      [m] Water level set-up
5      4.300 % Ru2perc    [m] Run-up 2%
6      3.774 % hsg        [m] Mean WL at seagrass incidence
7      3.870 % hveg       [m] Mean WL at vegetation incidence
8      3.936 % hmf        [m] Mean WL at midforest
9      3.936 % htoe       [m] Mean WL at diketoe
10     0.211 % Hrms_toe   [m] Incident wave height at diketoe
11     0.130 % Hrms_IG_toe [m] Infragravity wave height at diketoe
12     0.117 % Hrms_VLF_toe [m] Very Low Frequency wave height at ...
      diketoe
13     9.153 % Tm-1,0     [s] Spectral wave period
14     4.796 % RuVG       [m] van Gent's (2001) runup estimate
15     4.883 % RuVG_VLF   [m] van Gent's (2001) runup estimate ...
      with VLF
16     0.038 % R0         [-] Reflection Coefficient (offshore)
17     0.995 % Rd         [-] Reflection Coefficient (dike)
18     0.205 % KrSG       [-] Attenuation Coefficient Seagrass
19     0.910 % KrSM       [-] Attenuation Coefficient Saltmarsh
20     0.065 % KtOD       [-] Transmission Coefficient Offshore to ...
      Dike
21     0.158 % KtVM       [-] Transmission Coefficient Veg. ...
      incidence to midforest
22     0.823 % Kru        [-] Attenuation Coefficient of velocities
23     0.969 % KrF        [-] Attenuation Coefficient of drag forces
24     0.368 % Hrms_hp1   [m] Spectral High-pass wave height
25     0.105 % Hrms_lp1   [m] Spectral Low-pass wave height
26     0.258 % Hrms_hp2   [m] Zero-crossing High-pass wave height
27     0.056 % Hrms_lp2   [m] Zero-crossing Low-pass wave height
28     0.00000 % qOTmean  [l/s/m] Mean Overtopping discharge rate
29     0.00000 % qOTmax   [l/s/m] Maximum Overtopping discharge rate
30     0.00000 % qOTtot   [m3/m] Overtopping discharge
31     11.97283 % RcSWL   [m] Freeboard relative to Still WL
32     11.85464 % RcMWL   [m] Freeboard relative to Mean WL
33     11.83992 % Rc      [m] Freeboard relative to Mean Run-up
34     686.017 % Filesize [MB] Filesize
35     70.79 % Trun       [min] Simulation Runtime
36     1024579 % nt       [-] Timesteps

```

37	0.40	% maxbrsteep	[-]	Maximum breaking steepness
38	0.100	% dx min	[m]	Minimum grid size
39	1.000	% dx max	[m]	Maximum grid size
40	0.487	% dx mean	[m]	Mean grid size
41	100.0	% np	[-]	num points per wavelength
42	3554.0	% nx	[-]	Num of grid points
43	1731.236	% xmax	[m]	Domain width
44	-14.806	% zb0	[m]	offshore bed elevation
45	4.097	% h2perc	[m]	Extreme water level at diketoe

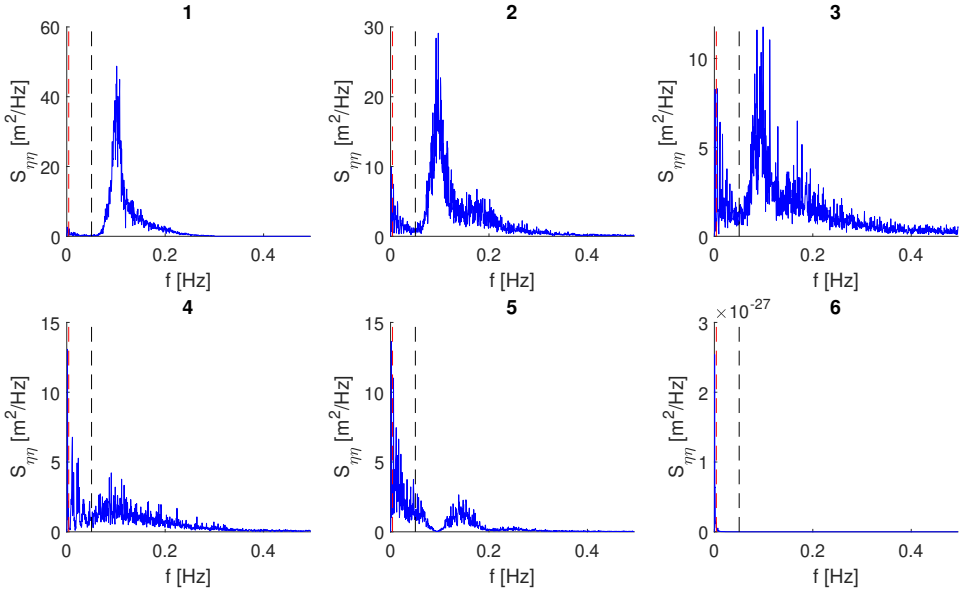
The same outputs are recompiled by `results.m` along with input conditions for each specific run. A `*.csv` file is written containing all the input conditions with all the results which feeds the flood risk prediction tool presented in Chapter 5. Not all the outputs have been used in the prediction tool due to scope limitation. However, future studies could focus on looking into more detailed aspects of vegetated hydrodynamics like streamwise velocities and drag forces in the vegetation forest relative to the upstream and downstream ends.

The Figure C.1 presented extension of results presented in Figure 4.7. The spectral evolution along the cross-shore transect has been presented scenario of vegetation and bare-bed. Frequency splitting between short-wind waves and infragravity was done and another splitting was done between infragravity and very low frequency waves to study effect of vegetation on all sea-state frequency components.

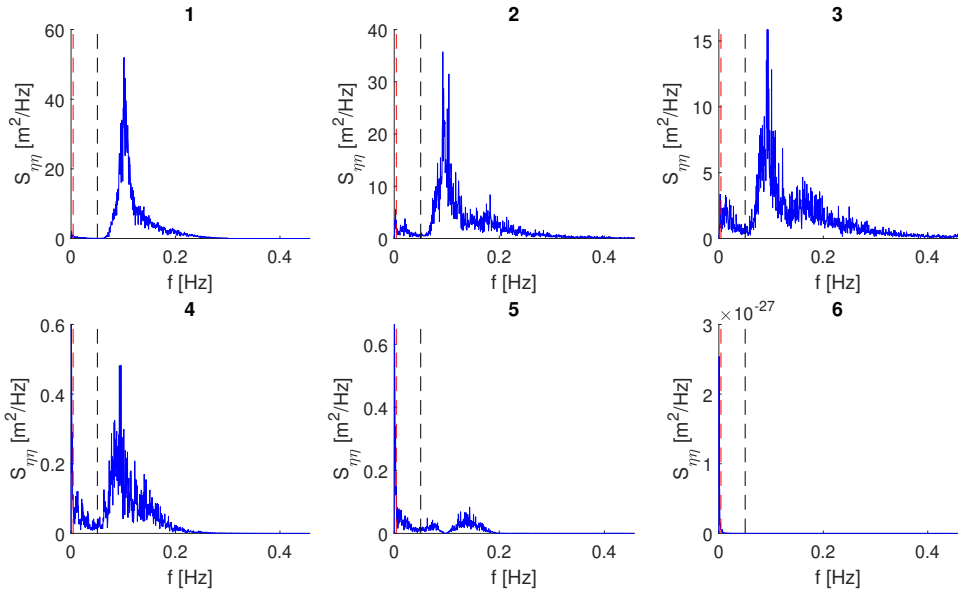
## C.2. COWEBS OF BAYESIAN NETWORK

The Figure C.2 presents coweb plots of both the prediction tools for saltmarshes and mangroves. The vertical axis has been scaled based on relative percentage values of each parameter. The lines in the plots could be followed to see the variation of Monte Carlo sampled values in each simulation. In total only 15 samples have been provided for explanatory purposes.

Based on only 15 samples per parameter the strength of copulas and non-parametric Bayesian Networks over discrete BNs in handling data could be elaborated through the order of magnitude of conditional probabilities required. In discrete BNs, for 15 variations of 13 saltmarsh parameters and 21 mangroves parameters, the order of magnitude of conditional probabilities required would have been around  $(O)^{15}$  for saltmarshes and  $(O)^{24}$  for mangroves. The extent of complexity and the ease with which the data was handled by the stochastic model and the non-parametric Bayesian network while making flood risk predictions is immense which makes it a superior approach in developing synthetic datasets.

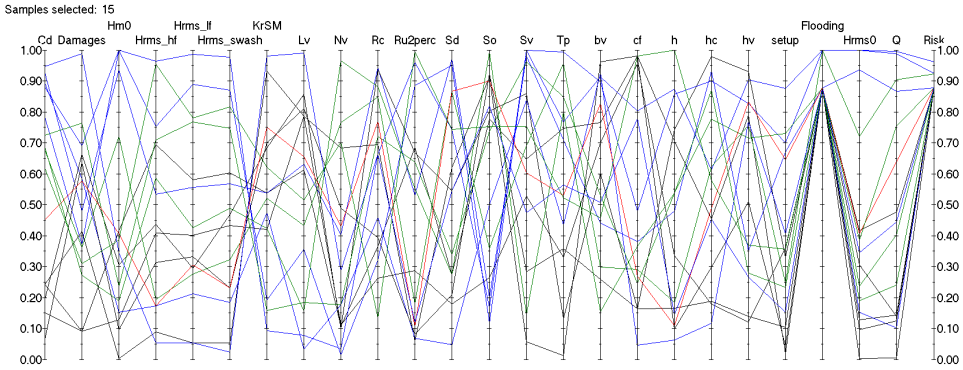
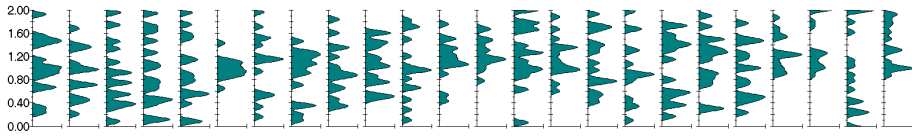


(a) Spectral output of 1000 waves in a bare-bed (no vegetation) case.

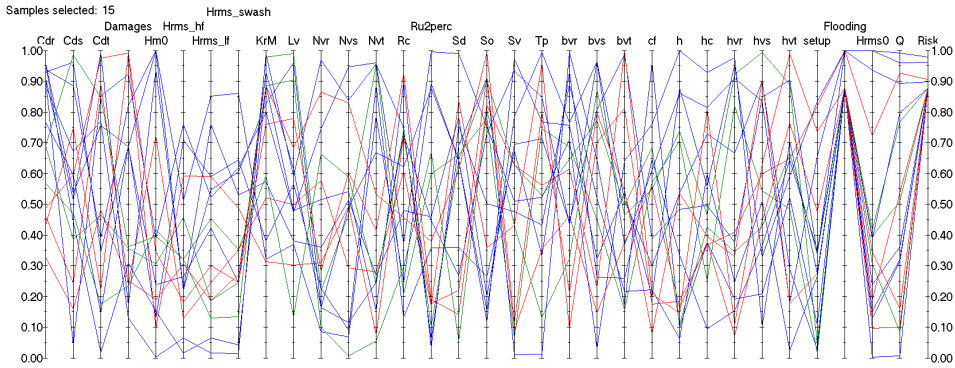
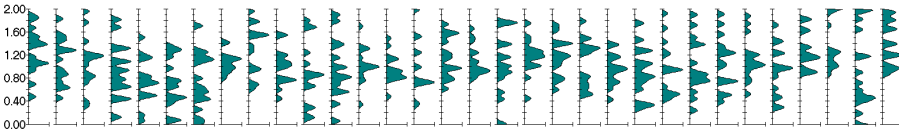


(b) Spectral output of 1000 waves with vegetation

**Figure C.1:** Spectral evolution across 6 output points is shown in the scenario of vegetation and without vegetation. Black dash lines represent splitting frequency between short-wind waves and infragravity while red dash lines represent splitting frequency between infragravity and very low frequency waves.



(a) CoWebs and density plots of Saltmarsh non-parametric Bayesian Network.



(b) CoWebs and density plots of Mangroves non-parametric Bayesian Network.

**Figure C.2:** CoWebs and density plots of all the parameters in both saltmarshes and mangroves prediction tools. Only 15 samples per parameter are presented which shows the capacity of copulas and non-parametric Bayesian Networks in handling data is a better way than discrete BNs. In discrete BNs the order of magnitude of conditional probabilities required would have been around  $(O)^{15}$  for saltmarshes and  $(O)^{24}$  for mangroves.

